Optimized energy management for hybrid powertrains with different power levels

Tianhong Wang

THÈSE DE DOCTORAT DE L'ETABLISSEMENT UNIVERSITÉ BOURGOGNE FRANCHE-COMTÉ

PRÉPARÉE A L'UNIVERSITÉ DE TECHNOLOGIE DE BELFORT-MONTBÉLIARD

Ecole doctorale n°37

Sciences Pour l'Ingénieur et Microtechniques

Doctorat de Énergétique

Par

Tianhong WANG

Gestion optimisée de l'énergie pour les chaines de traction hybrides avec différents niveaux de puissance

Thèse présentée et soutenue à Belfort, le 16/11/2022

Composition du Jury:

M. Mohamed Benbouzid	Professeur à l'Université de Brest	Président
M. Marek Jasinski	Professeur à l'École polytechnique de Varsovie	Rapporteur
Mme. Su Su	Professeure à l'Université Jiao Tong de Pékin	Rapportrice
M. Chen Liu	Maitre de conférences à l'Université de Zhengzhou	Examinateur
M. Fei Gao	Professeur à l'Université de Technologie de Belfort-Montbéliard	Directeur de thèse
M. Qi Li	Professeur à l'Université Jiaotong du Sud-ouest	Co Directeur de thèse
Mme. Elena Breaz	Maitre de conférences à l'Université de Technologie de Belfort-Montbéliard	Co-encadrant
M. Alexandre Ravey	Maitre de conférences à l'Université de Technologie de Belfort-Montbéliard	Co-encadrant

PH.D. THESIS OF THE UNIVERSITY BOURGOGNE FRANCHE-COMTÉ

PREPARED AT THE UNIVERSITY OF TECHNOLOGY OF BELFORT-MONTBÉLIARD

Doctoral School n°37

Engineering Sciences and Microtechnologies

Doctor of Philosophy (Ph.D.) in Energy

by

Tianhong WANG

Optimized energy management for hybrid powertrains with different power levels

Thesis presented and defended in Belfort, on 16/11/2022

Composition of Jury:

M. Mohamed Benbouzid	Professor at University of Brest	President
M. Marek Jasinski	Professor at Warsaw University of Technology	Reviewer
Mme. Su Su	Professor at Beijing Jiaotong University	Reviewer
M. Chen Liu	Associate professor at Zhengzhou University	Examiner
M. Fei Gao	Professor at University of Technology of Belfort-Montbéliard	Supervisor
M. Qi Li	Professor at Southwest Jiaotong University	Co-director of thesis
Mme. Elena Breaz	Associate professor at University of Technology of Belfort-Montbéliard	Co-supervisor
M. Alexandre Ravey	Associate professor at University of Technology of Belfort-Montbéliard	Co-supervisor

Titre: Gestion optimisée de l'énergie pour les chaines de traction hybrides avec différents niveaux de puissance

Mots-clés: Système d'alimentation hybride, Système multi-sources, Gestion de l'énergie, Distribution d'énergie

Résumé: L'application d'architectures hybrides dans le domaine des transports permet d'atténuer les problèmes de pollution de l'environnement et d'améliorer la qualité de l'air. Par conséquent, cette thèse est consacrée à la recherche de stratégies de gestion de l'énergie et de méthodes de distribution de puissance adaptées aux chaines de traction hybrides à différents niveaux de puissance. Dans ces systèmes, le coût élevé et la durabilité insuffisante des sources d'énergie sont les principales raisons qui limitent son application à grande échelle. Afin de minimiser la consommation d'hydrogène d'un véhicule électrique hybride batterie/pile à combustible et d'améliorer la durabilité des ses sources, une stratégie optimale de gestion économique de l'énergie est proposée dans cette thèse. De plus, afin d'optimiser la durée de vie de la structure hybride étudiée, cette thèse propose une stratégie de gestion de l'énergie optimisée basée sur la recherche extrême en ligne en tenant compte de la dégradation des sources d'énergie pour une application de tramway électrique hybride supercondensateur/pile à combustible. Enfin, l'architecture hybride propose à été dérivé en système multisource utilisant plusieurs systèmes de stockage d'énergie et plusieurs ensembles de piles à combustible afin de pouvoir répondre à des applications nécessitant des puissances de charge plus élevées. En conséquence, une stratégiede distribution d'énergie à performances constantes adapté à un système d'alimentation hybride multisource est également proposé. Les gestions présentées dans cette these ont fait l'objet d'une validation expérimentale grâce à un banc d'essai Hardware in the Loop.

Title: Optimized energy management for hybrid powertrains with different power levels

Keywords: Hybrid power system, Multi-source system, Energy management, Power distribution

Abstract: The application of hybrid power system in the field of transportation can alleviate environmental pollution problems and improve air quality. Therefore, this thesis is devoted to researching energy management strategies and power distribution methods suitable for hybrid power systems with different power levels. In the hybrid power systems, the high cost and insufficient durability of the power sources are the main reasons that restrict its large-scale application in the energy market. In order to minimize the equivalent hydrogen consumption of a battery/fuel cell hybrid electric vehicle and improve the durability of the power sources, an optimal system economic energy management strategy is proposed in this thesis. In addition, considering the change of power sources operating performance can further improve the optimization effect of the energy management strategy, this thesis also proposes an online extremum seeking-based optimized energy management strategy considering power sources degradation for a supercapacitor/fuel cell hybrid electric tram. Moreover, in order to apply the new energy hybrid power systems to higher power applications, a scheme of constructing a multi-source hybrid power system using multiple energy storage systems and multiple sets of fuel cells is proposed. Accordingly, a performance consistent power distribution method suitable for multi-source hybrid power system is also proposed. Furthermore, hardware-in-the-loop testing and physical experiments have verified the functionality and real-time suitability of the proposed strategies.

Université Bourgogne Franche-Comté
32, avenue de l'Observatoire
25000 Besançon

Acknowledgement

The research work of this thesis was done in the FEMTO-ST Institute, Energy Department, University Bourgogne Franche-Comte, UTBM, CNRS.

Firstly, I am very grateful to Prof. Mohamed Benbouzid, Prof. Marek Jasinski, Prof. Su Su, and Dr. Chen Liu for their kindly help in preparation for my thesis defense. In addition, I would like to express my sincerest gratitude to my supervisors Prof. Qi Li, Prof. Fei Gao, Dr. Elena Breaz, and Dr. Alexandre Ravey. In the first year of my Ph.D. study, I didn't know anything about the optimization and building of the hybrid electric vehicle model and the design of hardware experiments. My supervisors gave me the most meticulous guidance and full trust, which encouraged me to pursue academic research. Prof. Qi Li and Prof. Fei Gao patiently explained the modeling details of the vehicle to me, and guided me to design experiments to test my scientific research ideas. Their extensive professional knowledge and rigorous academic attitude have benefited me a lot, which will benefit me for the rest of my life. Dr. Elena Breaz and Dr. Alexandre Ravey helped me explore research content and guided me to write academic papers, and they gave me constructive suggestions and critical discussions to my thesis. It is my great privilege to work with them over the past few years. In addition, I sincerely thank Prof. Weirong Chen from Southwest Jiaotong University for his guidance and suggestions towards my future scientific career.

Secondly, I would like to convey my sincere appreciations to my dear colleagues in UTBM: Dr. Hao Bai, Dr. Hanqing Wang, Dr. Zhiguang Hua, Dr. Yang Zhou, Dr. Yu Wu, Dr. Shengrong Zhuo, Dr. Huan Luo, Dr. Bincong Jian, Mr. Liangzhen Yin, Mr. Yuchen Pu, Mr. Qian Li, Mr. Xinyang Hao, Mr. Xiaolei Ye, Mr. Rui Yang, for they have helped me a lot no matter in the academic researches and daily life.

Then, I would also like to thank my loved ones, my dear parents, grandma, sister, and grandfather in heaven, for your unconditional support along the way in any decision I made so that I can concentrate on my studies and have no worries.

Finally, I would like to express my heartfelt thanks to the China Scholarship Council (CSC) for funding during my Ph.D.

Table of contents

General Introduction

With the increase of population and the vigorous development of society, energy consumption in transportation, house heating, living lighting and other aspects has gradually increased. For further development, human demand for energy has also reached unprecedented levels [1–3]. Nevertheless, up to now, more than 80% of energy comes directly or indirectly from the combustion of fossil fuels such as coal, oil and natural gas [4–6]. Over the past two centuries, massive energy consumption has brought huge hidden dangers to the environment [7]. There is a direct inseparable relationship between the burning of fossil energy and the rising emissions of greenhouse gases, and it is also the main cause of climate change [8,9]. In order to more actively respond to global climate issues and improve the ecological environment, 171 countries jointly signed the "Paris Agreement on Climate Change" in 2016, and jointly agreed to limit the increase in global average temperature to well below 2 °C [10]. In order to implement this goal, China released the "Energy Production and Consumption Revolution Strategy" in 2016, proposing to achieve the goal of "carbon peaking" by 2030, and the proportion of renewable energy in total energy consumption should not be less than 20%. In addition, in 2017, the United States formulated a plan to achieve more than 50% of total energy from clean energy by 2025 and 100% by 2040. Besides, in the same year, France proposed a plan to stop coal-fired power generation in 2022 and halve total energy consumption by 2050. What's more, in 2018, the European Commission planned to achieve the goal that regenerative energy should account for no less than 32% of total energy consumption by 2030, and planned to achieve "carbon neutrality" by 2050. Furthermore, Germany also proposed in 2019 a plan to achieve more than 80% renewable energy in total power generation by 2050 [11–15]. Therefore, the further development and utilization of renewable and clean energy such as nuclear energy, solar energy, wind energy, and hydrogen energy have gradually become the trend of global energy development [2,16,17].

In this context, a lot of research work has been carried out in the field of sustainable energy, such as the investigation of photovoltaic (PV) power generation, wind turbines (WT), hydrogen energy and other clean energy sources. Among these new energy sources, different energy sources have different power generation characteristics. PV and WT are easily affected by the geographical environment and therefore have strong randomness and intermittence operating characteristics, which can't stably supply energy to the load [18–20]. Compared with these two energy sources, hydrogen energy has the advantages of high energy efficiency, easy transportation and high reliability. Therefore, hydrogen energy seems to have the most application prospect [21–23].

Further, according to existing research [2,8,16,24,25], the transportation domain consumes more than half of the fossil fuels (about 75%) and emits a large amount of black carbon. Therefore, the research and popularization of new energy vehicles helps reduce fuel consumption and improve air quality. It is

necessary to carry out in-depth research in the field of new energy vehicles [16,26,27]. Compared with plug-in hybrid electric vehicle (PHEV), pure electric vehicle (EV), and fuel cell vehicle (FCV), it is a more promising research direction to apply energy storage system (ESS) (such as battery and supercapacitor) and fuel cell (FC) to the field of transportation to form hybrid electric vehicle (HEV) [28,29]. The main properties of this type of ESS/FC HEV are high driving range like the traditional internal combustion engine vehicle, fast charging time (usually 3-5 minutes), silent operation capability, and zero-local emissions [24,30]. Therefore, in recent years, more and more scholars are investigating HEV. However, the widespread market application of dual-source hybrid system in the high-power occasions has not yet been accomplished, the main reasons are as follows [21,31,32]:

- Limited by power density, it is difficult for a dual-source hybrid system to meet the system power requirements of high-power applications (higher than 400 kW);
- Due to the limitations of technology and materials, the cost of developing higher-power power sources is relatively high;
- When operating under complex operating conditions, it is difficult to ensure the power generation performance of the power sources, and their durability and service life need to be improved.

In order to fill the above-mentioned research gap, a scheme of using multiple ESSs and multiple sets of FCs to build a multi-source hybrid system to supply electric power for high-power applications is proposed [33–35]. This type of power supply method can effectively increase the power level and redundancy of the system, reduce the development cost of high-power power sources, improve the reliability and stability of the system, and prolong the overall service life of the system [21,23,36]. In addition, the adoption of multi-source hybrid system power generation technology also makes the control method more flexible. We can remove the faulty generator unit in time without affecting the normal operation of the system through reasonable control methods, thereby increasing the fault tolerance of the system [21,37,38]. Therefore, it is necessary to study the multi-source hybrid power system applied in high-power applications.

In the dual-source hybrid power system and multi-source hybrid power system, it is necessary to fully consider the power generation characteristics of ESS and FC, and provide a reasonable energy management strategy (EMS) or power distribution method for the hybrid power systems according to different goals and operating conditions, which is of great significance for improving system stability, prolonging power sources service life, and optimizing fuel economy. Therefore, it is necessary to conduct in-depth research on EMS to properly coordinate the power allocation between the ESS and FC in the hybrid power systems.

In summary, the research on EMSs and control methods for hybrid power systems has very important commercial application value. Therefore, this thesis mainly studies the EMS of different hybrid power

systems. In addition, the research route of this thesis is shown in Fig. I, and the research contents of each chapter are as follows.

Chapter 1 introduces the research status of HEVs, the development status of hybrid electric trams, the research status of EMSs, and the research status of multi-source power generation systems. According to the analysis in the **Chapter 1**, the drawbacks of the current EMSs are highlighted, and the structure and the configuration of the powertrain can be determined.

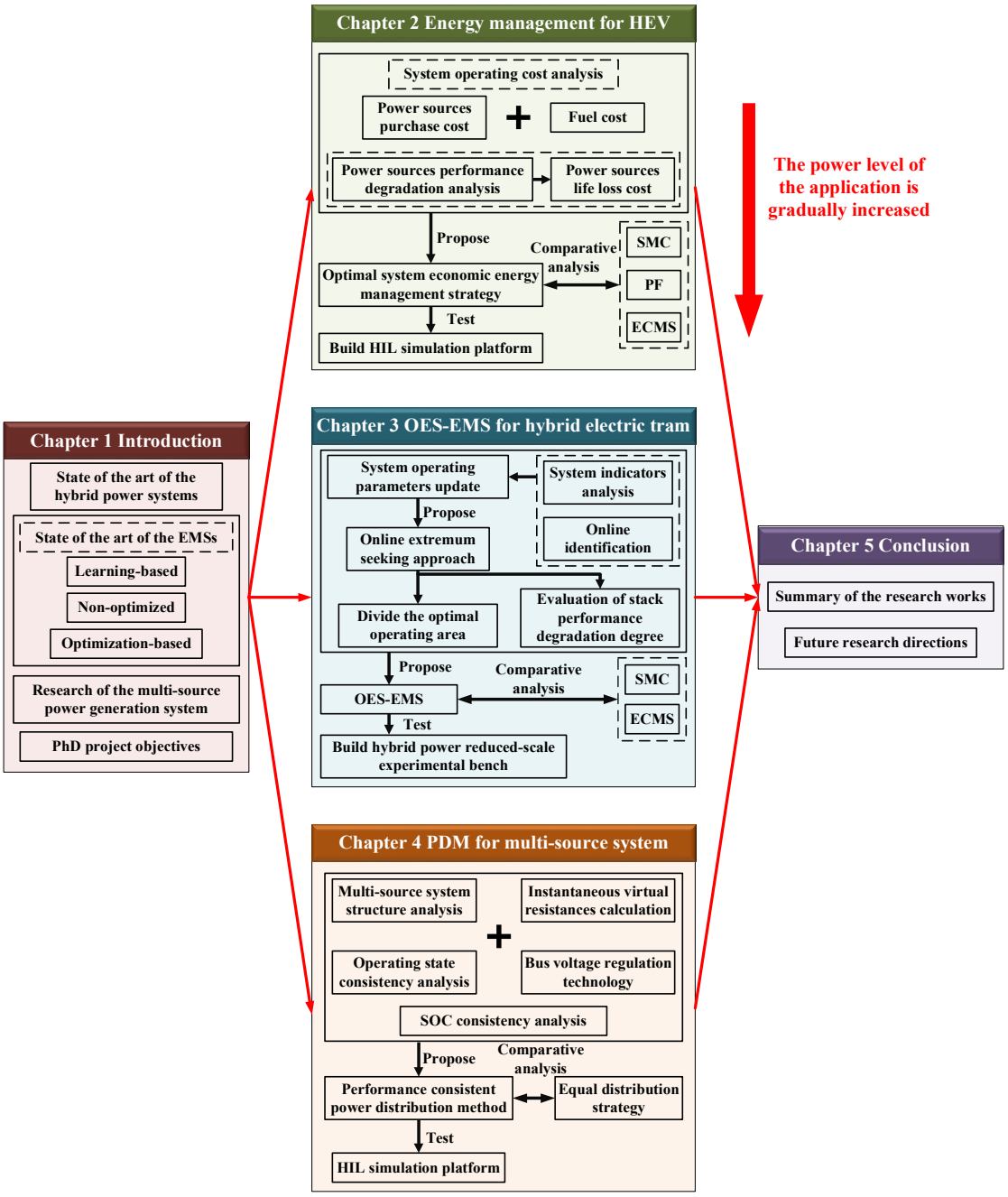

Figure I. The research route of this thesis.

In **Chapter 2**, various EMSs for the hybrid power systems are studied. Then, in order to minimize the equivalent hydrogen consumption of the system and improve the power sources durability, an optimal

system economic EMS for a hybrid electric vehicle is proposed. The proposed strategy, is experimentally validated on the hardware-in-the-loop (HIL) simulation platform.

The main purpose of **Chapter 3** is to present an online extremum seeking-based optimized EMS for a hybrid electric tram. This strategy considers that the operating performance of the power sources will vary with the operating conditions, so an online extremum seeking technology is used to estimate the maximum efficiency and maximum power operating points of the stack. In addition, this chapter constrains the fluctuation range of the supercapacitor's State of Charge (SOC) and divides a "safe operating zone" for the stack. A reduced-scale test platform powered by supercapacitor and FC is established, and verification experiments are carried out.

Chapter 4 mainly focuses on the research of multi-source hybrid power system suitable for high-power applications, and presents an operating state consistency power distribution method that considers multiple factors (such as batteries SOC consistency and stacks operating performance consistency). In addition, in order to facilitate the system expansion, this chapter also studies the virtual droop control algorithm. The validity verification is carried out on the HIL test platform.

Chapter 5 presents research contents in this PhD thesis, and also lists the future research works and directions.

Chapter 1. Introduction

This chapter presents a general introduction to the PhD thesis, including the current research and development status of the hybrid electric vehicles (HEVs), the research status of hybrid electric trams, a brief overview of the current state of research on energy management strategies (EMSs), and the research status of multi-source power systems. In this chapter, by analyzing the advantages and disadvantages of dual-source hybrid powertrain and multi-source hybrid powertrain, we decide to apply the dual-source hybrid power system to low-power level traffic vehicles (such as electric vehicles and trams below 400 kW) and the multi-source hybrid power system to high-power level rail traffic vehicles (such as high-speed Electrical Multiple Unit trains). In addition, by analyzing the advantages and disadvantages of different powertrain topologies of the HEV, we finally determined the powertrain topologies adopted in this thesis. Then, by analyzing the existing EMSs, we summarize the advantages and disadvantages of these strategies, which provide a basis for research on the formulation of subsequent EMSs. Thereafter, by investigating the current research on multi-source power systems, the structure and the research focus of the systems are determined in this thesis. In the final section of this chapter, we highlight the contributions of this PhD thesis.

1.1. State of the art of hybrid power systems

With the increasing improvement of material science, battery, supercapacitor (SC), and fuel cell (FC) have been widely used in many industries, especially in the field of transportation [8,16,39,40]. At present, the world's major automobile manufacturers have achieved certain technological achievements in the field of transportation powered by ESS and FC.

1.1.1. Hybrid electric vehicles research and development status

In order to accelerate the layout of the HEV industry, automobile manufacturers in the United States, Japan, South Korea, China and other countries have formulated HEV development strategies, and have basically broken through the HEV technical bottleneck [39,41].

General Motors (GM) has been developing the battery/FC HEVs since the 1990s. GM developed the first electric vehicle (EV) "Electrovan" powered by FC in 1996, with a maximum speed of 70 km/h and a cruising range of 240 km [27,42]. In 2000, GM successfully developed the FC vehicle "HydroGen1", which uses liquid hydrogen as fuel, with a maximum speed of 140 km/h and a cruising range of 400 km [43]. In addition, in 2005, GM exhibited the HEV "Sequel" at the Detroit Auto Show. This vehicle has a hydrogen fuel storage capacity of 8 kg and a cruising range of 480 km.

Hyundai started research on energy storage system (ESS)/FC HEV technology in 1998 and developed the HEV "Santa Fe" in 2000 [44,45]. In 2006, Hyundai independently developed the "Tucson" HEV,

and in 2013, Hyundai developed electric vehicle “ix35”. This vehicle adopts a powertrain with a rated power of 100 kW and has a cruising range of 594 km with one hydrogen refueling [46].

Due to lack of resources, Japan pays special attention to the application of new energy power generation technology in the field of vehicles [27]. Toyota has been researching HEV since 1996 and has developed many prototypes powered by battery and FC such as the “FCHV-1” (1996), “FCHV-2” (1997), “FCHV-3” (March 2001), “FCHV-4” (June 2001), “FCHV-5” (October 2001), “Toyota FCHV” (2002), and “Toyota FCHV-adv” (2008). In 2015, Toyota finally launched a mass-produced and commercial HEV “Mirai” with a cruising range of 480 km [47]. This means that the research and development of HEV begins to enter the early commercialization stage. In addition, in 1999, Honda also developed two prototypes, “FCX-V1” and “FCX-V2”. In 2002, Honda developed the “FCX-V4” HEV, which uses a 35 MPa high-pressure hydrogen storage tank and has a cruising range of 310 km. In 2008, Honda developed the “FCX Clarity”, which has a maximum cruising range of 390 km and successfully entered the global market [42]. The new-generation “Clarity” HEV was exhibited in Japan in 2016. This vehicle is equipped with a hydrogen storage tank that can hold 5 kg of hydrogen, the pressure can reach 70 MPa, and can drive about 750 km with one refueling [48,49].

China’s first HEV powered by battery and FC was jointly developed by Tsinghua University and Beijing Century Fuyuan Fuel Cell Company in 1998. This vehicle is an 8-seat small EV, its top speed is 20 km/h, and it can travel 80 km with one hydrogen refueling. In 2014, SAIC Roewe launched the “Roewe 950” plug-in hydrogen HEV with a cruising range of 430 km and a maximum speed of 160 km/h. In 2018, Yutong Bus launched the third-generation battery/FC electric bus “ZK6125FCEVG5”. The maximum speed of this vehicle is 69 km/h, the fueling time is only 10 minutes, and its cruising range can reach 500 km, which meets the market operation requirements.

In summary, automotive companies such as GM, Toyota, Hyundai, Honda and other international technology-leading vehicle manufacturers have completed the research and development of basic HEV performance and released mass-produced models, and have made significant progress in HEV technology.

1.1.2. Hybrid electric trams research and development status

In addition to applying hybrid power generation technology to the above-mentioned vehicles, more and more researchers apply it to trams (including locomotives and trains) in order to construct hybrid electric trams. This kind of tram can not only meet the needs of rapid population movement, but also effectively alleviate environmental pollution, so it has received extensive attention from many experts [50,51].

In 2002, led by the United States Department of Energy, the Fuel cell Propulsion Institute and Vehicle Projects LLC jointly developed the world’s first locomotive powered by FCs. The powertrain of this

locomotive is composed of two sets of FCs from Nuvera Fuel Cell Europe, Italy, in series, with a total power of 17 kW and a rated current of 135 A, which can guarantee continuous operation for more than 8 hours when working at full load [52]. In addition, Burlington Northen Santa Fe began developing FC hybrid locomotive for shunting yards in 2007. The powertrain of this locomotive consists of a FC with a rated power of 240 kW and two sets of lead-acid batteries [53].

In order to reduce the pollution caused by trams to the environment, Japan planned to start the development of new energy locomotives in 2000, and began to apply FC hybrid power generation technology to rail transit locomotives in 2006. In 2006, Japan's Railwar Technology Research Institute transformed a diesel hybrid locomotive into a FC hybrid locomotive. This locomotive has a top speed of 100 km/h, and the powertrain consists of a battery rated at 340 kW and two FCs rated at 65 kW. Its bus voltage is 450 V, and the capacity of the hydrogen storage tank is about 410 L [54,55]. In 2007, Japan launched a commercial battery/FC hybrid electric train. Its hybrid power system consists of a 360 kW battery and a 120 kW FC, the bus voltage is 1500 V, and the maximum speed of the train is 110 km/h [56,57]. This is also the first time in the world that FC hybrid technology has been used in commercial passenger train.

Denmark started the research and development plan of FC hybrid electric tram in 2007, and successfully developed Europe's first hybrid electric rail locomotive in 2010. The locomotive is powered by a FC rated at 105 kW and operates on the Vemb-Lemvig-Thyborøn Jernbane railway [58]. In addition, France's Alstom also exhibited the FC train "Coradia iLint" at the Rail Transit Technology Exhibition in Berlin, Germany in 2016. The powertrain of the "Coradia iLint" consists of a battery with a capacity of 110 kWh and a FC rated at 200 kW. Its maximum operating speed can reach 140 km/h and has a cruising range of 600-800 km with one hydrogen refueling [59,60].

In 2008, Southwest Jiaotong University started the research work on FC locomotive for the first time, and in 2013, developed China's first FC hybrid electric locomotive, which has a design speed of 65 km/h and a towing weight of 200 t. The locomotive adopts the HD-6 FC with a rated power of 150 kW provided by Ballard as the power source, and is equipped with lithium titanate batteries and SCs as the ESS [61]. Then in 2016, Southwest Jiaotong University and CRRC jointly developed the world's first commercial FC/SC hybrid electric tram. The power system of the tram uses two sets of 150 kW FCs and multiple sets of SCs, the maximum operating speed is 70 km/h, and it can carry 336 passengers [62]. In addition, Tsinghua University and CRRC successfully developed a FC hybrid electric tram in 2016. The power system of the tram adopts FC with a rated power of 150 kW, and is also equipped with batteries and SCs as the ESS. In addition, its design speed is 36 km/h, and it can run 70 km with a single hydrogen refueling [63].

1.1.3. Research on hybrid powertrain structure

From the above description, it can be seen that due to the inherent shortcomings of FCs such as slow dynamic response and inability to absorb braking energy from the vehicle, in order to ensure the safe, stable and efficient operation of the system, the powertrains of systems are generally powered by two or more energy devices (such as FC, battery, and SC) [40,41]. According to the investigation of the current commercial EVs and electric trams [39,41,64], it is found that the main components configuration of the system powertrains are "FC only", "supercapacitor + FC (SC + FC)", "battery + FC (Bat + FC)", and "supercapacitor + battery + FC (SC + Bat + FC)". The specific details are listed in TABLE 1.1. It can be seen from TABLE 1.1 that most of the system powertrain adopts the "Bat + FC" configuration, and a few use the "SC + FC" and "SC + Bat + FC" configuration. Considering that the major research purpose of this thesis is to study the EMSs of hybrid power systems, in addition, in order to comprehensively study hybrid power generation technology, we adopt two configurations of "Bat + FC" and "SC + Bat" in our research.

TABLE 1.1. Components configuration of different commercial EVs and electric trams powertrains.

Vehicle model	Year	Components configuration	Vehicle model	Year	Components configuration
Mazda Demio FC-EV	1997	Bat + FC	Mercedes-Benz F-Cell	2002	FC only
Nissan X-Trail FCV	2003	Bat + FC	Jeep Treo-Fuel cell	2004	FC only
Suzuki SX4-FCV Fuel cell vehicle	2004	SC + FC	Suzuki Wagon R-FCV	2005	FC only
Peugeot 207 Epure	2006	Bat + FC	Kiha E200	2007	Bat + FC
Mitsubishi Grandis FCV	2008	Bat + FC	Morgan LIFEcar	2008	SC + FC
Peugeot H2Origin	2008	Bat + FC	Sceni ZEV H2	2008	Bat + FC
Suzuki SX4-FCV	2008	SC + FC	Audi Q5 FCEV	2009	Bat + FC
Chevrolet Equinox fuel cell	2009	Bat + FC	Mercedes-Benz F800	2010	FC only
Chang an Z-SHINE FCV	2010	Bat + FC	FAW Besturn B70 FCV	2010	Bat + FC
Ford Focus FCV	2010	Bat + FC	VW Golf Sport Wagen HyMotion	2010	Bat + FC
Nissan Terra FCEV SUV	2012	FC only	Kia Borrego FCEV	2012	FC only
Nissan TeRRA SUV	2012	Bat + FC	BMW i8 Hydrogen Car	2012	Bat + FC
Honda FCX clarity	2014	FC only	Audi Sportback A7h-tron Quattro	2014	Bat + FC
Roewe 950 Fuel Cell	2014	Bat + FC	Volkswagen Golf Hymotion	2014	Bat + FC
Coradia iLint	2016	Bat + FC	Honda Clarity Fuel Cell	2017	Bat + FC
Toyota Mirai	2017	Bat + FC	Hyundai Tucson Fuel cell	2017	Bat + FC
BMW 5 series Gran fuel cell vehicle	2017	Bat + FC	Alfa Romeo MiTo FCEV	2017	Bat + FC
LRV	2017	SC + FC	100% LF-LRV	2018	SC + Bat + FC

Mercedes Benz New GLC-Fuel Cell	2018	Bat + FC	Hyundai Nexo	2018	Bat + FC

In hybrid power systems, it can be divided into different topological structures according to the different connection methods between the power sources and the DC/DC converter. Different powertrain designs have a direct impact on the complexity of system control and operational performance. According to existing research [8,24,39], there are a total of six different topologies (T1-T6), as shown in Fig. 1.1.

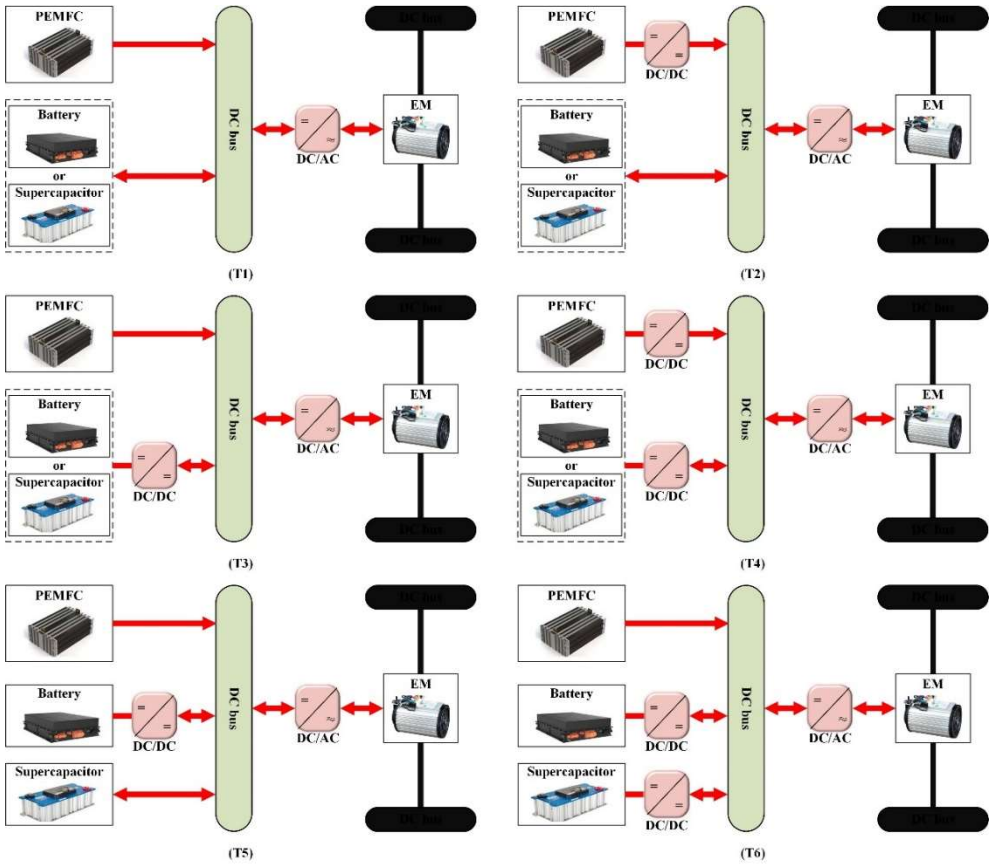

Figure 1.1. The different powertrain topologies of the hybrid power systems.

Fig. 1.1 (T1) is a relatively simple powertrain topology, the ESS (battery or supercapacitor) and FC are directly connected to the bus port. This topology does not require any DC/DC converter and is the simplest and most economical topology. Whereas, in this topology, the bus voltage directly determines the voltage level of the ESS and FC, which requires higher power generation parameters for the ESS and FC. Only when the output voltage of the ESS and FC matches the bus voltage, the vehicle can drive safely and stably. In addition, the ESS plays the role of stabilizing the bus voltage in this system and can be regarded as a voltage source. From the FC output characteristic curve, it can be seen that its output voltage changes with its output current, which can be regarded as a current source [24,65]. Therefore, when using this topology, the output power of each power source cannot be actively adjusted, and the passive adjustment can only be achieved by relying on the bus voltage fluctuation caused by the load fluctuation. When the load demand fluctuates greatly, it is difficult for the FC to meet the power

demand of the vehicle powertrain, which will reduce the operating efficiency and reliability of the system and accelerate the performance degradation of the FC. Therefore, this topology is generally not used in removable devices.

In Fig. 1.1 (T1), the output voltage of the FC cannot be directly matched with the bus voltage, and active energy management cannot be realized, which has certain shortcomings. In order to solve the shortcomings in topology (T1), a unidirectional DC/DC converter is usually connected in series with the output port of the FC, and the output voltage of the FC is adjusted by controlling the DC/DC converter, as shown in Fig. 1.1 (T2). In this topology, by controlling the DC/DC converter, the output power of the FC can be indirectly controlled, thereby realizing the energy management and distribution of the HEV. Therefore, it is possible to achieve the purpose that different power sources operate according to their respective operating characteristics. Although this topology can realize the management of the ESS and FC by adjusting the output current of the DC/DC converter, the ESS used in this topology is directly connected to the DC bus, so the requirements for ESS's voltage level are relatively strict. The topology is relatively simple, can achieve the purpose of energy management, and is easy to implement.

In Fig. 1.1 (T3), the ESS is connected to the bus through a bidirectional DC/DC converter. Compared with the topology (T2), topology (T3) reduces the restriction on the output voltage of the ESS, and can manage the charging and discharging of the ESS at the same time. Although this topology does not require the voltage level of the ESS to match the bus voltage, allowing more flexibility in the selection of the ESS, it has higher requirements on the FC output voltage. In addition, in general, the FC has the characteristics of "low voltage and high current", and its output voltage is usually lower than the bus voltage, so it is difficult to achieve the FC voltage matching the bus voltage [3,17,66]. In this topology, when the bus voltage fluctuates greatly, the FC output voltage will fluctuate violently. Therefore, topology (T3) is not conducive to maintaining the output performance of the FC.

In order to further stabilize the bus voltage, based on the topology (T2), a bidirectional DC/DC converter is added between the ESS and the DC bus to form the topology shown in Fig. 1.1 (T4) [67]. In this topology, not only the FC output reference power can be adjusted by controlling the DC/DC converter, but also the bus voltage can be adjusted. This topology makes the choice of power sources more flexible, and is more conducive to the realization of more demanding EMSs. However, the charging and discharging capacity of the ESS in this topology is limited by the bidirectional DC/DC converter, which may not be conducive to the stability of the system when the load changes sharply. In addition, because more DC/DC converters are added, the control becomes more complicated and the system cost is also increased.

Considering that the batteries have a low charge and discharge rate, they can provide energy continuously and stably, while SCs have higher power density and higher energy storage efficiency, but

they cannot continuously provide electricity [66,68]. Therefore, there are studies using the respective advantages of batteries and SCs to form a hybrid ESS, the topologies are shown in Fig. 1.1 (T5) and (T6). In the topologies (T5) and (T6), the battery is used as the main energy buffer device to compensate for the insufficient output power of the FC when the load changes. Since the SC can be charged and discharged quickly, it can quickly provide energy during acceleration, and can quickly recover regenerative braking energy during braking. In the topology (T5), the SC is directly connected to the DC bus, which can quickly release or recover energy. However, this topology requires that the rated voltage of the supercapacitor must match the DC bus voltage, otherwise it will easily lead to a shortened lifespan of the SC.

In order to make up for the disadvantage that the SC is directly connected to the bus, a bidirectional DC/DC converter can be connected in series to form a topology as shown in Fig. 1.1 (T6). In this topology, the SC is connected to the bus through a bidirectional DC/DC converter, which reduces the limitation of the topology (T5) on the rated voltage of the SC. Although the topologies (T5) and (T6) composed of three power sources (battery, SC, and FC) are relatively complete, the system topologies are complex and have more control quantities. Therefore, the complexity of power distribution is increased, and these topologies are more complicated to implement.

It can be seen from the above analysis that the powertrain of hybrid system is mainly composed of ESS, FC, DC/DC converters, and other components. Through the comparative analysis of different topologies, each topology has its own advantages and disadvantages, which are summarized in TABLE 1.2. Considering the characteristics of different topologies, we decided to use topologies (T2) and (T4) in this chapter to study EMSs for HEVs and hybrid electric trams.

TABLE 1.2. Comparative analysis of different HEV powertrain topologies.

Topology	Advantages	Drawbacks	Remark
T1	1. Less cost and mass 2. Simplest topology	1. Risk of bus current injection back to FC 2. Hard to split the power flow	Seldom used
T2	1. Better FC durability and performance 2. Easy to split the power flow	1. Floating bus voltage	Widely used
T3	1. Good startup performance 2. Low requirements for ESS	1. Easily damage power sources 2. Control strategy is more complex than T2	Seldom used
T4	1. Better control of both FC and ESS 2. Stable bus voltage	1. Increased cost and mass 2. Control strategy is more complex	Widely used
T5	1. Flexibility in energy allocation 2. Combined advantages of three energy sources	1. Increased complexity in control strategy than T1 – T3 2. Increased complexity in powertrain topology	Seldom used

T6	1. Flexibility in energy allocation 2. Better protection for power sources 3. Combined advantages of all power sources	1. Highest mass and cost 2. Lowest system efficiency 3. Most complex topology and control strategy	Seldom used

1.2. State of the art of hybrid power system energy management strategies

In the hybrid power systems, the EMS is the core content of the whole system, which plays a crucial role in determining the output power of different power sources in the system. The formulation principle of the EMS is to improve the fuel utilization rate as much as possible, prolong the service life of the power sources, and meet the dynamic response requirements of the system under the premise of ensuring the safe and stable operation of the system. According to existing research [39–41], EMSs in hybrid power systems can be divided into three categories: non-optimized EMSs, optimization-based EMSs, and learning-based EMSs, as shown in Fig. 1.2.

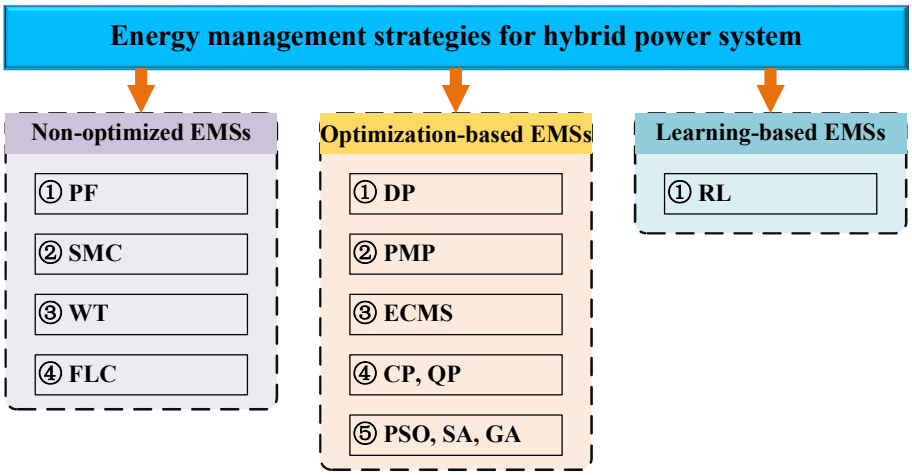

Figure 1.2. Classification of energy management strategies for hybrid power system.

1.2.1. Non-optimized energy management strategies

The non-optimized EMSs do not need to obtain the driving conditions of the vehicle in advance, but need to predefine logic rules according to the State of Charge (SOC) of the battery and the required power of the system. According to the different rules definition methods, it can be divided into EMSs based on certain rules and EMSs based on fuzzy logic [2,3,31]. Because these strategies have the advantages of low computational complexity, simple control, strong robustness and high reliability, this kind of EMS has been widely used in engineering practice. However, this type of strategy relies too much on engineering practice and expert experience, and it is difficult to improve energy utilization, and the pre-established rules cannot be adjusted in practical applications, which may easily lead to poor performance of the system under certain conditions [25,69].

The main idea of the state machine control (SMC) strategy is to divide the operating state of the system into multiple modes. In each mode, the power sources will run at a fixed operating point according to the current load power and SOC state of battery [70]. Based on the research background of EU-sponsored zero-emission ships (Zemships), Ref. [71] proposes a SMC strategy. This strategy is divided into 11 states according to the real-time demand power of the hybrid system, the battery SOC, and the maximum, minimum and optimal output power of the power sources. The simulation results show that the SMC strategy can ensure the continuous and stable operation of the system, but the optimization effect of this strategy on the hydrogen consumption and fuel utilization of the system is not further analyzed. In addition, in the Ref. [70], the state is divided according to the battery SOC and load power, and the output power of the FC is set according to the characteristics of each state. This belongs to the traditional SMC strategy, and in order to achieve better performance, the SMC strategy is often used in combination with other methods. Ref. [50] combines the SMC strategy with droop control, and the proposed strategy can further optimize the overall energy consumption level of the system. Ref. [72] divides the operating modes of the hybrid system according to the state machine theory, and then optimizes the power sources operating point in each mode through the equivalent fuel consumption minimum theory. The results show that the total energy consumption can be reduced by around 4.18% compared to the classical SMC strategy. Furthermore, the Refs. [73,74] also studied the SMC strategy according to different applications and different goals, and formulated power distribution rules according to the power generation characteristics of each power source.

The power following (PF) strategy aims to maintain the SOC of the ESS within the desired range under the premise of satisfying the load power. The strategy uses the difference between the current SOC and the ideal SOC of the battery to adjust the penalty factor to obtain the reference power of each power source. Specifically, when the SOC is higher than the ideal value, the reference power of the FC should be lower than the load power, otherwise it should be higher than the load power to balance the SOC [25,45,75].

The fuzzy logical control (FLC) is a control algorithm based on fuzzy set theory, fuzzy linguistic variables and fuzzy logic reasoning, and the key of the algorithm is to formulate rules of membership functions. The main feature of the FLC strategy is that the fuzzy controller design does not need to establish an accurate mathematical model of the controlled object, nor does it need to know the mathematical relationship between the controller's input and output. Like most non-optimized EMSs, this strategy relies on the researcher's engineering practice experience and has strong adaptability and robustness [25,70,76]. Refs. [77,78] proposed an EMS based on real-time FLC for a HEV power by battery and FC. This strategy takes the load power and the SOC of the battery as the input of the controller, the output power of the FC as the output of the controller, and optimizes the working state of the FC and balances the SOC of battery by formulating a reasonable membership function. In order to

improve the system operation efficiency and power sources durability, Ref. [79] proposed an EMS based on FLC. The study uses a fuzzy logic algorithm and takes battery's SOC and load demand power as input variables to determine the reference power of each power source. In [79], when the load demand power of the system and the battery's SOC are both low, the FC mainly charges the battery, and if the demand power is high and the SOC is also high, the FC and the battery jointly provide the demand power for the load. The experimental results show that reasonable rules can effectively improve the operating efficiency of the system and maintain the battery's SOC in the ideal range. In addition, Refs. [80,81] also apply FLC to the power distribution of hybrid power system.

The wavelet transform (WT) algorithm has been widely used in signal processing applications due to its ability to perform local signal analysis in both time and frequency domains. In the past decade, the WT algorithm has also been widely used in the field of energy management due to its unique advantages. The commonly used basis functions of the WT algorithm are Haar wavelet function, Morlet wavelet function, Daubechies wavelet function and Meyer wavelet function. Among them, the Harr wavelet function is the most widely used because of its convenience and practicality. In order to make the power sources operate according to their respective dynamic characteristics and smooth the power sources output power as much as possible, Ref. [82] proposed an EMS based on wavelet transform for a multi-source hybrid power system. In this study, Harr wavelet is used to decompose the load power into high frequency and low frequency parts, and the low frequency part is allocated to the FC to limit the fluctuation of the FC and prolong the lifetime of the stack, and the remaining high frequency part is allocated to the battery. Since the WT cannot reduce energy consumption and maintain SOC, WT is usually combined with other control methods to obtain better results. Refs. [62] and [83] both propose an EMS that combines WT with FLC. This strategy employs three layers of wavelet analysis and two fuzzy controllers. Firstly, the load power is decomposed by wavelet transform, and then the obtained power is input into the fuzzy controller to generate the reference power of each power source. Experimental results show that the proposed strategy can improve the average efficiency of the system.

In addition to the above-mentioned non-optimized strategies, some scholars use genetic algorithm (GA) and particle swarm optimization (PSO) algorithm to optimize fuzzy rules and membership functions to improve the accuracy and practicability of control strategies [29,84].

1.2.2. Optimization-based energy management strategies

According to the different degrees of dependence on driving conditions, optimization-based EMSs can be divided into two types: instantaneous optimization and global optimization. The instantaneous optimization strategies don't need to know the overall system driving information in advance, and the computational burden is small, so these strategies can be used in real-time applications. The global optimization strategies need to obtain the global operating condition information in advance. However,

in practical applications, the driving of vehicles has greater randomness. Therefore, these strategies are not easy to implement in real-time applications, and are often used to optimize other control methods offline. In practical applications, although the optimization-based EMSs can take into account the advantages and disadvantages of each power source and realize multi-objective control, their control algorithm is complex and require high performance of the controller [76,85].

Dynamic Programming (DP) is an optimization theory proposed by American mathematician Richard Bellman in the 1950s. This algorithm is often used to obtain the global optimal solution in the decision-making process, and can be divided into Stochastic Dynamic Programming (SDP) and Deterministic Dynamic Programming (DDP) [86]. In order to optimize the fuel economy of the hybrid power system composed of battery and FC, a multi-objective optimization EMS is proposed in [87], and the DP algorithm is used to solve the objective function. In addition, in [88], the DP algorithm is adopted to optimize the power distribution of a HEV. The results show that this strategy can effectively prolong the service life of the power sources and reduce the energy consumption of the system. With the goal of minimizing system cost and operating cost, Ref. [89] proposes an improved DP algorithm and compared it with the SMC strategy. The results show that the proposed algorithm can effectively reduce hydrogen consumption by about 15%. In order to reduce the dependence of the DP algorithm on driving information, a SDP algorithm is proposed in [90], which combined the random demand power prediction results to optimize the cost function. Ref. [91] uses DDP algorithm to optimize the charging and discharging strategy of hybrid electric vehicles. The results show that this strategy can effectively reduce fuel consumption by about 2%. However, because the computational burden of the DP algorithm is too large, this algorithm is only suitable for systems whose operating conditions are determined, and can only be implemented offline. Therefore, the DP algorithm is usually used as the optimal benchmark for comparison with the power allocation results of the new strategies.

Pontryagin's Minimum Principle (PMP) is also a global optimization algorithm, which is proposed by Soviet Russian mathematicians in 1956. The PMP algorithm mainly includes cooperative state equation, Hamiltonian function, system state equation and state constraints. The core idea of this algorithm is to transform the global constrained optimization problem into a local Hamiltonian function minimization problem to reduce the computational complexity [92]. By reasonably selecting the initial value of the cooperative state equation of the PMP algorithm, the optimization results of the algorithm can be greatly improved. In order to optimize the operating range of the FC, Ref. [93] proposes a power distribution strategy based on PMP algorithm, and uses the sequential quadratic programming algorithm to optimize the proposed strategy. The experimental results show that this strategy can effectively optimize the hydrogen consumption of the system and improve the power generation efficiency of power sources. In addition, in order to minimize the fuel consumption of the battery/FC hybrid power systems, Refs. [94] and [95] both adopt the PMP algorithm to optimize the reference power of the power sources. Although

the PMP algorithm has the same results as DP algorithm in theory, due to various simplification and omission factors, the control effect of PMP is often inferior to that of DP algorithm. However, the PMP algorithm can greatly reduce the computation time compared to DP algorithm. Ref. [96] points out that under the same conditions, it takes about 10 hours for the DP algorithm to complete all calculations, while the PMP algorithm only takes 20-30 minutes. The calculation amount of the PMP algorithm is huge, and it needs to select the initial value offline and obtain the working condition information in advance. Therefore, like the DP algorithm, this algorithm is difficult to implement in real-time applications [25,39].

When the objective function and constraints meet certain conditions, algorithms such as convex programming (CP) and quadratic programming (QP) can also be used to solve the optimal solution [39,40]. The CP algorithm is suitable for optimization problems in which the objective function is a convex function and the feasible region of the control variable is a convex set. Ref. [97] aims to minimize the sum of fuel consumption cost and system operating cost, and uses the CP algorithm to optimize the reference power of each power source and the configuration of powertrain components. The results show that this algorithm has a fast solution speed and good optimization effect. The QP requires the objective function to be a quadratic polynomial. Ref. [98] uses QP algorithm to study the energy management of a HEV, and the results show that the overall energy consumption level of the system has been reduced.

In addition, heuristic algorithm, also known as swarm intelligence algorithm, can also be used to search and solve the global optimal solution of the objective function. Commonly used heuristic algorithms include GA, PSO algorithm and simulated annealing (SA) algorithm [99–102]. Ref. [103] comprehensively considers multiple optimization indicators such as hydrogen consumption and vehicle acceleration performance, and uses GA to solve the multi-objective optimal solution. Simulation results demonstrate the effectiveness of the proposed EMS. In order to optimize the hydrogen consumption of a multi-source power generation system, Ref. [104] proposes an EMS based on PSO algorithm. The results show that compared with equidistributional method, the proposed EMS can effectively reduce the hydrogen consumption of the system.

Due to the poor real-time performance of global optimization methods, instantaneous optimization-based EMSs are often used in practical applications. According to existing research, there are mainly two kinds of instantaneous optimization EMSs: model predictive control (MPC) strategy and equivalent consumption minimization strategy (ECMS) [39]. In order to optimize the fuel economy of a battery/FC hybrid bus, Ref. [105] introduces the concept of equivalent hydrogen consumption to optimize the system energy distribution strategy. In addition, Ref. [106] designs a MPC model using Markov chains in order to simulate 8 different driving behaviors, and uses the k-means algorithm to classify the driving patterns.

1.2.3. Learning-based energy management strategies

With the rapid development of computer technology, in recent years, in addition to the above two types of EMSs (non-optimized EMS and optimization-based EMS), more and more researchers try to use artificial intelligence algorithms for power distribution. The EMS based on intelligent algorithm adopts machine learning as the framework, and can distribute the output power of each power source online. This kind of method continuously improves the strategy by learning the historical data of power distribution, and finally achieves the purpose of improving the system performance and hydrogen consumption. Since 2014, reinforcement learning (RL) technology has been introduced into the power distribution of hybrid systems [107], and later, artificial intelligence methods based on algorithms such as Q-learning, deep Q-network, Deep Deterministic Policy Gradient (DDPG), and state-action-reward-state-action (SARSA) have been gradually developed [108,109]. In Refs. [107,110], the Q-learning algorithm is used to optimize the reference power decision-making process of each power source. The experimental results show that the proposed strategy can effectively reduce the hydrogen consumption of the system. In addition, in order to obtain better control performance, Ref. [108] uses cosine similarity-based method to update the state transition matrix online. Ref. [109] proposes a method to solve the energy management problem using the SARSA algorithm, which can reduce the fuel consumption of the system by 11.9%.

Through the detailed analysis of the existing EMSs in the above three subsections, the advantages and disadvantages of each strategy for hybrid power systems could be summarized in TABLE 1.3.

TABLE 1.3. Summary of benefits and drawbacks of different EMSs.

Classification	Strategy	Benefits	Drawbacks
Non-optimized EMS	Deterministic rule	1. Least computation burden 2. Simple and easy to implement	1. Rely on expertise knowledge 2. Poor adaptability towards condition changes
	Fuzzy logic	1. Computation-friendly 2. High robustness	1. Sensitive to driving cycle 2. Multiple fuzzy membership parameters need recalibration in different driving cycles
Global optimization-based EMS	PMP	1. Near global optimality (close to DP)	1. Complexity in mathematical theory
	DP	1. Global optimality 2. Benchmark to other EMSs	1. Curse of dimensionality 2. High computation burden 3. Requires all condition information
	CP	1. Less computation burden than DP 2. Sub-global optimality	1. Hardly to achieve the global optimal results 2. System must comply with convexification
	QP	1. Less computation burden than	1. Simplified model may degrade

		DP 2. Subset of convex optimization 3. Availability of commercial solver	performance optimality
	GA	1. Support multiple objectives 2. Applicable to non-differentiable objective functions	1. Risk of stuck into local optima 2. Time consuming 3. Searching results depend on the initial population
	PSO	1. Robust to initial population size 2. Less parameter tuning	1. Less adaptability towards different operation conditions 2. Extra memory requirement
Real-time optimization-based EMS	ECMS	1. High computational efficiency 2. Can be applied in practical applications	1. Optimal EF sensitive to operation conditions 2. The sum of local optima is not the global optima
	MPC	1. Real-time optimization 2. Capacity of handling complex time-varying constrained system	1. Prediction horizon sensitivity
Learning-based EMS	RL	1. Model-free 2. Real-time	1. No clear guidance in choosing immediate cost for multi-objective global optimization 2. Rely on training data

1.3. Research status of multi-source power systems

As mentioned in the previous description, in order to apply the hybrid systems to higher power level applications, more and more researchers study the control and power distribution methods of the multi-source power systems [21,35,111]. Compared with the dual-source power system, the use of multi-source power system can not only improve the power level of the system without increasing the development cost of high-power power sources, but also ensure the power supply stability of the system and improve the durability of power sources [34,37,112]. In addition, for the multi-source system, the power allocation among different power sources is not trivial, which will affect multiple operating indicators of the system. Therefore, another core research content of this thesis is the reasonable and effective power distribution of multi-source power systems.

A multi-source power system (e.g. multi-stack FC system and multi-battery power system) consists of several power sources and has some different structures. For example, parallel-connected, serial-connected, and series-parallel-connected structures can be used to link the power sources together [32]. Different structures have different effects on the performance and stability of the system. It should be noted that since the connection structure used in the multi-battery power system mainly depends on the requirements of the system current or voltage, the current research mainly discusses the structure of the

multi-stack FC system. In order to further study the influence of different structures on the output performance of the systems, Ref. [113] summarizes the structure of the multi-stack FC system, and establishes an experimental platform to test the above three structures. The results show that, compared with the other two structures, the parallel structure is more stable and more suitable for complex applications. Ref. [114] builds a dynamic model of dual-stack FCs in parallel, and conducts simulation tests on the built model under normal and fault conditions. The results show that the parallel-connected structure is suitable for the actual vehicle environment. In addition, referring to the Ref. [114], Ref [22] also designs a dual-stack power generation system consisting of two sets of FCs in parallel, each set of FC is connected to the DC bus through a DC/DC converter. Experiments show that the parallel-connected structure has good power generation efficiency and is suitable for operation in complex working modes. That is the reason why this thesis employs the parallel-connected structure in the multi-stack FC system and multi-battery power system.

In order to make the control of each power source in the multi-source power system more flexible and improve the system stability and controllability, it is usually necessary to configure a DC/DC converter for each power source. Therefore, researchers also have some research on the control of DC/DC converters in multi-source systems. In order to reduce the difference of the output current between the power sources, an improved droop control method is proposed in [115]. In this study, the output voltage of each DC/DC converter is changed by adjusting the droop coefficient, so as to achieve the purpose of current sharing of each power source. Further, in order to reduce the difference between the actual output current and the reference current, and to solve the problem of the bus voltage drop due to the addition of the droop coefficient, a droop control algorithm based on virtual impedance is proposed in [21]. In addition, Refs.[116,117] study the control technology of parallel DC/DC, which makes the DC/DC parallel distributed control of multi-source power systems easier to realize.

In addition, for multi-source power systems, the implementation of reasonable power distribution methods is of great significance for improving system performance and optimizing fuel economy. In the multi-stack FC system, the operating characteristics of the stacks are usually non-uniform. Therefore, Ref. [33] proposes a method to adaptively adjust the output power of each stack according to its performance, thus to reduce the performance differences among the stacks. Ref. [35] proposes a coordinated EMS based on SOC consistency for a multi-source hybrid power system to ensure that the SOC of the multi-battery system is as consistent as possible. In addition, in order to improve the operating economy of the dual-stack fuel cell system, Ref. [36] establishes a system efficiency model by analyzing the operating characteristics of the stack, and proposes an instantaneous efficiency optimization method. In order to improve the operating performance of multi-source power generation system, Ref. [118] proposes an optimized power distribution management method by analyzing the power generation characteristics of the system off-line. The superiority of the proposed method is

verified by comparing with the Daisy chain allocation and average allocation methods. Moreover, there are also some other power allocation methods for multi-source power systems, such as global fuel optimization control based on Karush-Kuhn-Tucker condition [119], equivalent fitting circle method to optimize system efficiency [120], and current distribution method based on model predictive control [121].

To summarize, there have been many studies on multi-source systems, such as system structure research, control algorithm research, and power distribution method research, which provide inspiration for our research content.

1.4. PhD project objectives

This thesis takes the dual-source hybrid power system (powered by ESS and FC) and multi-source hybrid power system (powered by multiple sets of batteries and multiple sets of FCs) as the research objects, and the main research contents include: 1) Research on EMSs of dual-source hybrid power system (different powertrain structures and configurations); 2) Research on performance consistent power distribution method for multi-source hybrid power system; 3) In order to facilitate the verification of the EMS and power distribution method mentioned above, hardware-in-the-loop (HIL) simulation platform and physical reduced-scale experimental platform are established.

1) Propose an optimal system economic energy management strategy for a battery/FC hybrid electric vehicle

As can be seen from the previous description, in the hybrid power system, the high cost and insufficient durability of the power sources are the main reasons that restrict the large-scale application of ESS/FC hybrid systems in the energy market. In order to minimize the equivalent hydrogen consumption of a HEV and improve the power sources durability, this thesis proposes an optimal system economic energy management strategy. This strategy studies the coupling relationship between power sources life loss and output power by analyzing the impact of output power on power sources durability, and converts life loss into system operating costs. In addition, considering the equivalent hydrogen consumption cost of the battery during operation, a system operating cost function is formulated. In the cost function, the SOC fluctuation of the battery is also considered. In order to improve the operating efficiency and performance of the FC, a high-efficiency zone is also identified for the stack. Finally, the sequential quadratic programming algorithm is used to solve the optimal value of the formulated cost function.

2) Propose an online extremum seeking-based optimized EMS for a SC/FC hybrid electric tram

Considering the change of power sources operating performance can further improve the optimization effect of the EMS, this thesis proposes an online extremum seeking-based optimized EMS considering power sources degradation for a SC/FC hybrid electric tram. In order to improve the operating

performance of the stack, this thesis divides a "safe operating zone" for the stack by analyzing its output characteristics. In addition, an online identification algorithm is proposed to update the zone boundary value in real time to ensure the efficiency operation of the system. Since the SC has the disadvantage of low energy density, in order to ensure the consistency of the initial and final SOC states of the SC and ensure the continuous operation of the tram, the SOC fluctuation constraint is considered in the proposed EMS. Moreover, in order to further protect the power sources, this strategy also limits the power fluctuation range of the power sources.

3) Propose a performance consistent power distribution method for a multi-source hybrid power system

Another work focus of this thesis is the research of multi-source hybrid power system suitable for the high-power applications such as high-speed Electrical Multiple Unit trains, and a performance consistent power distribution method considering multiple factors is proposed. The presented power distribution method distributes the power among the power sources in the hybrid system according to the SOC of batteries and the operating state of stacks. In addition, taking into consideration that in the multi-source hybrid power system, a certain power source (battery or FC) may suddenly fail and cannot work, and also in order to realize the "plug and play" function and facilitate system expansion, this thesis presents a virtual droop control algorithm and an instantaneous virtual resistances calculation technology. According to the real-time operating state of each power source, the adjustment factors are designed to adaptively adjust the droop coefficients to control the converters output the reference power. Furthermore, to maintain the bus voltage stability, a voltage regulation technology is also presented.

4) Construction of HIL simulation platform and physical reduced-scale experimental bench

This thesis introduces in detail the structure of various hybrid systems suitable for transportation field, analyzes the operating characteristics of each component in the system, and establishes the corresponding mathematical model. Based on OP5600 real-time simulator and RT-LAB simulation development software, a HIL simulation platform consisting of DSP, signal generation/conditioning circuits, and system simulation model is built. In addition, in order to test the actual effect of the proposed method, a corresponding physical reduced-scale experiment platform is also built. The established HIL simulation platform and physical reduced-scale test platform provide a research basis for power distribution methods.

1.5. Publication list

This PhD thesis has contributed to 6 publications, which are listed as below:

Papers have been published in international journals:

1. **Tianhong Wang**, Qi Li, Yibin Qiu, Weirong Chen, Alexandre Ravey, Elena Breaz, and Fei Gao.

Power Optimization Distribution Method for Fuel Cell System Cluster Comprehensively Considering System Economy. ***IEEE Transactions on Industrial Electronics***, 2022, 69(12): 12898-12911. **(Q1, IF = 8.162)**

2. **Tianhong Wang,** Qi Li, Liangzhen Yin, Weirong Chen, Elena Breaz, and Fei Gao. Hierarchical Power Allocation Method Based on Online Extremum Seeking Algorithm for Dual-PEMFC/Battery Hybrid Locomotive. ***IEEE Transactions on Vehicular Technology***, 2021, 70(6): 5679-5692. **(Q1, IF = 6.239)**
3. **Tianhong Wang**, Qi Li, Xiaotong Wang, Weirong Chen, Elena Breaz, and Fei Gao. A Power Allocation Method for Multistack PEMFC System Considering Fuel Cell Performance Consistency. ***IEEE Transactions on Industry Applications***, 2020, 56(5): 5340–5351. **(Q1, IF = 4.079)**
4. Qi Li, **Tianhong Wang**, Shihan Li, Weirong Chen, Hong Liu, Elena Breaz, and Fei Gao. Online extremum seeking-based optimized energy management strategy for hybrid electric tram considering fuel cell degradation. ***Applied Energy***, 2021, 285: 116505. **(ESI highly-cited and Hot paper, Q1, IF = 11.446)**

Papers presented in international conferences:

1. **Tianhong Wang**, Qi Li, Weirong Chen, Qian Li, Alexandre Ravey, Elena Breaz, and Fei Gao. Multi-Mode Power Allocation Strategy Based on Kalman Filter Algorithm for Hybrid Electric Vehicle. ***2021 IEEE Transportation Electrification Conference and Expo (ITEC)***, 2021, 136-141.
2. Noureddine Bouisalmane, **Tianhong Wang**, Elena Breaz, Said Doubabi, Damien Paire, Jorn Oubraham, Michael Levy, and Fei Gao. Hydrogen consumption minimization with optimal power allocation of multi-stack fuel cell system using particle swarm optimization. ***2021 IEEE Transportation Electrification Conference and Expo (ITEC)***, 2021, 154-160.

References

[1] J. Jiang, Q. Jiang, J. Chen, X. Zhou, S. Zhu, T. Chen, Advanced Power Management and Control for Hybrid Electric Vehicles: A Survey, Wireless Communications and Mobile Computing. 2021 (2021) 1–12. https://doi.org/10.1155/2021/6652038.

[2] M. Kandidayeni, J.P. Trovão, M. Soleymani, L. Boulon, Towards health-aware energy management strategies in fuel cell hybrid electric vehicles: A review, International Journal of Hydrogen Energy. 47 (2022) 10021–10043. https://doi.org/10.1016/j.ijhydene.2022.01.064.

[3] Q. Li, T. Wang, S. Li, W. Chen, H. Liu, E. Breaz, F. Gao, Online extremum seeking-based optimized energy management strategy for hybrid electric tram considering fuel cell degradation, Applied Energy. 285 (2021) 116505. https://doi.org/10.1016/j.apenergy.2021.116505.

[4] World Energy Outlook 2020, OECD, 2020. https://doi.org/10.1787/557a761b-en.

[5] World - Renewable and Waste Energy Statistics (Edition 2020), (2017). https://doi.org/10.1787/4b51d740-en.

[6] D.M.L. González, J.G. Rendon, Opportunities and challenges of mainstreaming distributed energy resources towards the transition to more efficient and resilient energy markets, Renewable and Sustainable Energy Reviews. 157 (2022) 112018. https://doi.org/10.1016/j.rser.2021.112018.

[7] Z. Li, Z. Zheng, R. Outbib, Adaptive Prognostic of Fuel Cells by Implementing Ensemble Echo State Networks in Time-Varying Model Space, IEEE Trans. Ind. Electron. 67 (2020) 379–389. https://doi.org/10.1109/TIE.2019.2893827.

[8] H.S. Das, C.W. Tan, A.H.M. Yatim, Fuel cell hybrid electric vehicles: A review on power conditioning units

and topologies, Renewable and Sustainable Energy Reviews. 76 (2017) 268–291. https://doi.org/10.1016/j.rser.2017.03.056.
[9] Y.-H. Hung, Y.-M. Tung, C.-H. Chang, Optimal control of integrated energy management/mode switch timing in a three-power-source hybrid powertrain, Applied Energy. 173 (2016) 184–196. https://doi.org/10.1016/j.apenergy.2016.04.025.
[10] Paris climate agreement, (n.d.). https://doi.org/10.1036/1097-8542.br0612171.
[11] J.-F. Li, Z.-Y. Ma, Y.-X. Zhang, Z.-C. Wen, Analysis on energy demand and CO2 emissions in China following the Energy Production and Consumption Revolution Strategy and China Dream target, Advances in Climate Change Research. 9 (2018) 16–26. https://doi.org/10.1016/j.accre.2018.01.001.
[12] N. Li, R. Yuan, J. Wang, Analysis of current and future energy inequality by energy categories in China, Sustainable Production and Consumption. (2022). https://doi.org/10.1016/j.spc.2022.04.029.
[13] S. Teske, ed., Achieving the Paris Climate Agreement Goals, Springer International Publishing, 2019. https://doi.org/10.1007/978-3-030-05843-2.
[14] P.J. Thimet, G. Mavromatidis, Review of model-based electricity system transition scenarios: An analysis for Switzerland, Germany, France, and Italy, Renewable and Sustainable Energy Reviews. 159 (2022) 112102. https://doi.org/10.1016/j.rser.2022.112102.
[15] R. Krikštolaitis, V. Bianco, L. Martišauskas, S. Urbonien\.e, Analysis of Electricity and Natural Gas Security. A Case Study for Germany, France, Italy and Spain, Energies. 15 (2022) 1000. https://doi.org/10.3390/en15031000.
[16] T. Rudolf, T. Schurmann, S. Schwab, S. Hohmann, Toward Holistic Energy Management Strategies for Fuel Cell Hybrid Electric Vehicles in Heavy-Duty Applications, Proceedings of the IEEE. 109 (2021) 1094–1114. https://doi.org/10.1109/jproc.2021.3055136.
[17] T. Wang, Q. Li, Y. Qiu, L. Yin, L. Liu, W. Chen, Efficiency Extreme Point Tracking Strategy Based on FFRLS Online Identification for PEMFC System, IEEE Trans. Energy Convers. 34 (2019) 952–963. https://doi.org/10.1109/TEC.2018.2872861.
[18] D. Ton, J. Reilly, Microgrid controller initiatives: an overview of R&D by the US Department of Energy, IEEE Power and Energy Magazine. 15 (2017) 24–31.
[19] A. Kwasinski, W. Weaver, R.S. Balog, Microgrids and other local area power and energy systems, Cambridge University Press, 2016.
[20] H. Rudnick, L. Barroso, Flexibility needed: Challenges for future energy storage systems [guest editorial], IEEE Power and Energy Magazine. 15 (2017) 12–19.
[21] T. Wang, Q. Li, X. Wang, W. Chen, E. Breaz, F. Gao, A Power Allocation Method for Multistack PEMFC System Considering Fuel Cell Performance Consistency, IEEE Trans. on Ind. Applicat. 56 (2020) 5340–5351. https://doi.org/10.1109/TIA.2020.3001254.
[22] A.D. Bernardinis, M.-C. Péra, J. Garnier, D. Hissel, G. Coquery, J.-M. Kauffmann, Fuel cells multi-stack power architectures and experimental validation of 1kW parallel twin stack PEFC generator based on high frequency magnetic coupling dedicated to on board power unit, Energy Conversion and Management. 49 (2008) 2367–2383. https://doi.org/10.1016/j.enconman.2008.01.022.
[23] T. Wang, Q. Li, H. Yang, L. Yin, X. Wang, Y. Qiu, W. Chen, Adaptive current distribution method for parallel-connected PEMFC generation system considering performance consistency, Energy Conversion and Management. 196 (2019) 866–877. https://doi.org/10.1016/j.enconman.2019.06.048.
[24] X. Lü, Y. Wu, J. Lian, Y. Zhang, C. Chen, P. Wang, L. Meng, Energy management of hybrid electric vehicles: A review of energy optimization of fuel cell hybrid power system based on genetic algorithm, Energy Conversion and Management. 205 (2020) 112474. https://doi.org/10.1016/j.enconman.2020.112474.
[25] R. Xiong, H. Chen, C. Wang, F. Sun, Towards a smarter hybrid energy storage system based on battery and ultracapacitor - A critical review on topology and energy management, Journal of Cleaner Production. 202 (2018) 1228–1240. https://doi.org/10.1016/j.jclepro.2018.08.134.
[26] T. Wang, Q. Li, X. Wang, Y. Qiu, M. Liu, X. Meng, J. Li, W. Chen, An optimized energy management strategy for fuel cell hybrid power system based on maximum efficiency range identification, Journal of

Power Sources. 445 (2020) 227333. https://doi.org/10.1016/j.jpowsour.2019.227333.
[27] A. Ajanovic, R. Haas, Prospects and impediments for hydrogen and fuel cell vehicles in the transport sector, International Journal of Hydrogen Energy. 46 (2021) 10049–10058. https://doi.org/10.1016/j.ijhydene.2020.03.122.
[28] Vehicle Propulsion Systems, Springer Berlin Heidelberg, 2008. https://doi.org/10.1007/978-3-540-74692-8.
[29] A. Poursamad, M. Montazeri, Design of genetic-fuzzy control strategy for parallel hybrid electric vehicles, Control Engineering Practice. 16 (2008) 861–873. https://doi.org/10.1016/j.conengprac.2007.10.003.
[30] M.A. Soumeur, B. Gasbaoui, O. Abdelkhalek, J. Ghouili, T. Toumi, A. Chakar, Comparative study of energy management strategies for hybrid proton exchange membrane fuel cell four wheel drive electric vehicle, Journal of Power Sources. 462 (2020) 228167. https://doi.org/10.1016/j.jpowsour.2020.228167.
[31] T. Wang, Q. Li, L. Yin, W. Chen, E. Breaz, F. Gao, Hierarchical Power Allocation Method Based on Online Extremum Seeking Algorithm for Dual-PEMFC/Battery Hybrid Locomotive, IEEE Transactions on Vehicular Technology. 70 (2021) 5679–5692. https://doi.org/10.1109/tvt.2021.3078752.
[32] T. Wang, Q. Li, L. Yin, W. Chen, Hydrogen consumption minimization method based on the online identification for multi-stack PEMFCs system, International Journal of Hydrogen Energy. 44 (2019) 5074–5081. https://doi.org/10.1016/j.ijhydene.2018.09.181.
[33] X. Meng, Q. Li, T. Huang, X. Wang, G. Zhang, W. Chen, A Distributed Performance Consensus Control Strategy of Multistack PEMFC Generation System for Hydrogen EMU Trains, IEEE Transactions on Industrial Electronics. 68 (2021) 8207–8218. https://doi.org/10.1109/tie.2020.3016243.
[34] G. Zhang, Q. Li, W. Chen, X. Meng, Synthetic strategy combining speed self-adjusting operation control and adaptive power allocation for fuel cell hybrid tramway, IEEE Transactions on Industrial Electronics. 68 (2020) 1454–1465.
[35] Y. Han, Q. Li, T. Wang, W. Chen, L. Ma, Multisource coordination energy management strategy based on SOC consensus for a PEMFC–battery–supercapacitor hybrid tramway, IEEE Transactions on Vehicular Technology. 67 (2017) 296–305.
[36] X. Han, F. Li, T. Zhang, T. Zhang, K. Song, Economic energy management strategy design and simulation for a dual-stack fuel cell electric vehicle, International Journal of Hydrogen Energy. 42 (2017) 11584–11595. https://doi.org/10.1016/j.ijhydene.2017.01.085.
[37] N. Marx, D. Hissel, F. Gustin, L. Boulon, K. Agbossou, On Maximizing the Steady-State Efficiency of a Multi-Stack Fuel Cell System, in: 2018 IEEE Vehicle Power and Propulsion Conference (VPPC), IEEE, 2018. https://doi.org/10.1109/vppc.2018.8605036.
[38] D.C.T. Cardenas, N. Marx, L. Boulon, F. Gustin, D. Hissel, Degraded Mode Operation of Multi-Stack Fuel Cell Systems, in: 2014 IEEE Vehicle Power and Propulsion Conference (VPPC), IEEE, 2014. https://doi.org/10.1109/vppc.2014.7007041.
[39] X. Hu, J. Han, X. Tang, X. Lin, Powertrain Design and Control in Electrified Vehicles: A Critical Review, IEEE Transactions on Transportation Electrification. 7 (2021) 1990–2009. https://doi.org/10.1109/tte.2021.3056432.
[40] A. Biswas, A. Emadi, Energy Management Systems for Electrified Powertrains: State-of-the-Art Review and Future Trends, IEEE Transactions on Vehicular Technology. 68 (2019) 6453–6467. https://doi.org/10.1109/tvt.2019.2914457.
[41] Mustafa \.Inci, M. Büyük, M.H. Demir, Göktürk \.Ilbey, A review and research on fuel cell electric vehicles: Topologies, power electronic converters, energy management methods, technical challenges, marketing and future aspects, Renewable and Sustainable Energy Reviews. 137 (2021) 110648. https://doi.org/10.1016/j.rser.2020.110648.
[42] Y. Luo, Y. Wu, B. Li, T. Mo, Y. Li, S.-P. Feng, J. Qu, P.K. Chu, Development and application of fuel cells in the automobile industry, Journal of Energy Storage. 42 (2021) 103124. https://doi.org/10.1016/j.est.2021.103124.
[43] Modern Electric, Hybrid Electric, and Fuel Cell Vehicles, Third Edition, CRC Press, 2018. https://doi.org/10.1201/9780429504884.

[44] B. Ahn, T. Lim, Fuel Cell Vehicle Development at Hyundai-Kia Motors, in: 2006 International Forum on Strategic Technology, IEEE, 2006. https://doi.org/10.1109/ifost.2006.312284.
[45] M. Li, Y. Bai, C. Zhang, Y. Song, S. Jiang, D. Grouset, M. Zhang, Review on the research of hydrogen storage system fast refueling in fuel cell vehicle, International Journal of Hydrogen Energy. 44 (2019) 10677–10693. https://doi.org/10.1016/j.ijhydene.2019.02.208.
[46] TU Delft researchers use Hyundai ix35 Fuel Cell for mobile power, Fuel Cells Bulletin. 2016 (2016) 4. https://doi.org/10.1016/s1464-2859(16)30074-8.
[47] Toyota Mirai fuel cell electric vehicle relies on Gore technology, Membrane Technology. 2016 (2016) 4. https://doi.org/10.1016/s0958-2118(16)30055-6.
[48] S. Tanaka, K. Nagumo, M. Yamamoto, H. Chiba, K. Yoshida, R. Okano, Fuel cell system for Honda CLARITY fuel cell, ETransportation. 3 (2020) 100046. https://doi.org/10.1016/j.etran.2020.100046.
[49] S. Satyapal, 2016 Annual Progress Report: DOE Hydrogen and Fuel Cells Program, Office of Scientific and Technical Information (OSTI), 2017. https://doi.org/10.2172/1347209.
[50] Q. Li, H. Yang, Y. Han, M. Li, W. Chen, A state machine strategy based on droop control for an energy management system of PEMFC-battery-supercapacitor hybrid tramway, International Journal of Hydrogen Energy. 41 (2016) 16148–16159. https://doi.org/10.1016/j.ijhydene.2016.04.254.
[51] T. Omura, R. Shimamune, H. Nomoto, T. Kaneko, M. Shimada, E. Toyota, 1101 Development for performance improvement of NE Train (Hybrid System), The Proceedings of the Transportation and Logistics Conference. 2005.14 (2005) 407–410. https://doi.org/10.1299/jsmetld.2005.14.407.
[52] A. Miller, D. Barnes, Advanced Underground Vehicle Power and Control Fuel Cell Mine Locomotive, (2002) 7.
[53] A.R. Miller, K.S. Hess, D.L. Barnes, T.L. Erickson, System design of a large fuel cell hybrid locomotive, Journal of Power Sources. 173 (2007) 935–942. https://doi.org/10.1016/j.jpowsour.2007.08.045.
[54] W. Zhang, L. Xu, J. Li, M. Ouyang, Y. Liu, Q. Han, Y. Li, Comparison of daily operation strategies for a fuel cell/battery tram, International Journal of Hydrogen Energy. 42 (2017) 18532–18539.
[55] H. Abiko, Development of hybrid railcars and catenary and battery-powered hybrid railcar system, JR East Technical Review. (2012).
[56] R. Furuta, J. Kawasaki, K. Kondo, Hybrid traction technologies with energy storage devices for nonelectrified railway lines, IEEJ Transactions on Electrical and Electronic Engineering. 5 (2010) 291–297.
[57] N. Shiraki, H. Satou, S. Arai, A hybrid system for diesel railcar series Ki-Ha E200, in: The 2010 International Power Electronics Conference - ECCE ASIA -, IEEE, Sapporo, Japan, 2010: pp. 2853–2858. https://doi.org/10.1109/IPEC.2010.5542319.
[58] T.W. Bennedsgaard, I.C. Klaas, M. Vaarst, Reducing use of antimicrobials — Experiences from an intervention study in organic dairy herds in Denmark, Livestock Science. 131 (2010) 183–192. https://doi.org/10.1016/j.livsci.2010.03.018.
[59] M.Y. Mustafa, A. Al-Mahadin, B.E. Kanstad, R.K. Calay, Fuel cell technology application for Dubai rail systems, in: 2018 Advances in Science and Engineering Technology International Conferences (ASET), IEEE, Abu Dhabi, 2018: pp. 1–7. https://doi.org/10.1109/ICASET.2018.8376798.
[60] Alstom Coradia iLint fuel cell powered train in first test run, Fuel Cells Bulletin. 2017 (2017) 15. https://doi.org/10.1016/s1464-2859(17)30132-3.
[61] F. Peng, W. Chen, Z. Liu, Q. Li, C. Dai, System integration of China's first proton exchange membrane fuel cell locomotive, International Journal of Hydrogen Energy. 39 (2014) 13886–13893.
[62] Q. Li, W. Chen, Z. Liu, M. Li, L. Ma, Development of energy management system based on a power sharing strategy for a fuel cell-battery-supercapacitor hybrid tramway, Journal of Power Sources. 279 (2015) 267–280. https://doi.org/10.1016/j.jpowsour.2014.12.042.
[63] W. Zhang, J. Li, L. Xu, M. Ouyang, Optimization for a fuel cell/battery/capacity tram with equivalent consumption minimization strategy, Energy Conversion and Management. 134 (2017) 59–69. https://doi.org/10.1016/j.enconman.2016.11.007.
[64] O. Siddiqui, I. Dincer, A review on fuel cell-based locomotive powering options for sustainable

transportation, Arabian Journal for Science and Engineering. 44 (2019) 677–693.
[65] K. Ettihir, L. Boulon, M. Becherif, K. Agbossou, H.S. Ramadan, Online identification of semi-empirical model parameters for PEMFCs, International Journal of Hydrogen Energy. 39 (2014) 21165–21176. https://doi.org/10.1016/j.ijhydene.2014.10.045.
[66] Q. Li, T. Wang, C. Dai, W. Chen, L. Ma, Power Management Strategy Based on Adaptive Droop Control for a Fuel Cell-Battery-Supercapacitor Hybrid Tramway, IEEE Trans. Veh. Technol. 67 (2018) 5658–5670. https://doi.org/10.1109/TVT.2017.2715178.
[67] Hybrid Fuel Cell Based Energy System Case Studies, in: Modeling and Control of Fuel Cells, IEEE, 2010. https://doi.org/10.1109/9780470443569.ch9.
[68] Y. Haitao, Z. Yulan, S. Zechang, W. Gang, Model-based power control strategy development of a fuel cell hybrid vehicle, Journal of Power Sources. 180 (2008) 821–829. https://doi.org/10.1016/j.jpowsour.2008.01.041.
[69] T. Wang, Q. Li, W. Chen, T. Liu, Application of energy management strategy based on state machine in fuel cell hybrid power system, in: 2017 IEEE Transportation Electrification Conference and Expo, Asia-Pacific (ITEC Asia-Pacific), IEEE, 2017. https://doi.org/10.1109/itec-ap.2017.8080854.
[70] S.N. Motapon, L.-A. Dessaint, K. Al-Haddad, A Comparative Study of Energy Management Schemes for a Fuel-Cell Hybrid Emergency Power System of More-Electric Aircraft, IEEE Transactions on Industrial Electronics. 61 (2014) 1320–1334. https://doi.org/10.1109/tie.2013.2257152.
[71] J. Han, J.-F. Charpentier, T. Tang, An Energy Management System of a Fuel Cell/Battery Hybrid Boat, Energies. 7 (2014) 2799–2820. https://doi.org/10.3390/en7052799.
[72] Q. Li, B. Su, Y. Pu, Y. Han, T. Wang, L. Yin, W. Chen, A State Machine Control Based on Equivalent Consumption Minimization for Fuel Cell/ Supercapacitor Hybrid Tramway, IEEE Trans. Transp. Electrific. 5 (2019) 552–564. https://doi.org/10.1109/TTE.2019.2915689.
[73] P. Garcia, L.M. Fernandez, C.A. Garcia, F. Jurado, Energy Management System of Fuel-Cell-Battery Hybrid Tramway, IEEE Transactions on Industrial Electronics. 57 (2010) 4013–4023. https://doi.org/10.1109/tie.2009.2034173.
[74] A. Benrabeh, F. Khoucha, O. Herizi, M.E.H. Benbouzid, A. Kheloui, FC/battery power management for electric vehicle based interleaved DC-DC boost converter topology, in: 2013 15th European Conference on Power Electronics and Applications (EPE), IEEE, 2013. https://doi.org/10.1109/epe.2013.6634610.
[75] Y. Yan, Q. Li, W. Chen, B. Su, J. Liu, L. Ma, Optimal Energy Management and Control in Multimode Equivalent Energy Consumption of Fuel Cell/Supercapacitor of Hybrid Electric Tram, IEEE Transactions on Industrial Electronics. 66 (2019) 6065–6076. https://doi.org/10.1109/tie.2018.2871792.
[76] D.-D. Tran, M. Vafaeipour, M.E. Baghdadi, R. Barrero, J.V. Mierlo, O. Hegazy, Thorough state-of-the-art analysis of electric and hybrid vehicle powertrains: Topologies and integrated energy management strategies, Renewable and Sustainable Energy Reviews. 119 (2020) 109596. https://doi.org/10.1016/j.rser.2019.109596.
[77] B. Vural, A.R. Boynuegri, I. Nakir, O. Erdinc, A. Balikci, M. Uzunoglu, H. Gorgun, S. Dusmez, Fuel cell and ultra-capacitor hybridization: A prototype test bench based analysis of different energy management strategies for vehicular applications, International Journal of Hydrogen Energy. 35 (2010) 11161–11171. https://doi.org/10.1016/j.ijhydene.2010.07.063.
[78] H. Hemi, J. Ghouili, A. Cheriti, A real time fuzzy logic power management strategy for a fuel cell vehicle, Energy Conversion and Management. 80 (2014) 63–70. https://doi.org/10.1016/j.enconman.2013.12.040.
[79] K.-S. Jeong, W.-Y. Lee, C.-S. Kim, Energy management strategies of a fuel cell/battery hybrid system using fuzzy logics, Journal of Power Sources. 145 (2005) 319–326. https://doi.org/10.1016/j.jpowsour.2005.01.076.
[80] Q. Li, W. Chen, Y. Li, S. Liu, J. Huang, Energy management strategy for fuel cell/battery/ultracapacitor hybrid vehicle based on fuzzy logic, International Journal of Electrical Power & Energy Systems. 43 (2012) 514–525. https://doi.org/10.1016/j.ijepes.2012.06.026.
[81] S. Caux, W. Hankache, M. Fadel, D. Hissel, On-line fuzzy energy management for hybrid fuel cell systems,

International Journal of Hydrogen Energy. 35 (2010) 2134–2143. https://doi.org/10.1016/j.ijhydene.2009.11.108.
[82] X. Zhang, C.C. Mi, A. Masrur, D. Daniszewski, Wavelet-transform-based power management of hybrid vehicles with multiple on-board energy sources including fuel cell, battery and ultracapacitor, Journal of Power Sources. 185 (2008) 1533–1543. https://doi.org/10.1016/j.jpowsour.2008.08.046.
[83] O. Erdinc, B. Vural, M. Uzunoglu, A wavelet-fuzzy logic based energy management strategy for a fuel cell/battery/ultra-capacitor hybrid vehicular power system, Journal of Power Sources. 194 (2009) 369–380. https://doi.org/10.1016/j.jpowsour.2009.04.072.
[84] R. Zhang, J. Tao, GA-Based Fuzzy Energy Management System for FC/SC-Powered HEV Considering H2 Consumption and Load Variation, IEEE Transactions on Fuzzy Systems. 26 (2018) 1833–1843. https://doi.org/10.1109/tfuzz.2017.2779424.
[85] L. Xu, F. Yang, J. Li, M. Ouyang, J. Hua, Real time optimal energy management strategy targeting at minimizing daily operation cost for a plug-in fuel cell city bus, International Journal of Hydrogen Energy. 37 (2012) 15380–15392. https://doi.org/10.1016/j.ijhydene.2012.07.074.
[86] C. Wang, Dynamic programming and the Lagrange multipliers, Journal of Mathematical Analysis and Applications. 150 (1990) 551–561. https://doi.org/10.1016/0022-247x(90)90122-v.
[87] L. Xu, C.D. Mueller, J. Li, M. Ouyang, Z. Hu, Multi-objective component sizing based on optimal energy management strategy of fuel cell electric vehicles, Applied Energy. 157 (2015) 664–674. https://doi.org/10.1016/j.apenergy.2015.02.017.
[88] B.-C. Chen, Y.-Y. Wu, H.-C. Tsai, Design and analysis of power management strategy for range extended electric vehicle using dynamic programming, Applied Energy. 113 (2014) 1764–1774. https://doi.org/10.1016/j.apenergy.2013.08.018.
[89] D. Fares, R. Chedid, F. Panik, S. Karaki, R. Jabr, Dynamic programming technique for optimizing fuel cell hybrid vehicles, International Journal of Hydrogen Energy. 40 (2015) 7777–7790. https://doi.org/10.1016/j.ijhydene.2014.12.120.
[90] T. Fletcher, R. Thring, M. Watkinson, An Energy Management Strategy to concurrently optimise fuel consumption & PEM fuel cell lifetime in a hybrid vehicle, International Journal of Hydrogen Energy. 41 (2016) 21503–21515. https://doi.org/10.1016/j.ijhydene.2016.08.157.
[91] T. Nüesch, P. Elbert, M. Flankl, C. Onder, L. Guzzella, Convex Optimization for the Energy Management of Hybrid Electric Vehicles Considering Engine Start and Gearshift Costs, Energies. 7 (2014) 834–856. https://doi.org/10.3390/en7020834.
[92] N.W. Kim, D.H. Lee, C. Zheng, C. Shin, H. Seo, S.W. Cha, Realization of pmp-based control for hybrid electric vehicles in a backward-looking simulation, International Journal of Automotive Technology. 15 (2014) 625–635. https://doi.org/10.1007/s12239-014-0065-z.
[93] K. Ettihir, L. Boulon, K. Agbossou, Optimization-based energy management strategy for a fuel cell/battery hybrid power system, Applied Energy. 163 (2016) 142–153. https://doi.org/10.1016/j.apenergy.2015.10.176.
[94] K. Song, X. Wang, F. Li, M. Sorrentino, B. Zheng, Pontryagin's minimum principle-based real-time energy management strategy for fuel cell hybrid electric vehicle considering both fuel economy and power source durability, Energy. 205 (2020) 118064. https://doi.org/10.1016/j.energy.2020.118064.
[95] K. Simmons, Y. Guezennec, S. Onori, Modeling and energy management control design for a fuel cell hybrid passenger bus, Journal of Power Sources. 246 (2014) 736–746. https://doi.org/10.1016/j.jpowsour.2013.08.019.
[96] Z. Song, X. Zhang, J. Li, H. Hofmann, M. Ouyang, J. Du, Component sizing optimization of plug-in hybrid electric vehicles with the hybrid energy storage system, Energy. 144 (2018) 393–403. https://doi.org/10.1016/j.energy.2017.12.009.
[97] X. Hu, N. Murgovski, L.M. Johannesson, B. Egardt, Optimal Dimensioning and Power Management of a Fuel Cell/Battery Hybrid Bus via Convex Programming, IEEE/ASME Transactions on Mechatronics. 20 (2015) 457–468. https://doi.org/10.1109/tmech.2014.2336264.
[98] X. Wang, Q. Li, T. Wang, Y. Han, W. Chen, Optimized Energy Management Strategy Based on SQP

Algorithm for PEMFC Hybrid Locomotive, in: 2019 IEEE Transportation Electrification Conference and Expo, Asia-Pacific (ITEC Asia-Pacific), IEEE, 2019. https://doi.org/10.1109/itec-ap.2019.8903778.
[99] Electromobility Studies Based on Convex Optimization: Design and Control Issues Regarding Vehicle Electrification, IEEE Control Systems. 34 (2014) 32–49. https://doi.org/10.1109/mcs.2013.2295709.
[100] J.P.F. Trovao, V.D.N. Santos, P.G. Pereirinha, H.M. Jorge, C.H. Antunes, A Simulated Annealing Approach for Optimal Power Source Management in a Small EV, IEEE Transactions on Sustainable Energy. 4 (2013) 867–876. https://doi.org/10.1109/tste.2013.2253139.
[101] Z. Wang, B. Huang, W. Li, Y. Xu, Particle Swarm Optimization for Operational Parameters of Series Hybrid Electric Vehicle, in: 2006 IEEE International Conference on Robotics and Biomimetics, IEEE, 2006. https://doi.org/10.1109/robio.2006.340289.
[102] Z. Chen, C.C. Mi, R. Xiong, J. Xu, C. You, Energy management of a power-split plug-in hybrid electric vehicle based on genetic algorithm and quadratic programming, Journal of Power Sources. 248 (2014) 416–426. https://doi.org/10.1016/j.jpowsour.2013.09.085.
[103] F. Odeim, J. Roes, A. Heinzel, Power Management Optimization of an Experimental Fuel Cell/Battery/Supercapacitor Hybrid System, Energies. 8 (2015) 6302–6327. https://doi.org/10.3390/en8076302.
[104] N. Bouisalmane, T. Wang, E. Breaz, S. Doubabi, D. Paire, J. Oubraham, M. Levy, F. Gao, Hydrogen consumption minimization with optimal power allocation of multi-stack fuel cell system using particle swarm optimization, in: 2021 IEEE Transportation Electrification Conference & Expo (ITEC), IEEE, 2021. https://doi.org/10.1109/itec51675.2021.9490111.
[105] L. Xu, J. Li, J. Hua, X. Li, M. Ouyang, Adaptive supervisory control strategy of a fuel cell/battery-powered city bus, Journal of Power Sources. 194 (2009) 360–368. https://doi.org/10.1016/j.jpowsour.2009.04.074.
[106] L. Li, S. You, C. Yang, B. Yan, J. Song, Z. Chen, Driving-behavior-aware stochastic model predictive control for plug-in hybrid electric buses, Applied Energy. 162 (2016) 868–879. https://doi.org/10.1016/j.apenergy.2015.10.152.
[107] X. Lin, Y. Wang, P. Bogdan, N. Chang, M. Pedram, Reinforcement learning based power management for hybrid electric vehicles, in: 2014 IEEE/ACM International Conference on Computer-Aided Design (ICCAD), IEEE, 2014. https://doi.org/10.1109/iccad.2014.7001326.
[108] X. Lin, B. Zhou, Y. Xia, Online Recursive Power Management Strategy Based on the Reinforcement Learning Algorithm With Cosine Similarity and a Forgetting Factor, IEEE Transactions on Industrial Electronics. 68 (2021) 5013–5023. https://doi.org/10.1109/tie.2020.2988189.
[109] Z. Chen, L. Li, X. Hu, B. Yan, C. Yang, Temporal-Difference Learning-Based Stochastic Energy Management for Plug-in Hybrid Electric Buses, IEEE Transactions on Intelligent Transportation Systems. 20 (2019) 2378–2388. https://doi.org/10.1109/tits.2018.2869731.
[110] R.C. Hsu, S.-M. Chen, W.-Y. Chen, C.-T. Liu, A Reinforcement Learning Based Dynamic Power Management for Fuel Cell Hybrid Electric Vehicle, in: 2016 Joint 8th International Conference on Soft Computing and Intelligent Systems (SCIS) and 17th International Symposium on Advanced Intelligent Systems (ISIS), IEEE, 2016. https://doi.org/10.1109/scis-isis.2016.0104.
[111] N. Marx, L. Boulon, F. Gustin, D. Hissel, K. Agbossou, A review of multi-stack and modular fuel cell systems: Interests, application areas and on-going research activities, International Journal of Hydrogen Energy. 39 (2014) 12101–12111. https://doi.org/10.1016/j.ijhydene.2014.05.187.
[112] S. Boddu, V. Agarwal, Maximum Power Extraction From Series-Connected Fuel Cell Stacks by the Current Compensation Technique, IEEE Transactions on Power Electronics. 30 (2015) 582–589. https://doi.org/10.1109/tpel.2014.2311323.
[113] N. Marx, J. Cardozo, L. Boulon, F. Gustin, D. Hissel, K. Agbossou, Comparison of the Series and Parallel Architectures for Hybrid Multi-Stack Fuel Cell - Battery Systems, in: 2015 IEEE Vehicle Power and Propulsion Conference (VPPC), IEEE, 2015. https://doi.org/10.1109/vppc.2015.7352915.
[114] J. Garnier, A.D. Bernardinis, M.-C. Péra, D. Hissel, D. Candusso, J.-M. Kauffmann, G. Coquery, Study of a PEFC power generator modular architecture based on a multi-stack association, Journal of Power Sources.

156 (2006) 108–113. https://doi.org/10.1016/j.jpowsour.2005.08.031.
[115] J.-W. Kim, H.-S. Choi, B.H. Cho, A novel droop method for converter parallel operation, IEEE Transactions on Power Electronics. 17 (2002) 25–32. https://doi.org/10.1109/63.988666.
[116] S.K. Mazumder, M. Tahir, K. Acharya, Master–Slave Current-Sharing Control of a Parallel DC–DC Converter System Over an RF Communication Interface, IEEE Transactions on Industrial Electronics. 55 (2008) 59–66. https://doi.org/10.1109/tie.2007.896138.
[117] S.K. Mazumder, M. Tahir, S.L. Kamisetty, Wireless PWM Control of a Parallel DC–DC Buck Converter, IEEE Transactions on Power Electronics. 20 (2005) 1280–1286. https://doi.org/10.1109/tpel.2005.857527.
[118] J.E. Garcia, D.F. Herrera, L. Boulon, P. Sicard, A. Hernandez, Power sharing for efficiency optimisation into a multi fuel cell system, in: 2014 IEEE 23rd International Symposium on Industrial Electronics (ISIE), IEEE, 2014. https://doi.org/10.1109/isie.2014.6864614.
[119] R. Suresh, G. Sankaran, S. Joopudi, S.R. Choudhury, S. Narasimhan, R. Rengaswamy, Optimal power distribution control for a network of fuel cell stacks, Journal of Process Control. 74 (2019) 88–98. https://doi.org/10.1016/j.jprocont.2017.12.006.
[120] Y. Yan, Q. Li, W. Chen, W. Huang, J. Liu, Hierarchical Management Control Based on Equivalent Fitting Circle and Equivalent Energy Consumption Method for Multiple Fuel Cells Hybrid Power System, IEEE Transactions on Industrial Electronics. 67 (2020) 2786–2797. https://doi.org/10.1109/tie.2019.2908615.
[121] R. Long, S. Quan, L. Zhang, Q. Chen, C. Zeng, L. Ma, Current sharing in parallel fuel cell generation system based on model predictive control, International Journal of Hydrogen Energy. 40 (2015) 11587–11594. https://doi.org/10.1016/j.ijhydene.2015.04.148.

Chapter 2. Optimal economic energy management strategy for a light-duty hybrid electric vehicle

2.1. Introduction

The research object of this chapter is a hybrid power system for a light-duty vehicle, which adopts a power supply mode with a dual power sources structure (lithium-ion battery energy storage power supply and hydrogen fuel cell power generation device). As descripted in the **Chapter 1**, the lithium-ion battery has the characteristics of high specific power but unable to continuously provide stable power. In addition, the fuel cell (FC) has the characteristics of large specific energy but insufficient dynamic response capabilities [1,2]. Therefore, a hybrid battery/FC power supply structure is usually used to power the vehicle, and a reliable energy management strategy (EMS) should be designed according to the respective operating characteristics of the power sources to improve the reliability of the system operation [3,4]. EMS plays an important role in the entire hybrid power vehicle, and researchers usually design different EMSs according to different operating goals (e.g., battery state of charge (SOC) fluctuation, operating performance and lifetime of power sources, system fuel utilization rate, and vehicle dynamic performance). Designing effective control algorithms and EMSs are beneficial to improve system operating performance and extend its service life. Therefore, it is necessary to develop a more in-depth investigation of the EMSs for the hybrid electric vehicle (HEV).

The formulation principle of the EMSs is to maximize the fuel utilization and extend the service life of the power sources under the premise of meeting the power demand of the system, while taking into account the charging and discharging safety of the battery [5]. Usually the FC is used as the power source to provide continuous and stable electrical energy to the load. The battery or other energy storage component (e.g. supercapacitor, etc.) is used as the power source to meet the rapidly changing power demand of the load and recover the braking power of the vehicle [6]. Based on the research of [7–9], high operating cost and low durability of power sources are two mainly factors that limit the widespread commercial usage of hybrid technology. Besides, as discussed in **Chapter 1**, most of the existing strategies focus only on ameliorating fuel consumption or system operating efficiency, but do not fully consider the impact of other factors such as power sources performance degradation. Therefore, in order to minimize the total fuel consumption of the system while prolonging the lifetime of the battery and FC, this chapter puts forward an optimal economic EMS that considering the lifetime loss of power sources.

This chapter is organized as following: section 2.2 introduces the structure of light-duty vehicle and modeling of primary components including battery, FC, and DC/DC converter. Section 2.3 is dedicated to the proposed EMS, while presenting other benchmark EMSs as well. Section 2.4 introduces the construction of the hardware-in-the-loop (HIL) simulation platform in detail. In addition, the

experimental validation and the experimental results analysis are also included in section 2.4. Finally, the major conclusions of this chapter are presented in section 2.5.

2.2. Hybrid power system structure and components modeling

The research objective of this chapter is a 64V hybrid electric vehicle developed by Clean Energy Laboratory of Southwest Jiaotong University (SWJTU) [3,10]. The hybrid powertrain of this vehicle is composed by a battery and a FC. The battery and FC play an important role in the powertrain, and they are responsible for providing the necessary electric energy for the operation of the vehicle. In order to facilitate the study of EMSs, it is first necessary to model each component of the HEV. This subsection introduces the system architecture of the developed vehicle, the modeling of the powertrain components including battery and FC, and the modeling of the power converter.

2.2.1. Vehicle model and powertrain structure

The appearance and basic structure of the vehicle employed in this chapter is depicted in Fig. 2.1, this is a low-speed campus sightseeing vehicle that can carry 12 people. As shown in Fig. 2.1, the battery is directly connected to the DC bus and is used as an energy storage system to hold the DC-link voltage and recover the braking power of the HEV. Besides, the FC is connected to a unidirectional boost DC/DC in series to supply the steady-state power for the vehicle. In order to ensure that the powertrain could provide enough electric energy to meet the vehicle's demand for speed, it is necessary to analyze the vehicle dynamics.

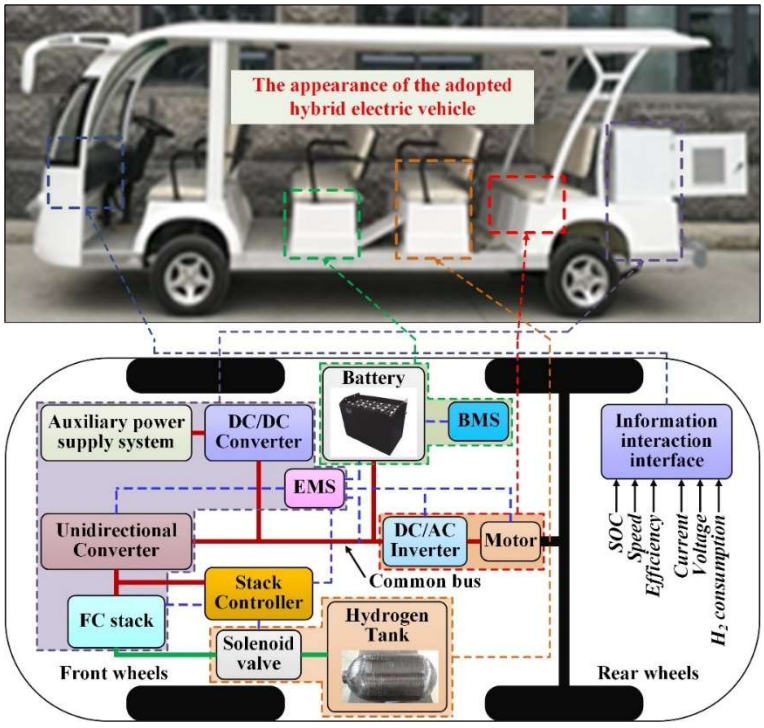

Figure 2.1. Vehicle's appearance and structure.

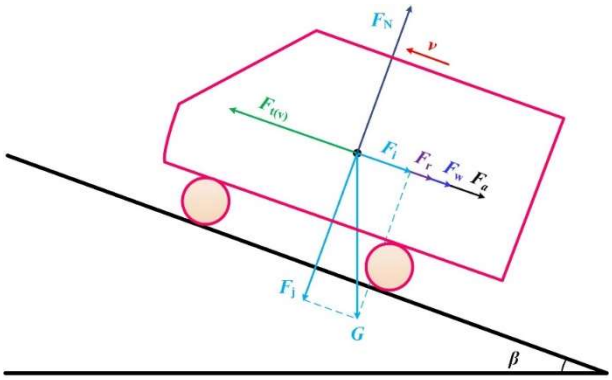

Figure 2.2. Analysis diagram of the forces acting on a vehicle.

As depicted in Fig. 2.2, when a vehicle is driving on the road, the gravity can be decomposed into parallel and vertical components. In this figure, v is the speed of the vehicle, $F_{t(v)}$ represents the traction or braking force, F_r is the rolling friction force, F_a is the acceleration friction force, F_w represents the aerodynamic friction force, G represents the gravity on the vehicle, F_i is the climbing resistance force generated by the gravity component, and F_j is the vertical road component of gravity. In addition, F_N is the ground support force and β is the slope angle. According to the principle of power balance, it can be known that the force of the vehicle has the following functional relationship.

$$F_{t(v)} = F_i + F_r + F_w + F_a . \tag{2.1}$$

The $F_{t(v)}$ is generated by the torque applied by the motor to the wheels through the transmission system. In addition, the driving power of the vehicle is provided by the battery and FC. Therefore, the power demand of the DC bus (P_{demand}) can be calculated by Eq. (2.2) [11]:

$$P_{demand} = \frac{P_{t(v)}}{\eta_{drive} \times \eta_{DC/AC} \times \eta_{EM}} = \frac{F_{t(v)} \times v}{\eta_{drive} \times \eta_{DC/AC} \times \eta_{EM}} = P_{bat} + P_{FC} \times \eta_{DC/DC} \tag{2.2}$$

where η_{drive}, $\eta_{DC/AC}$, $\eta_{DC/DC}$, and η_{EM} respectively represent transmission system efficiency, inverter efficiency, the efficiency of the DC/DC converter, and the electric machine efficiency. In addition, v is the speed of the vehicle. In order to facilitate the design, in this thesis, the efficiency of these components is assumed to be a fixed value. In addition, P_{bat} and P_{FC} are the output power of battery and FC, respectively.

The rolling friction force is mainly affected by the vertical component F_j and the rolling friction coefficient f, as denoted by Eq. (2.3).

$$\begin{cases} F_r = F_j \times f \\ F_j = G \times \cos(\beta) = Mg \times \cos(\beta) \end{cases} \tag{2.3}$$

where M is the mass of the vehicle and g represents the gravitational acceleration. Please note that since we can't estimate the inclination angle of the road, the angle β in this thesis is taken as 0.

In addition, the aerodynamic friction force is caused by the movement of the vehicle, mainly determined by the speed of the vehicle and the area of the front surface (A), which can be expressed as [12]:

$$F_w = \frac{1}{2} C_D \times A \times \rho \times v^2 \tag{2.4}$$

here, C_D is the aerodynamic drag coefficient and ρ represents the air density. Besides, the resistance force caused by the acceleration of the vehicle can be calculated by Eq. (2.5).

$$F_a = Ma \tag{2.5}$$

where a is the acceleration of the vehicle. Moreover, when a vehicle is driving on a slope, it is affected by the vehicle's gravity, which will cause climbing resistance force in the horizontal direction, as denoted by Eq. (2.6).

$$F_i = Mg \times \sin(\beta) \tag{2.6}$$

TABLE 2.1. Primary parameters of the adopted HEV.

HEV			
Capacity	12 persons	Mass	1350 kg
Max load	800 kg	Max speed	30 km/h
Size	520*149*208 cm^3	Tire radius	0.27 m
DC/AC converter efficiency	95%	Vehicle front surface	2.5 m^2
DC/DC converter efficiency	90%	Air density	1.21 kg/m^3
Gravitational acceleration	9.8 m/s^2	Transmission system efficiency	90%
Rolling friction coefficient	0.015	Aerodynamic coefficient	0.65

In order to meet the requirements of vehicle traction power, the size of the powertrain needs to be configured according to the parameters of the vehicle. The key specifications of the developed vehicle are listed in TABLE 2.1. It should be noted that the main research focus of this chapter is to investigate the EMSs for a light-duty HEV, so we don't conduct optimization studies on the components parameters of the powertrain.

TABLE 2.2. Primary parameters of the powertrain.

Battery pack			
Type	Lithium-ion	Serial number	20
Single cell rated voltage	3.2 V	Capacity	60 Ah
Maximum charge current	60 A (1 C)	Maximum discharge current	120 A (2 C)
FC			
Rated power	3 kW	Rated voltage	43.2 V
Rated current	70 A	H_2 pressure	0.45-0.55 Bar

According to the above parameters and analysis, it can be known that the maximum traction power required by the developed vehicle is about 6 kW. Therefore, we utilize a battery pack capable of

continuous output of 3 kW, and we also use a FC with a rated power of 3 kW to provide electric energy. In addition, the key parameters of the powertrain are listed in TABLE 2.2.

2.2.2. Battery model

Since the FC can't recover the braking power of the system, and the dynamic response capability is insufficient, in order to strengthen the response ability of the system, the energy storage system plays a very important role in the HEV. Although there are many batteries (e.g. lead-acid battery) currently used in HEV, considering the advantages of lithium-ion battery in terms of specific energy, service life, and specific power, this thesis utilize this type of battery as the energy storage device for hybrid system. Therefore, we need to conduct modeling research on the lithium-ion battery.

Fig. 2.3 shows the typical discharge curve of a lithium-ion battery. As can be seen from this figure, the discharging process of the battery can be divided into three areas, area A is [0, Q_{exp}], area B is [Q_{exp}, Q_{nom}], and area C is [Q_{nom}, Q]. In area A, the battery output voltage decreases linearly with the increase in discharge capacity. In area B, the battery is in normal operation and the output voltage fluctuation is small. In area C, its output voltage drops rapidly with the consumption of electric energy.

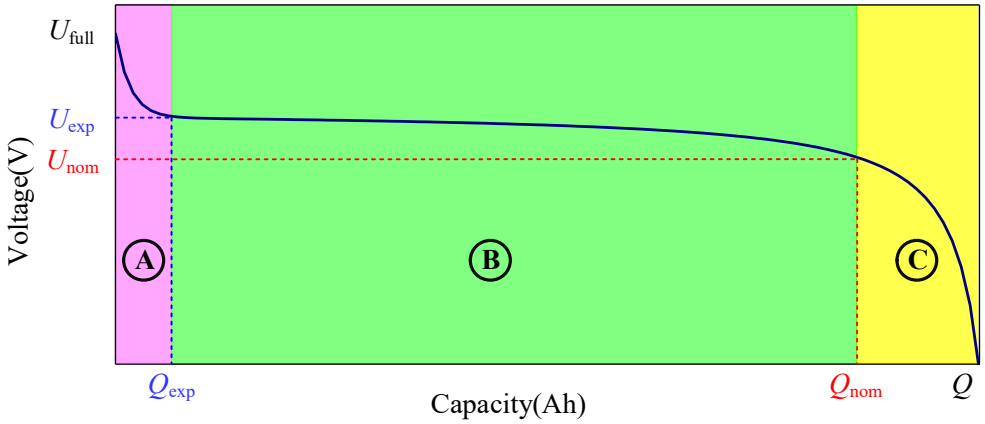

Figure 2.3. Typical discharge curve of battery.

In addition, U_{full} represents the maximum voltage of the battery, and Q is the maximum capacity of the battery. U_{exp} and Q_{exp} are the corresponding voltage and discharge amount of the battery at the end of area A, respectively. U_{nom} and Q_{nom} are the corresponding voltage and discharge amount of the battery at the end of area B, respectively.

Based on the research of [13,14], the battery model can be simplified into a circuit composed of resistor R and capacitor C, which can be divided into Rint model, PNGV model, and Thevenin model, as depicted in Fig. 2.4. These models have the characteristics of simplicity and easy parameter identification.

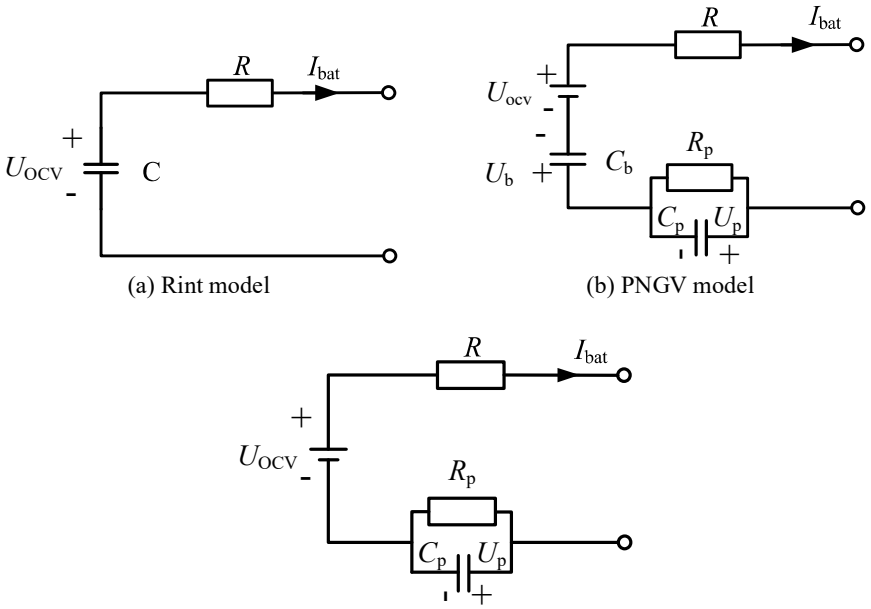

(a) Rint model (b) PNGV model

(c) Thevenin model

Figure 2.4. Battery model.

In addition, based on a large amount of experimental data, Shepherd first proposed a method to describe the electrochemical properties of batteries using voltage and current in 1965 [15]. Since then, this model has been continuously revised by many researchers in order to describe more accurately the characteristics of lithium-ion batteries. In 2009, on the basis of the Shepherd model, O. Tremblay proposed an improved Shepherd model, in which the output voltage of the battery is calculated as shown in Eq. (2.7) [16,17].

$$\begin{cases} U_{bat} = E_0 - RI_{bat} - K\dfrac{Q}{Q - I_{bat}t}\left(I_{bat}t + i^*\right) + A_1 \cdot \exp\left(-\dfrac{I_{bat}t}{A_2}\right) & I_{bat} > 0 \\ U_{bat} = E_0 - RI_{bat} - K\dfrac{Q}{Q - I_{bat}t}I_{bat}t - K\dfrac{Q}{I_{bat}t - 0.1Q}t^* + A_1 \cdot \exp\left(-\dfrac{I_{bat}t}{A_2}\right) & I_{bat} < 0 \end{cases} \tag{2.7}$$

here, E_0 is the voltage constant, U_{bat} is the output voltage of the battery, R represents the internal resistance of the battery and I_{bat} is the output current of the battery. K represents the internal polarization resistance, and Q represents the rated capacity of the battery. i^* is the current of the battery after passing through the filter. The purpose of this parameter is to solve the algebraic loop problem generated during the actual operation of the model. In addition, $KQ/(Q - I_{bat}t)$ indicates that during the discharge process, the internal polarization resistance will continue to increase, A_1 represents the maximum voltage in the polarization area, and A_2 represents the discharge time constant of the battery. Since the amplitude of the exponential term approaches 0 at the end of area A, it is generally taken as $A_2 = 3/Q_{exp}$. Moreover, I_{bat}t represents the actual discharge capacity, which can be expressed by:

$$I_{\text{bat}}t = \frac{1}{3600}\left(3600 \times \left(\frac{1-SOC_0}{100}\right)Q + \int I_{\text{bat}}dt\right) \tag{2.8}$$

where SOC_0 is the initial SOC value of the battery, and it can be measured by the open circuit voltage method, as expressed in Eq. (2.9)[18].

$$SOC_0 = \frac{U_{\text{OCV}} - U_{\text{OCV\_1}}}{U_{\text{OCV\_1}} - U_{\text{OCV\_0}}} \tag{2.9}$$

where U_{OCV} represents the open circuit voltage of the battery, $U_{\text{OCV\_1}}$ represents the open circuit voltage when the battery capacity is 100%, and $U_{\text{OCV\_0}}$ represents the open circuit voltage when the battery capacity is 0.

Moreover, Fig. 2.5 is the schematic diagram of the adopted model, which has been included in Matlab's SimpowerSystems and is widely used in the simulation of hybrid power systems.

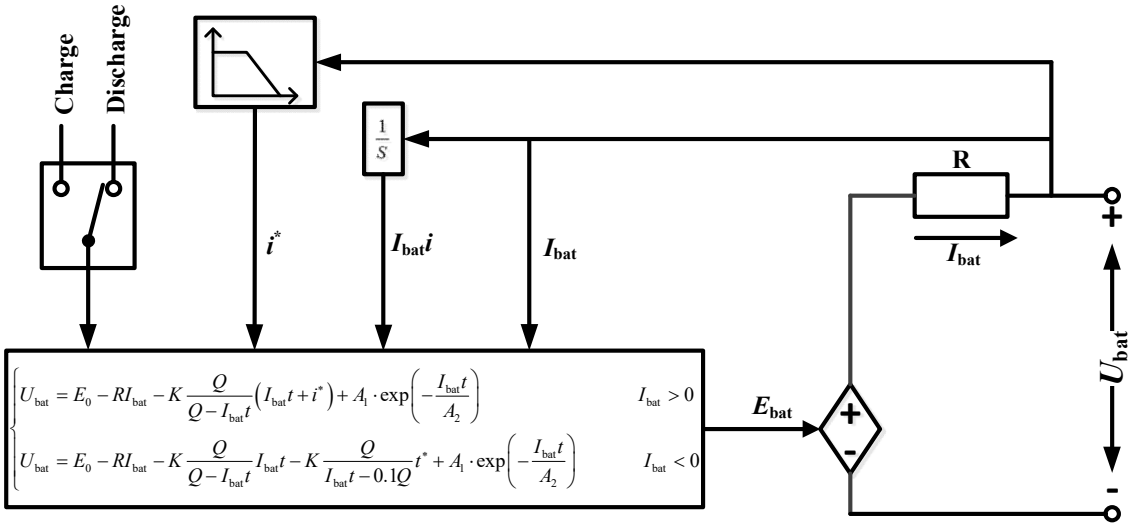

Figure 2.5. Lithium-ion battery model schematic.

According to the datasheet of the selected battery, three sets of data of [U_{full}, Q], [U_{exp}, Q_{exp}], and [U_{nom}, Q_{nom}] can be obtained, and then the parameters in the built battery model can be calculated by using Eq. (2.10):

$$\begin{cases} U_{\text{full}} = E_0 + A - RI_{\text{bat}} \\ U_{\text{exp}} = E_0 - RI_{\text{bat}} - K\dfrac{Q}{Q - Q_{\text{exp}}}(Q_{\text{exp}} + I_{\text{bat}}) + A \cdot \exp(-\dfrac{3}{Q_{\text{exp}}}Q_{\text{exp}}) \\ U_{\text{nom}} = E_0 - RI_{\text{bat}} - K\dfrac{Q}{Q - Q_{\text{nom}}}(Q_{\text{nom}} + I_{\text{bat}}) + A \cdot \exp(-\dfrac{3}{Q_{\text{exp}}}Q_{\text{nom}}) \end{cases} \tag{2.10}$$

The SOC of the battery can be calculated by the ampere-hour integration method, as expressed in Eq.

(2.11) [19,20]:

$$SOC = SOC_0 - \frac{1}{Q}\int_0^T I_{bat}\,dt \tag{2.11}$$

This chapter calibrates the model parameters by measuring the actual output data of the battery. The main parameters of the built battery model are listed in TABLE 2.3.

TABLE 2.3. The built battery model parameters.

battery model			
Maximum capacity	60 Ah	Fully charged voltage	69.84 V
Nominal discharge current	17.39 A	Capacity at nominal voltage	56.17 Ah
Nominal voltage	62 V	Internal resistance	0.062 Ω

Furthermore, Fig. 2.6 shows the comparison results between the actual operation data and the model simulation data of a lithium-ion battery with a rated voltage of 64 V (capacity of 60 Ah). Obviously, the error between the experimental data and the simulation results is small, which can prove that the built model can simulate the charging and discharging process of the battery well, thereby verifying the accuracy of the model.

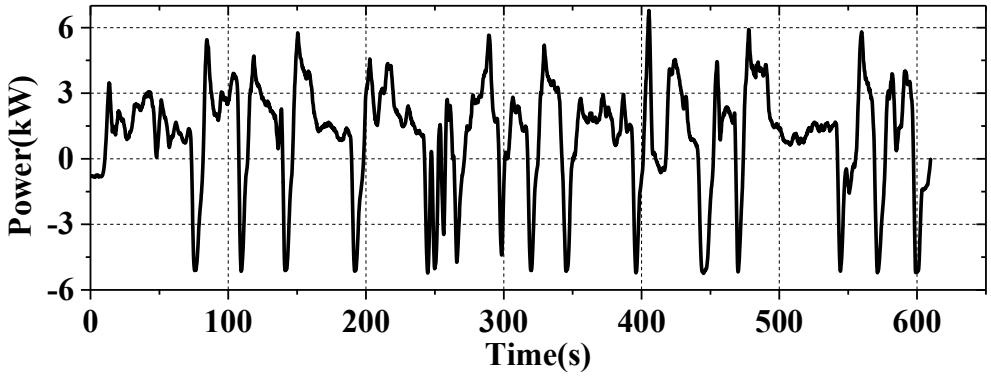

(a) Battery output power

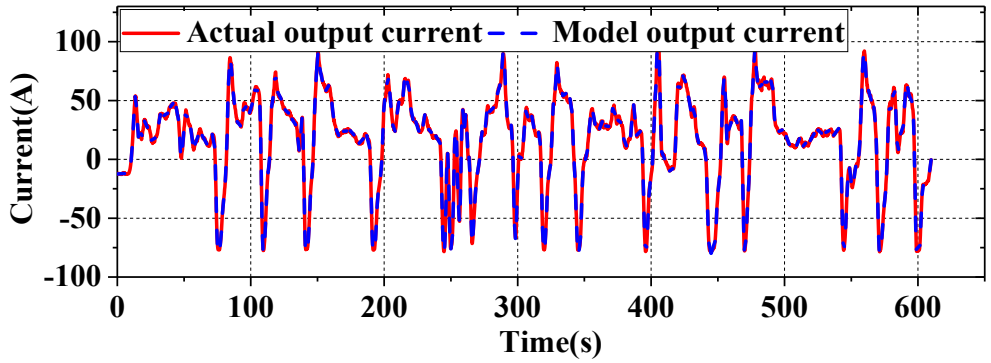

(b) Output current curves

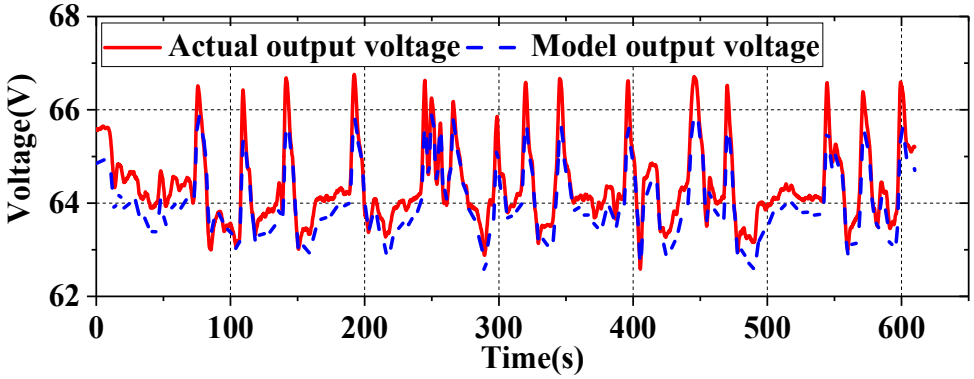

(c) Output voltage curves

Figure 2.6. Lithium-ion battery model validation for variable loading.

In addition, according to the experimental test [10], the relationship between the open circuit voltage and the SOC is depicted in Fig. 2.7 (a). Moreover, the internal resistance of the battery is also related to the SOC, as shown in Fig. 2.7 (b).

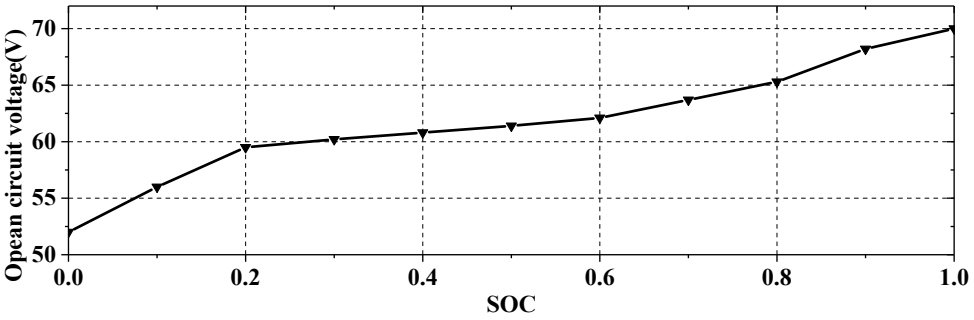

(a) Open circuit voltage

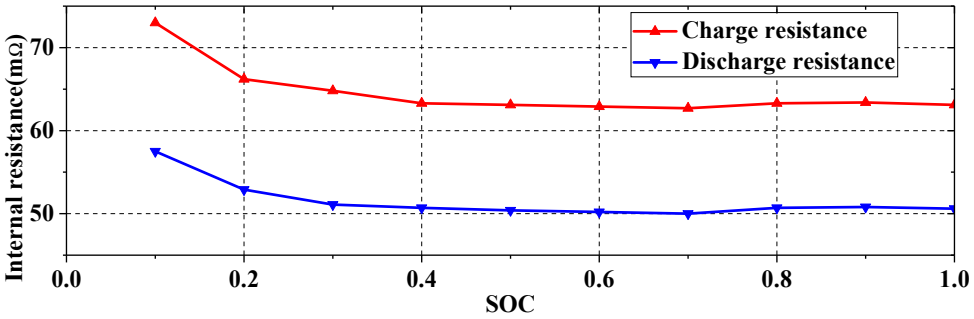

(b) Internal resistance

Figure 2.7. The characteristics of the battery.

It can be seen from Fig. 2.7 that there is a polynomial function relationship between the open circuit voltage, internal resistance and SOC, as shown in Eq. (2.12).

$$\begin{cases} U_{\mathrm{OCV}} = a_0 SOC^2 + a_1 SOC + a_2 \\ R_{\mathrm{dis}} = b_0 SOC^2 + b_1 SOC + b_2 \\ R_{\mathrm{chg}} = c_0 SOC^2 + c_1 SOC + c_2 \end{cases} \tag{2.12}$$

here, R_{dis} and R_{chg} denote the internal resistance during the charging and discharging, respectively. The

fitting coefficients can be obtained by identifying the curves shown in Fig. 2.7. Furthermore, the efficiency of the battery can be expressed as [19]:

$$\begin{cases} \eta_{\text{dis}} = \dfrac{1+\sqrt{1-\dfrac{4R_{\text{dis}}P_{\text{bat}}}{U_{\text{OCV}}^2}}}{2} \\ \eta_{\text{chg}} = \dfrac{2}{1+\sqrt{1-\dfrac{4R_{\text{chg}}P_{\text{bat}}}{U_{\text{OCV}}^2}}} \end{cases} \tag{2.13}$$

where η_{dis} is the battery discharging efficiency and η_{dis} is the battery discharging efficiency. According to Fig. 2.7 and Eq. (2.13), the battery charging and discharging efficiency surfaces are shown in Fig. 2.8.

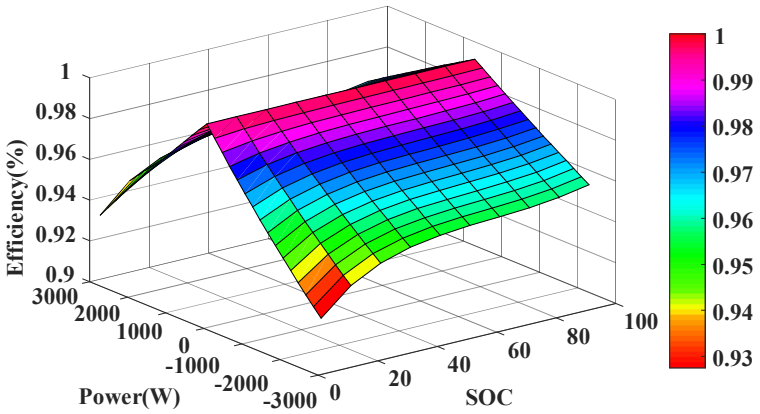

Figure 2.8. Battery charging and discharging efficiency surface.

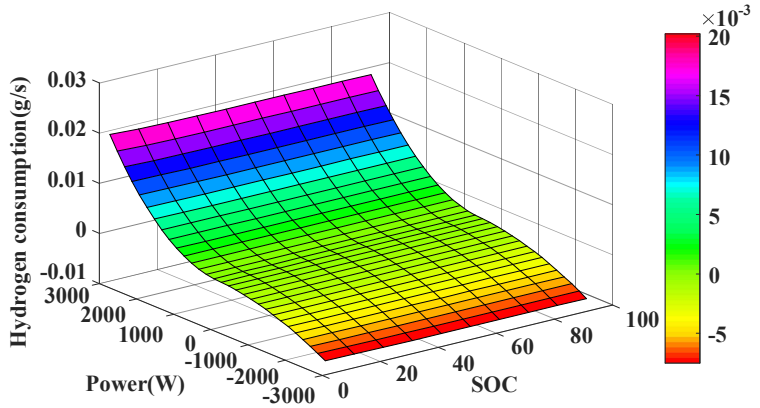

Figure 2.9. Battery equivalent hydrogen consumption surface.

Based on the research in [21,22], this thesis expresses the equivalent fuel consumption of the battery as:

$$C_{\text{bat}} = \begin{cases} \dfrac{d_0 P_{\text{bat}} + d_1}{\eta_{\text{dis}}\eta_{\text{chg,avg}}} & P_{\text{bat}} \geq 0 \\ \left(d_0 P_{\text{bat}} + d_1\right)\eta_{\text{chg}}\eta_{\text{dis,avg}} & P_{\text{bat}} < 0 \end{cases} \tag{2.14}$$

here, C_{bat} is the equivalent fuel consumption rate of the battery. The $\eta_{\text{chg,avg}}$ is battery average charging

efficiency and the $\eta_{chg,avg}$ represents battery average discharging efficiency. In addition, d_0 and d_1 represent the hydrogen consumption rate coefficients. According to Eq. (2.14), the equivalent fuel consumption rate surface of battery can be calculated, as depicted in Fig. 2.9.

2.2.3. Hydrogen power source model

FC is a strongly coupled, multi-input electrochemical power generation device that can convert chemical energy into electrical energy. There are many types of FCs, and proton exchange membrane FC is used in this chapter because it is very suitable for automotive application [3]. As one of the power sources in HEV, FC also needs to be modeled and analyzed. Usually a series of physical and chemical changes occur during the operation of the stack, and each process has a certain resistance [23]. The output voltage loss caused by these resistances could be mainly divided into activation voltage loss, ohmic voltage loss, and concentration voltage loss. Based on the research of [24,25], the output voltage of the single cell could be expressed as:

$$U_{cell} = E_{OC} - U_{act} - U_{ohmic} - U_{conc} \tag{2.15}$$

here, E_{OC} is the open circuit voltage, U_{act}, U_{ohmic}, and U_{conc} respectively represent activation voltage loss, ohmic voltage loss, and concentration voltage loss. The E_{oc}, U_{act}, U_{ohmic}, and U_{ocnc} can be further expressed as [7]:

$$\begin{cases} E_{OC} = K_c\left(E^0 + (T-298)\dfrac{\Delta S^0}{2F} + \dfrac{RT}{2F}\ln\left(P_{H_2}\sqrt{P_{O_2}}\right)\right) \\ U_{act} = \dfrac{1}{\tau_d s + 1} \times N_{cell} A \ln\left(\dfrac{I_{FC}}{i_0}\right) \\ U_{ohmic} = r_{ohm} I_{FC} \\ U_{conc} = \dfrac{RT}{NF} \times \ln\left(1 - \dfrac{I_{FC}}{i_{max}}\right) \end{cases} \tag{2.16}$$

where K_c is the rated voltage constant, ΔS^0 represents the entropy change of the system, and the value is -44.43 J/(mol*K). E^0 represents the stack electromotive force at standard atmospheric pressure, and the value is 1.229 V. F represents the Faraday constant, with a value of 96485 A*s/mol, R denotes gas constant (the value is 8.3145 J/(mol*K)), and T represents the operating temperature of the stack. Besides, P_{O2} is oxygen pressure in the cathode side and P_{H2} stands for hydrogen pressure in the anode side. τ_d is the time constant of the dynamic response of the stack, N_{cell} stands for the number of cells, I_{FC} is the drawn current from the stack, and r_{ohm} is the internal resistance of the FC. i_0 is the exchange current, A is the Tafel slope, and i_{max} represents the maximum current of the stack.

The specific values of the built FC model are shown in TABLE 2.4. It should be noted that the FC power generation parameters in actual operation will fluctuate as the operating temperature changes. In the model built in this thesis, it is assumed that the operating temperature of the stack is a fixed value (303K),

so its operating performance (e.g. operating efficiency and hydrogen consumption rate) will not change.

TABLE 2.4. The built model parameters' values.

FC model			
Resistance	0.2134Ω	Oxidant composition	21%
Hydrogen utilization rate	91.43%	System temperature	303K
Oxidant utilization	7.36%	Fuel supply pressure	0.5bar
Exchange current	0.2139A	Air supply pressure	0.5bar
Exchange coefficient	0.3611	Nernst voltage	1.1715V

In addition, the output characteristic curve of used stack and the output characteristic curve of the built model are depicted in Fig. 2.10. It can be seen that the error between the model output curve and the actual stack output curve is very small, which can verify the effectiveness of the built model.

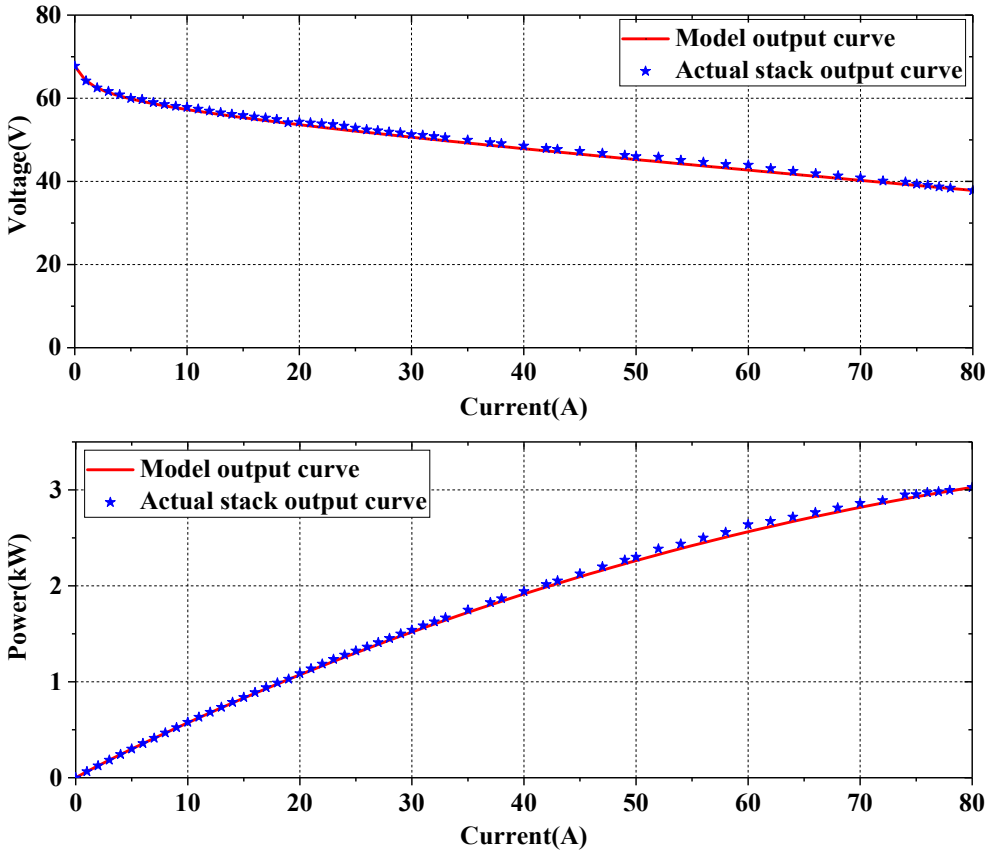

Figure 2.10. Fuel cell output polarization curve.

The operating efficiency of the system is an important indicator for evaluating the performance of the EMS. In this subsection, the operating efficiency of the FC system is analyzed. Its power generation efficiency can be defined as the ratio of the output electric energy of the stack to the chemical energy contained in the supplied hydrogen [26]. When 1 mol of hydrogen is completely combusted in an environment of 25 ℃ (the product is liquid water), it will generate 286.02 kJ of heat, so 286.02 kJ*mol^{-1} is defined as the high heating value (ΔH_{HHV}) of hydrogen. Since the FC generates electric energy

through electrochemical reactions, there is loss in each step of the reaction, so a part of the chemical energy can't be converted into electric energy, and the energy that can be converted into electric energy corresponds to the Gibbs free energy ΔG. Assuming that all ΔG can be converted into electrical energy, theoretically the output efficiency of the FC stack can reach:

$$\eta_{\mathrm{HHV}} = \frac{-\Delta G}{-\Delta H_{\mathrm{HHV}}} = \frac{237.34}{286.02} = 83\% \tag{2.17}$$

where η_{HHV} represents the high heat efficiency of the stack. In addition, the FC stack efficiency (η_{stack}) can be defined by [3,19,27]:

$$\eta_{\mathrm{HHV}} = \frac{P_{\mathrm{FC}}}{P_{\mathrm{H_2}}} = \frac{\dfrac{U_{\mathrm{cell}} I_{\mathrm{FC}}}{-\Delta H_{\mathrm{HHV}} I_{\mathrm{FC}}}}{2F} = \frac{U_{\mathrm{cell}}}{1.482} \tag{2.18}$$

where U_{cell} is a single cell output voltage. It should be noted that in practical applications, other auxiliary systems are usually required, such as air compressor, cooling circulation systems, etc. to ensure the normal and stable operation of the stack. Therefore, the efficiency of the FC system (η_{FCS}) can be expressed as:

$$\eta_{\mathrm{FCS}} = \eta_{\mathrm{HHV}} \eta_{\mathrm{DC/DC}} \frac{P_{\mathrm{net}}}{P_{\mathrm{FC}}} = \eta_{\mathrm{HHV}} \eta_{\mathrm{DC/DC}} \frac{P_{\mathrm{FC}} - P_{\mathrm{aux}}}{P_{\mathrm{FC}}} = \eta_{\mathrm{HHV}} \eta_{\mathrm{DC/DC}} \left(1 - \frac{P_{\mathrm{aux}}}{P_{\mathrm{FC}}}\right) \tag{2.19}$$

where P_{net} represents the net output power of the FC system and P_{aux} represents the power consumed by the auxiliary systems. Based on the experimental data obtained from experimental tests and using Eq. (2.19), the output efficiency curve of the FC system used in this chapter can be calculated.

Based on the research of [12] and [27], in the low power range, as the output power increases, the system efficiency will increase and reach the maximum value. Furthermore, as the power generated by the stack increases, the consumption of auxiliary devices in the system also increases correspondingly, resulting in a decrease in system efficiency. Therefore, the system has a maximum efficiency operating point (MEOP). When designing the EMS, it is necessary to ensure that the FC operates around this power point (MEOP) as much as possible.

In addition, the fuel consumption of the whole system is another important indicator in the HEV. Based on the research of [5,21], the hydrogen consumption rate of the FC can be calculated by:

$$C_{\mathrm{FC}} = \frac{P_{\mathrm{FC}}}{2U_{\mathrm{cell}}F} \tag{2.20}$$

where C_{FC} represents the hydrogen consumption rate of the FC (the unit is g/s). Considering that the molar mass of the hydrogen is 2.02 g/mol, Eq. (2.20) can be rewritten as:

$$C_{\mathrm{FC}} = \frac{2.02 P_{\mathrm{FC}}}{2 U_{\mathrm{cell}} F} = 1.05 \times \frac{P_{\mathrm{FC}}}{U_{\mathrm{cell}}}. \tag{2.21}$$

Since there are other auxiliary equipment consumption in the system, the hydrogen consumption of the FC power generation system can be expressed as:

$$C_{\mathrm{FCS}} = 1.05 \times \frac{\frac{P_{\mathrm{FC}}}{\eta_{\mathrm{DC/DC}}} + P_{\mathrm{aux}}}{U_{\mathrm{cell}}}. \tag{2.22}$$

According to Eq. (2.22), the hydrogen consumption rate of the FC system can be obtained. Furthermore, the total mass of fuel consumption by the system can be calculated by [6,20]:

$$M_{\mathrm{H_2}} = \int_o^{\mathrm{T}} C_{\mathrm{FCS}} dt \tag{2.23}$$

where M_{H2} is the total mass of hydrogen.

2.2.4. DC/DC converter model

According to our previous research [10], the output voltage of the FC fluctuates greatly (67.76 V @ 0 A and 37.83 V @ 80 A). In order to provide stable electrical energy to the HEV, it is necessary to connect the FC to the DC bus port through a DC/DC converter. In addition, the DC/DC converter is also the core part of the entire hybrid power system. It can control the energy flow of the hybrid system by adjusting the output power of the converter, which is the basis for the realization of EMSs and other control algorithms. At present, the commonly used converter topologies include Buck, Boost, Buck-Boost, Sepic, and Cuk. From the operating characteristics of each topology, although the voltage conversion can be achieved, each has its own advantages and disadvantages. According to the power generation characteristics of the FC and the system structure, the converter topology I adopted in this chapter is shown in Fig. 2.11, which is a Boost converter.

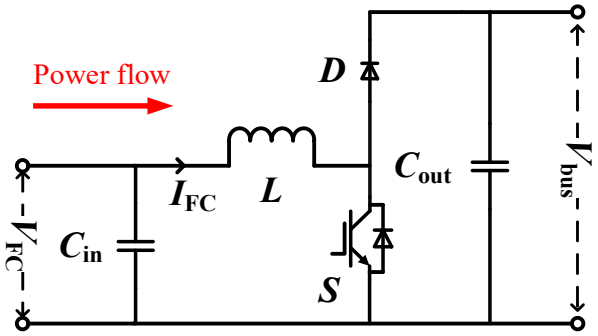

Figure 2.11. Boost DC/DC converter topology.

In Fig. 2.11, S is a switching device, L is an energy storage inductor, C_{in} is an input filter capacitor, D is a synchronous diode, and C_{out} is an output filter capacitor. The FC output reference current or power can

be controlled by adjusting the PWM duty cycle. It should be noted that, in order to simplify the control algorithm, this chapter uses the average circuit model to replace the boost DC/DC converter model. The switching element is replaced by a controlled source, and the modified DC/DC converter model is shown in Fig. 2.12.

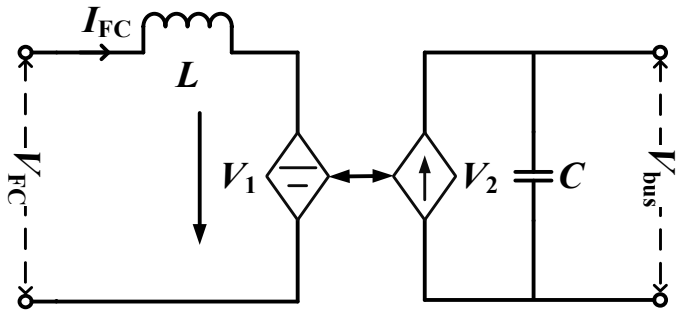

Figure 2.12. The average circuit model.

In this model, the inductor value is 3000 mH, and the output capacitor parameter is set to 72 V/5000*e*-6 F. In addition, the system control method is depicted in Fig. 2.13.

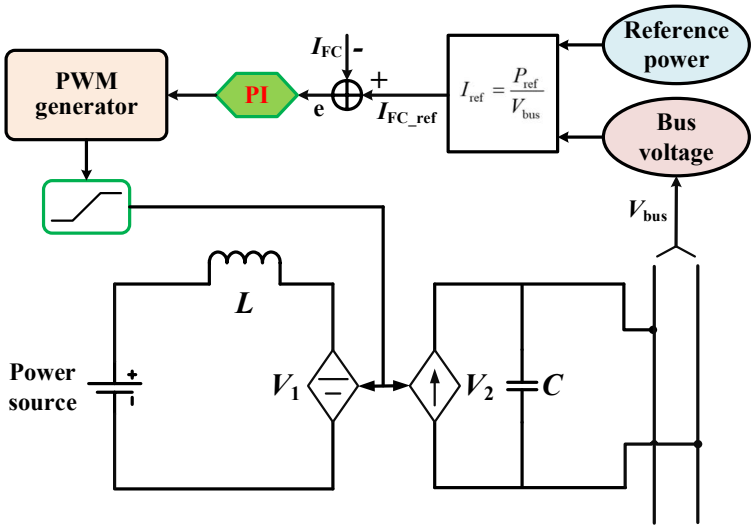

Figure 2.13. Control framework of the DC/DC converter.

In Fig. 2.13, P_{ref} is the reference power of the power source, and I_{ref} represents the reference current calculated based on the reference power. In this chapter, the PI control algorithm is used to realize the power conversion. Through repeated tests, set the proportional gain to 0.1 and the integral gain to 0.05.

2.3. Optimal system economic energy management strategy

Up to now, scientific researchers have conducted a large number of investigations on hybrid powertrain (such as EMSs and component configuration optimization), which has made a huge breakthrough in the cost of hybrid powertrain manufacturing, but its market utilization rate is still limited [28,29]. The main reason is that compared with the traditional internal combustion engine, its operating cost is still high,

so it is difficult to achieve large-scale application in the energy market [30,31]. In addition, the complex application environment of vehicles will aggravate the degradation rate of the power sources performance, results in insufficient durability. Another important factor restricting the large-scale application of hybrid battery/FC structure in the energy market is that its service life is lower than market expectations [7,32]. In other words, the durability and the cost are two bottlenecks that limit the widespread use of hybrid systems in the energy market. In addition, according to the literature review in **Chapter 1**, although there have been a lot of researches on EMSs of hybrid system, most of the researches ignore the changes in power sources performance, which is not conducive to effectively extending the life cycle of the hybrid system. Therefore, considering the fuel economy of the system and the durability of the power sources is of great significance to expand the application range of the hybrid battery/FC structure. Based on the above reasons, this chapter presents an optimal system economic energy management strategy considering lifetime loss of power sources for a HEV.

From the summary of existing EMSs in **Chapter 1**, power following (PF) strategy and state machine control (SMC) strategy are the two most common rule-based EMSs [9,33]. They have the advantages of simple principle and easy implementation, and are often used in engineering applications [34]. Equivalent consumption minimization strategy (ECMS) is an EMS based on local real-time optimization. This strategy is aimed at optimizing the total instantaneous hydrogen consumption of the system, and it can be applied online, so it is used in many occasions [21,35]. In order to verify the optimization effect of the presented strategy and highlight the advantages of the proposed strategy, the above three EMSs (PF, SMC, and ECMS) are used as the test benchmarks to compare with the proposed strategy. These strategies will be carefully analyzed in the following subsections.

2.3.1. Rule-based control strategies

The rule-based EMSs don't need to obtain the driving conditions of the vehicle in advance, but need to predefine logical rules based on the SOC and required power of the battery in the system. Since this kind of methods have the advantages of low computational complexity, simple control, high reliability, etc., they have been widely used in practical applications. Whereas, these strategies rely too much on engineering practice and expert experience, and it is difficult to improve energy utilization. Moreover, the pre-established rules can't be adjusted in actual applications, resulting in poor performance of the systems under certain conditions [3,36,37].

2.3.1.1. Power following control strategy

On the premise of ensuring the safe operation of the vehicle, in order to maintain the SOC within the constrained range, the PF strategy adjusts the output power of the power sources according to the load power demand and the real-time SOC of the battery. When the battery SOC is higher that the upper limit, the output power of the FC will be reduced so that the battery can provide electrical energy to the load

in order to reduce its SOC. In addition, when the battery SOC is lower than the minimum value, the FC output power must not only meet the load power demand, but also charge the battery. Specifically, it can be divided into two states: Run mode and Stand mode.

1) Run mode

In this mode, when the SOC is within a certain range, both the battery and the FC operate normally to provide electric energy to the load. If the SOC is low, the FC not only provides energy for the load but also needs to charge the battery. The specific allocation of reference power between the battery and FC is as follows:

$$\begin{cases} P_{\text{FC\_ref}} = P_{\text{demand}} - P_{\text{bat\_ref}} \\ P_{\text{bat\_ref}} = P_{\text{bat\_rate}} \times \dfrac{SOC - SOC^*}{\Delta SOC} \\ SOC^* = \dfrac{1}{2}\left(SOC_{\text{H}} + SOC_{\text{L}}\right) \\ \Delta SOC = \dfrac{1}{2}\left(SOC_{\text{H}} - SOC_{\text{L}}\right) \end{cases} \tag{2.24}$$

where $P_{\text{bat\_ref}}$ is the battery reference power, $P_{\text{FC\_ref}}$ represents the FC reference power, SOC^* is the predetermined value of the battery SOC, SOC_{H} represents the upper limit of SOC, and SOC_{L} is the lower limit of SOC. In this chapter, the upper and lower limits of battery are 80% and 30%, respectively.

2) Stand mode

When the load demand power is small and the battery SOC is large, the system runs in this mode. The FC continues to output the lowest power, and the battery follows the fluctuation of the load power to maintain power balance. The reference power distribution is as follows:

$$P_{\text{bat\_ref}} = P_{\text{demand}} - P_{\text{FC\_min}} \tag{2.25}$$

where $P_{\text{FC\_min}}$ represents the lowest output power of FC.

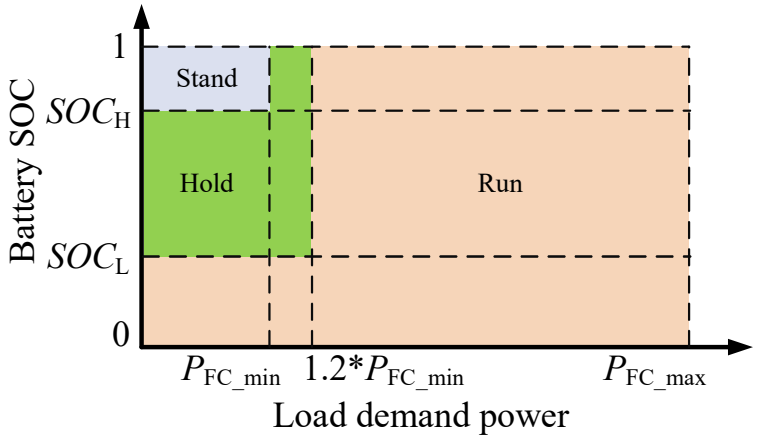

Figure 2.14. Power following strategy operation mode design.

The operating mode of the system can be determined according to the load demand power and the battery SOC. When the demand power is greater that 1.2*P_{FC_min} or the battery SOC is less that SOC_L, the system is in Run model. When the battery SOC is higher than the SOC_H and the load demand power is lower than the minimum output power of the FC, the system is in Stand mode. In other cases, the system keeps running in the previous state. The specific rules of modes division are depicted in Fig. 2.14.

In addition, in order to ensure the safe operation of the power sources, the following constraints on their reference power are also required.

$$\begin{cases} P_{bat\_min} \le P_{bat\_ref} \le P_{bat\_max} \\ P_{FC\_min} \le P_{FC\_ref} \le P_{FC\_max} \\ -\Delta P_{FC} \le \dfrac{dP_{FC\_ref}}{dt} \le \Delta P_{FC} \end{cases} \tag{2.26}$$

where P_{bat_min} and P_{bat_max} represents the allowable minimum and maximum output power of the battery, respectively. In addition, P_{FC_max} represents the maximum output power of the FC, and ΔP_{FC} is the maximum allowable change in the output power of the FC, which is generally defined as 12.5% of the rated power of the FC, as shown in Eq. (2.27) [38].

$$\Delta P_{FC} = 12.5\% \times P_{FC\_rate}\,. \tag{2.27}$$

2.3.1.2. State machine control strategy

The core idea of SMC is to set the reference power of the power sources according to the SOC of the battery and the required power of the load, so as to adjust the SOC within the constrained operating range. The strategy implementation process is as follows:

TABLE 2.5. The rules of SMC strategy [34,39].

SOC status	P_{deman} status	State	P_{FC_ref}
High (SOC > SOC_H)	$P_{demand} < P_{FC\_min}$	State = 1	$P_{FC\_ref} = P_{FC\_min}$
	$P_{demand} \in [P_{FC\_min}, P_{FC\_max}]$	State = 2	$P_{FC\_ref} = P_{demand}$
	$P_{load} > P_{FC\_max}$	State = 3	$P_{FC\_ref} = P_{FC\_max}$
Normal (SOC_L < SOC < SOC_H)	$P_{demand} < P_{FC\_MEP}$	State = 4	$P_{FC\_ref} = P_{FC\_MEP}$
	$P_{demand} \in [P_{FC\_MEP}, P_{FC\_max}]$	State = 5	$P_{FC\_ref} = P_{demand}$
	$P_{demand} > P_{FC\_max}$	State = 6	$P_{FC\_ref} = P_{FC\_max}$
Low (SOC < SOC_L)	$P_{demand} < P_{FC\_max} + P_{bat\_min}$	State = 7	$P_{FC\_ref} = P_{demand} - P_{bat\_min}$
	$P_{demand} \in [P_{FC\_max} + P_{bat\_min}, P_{FC\_max}]$	State = 8	$P_{FC\_ref} = P_{demand}$
	$P_{demand} > P_{FC\_max}$	State = 9	$P_{FC\_ref} = P_{FC\_max}$

Firstly, set the optimal operating range of battery SOC based on engineering experience. Secondly, calculate the reference power of the power sources based on the load demand power and the battery SOC. Finally, limit the output power of each power source to ensure its safe operation. The SMC strategy

designed in this chapter divides the battery and FC output power into 9 states to make each power source operate as smoothly as possible and avoid drastic changes in its output power. The specific rules are listed in TABLE 2.5.

According to the different SOC of the battery, the SOC can be divided into three areas: high (SOC > SOC_H), normal (SOC_L < SOC < SOC_H), and low (SOC < SOC_L). The specific operation process is as follows:

a) State 1 – high SOC and $P_{demand} < P_{FC\_min}$: In this state, the FC outputs at its minimum. When the demand power of load is less than the minimum output power of the FC, the battery absorbs the remaining energy.
b) State 2 – high SOC and $P_{demand} \in [P_{FC\_min}, P_{FC\_max}]$: In this scenario, the FC outputs the load demand power, and the battery doesn't output or absorb power.
c) State 3 – high SOC and $P_{demand} > P_{FC\_max}$: In this case, the FC outputs at maximum power, and the system power shortage will be provided by the battery. In this mode, the battery is in a discharged state, and the SOC will decrease.
d) State 4 – normal SOC and $P_{demand} < P_{FC\_opt}$: In this state, since the output efficiency of the FC is low when it is operating in the low-power area, the reference power of the FC is set as the power at the maximum efficiency point. Therefore, the battery will work in the charging mode in this state, and the SOC will increase.
e) State 5 – normal SOC and $P_{demand} \in [P_{FC\_opt}, P_{FC\_max}]$: In this case, as in State 2, the FC works in load power following mode, and the battery doesn't output power.
f) State 6 – normal SOC and $P_{demand} > P_{FC\_max}$: This state is similar to State 3, the FC works at maximum power, and the battery provides the remaining power of the system, which reduces the battery SOC.
g) State 7 – low SOC and $P_{demand} < P_{FC\_max} + P_{bat\_min}$: In this state, since the SOC is relatively low, the fuel cell not only needs to meet the load power demand, but also needs to charge the battery with the maximum charging power.
h) State 8 – low SOC and $P_{demand} \in [P_{FC\_max} + P_{bat\_min}, P_{FC\_max}]$: In this state, the FC is used to meet the load power demand.
i) State 9 – low SOC and $P_{demand} > P_{FC\_max}$: In this scenario, the FC outputs at maximum power, and the battery is used to provide insufficient power.

This control strategy is simple to control and easy to implement. Whereas, the disadvantage is that, in order to keep the battery in the best working state, it is inevitable that the FC operation state can't be taken into account, which is not conducive to maintain the power generation performance of the stack [4].

2.3.2. Equivalent consumption minimization strategy

The ECMS is based on the principle of equivalent hydrogen consumption for power allocation. This strategy uses the functional relationship between FC hydrogen consumption rate and output power, converts battery electric energy into hydrogen consumption, and converts the system hydrogen optimization problem into an optimal value solution problem [40]. Furthermore, this strategy minimizes the hydrogen consumption of the system per unit cycle to obtain the optimal fuel economy of the system [5,21].

In this chapter, the total hydrogen consumption of the hybrid system is determined by the indirect equivalent hydrogen consumption of the battery and the direct hydrogen consumption of the FC. The hydrogen consumption of the FC can be calculated by Eq. (2.22). In addition, the equivalent hydrogen consumption of battery can be obtained through Eq. (2.14). Therefore, the problem of minimum total hydrogen consumption in the system can be redefined as [22]:

$$P_{\mathrm{FC\_ref}} = \min C_{\mathrm{sys}} = \min\left(C_{\mathrm{FCS}} + \lambda_{\mathrm{bat}} C_{\mathrm{bat}}\right) \tag{2.28}$$

where λ_{bat} is the penalty coefficient, which can be expressed as:

$$\lambda_{\mathrm{bat}} = 1 - \frac{2\beta\left(SOC - \frac{1}{2}\left(SOC_{\mathrm{H}} + SOC_{\mathrm{L}}\right)\right)}{SOC_{\mathrm{H}} - SOC_{\mathrm{L}}} \tag{2.29}$$

here, β is used to determine the fluctuation range of the battery SOC. In order to ensure the safe and stable operation of the system, the following constraints are formulated.

$$\begin{cases} SOC_{\mathrm{L}} \le SOC \le SOC_{\mathrm{H}} \\ U_{\mathrm{bat\_min}} \le U_{\mathrm{bat}} \le U_{\mathrm{bat\_max}} \\ P_{\mathrm{FC\_min}} \le P_{\mathrm{FC}} \le P_{\mathrm{FC\_max}} \end{cases} \tag{2.30}$$

where $U_{\mathrm{bat\_min}}$ and $U_{\mathrm{bat\_max}}$ respectively represent the minimum and maximum output voltage of the battery. These two values can be obtained from Fig. 2.5 (a). Under the premise of satisfying the constraints of Eq. (2.30), the analytical solution of formula (2.28) can be expressed as [22]:

$$P_{\text{bat\_ref}}=\begin{cases}\dfrac{U_{\text{bat\_min}}\left(U_{\text{OCV}}-U_{\text{bat\_min}}\right)}{R_{\text{bat\_dis}}} & \alpha\le x_{\min}\\ \dfrac{U_{\text{OCV}}^2}{4R_{\text{bat\_dis}}}\left(1-\alpha^2\right) & x_{\min}\le\alpha\le 1\\ 0 & 1<\alpha\le\dfrac{1}{\eta_{\text{dis\_avg}}\eta_{\text{chg\_avg}}}\\ \dfrac{U_{\text{OCV}}^2\left(1-\left(\alpha\eta_{\text{dis\_avg}}\eta_{\text{chg\_avg}}\right)^2\alpha\right)}{4R_{\text{bat\_chg}}} & \dfrac{1}{\eta_{\text{dis\_avg}}\eta_{\text{chg\_avg}}}<\alpha\le\dfrac{x_{\max}}{\eta_{\text{dis\_avg}}\eta_{\text{chg\_avg}}}\\ -\dfrac{U_{\text{bat\_max}}\left(U_{\text{bat\_min}}-U_{\text{OCV}}\right)}{R_{\text{bat\_chg}}} & \alpha\ge\dfrac{x_{\max}}{\eta_{\text{dis\_avg}}\eta_{\text{chg\_avg}}}\end{cases} \tag{2.31}$$

with:

$$\begin{cases}\alpha=\dfrac{\lambda_{\text{bat}}}{\eta_{\text{cha\_avg}}}\\ x_{\min}=\sqrt{1+4U_{\text{bat\_min}}\dfrac{U_{\text{bat\_min}}-U_{\text{OCV}}}{U_{\text{OCV}}^2}}\\ x_{\max}=\sqrt{1+4U_{\text{bat\_max}}\dfrac{U_{\text{bat\_max}}-U_{\text{OCV}}}{U_{\text{OCV}}^2}}\end{cases} \tag{2.32}$$

The use of formulas (2.31) and (2.32) can realize the application of ECMS in the HEV.

2.3.3. Optimal system economic energy management strategy design

The major research purpose of this chapter is to reduce the operating cost of the system and to improve the durability of the power sources. In addition, the presented optimal system economic EMS is mainly implemented through two processes. The first process is to formulate the system objective function, and the second process is to use the optimization algorithm to solve the objective function. We will elaborate on the realization of each process in the following subsections.

2.3.3.1. System operating cost function formulation

The main factors that affect the operating cost of the system include battery and FC lifetime loss, system fuel consumption, and battery charge-discharge depth. The following is a detailed analysis of these factors in order to formulate an objective function for evaluating the operating cost of the system.

The aging of battery is a long-term gradual process, and the battery cycle life is mainly affected by various factors such as the depth of charge and discharge. With the continuous charge and discharge of the battery, its performance will gradually deteriorate, and the most obvious feature is capacity attenuation. Based on the research [41], the capacity degradation of battery can be calculated by the following formula:

$$Q_{\text{loss}} = Be^{-\left(\frac{C+D\times c_{\text{rate}}}{RT}\right)} \times \left(A_{\text{h}}\right)^{z} \tag{2.33}$$

here, Q_{loss} is the battery capacity loss percentage, B is the pre-exponential factor, c_{rate} is the current rate, R is the gas constant, T is the temperature, z is the power low factor, A_{h} is the Ah-through, C is the activation energy coefficient, and D is the activation energy increment coefficient. However, the Eq. (2.33) cannot be used to calculate the battery dynamic process capacity loss. Based on the damage accumulation theory, a capacity loss model suitable for battery dynamic process is derived [42–44].

$$Q_{\text{loss,k+1}} - Q_{\text{loss,k}} = \Delta A_{\text{h}} z B^{\frac{1}{z}} e^{-\left(\frac{C+D\times c_{\text{rate}}}{zRT}\right)} Q_{\text{loss,k}}^{\frac{z-1}{z}} \tag{2.34}$$

with:

$$\Delta A_{\text{h}} = \frac{1}{3600}\left|I_{\text{bat}}\right|\left(t_{\text{k+1}} - t_{\text{k}}\right) \tag{2.35}$$

where $Q_{\text{loss,k+1}}$ and $Q_{\text{loss,k}}$ are the capacity loss at $t_{\text{k+1}}$ and t_{k}. According to the above description, the formulated battery cycle life evaluation method is as follows:

$$D_{\text{bat\_loss}} = \frac{U_{\text{bat}} Q}{1000\times 0.2} \times \frac{\left|I_{\text{bat}}\right|\Delta t}{3600 N_{\text{p}}} z B^{\frac{1}{z}} e^{-\left(\frac{C+D\cdot c_{\text{rate}}}{zRT}\right)} Q_{\text{loss,k}}^{\frac{z-1}{z}} \tag{2.36}$$

where N_{p} is the number of batteries.

In addition, according to the research of [30,31], working conditions have a greater impact on the operating performance of the stack. The driving cycle is mainly composed of four conditions: start-stop, low power, high power, and load changing. The above factors will accelerate the degradation of stack performance, which is not conducive to maintain the healthy and long-life operation of the system. Therefore, on the basis of the existing research [30], this subsection formulates the functional relationship of the influence of output power on the lifetime of FC as follows:

$$D_{\text{FC\_loss}} = D_{\text{on/off}} + D_{\text{low}} + D_{\text{high}} + D_{\text{chg}} \tag{2.37}$$

here, $D_{\text{FC\_loss}}$ represents the performance degradation rate of stack, which is generally expressed in voltage or percentage form. D_{low} is the performance degradation caused by FC in a low power operating state, D_{high} is the lifetime loss during high power operation, D_{chg} represents the degradation caused by the change of the output power of the stack, and $D_{\text{on/off}}$ is the degradation of the stack caused by start and stop. These parameters are defined as follows:

$$\begin{cases} D_{\text{low}} = t_1' \times U_1' \\ D_{\text{high}} = t_2' \times U_2' \\ D_{\text{chg}} = \dfrac{\sum_{i=1}^{n} \Delta P_{\text{FC,i}} \times U_3'}{N_{\text{cell}}} = \dfrac{\sum \left| P_{\text{FC}}(t) - P_{\text{FC}}(t-1) \right| \times U_3'}{N_{\text{cell}}} \\ D_{\text{on/off}} = n \times U_4' \end{cases} \tag{2.38}$$

where t_1' is the total operating time of the stack at low power and U_1' represents the degradation rate of the stack during low power operation. In addition, t_2' represents the total operating time of the stack at high power and U_2' is the degradation rate of the stack during high power operation. Moreover, $\Delta P_{\text{FC,i}}$ is the fluctuation of the output power of the stack at the *i*-th moment, P_{FC}(t) represents the stack output power at the current moment, P_{FC}(t-1) represents FC output power at the previous moment, and U_3' represents the degradation rate of the stack when its output power changes. Furthermore, n represents the number of start and stop of the stack during operation and U_4' is the degradation rate of the stack voltage caused by the start and stop actions.

In addition to the degradation of battery and FC operating performance, fuel consumption is another important factor affecting system cost. Based on the concept of equivalent hydrogen consumption, the total hydrogen consumption can be calculated by [19]:

$$C_{\text{total}} = C_{\text{bat}} + C_{\text{FCS}} . \tag{2.39}$$

According to above description, using the battery capacity loss evaluation method shown in Eq. (2.36) and the stack lifetime loss evaluation formula shown in Eq. (2.37), the lifetime loss of the power sources during system operation can be converted into operating costs. Then, considering the hydrogen consumption cost of the system, the system economy objective function can be formulated, as shown below:

$$J_{\text{total}} = \min\left(C_{\text{FC\_D}} + C_{\text{H}_2} + C_{\text{bat\_D}} + D_{\text{SOC}} \right) \tag{2.40}$$

with:

$$\begin{cases} C_{\text{FC\_D}} = N_{\text{FC}} \times K_{\text{FC}} \times \dfrac{D_{\text{FC\_loss}}}{10\% \times U_{\text{rated,init}}} \times P_{\text{FC\_rated}} \times \beta_{\text{FC}} \\ C_{\text{H}_2} = C_{\text{total}} \times \beta_{\text{H}_2} \\ C_{\text{bat\_D}} = \int_0^{\text{T}} D_{\text{Bat\_loss}} dt \times \beta_{\text{bat}} \\ D_{\text{SOC}} = D_{\text{P}} \int_0^{\text{T}} \left(SOC - SOC_{\text{init}} \right)^2 dt \end{cases} \tag{2.41}$$

here, $P_{\text{FC\_rated}}$ is the rated power of the adopted FC, β_{FC} is unit price of the stack, β_{H2} is unit price of the hydrogen, and β_{bat} is unit price of the battery. In addition, the function of the coefficient D_{P} is to restrict

the fluctuation range of the battery SOC. The larger the value of D_P, the better the effect. Moreover, the coefficient K_{FC} is used to limit the stack to run as far as possible in the divided high-efficiency operating zone [4,20]. Furthermore, the specific values of the coefficients in the objective function are listed in TABLE 2.6.

TABLE 2.6. Coefficients values in the objective function.

Parameter	Value
Low power operation	$U'_1 = 8.662$ μV/h
High power operation	$U'_2 = 10$ μV/h
Load changing	$U'_3 = 0.0441$ μV/ΔkW
Start-stop	$U'_4 = 13.79$ μV

To ensure the safe and stable operation of the HEV, the equality and inequality constraints shown below are taken into account in the formulated cost function.

$$\begin{cases} P_{FC\_min} \le P_{FC} \le P_{FC\_max} \\ -\Delta P_{FC} \le \dfrac{dP_{FC}}{dt} \le \Delta P_{FC} \\ P_{bat\_min} \le P_{bat} \le P_{bat\_max} \\ P_{FC} + P_{bat} = P_{demand} \end{cases} \tag{2.42}$$

here, P_{FC_min} and P_{FC_max} are the minimum output power and maximum output power of the stack, respectively. In addition, ΔP_{FC} is used to limit the dynamic power fluctuations of the stack. Moreover, P_{bat_min} and P_{bat_max} are the minimum output power and maximum output power of the battery, respectively. After formulating the cost function, sequential quadratic programming (SQP) algorithm is used to solve the optimal value of the objective function to obtain the most economical operating cost [19]. We will introduce the process of using the SQP algorithm to solve the objective function in the next subsection.

2.3.3.2. Sequential quadratic programming algorithm

The main core process of the SQP algorithm is to decompose the complex nonlinear optimization problem into a series of quadratic programming sub-problems. This algorithm optimizes the solutions of the sub-problems through continuous iteration to search for the optimal solution of the objective function. The SQP algorithm has the advantages of fast convergence speed and high solving efficiency. It is one of the commonly used methods for solving nonlinear constrained optimization problems [45]. The following is the specific solution process.

According to the solution form of the SQP algorithm, the constraints shown in Eq. (2.42) are simplified into the linear function form, as follows:

$$\begin{cases} g_{\mathrm{i}}(x)=0, \ \ i=1,2,\cdots,m_{\mathrm{e}} \\ g_{\mathrm{i}}(x)\le 0, \ \ i=m_{\mathrm{e}}+1,m_{\mathrm{e}}+2,\cdots,m \end{cases} \rightarrow \begin{cases} g_1(x)=-P_{\mathrm{FC}}-P_{\mathrm{bat}}+P_{\mathrm{demand}} \\ g_2(x)=P_{\mathrm{FC}}+P_{\mathrm{bat}}-P_{\mathrm{demand}} \\ g_3(x)=P_{\mathrm{FC}}-P_{\mathrm{FC\_max}} \\ g_4(x)=P_{\mathrm{bat}}-P_{\mathrm{bat\_max}} \\ g_5(x)=\dfrac{dP_{\mathrm{FC}}}{dt}-D_{\mathrm{FC}}\times\Delta P_{\mathrm{FC}} \\ g_6(x)=-P_{\mathrm{FC}}+P_{\mathrm{FC\_min}} \\ g_7(x)=-P_{\mathrm{bat}}+P_{\mathrm{bat\_min}} \\ g_8(x)=-\dfrac{dP_{\mathrm{FC}}}{dt}-D_{\mathrm{FC}}\times\Delta P_{\mathrm{FC}} \end{cases} \tag{2.43}$$

where g_1 and g_2 represents equality constraints, g_3-g_8 represent inequality constraints in the system, and $m_{\mathrm{e}} = 2$, $m = 8$. Using Taylor expansion, the objective function (2.40) can be simplified into a quadratic function form at the iteration point x_{k}:

$$\begin{cases} \min f_{\mathrm{SQP}}=\dfrac{1}{2}[x-x_{\mathrm{k}}]^{\mathrm{T}}\nabla^2 f(x_{\mathrm{k}})[x-x_{\mathrm{k}}]+\nabla f(x_{\mathrm{k}})^{\mathrm{T}}[x-x_{\mathrm{k}}] \\ s.t. \ \ i=1,2,\cdots,m_{\mathrm{e}}, \ \ \nabla g_{\mathrm{i}}(x_{\mathrm{k}})^{\mathrm{T}}[x-x_{\mathrm{k}}]+g_{\mathrm{i}}(x_{\mathrm{k}})=0 \\ \quad i=m_{\mathrm{e}}+1,m_{\mathrm{e}}+2,\cdots,m, \ \ \nabla g_{\mathrm{i}}(x_{\mathrm{k}})^{\mathrm{T}}[x-x_{\mathrm{k}}]+g(x_{\mathrm{k}})\le 0 \end{cases} \\ \rightarrow s=x-x_{\mathrm{k}} \Rightarrow \begin{cases} \min \dfrac{1}{2}s^{\mathrm{T}}H_{\mathrm{k}}s+c^{\mathrm{T}}s \\ s.t. \ \ A_{\mathrm{eq}}=B_{\mathrm{eq}} \\ \quad As\le B \end{cases} \tag{2.44}$$

here, s represents the vector matrix of control variables in the quadratic programming sub-problem. In order to classify the above formula as the standard form of quadratic programming, set the following symbols.

$$\begin{cases} H=\nabla^2 f_{\mathrm{SQP}}(x_{\mathrm{k}}) \\ C=\nabla f_{\mathrm{SQP}}(x_{\mathrm{k}}) \\ A_{\mathrm{eq}}=\left[\nabla g_1(x_{\mathrm{k}}),\nabla g_2(x_{\mathrm{k}}),\cdots,\nabla g_{m_{\mathrm{e}}}(x_{\mathrm{k}})\right]^{\mathrm{T}} \\ A=\left[\nabla g_{m_{\mathrm{e}}+1}(x_{\mathrm{k}}),\nabla g_{m_{\mathrm{e}}+2}(x_{\mathrm{k}}),\cdots,\nabla g_m(x_{\mathrm{k}})\right]^{\mathrm{T}} \\ B_{\mathrm{eq}}=\left[g_1(x_{\mathrm{k}}),g_2(x_{\mathrm{k}}),\cdots,g_{m_{\mathrm{e}}}(x_{\mathrm{k}})\right]^{\mathrm{T}} \\ B=\left[g_{m_{\mathrm{e}}+1}(x_{\mathrm{k}}),g_{m_{\mathrm{e}}+2}(x_{\mathrm{k}}),\cdots,g_m(x_{\mathrm{k}})\right]^{\mathrm{T}} \end{cases} \tag{2.45}$$

here, H represents the positive definite approximation of the Hessian matrix, C represents the first derivative of the objective function at the iteration point x_{k}, A_{eq} represents the gradient equality constraint of $\nabla g_{\mathrm{i}}(x_{\mathrm{k}})^2$, A is the gradient inequality constraint of $\nabla g_{\mathrm{i}}(x_{\mathrm{k}})^2$, B_{eq} represents the negative number of the equality constraint of $-g_{\mathrm{i}}(x_{\mathrm{k}})$, and B represents the negative number of the inequality constraint of $-g_{\mathrm{i}}(x_{\mathrm{k}})$. Through the above analysis, the Lagrangian function shown in Eq. (2.46) can be used to solve the quadratic programming sub-problem.

$$\min L(s,\lambda) = \frac{1}{2} s^T Hs + c^T s + \lambda(As - B) \tag{2.46}$$

where $\lambda = 8$ represents the Lagrangian multiplier, and $As - B$ represents the constraint of g_i. The extreme condition of the multivariate equation $L(s, \lambda)$ can be expressed as $\nabla L(s, \lambda)$, and the solution process is as follows:

$$\begin{cases} Hs + c + A^T\lambda \\ As - B = 0 \end{cases} \rightarrow \begin{bmatrix} H & A \\ A & 0 \end{bmatrix} \begin{bmatrix} s \\ \lambda \end{bmatrix} = \begin{bmatrix} -c \\ B \end{bmatrix} \tag{2.47}$$

where the initial value of λ is [0, 0, 0, 0, 0, 0, 0, 0], and the initial value of H is [1, 0; 0, 1]. In order to update the values of s and λ in Eq. (2.47), the active-set algorithm is used to iterate, as follows:

$$f_{SQP}(x_k + a_k s_k) < f_{SQP}(x_{k+1}) \tag{2.48}$$

where k represents the number of iterations, and a_k is the search step size. In addition, the initial value of s is set to [0, 0]. By continuously iterating x_{k+1} and λ_{k+1}, the optimal solution of the objective function can be found. The specific iterative solution steps are as follows:

Step 1: Set the initial point x_0 of the system and the convergence accuracy ε, set $H_0 = I$, $k = 0$;

Step 2: Simplify the objective function at the iteration point x_k to a quadratic programming problem as shown in Eq. (2.44);

Step 3: Solve the above quadratic programming problem, let $s_k = s^*$;

Step 4: Carry out a one-dimensional search for the cost function under constraint conditions to obtain the next iteration point x_{k+1};

Step 5: If the termination rule is satisfied at the iteration point x_{k+1}, then x_{k+1} is taken as the optimal solution, $f(x_{k+1})$ is taken as the optimal cost of the objective function, and the calculation is terminated. Otherwise, go to the next step;

Step 6: Modify H_{k+1}, set $k = k+1$, and return to *Step 2* for looping.

By solving the objective function through the above steps, the system reference power P_{FC_ref} and P_{bat_ref} could be obtained, and the proposed EMS can be realized.

2.4. Online hardware-in-the-loop simulation platform design and analysis of experimental results

Considering that it is neither economical nor safe to directly verify the proposed strategies on an actual HEV. Before actual application, I first use simulation technology to test the operational performance of the proposed strategies. Using simulation technology to assist system design and method development

can effectively reduce research and development costs, improve product stability and greatly shorten the development cycle. As the most time-saving and economical verification method, simulation technology has been widely used in the early stage of product design, covering fields including communications, aerospace, power electronics, new energy transportation, and chemical engineering [7].

Please note that although the above mentioned strategies can be verified through the Matlab/Simulink environment, their real-time adaptability can't be verified. Therefore, this thesis develops an online HIL simulation test platform based on a real-time digital simulator (OP5600).

2.4.1. Description of RT-LAB test platform

RT-LAB is a set of software developed by Opal-RT Technologies in Canada that can be used to develop simulation models that run in real-time. The simulation system is based on FPGA +CPU architecture and is mainly used in power systems and power electronics. Based on the real-time simulator (see Fig. 2.15), the simulation model developed in Matlab/Simulink or MATRKx/SystemBuild can be converted into C code and complied by the RT-LAB integrated compiler. The executable C code is uploaded to the digital simulator OP5600 through the network connection TCP/IP protocol (using a network cable). The OP5600 is equipped with two six-core processors with a main frequency of 3.3 GHz, and the Linux operating system is used for processing. In addition, this simulator can send and receive a variety of digital and analog signals through the Xilinx Spartan-3 FPGA I/O board. The I/O board has 16 differential analog input signal interfaces, and the input voltage range is -20 V~20 V, 16 analog output signal interfaces, the output voltage range is -16 V~16 V, and 32 digital input interfaces, 32 digital output interfaces. According to the different needs of users, RT-LAB can be used in HIL system and Rapid Control Prototyping (RCP) system.

Figure 2.15. Outline of OP5600.

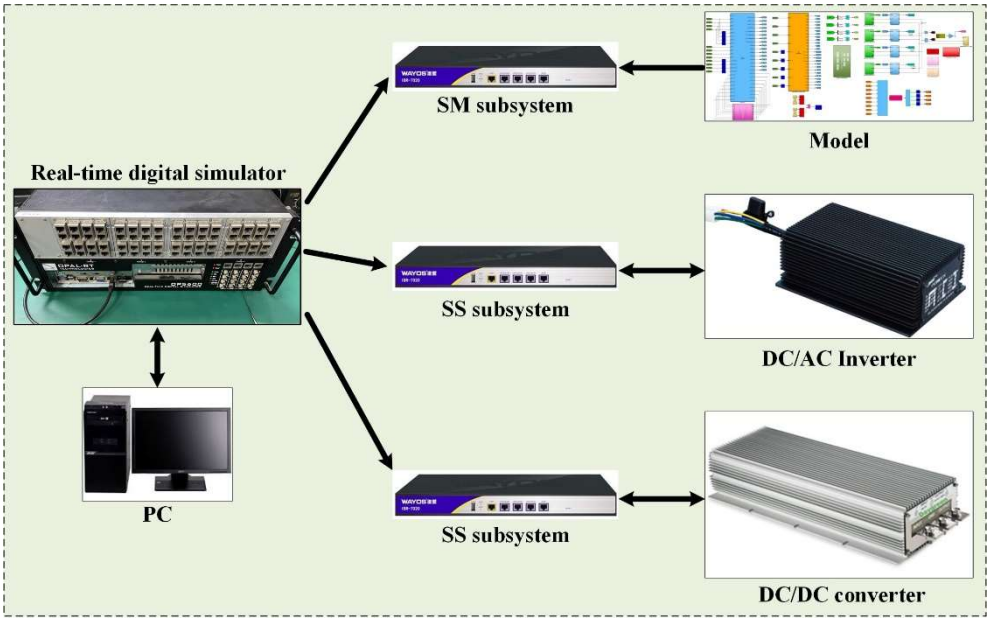

Figure 2.16. RCP simulation system.

Fig. 2.16 depicts the structure block diagram of the RCP control system, including an OP5600 real-time digital simulator, a PC installed with RT-LAB and Matlab development environment, and a hybrid hardware system composed of a battery, a FC, and a unidirectional DC/DC converter. In this mode of operation, the real-time simulator is equivalent to the controller of the entire hardware system. It needs to control the DC/DC converter and manage the output power of different power sources. In addition, in this system, according to the different functions of the top-level subsystems, it can be divided into two subsystems, SM and SS. The specific functions are as follows:

1) SM subsystem

The SM subsystem is the main subsystem, which is mainly used for system protection, algorithm calculation, lowest level control, and synchronization network. There is only one SM subsystem in each model.

2) SS subsystem

The SS subsystem is a secondary subsystem, which is mainly used to process the modules that need to be calculated in the model. Each model can contain multiple SS subsystem.

Using the RCP system can quickly verify the effectiveness and practicability of the proposed strategy. Whereas, since there are power devices in the system, it may be dangerous to use the RCP to develop a new algorithm.

Figure 2.17 shows the structure of the HIL simulation system, which includes an OP5600 real-time digital simulator, a PC with RT-LAB compilation software and Matlab simulation software, DSP controller, and communication interface circuit. The simulator is used to simulate the work response of

the hardware system, and other control algorithms are implemented in the DSP. Different from the RCP system, in addition to the SM and SS subsystems, HIL simulation system also includes a SC subsystem. The SC subsystem is mainly composed of the oscilloscopes and is used to monitor the operation of the entire system. The HIL simulation platform can test the operating performance of the proposed method without actual hardware conditions. This system imports the hardware model and the actual control method into the simulation loop to realize the real-time data interaction function. It has the advantages of actually reflecting the operating characteristics of each component, discovering hidden defects in the system in time, and minimizing risks and costs in actual commissioning and operation. This system puts all power device models into the real-time simulator, which makes it possible to test various boundary conditions of the system without damaging any equipment, thus reducing development risks. Therefore, in order to verify the effectiveness of the proposed strategy, this thesis sets up an online HIL simulation platform based on real-time simulator and Matlab/Simulink software.

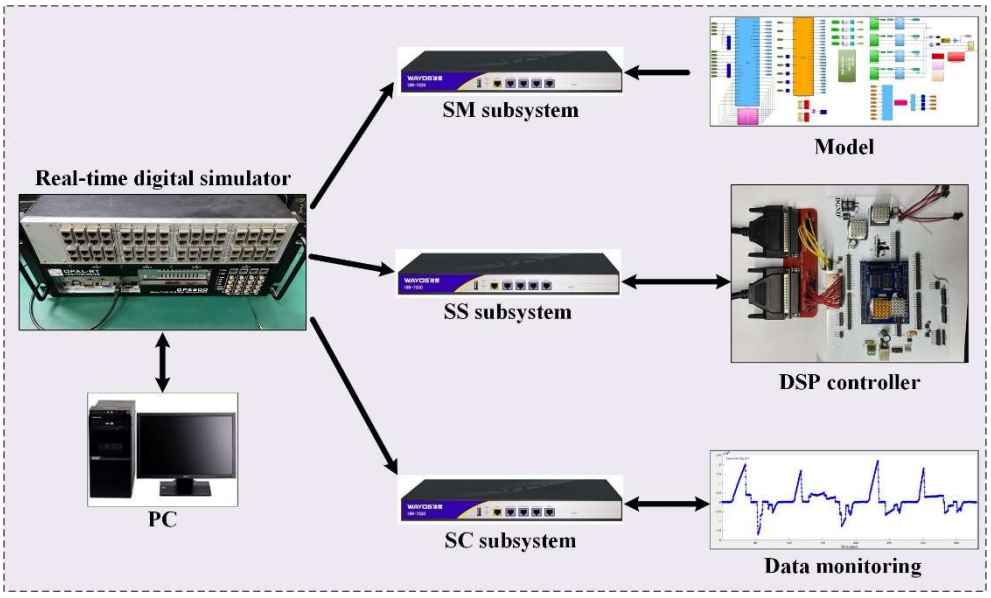

Figure 2.17. HIL simulation system.

2.4.2. HIL test platform construction

Based on the OP5600 simulator, the HIL test platform developed in this chapter can be divided into two parts:

1) System modeling

According to the topological structure selection of the hybrid system, the selection of each power source and the analysis of the mathematical model in the previous subsection, the HEV system model has been built (see section 2.2). This work is completed in Matlab/Simulink, the built model is compiled through the host computer and then imported into the simulator using TCP/IP communication, and the structure diagram is depicted in Fig. 2.18. The built hybrid system model is shown in Fig. 2.19.

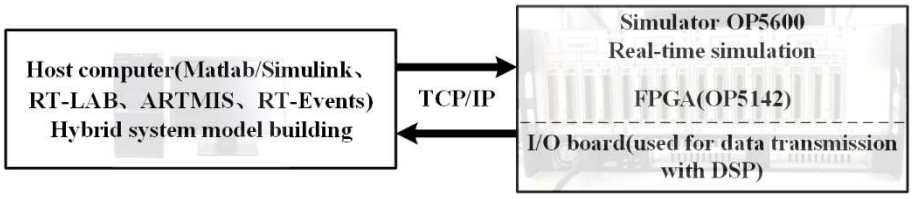

Figure 2.18. Simulation structure diagram.

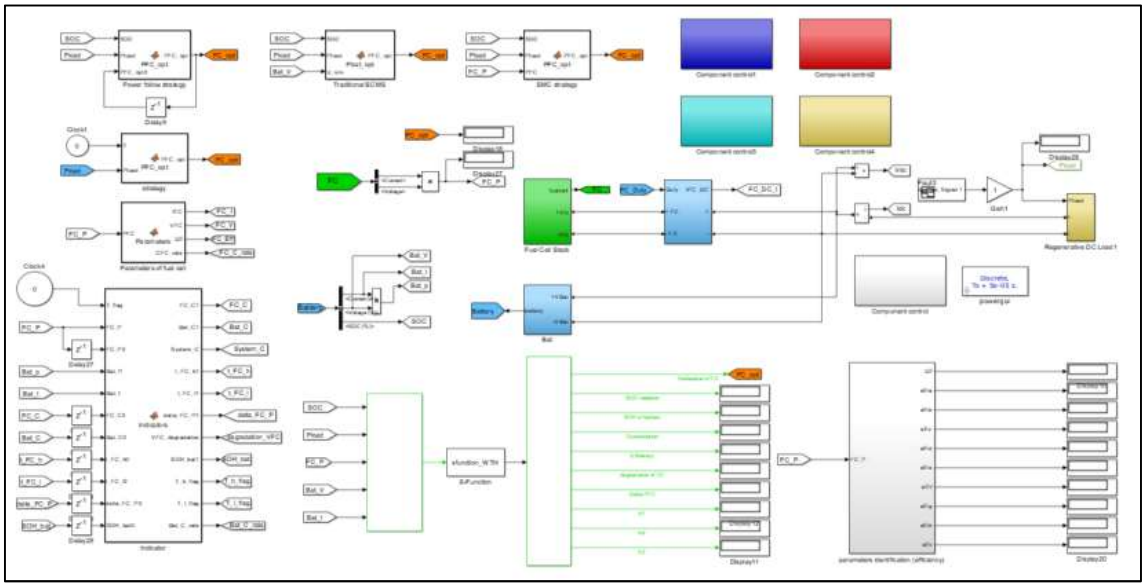

Figure 2.19. The built hybrid system model.

2) Interaction between control strategies and simulation system

As shown in Fig. 2.17, after building the system model, a power allocation strategy is needed to control the output power of each power source in the system. This part of the work is mainly to compile the proposed strategy into the DSP controller in the form of C code, and build the peripheral hardware circuit for connecting the simulator and the DSP. The structure is depicted in Fig. 2.20.

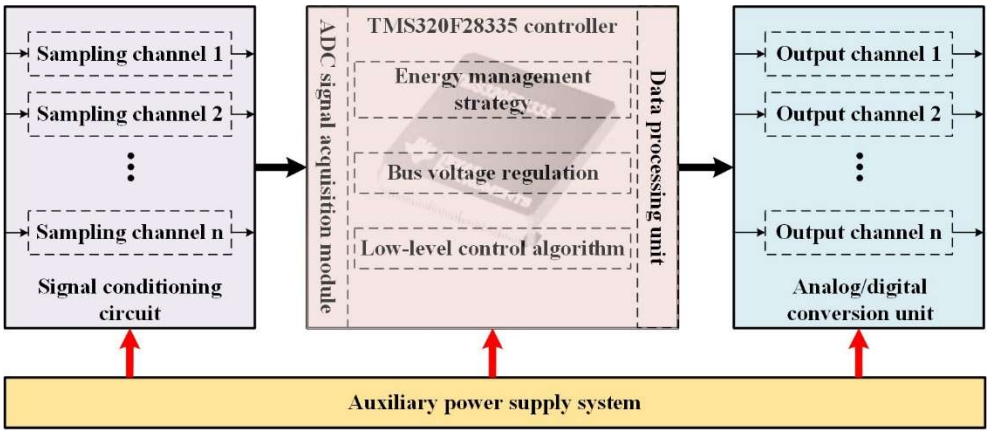

Figure 2.20. The peripheral control hardware structure diagram.

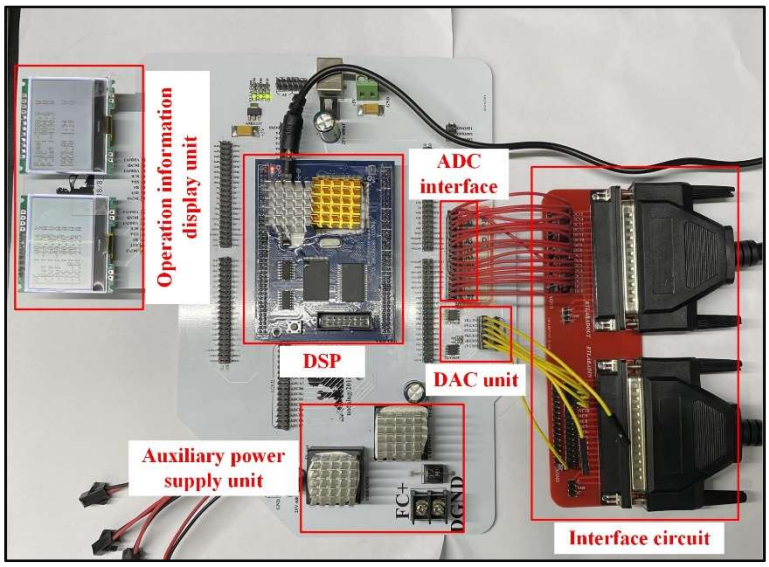

Figure 2.21. Peripheral hardware circuit.

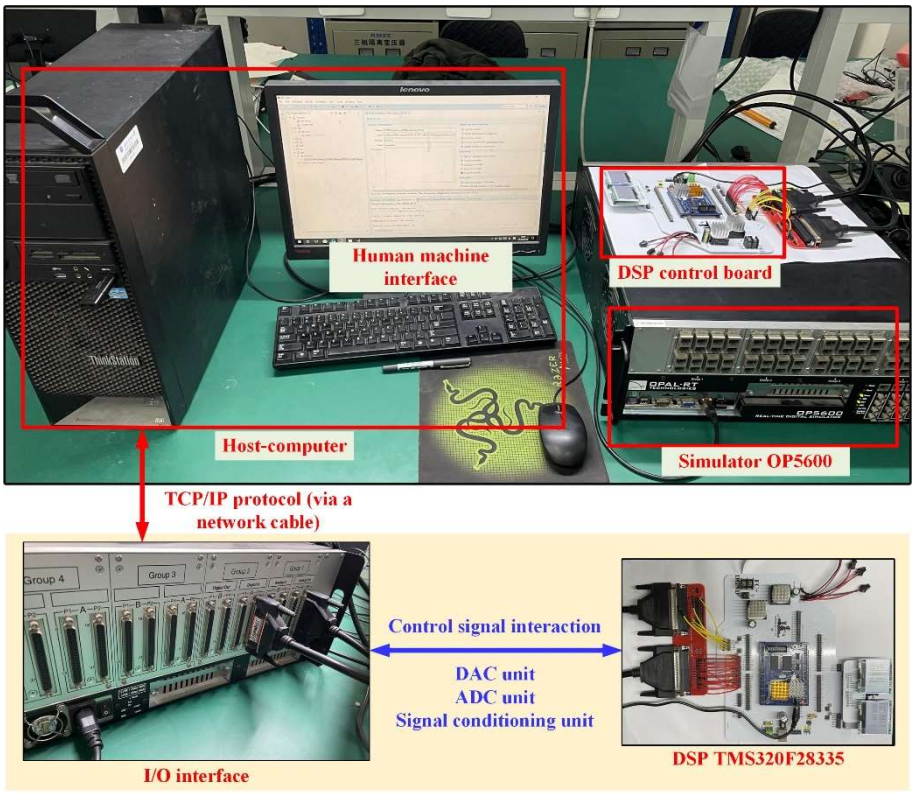

Figure 2.22. Actual picture of the HIL simulation test platform.

The DSP controller used in this thesis is TMS320F28335 provided by Texas Instruments (TI). The main frequency of TMS320F28335 is 150 MHz, and it has powerful data processing and computing capabilities. Considering that the input voltage range of the analog/digital conversion (ADC) unit of this DSP is 0 V-3 V, and the maximum output voltage of the I/O board of the simulator OP5600 is 16 V, it is necessary to add a signal conditioning circuit to match the voltage, protect the DSP and improve the sampling accuracy. In addition, the control signal generated by the DSP is transferred to the simulator

through the digital/analog conversion (DAC) unit. In order to facilitate experimental testing, I build all the peripheral hardware circuits on a control board, as depicted in Fig. 2.20.The built HIL simulation platform is depicted in Fig. 2.22, which mainly consists of a simulation system and hardware circuits.

2.4.3. Experimental verification and results analysis

In order to evaluate the operation effect of the above-mentioned EMSs and carry out performance comparison analysis, this chapter conducts experimental verification based on the HIL simulation platform shown in Fig. 2.22. On this platform, the driving cycle adopted is depicted in Fig. 2.23 (a). This driving cycle is from the actual HEV (see Fig. 2.1), and the driving route is the campus route of SWJTU, as depicted in Fig. 2.23 (c). In addition, the operating period of this working condition is about 1503 s, the operating speed range is 0-30 km/h, and the calculated power fluctuation range is -3-6 kW, as shown in Fig. 2.23 (b).

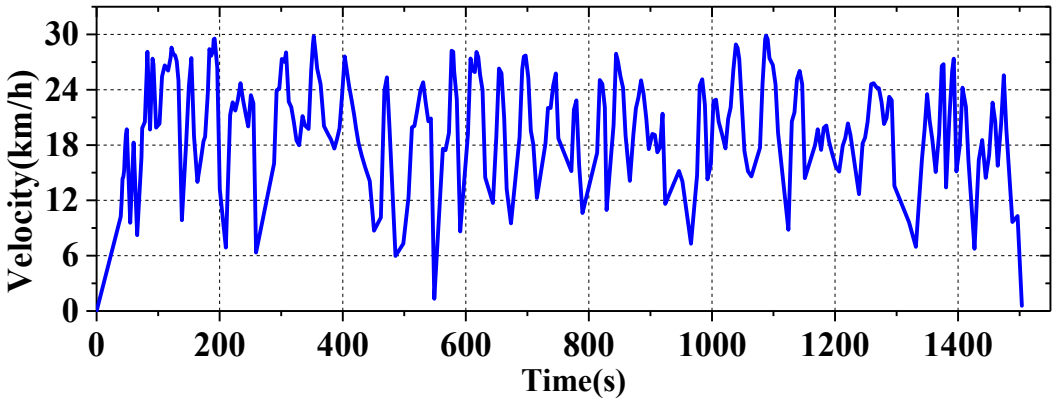

(a) The driving cycle of HEV

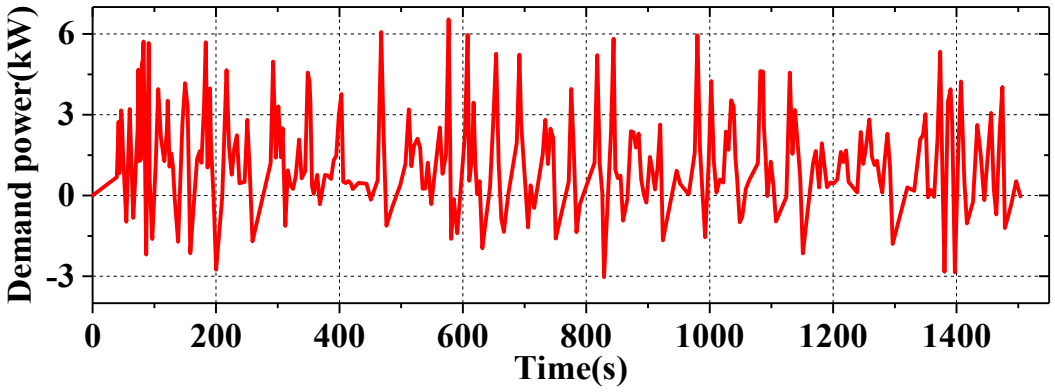

(b) Demand power of the HEV

(c) Driving route

Figure 2.23. Driving cycle information.

The main power generation parameters of the energy storage battery and FC adopted in this chapter are listed in TABLE 2.2. In addition, the power generation characteristics of the power sources have been carefully analyzed in the previous sections. In the following subsections, the experimental results will be analyzed in detail.

2.4.3.1. Output power analysis of each power source

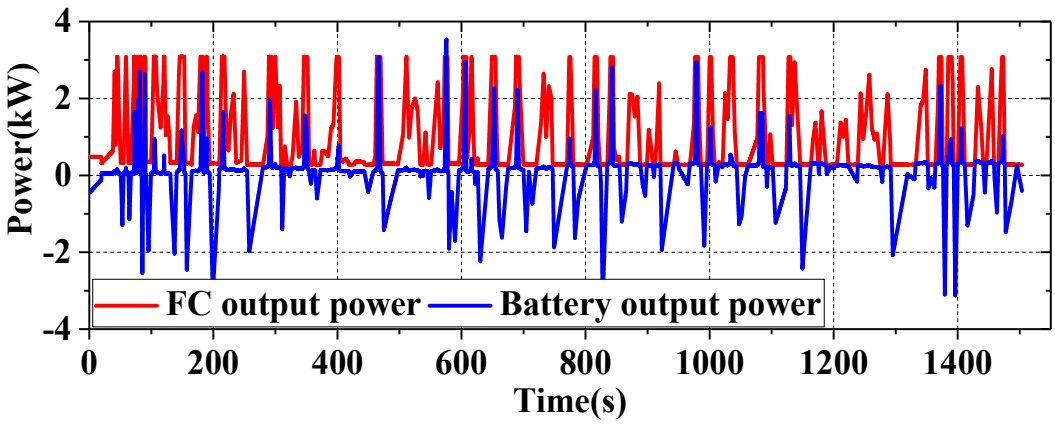

(a) PF control strategy

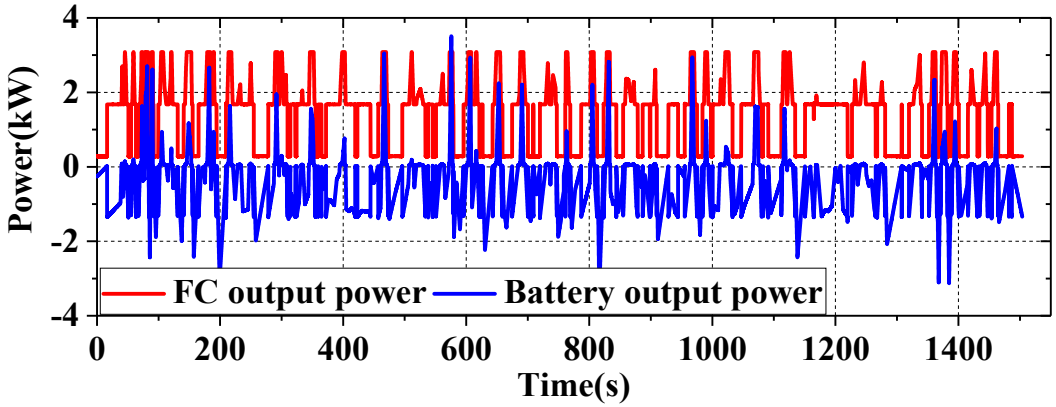

(b) SMC strategy

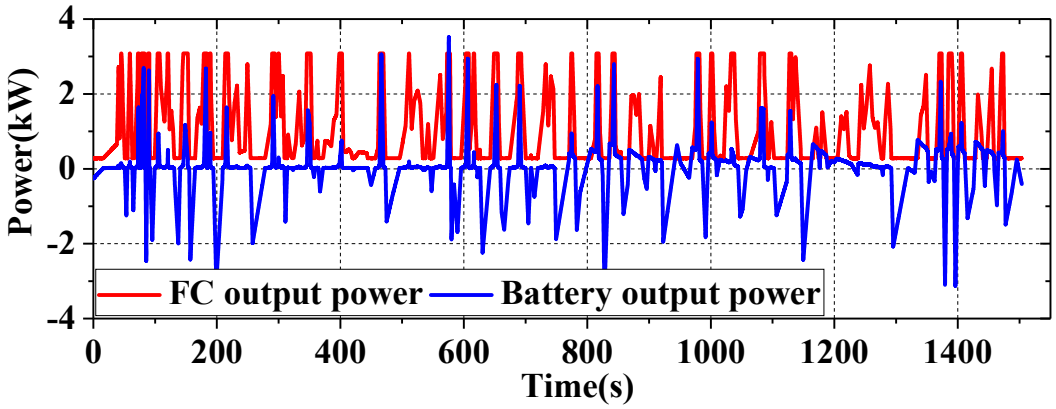

(c) ECMS

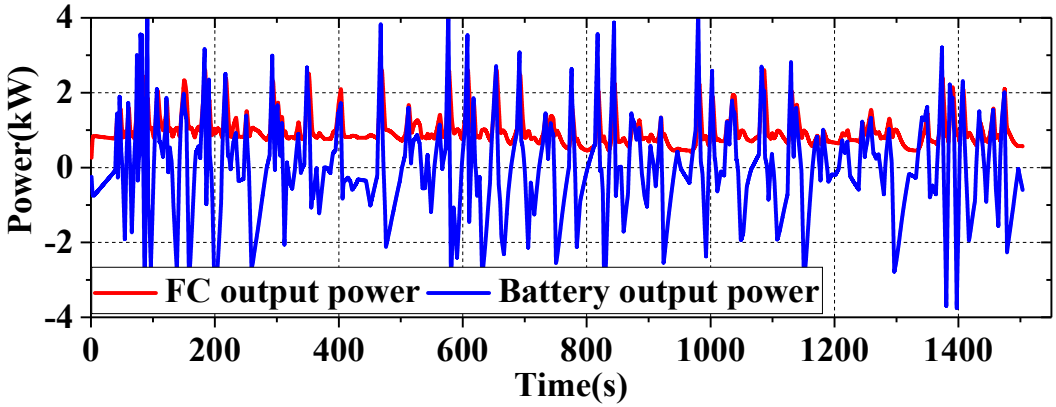

(d) The proposed optimal system economic EMS

Figure 2.24. Power distribution curves of different power sources under the control of different EMSs.

The battery and FC output power curves under the control of different EMSs are shown in Fig. 2.24. Specific indicators are analyzed in the next subsection. It can be clearly observed from Fig. 2.24 that all the strategies can fulfill the load demand, while the FC as a power source only provides electrical energy for the hybrid system (which can provide power to the load and the energy storage battery at the same time), and cannot absorb the system braking power. In addition, the battery not only provides the required instantaneous power to the HEV but also quickly recovers system braking and excess energy.

2.4.3.2. Performance evaluation on different EMSs

Fig. 2.24 presents the power output curves of the battery and FC using different EMSs (PF, SMC, ECMS and the proposed EMS). To test the performance of the proposed optimal system economic EMS, the SOC fluctuation of battery, the efficiency of FC, system hydrogen consumption, operating stress of each power source, voltage degradation of FC and operating cost of system are analyzed in this section.

- **SOC fluctuation range comparative analysis**

As the only energy storage system in the HEV, the battery plays a particularly important role. The SOC curves of battery under the control of different strategies are presented in Fig. 2.25. In order to facilitate the comparison of experimental results, the initial SOC values in all the strategies are set to the same value (about 55%).

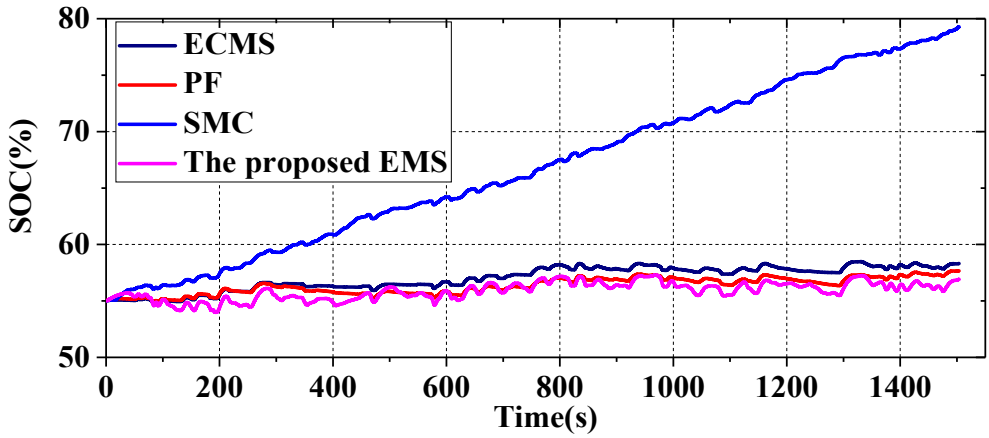

Figure 2.25. The SOC curves of battery under the control of different strategies.

In Fig. 2.25, the end-state battery SOC of the presented EMS, SMC strategy, PF control strategy and the ECMS are 56.91% (ΔSOC is about 1.91%), 79.28% (ΔSOC is about 24.28%), 57.67% (ΔSOC is about 2.67%), and 58.31% (ΔSOC is about 3.31%), respectively. Obviously, the presented EMS can ensure that the battery end-state SOC is close to its beginning state SOC. Compared with the other strategies, the SOC of proposed EMS has the smallest variation between the beginning state and end state, which helps to guarantee the stable and continuous operation of the hybrid electric vehicle [46].

- **Comparative analysis of the efficiency and hydrogen consumption**

The efficiency of the FC can be calculated by Eq. (2.19). Fig. 2.26 shows the efficiency curves of FCs under the control of different strategies. When using the proposed EMS, the average efficiency of the FC is 37.49%, which is 14.73% higher than that of the ECMS, 14.81% higher than that of the PF control strategy, and 9.65% higher than that of the SMC strategy. It can be seen that the proposed EMS can improve the operating efficiency of the FC and improve the system economy.

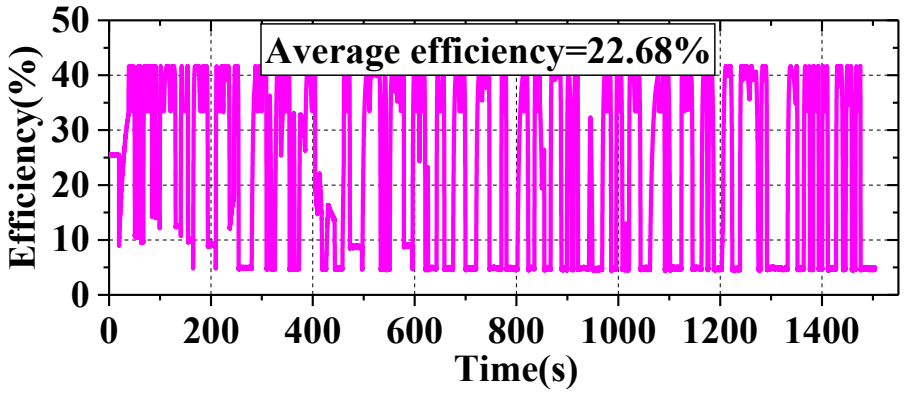

(a) PF control strategy

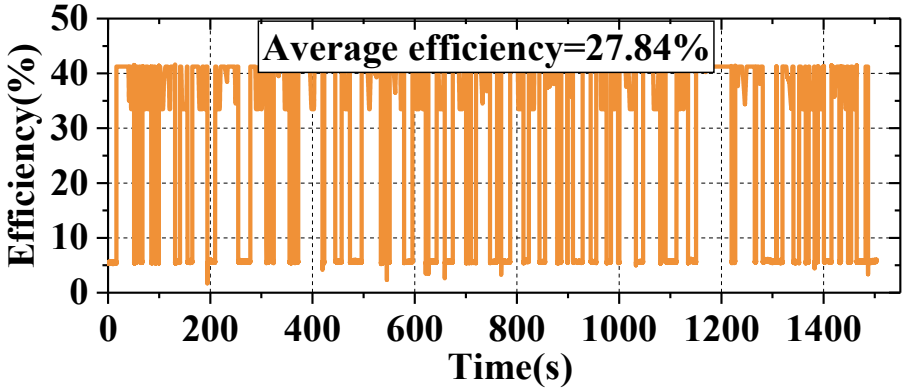

(b) SMC strategy

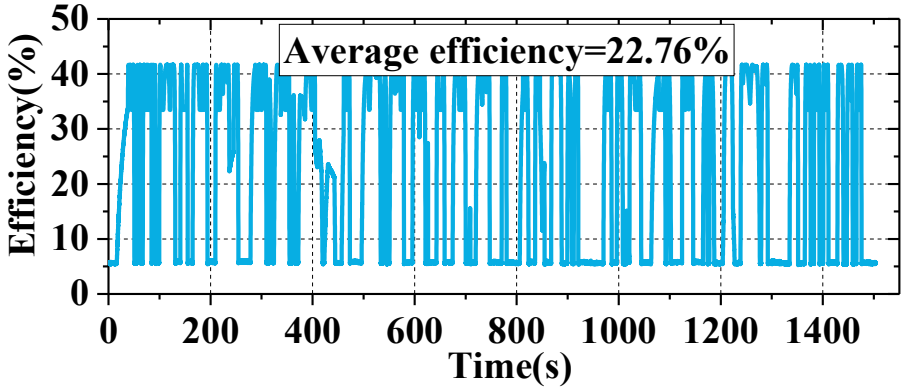

(c) ECMS

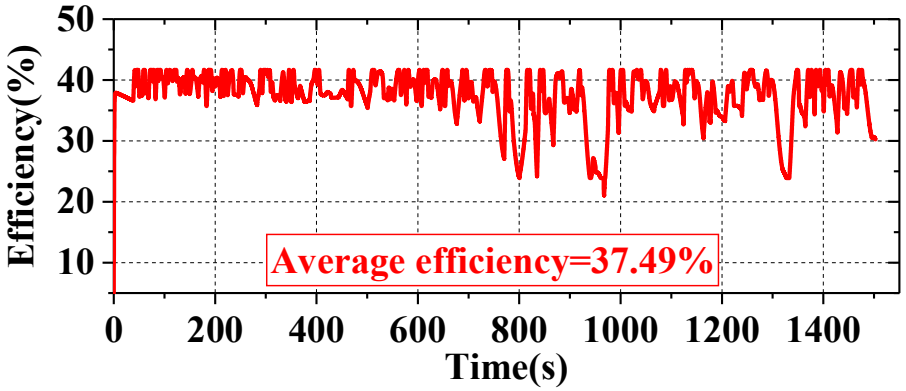

(d) The proposed optimal system economic EMS

Figure 2.26. Efficiency curves using different strategies.

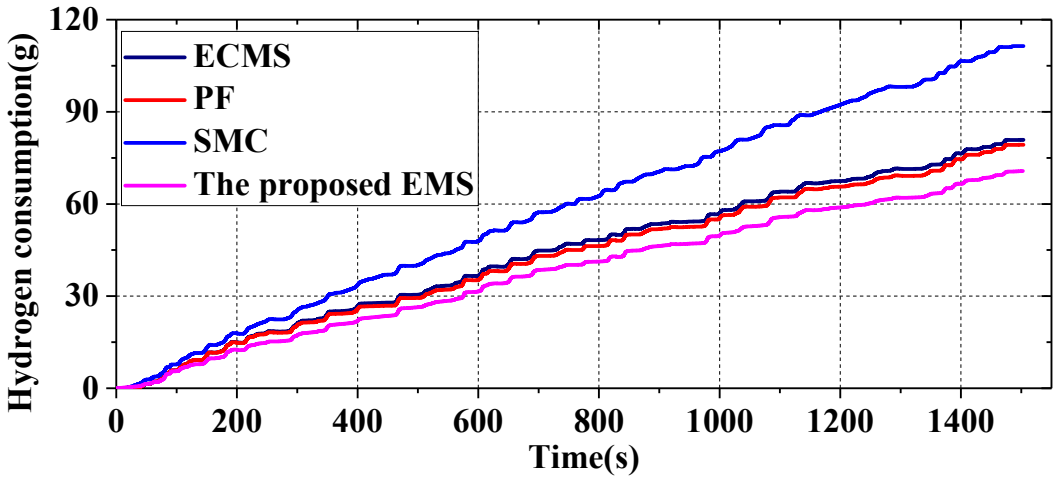

Figure 2.27. Total hydrogen consumption curves using different strategies.

In addition, by calculating the equivalent hydrogen consumption rate of the battery and the fuel consumption rate of the stack in real-time, the total amount of hydrogen consumption can be obtained, as shown in Fig. 2.27. The total mass of hydrogen consumed by the system using SMC strategy, PF control strategy, ECMS and the presented EMS is 111.39 g, 79.29 g, 76.83 g, and 70.73 g, respectively. It can be seen that in these strategies, the total hydrogen consumption of the presented EMS is the smallest.

- **Comparative analysis of the power sources operating stress**

It can be obtained from [27,47] that the smaller the operating stress, the smaller the frequency and amplitude of the power sources (battery and FC) output current and power variation, and the better it is to maintain power sources performance. In this thesis, the stress on each power supply is able to be decided by wavelet transform. The output power of battery and FC is decomposed by using the Haar wavelet transform which is securable in the MATLAB toolbox. This decomposition could be used as an especially effective tool to separate the high-frequency and low-frequency subassemblies [34]. The Haar wavelet transform is able to provide a filter to extract the characteristics of sharp changes and transient signals. In addition, the loss of signal edge information is minimized compared with the traditional filtering techniques. The average value of high-frequency subassembly of each power supply is close to zero, and the standard deviation δ of this component could provide a clear indication of how often each power supply is solicited [48]. Based on the output power curves of the battery (see Fig. 2.24), the operating stress analysis results of battery under the control of different strategies are presented in Fig. 2.28.

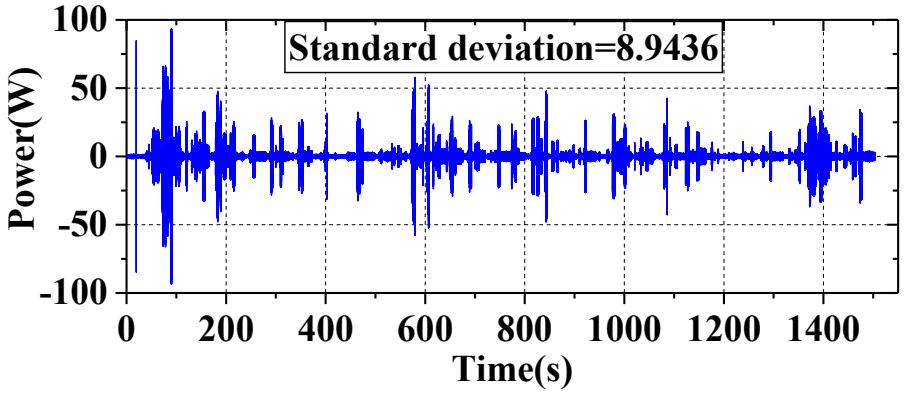

(a) PF control strategy

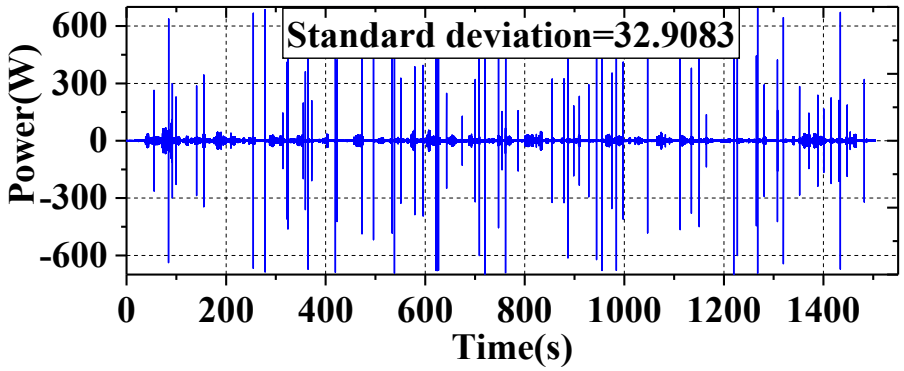

(b) SMC strategy

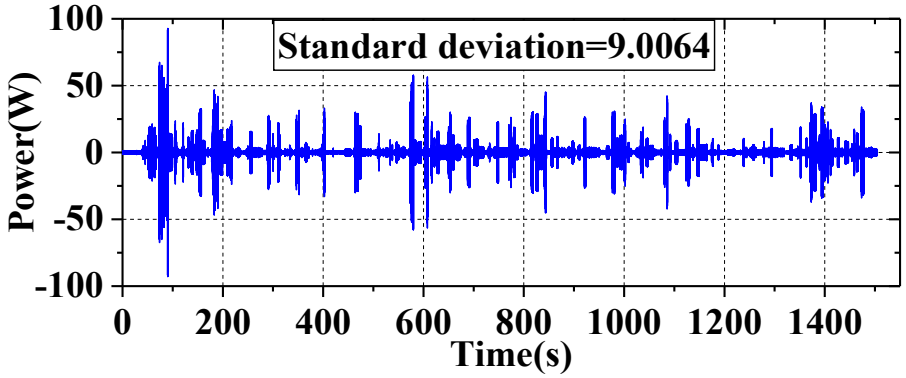

(c) ECMS

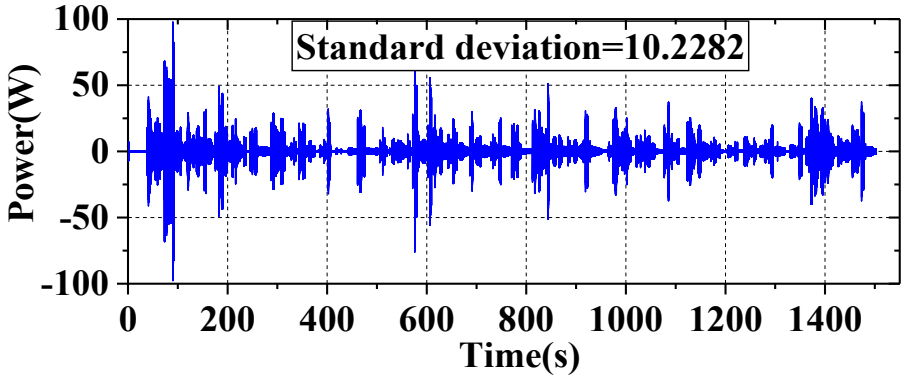

(d) The proposed optimal system economic EMS

Figure 2.28. Operating stress analysis of battery using different strategies.

Furthermore, based on the above description, the operating stress analysis results of FC using different strategies are depicted in Fig. 2.29.

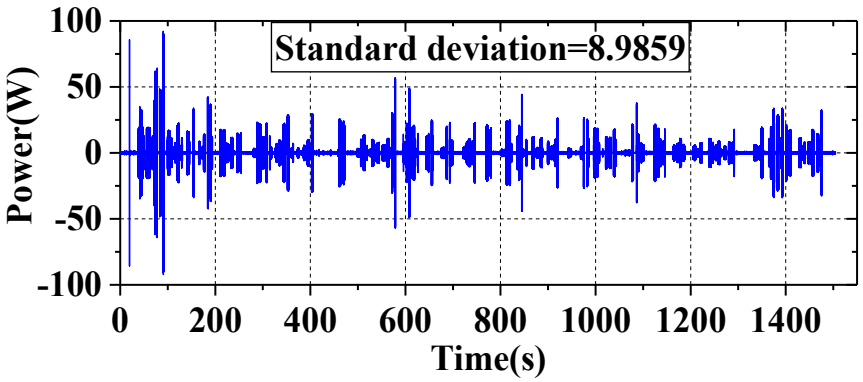

(a) PF control strategy

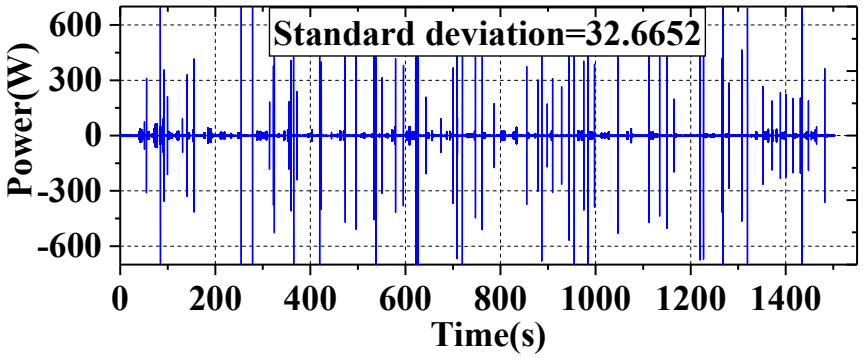

(b) SMC strategy

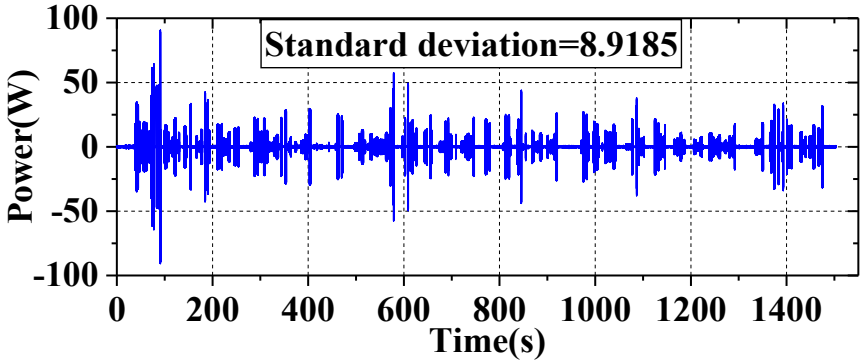

(c) ECMS

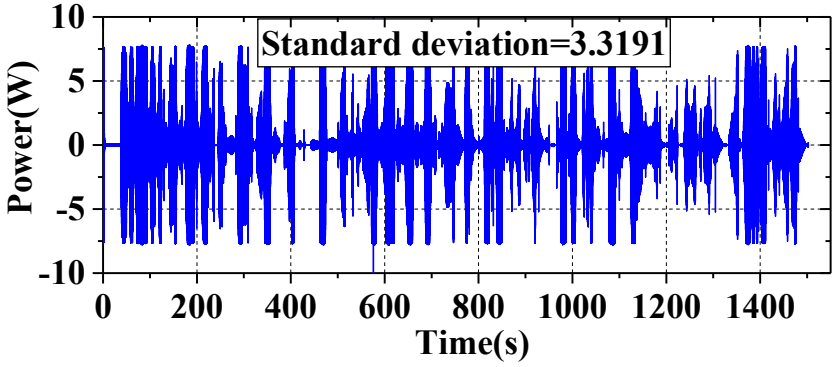

(d) The proposed optimal system economic EMS

Figure 2.29. Power fluctuation rate distribution of FC using different strategies.

As can be seen from Fig. 2.28 and Fig. 2.29, under the control of PF control strategy, the operating stress of the battery and the FC are 8.9436 and 8.9859, respectively. When controlled by the SMC strategy, the operating stress of the battery and the FC are 32.9083 and 32.6652, respectively. When using the ECMS, the operating stress of the battery and the FC are 9.0064 and 8.9185, respectively. Under the control of the presented EMS, the operating stress of the battery and FC are 10.2282 and 3.3191, respectively. It can be seen that compared with the other EMSs (PF, SMC, and ECMS), the operating stress of FC is the lowest under the control of the presented EMS. Thence, the presented strategy can effectively smooth the fluctuation of FC output power, thereby prolonging the lifetime of FC. Although the operating stress of battery is not the lowest, battery has the advantages of strong durability and long cycle lifespan, so it can be proved that the proposed optimal system economic EMS can improve the system lifetime.

- **Comparative analysis of the power sources lifetime degradation**

The state of health of the battery indicates the degree of lifetime degradation of the battery [49,50], according to the datasheet of the battery and Eq. (2.36), the lifetime degradation of the battery can be calculated when using different EMSs. The results are shown in Fig. 2.30. What's more, based on Eq. (2.37), the lifetime loss of FC caused by power fluctuation can be calculated. The voltage degradation of each stack when using different strategies is shown in Fig. 2.31.

It can be seen from the above figures that under the control of the proposed EMS, the FC lifetime degradation is the lowest. Although the lifetime degradation degree of the battery is not the lowest when the proposed EMS is used, the purchase cost of the battery is lower than that of FC, so it is generally beneficial to reduce the operating cost of the power sources in the HEV.

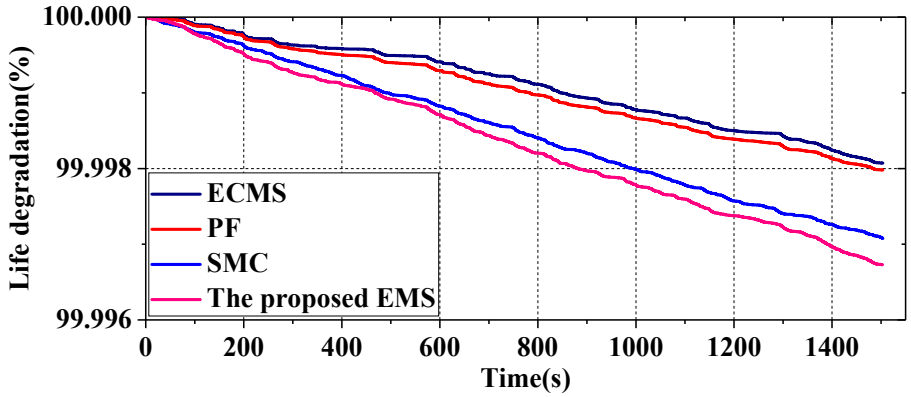

Figure 2.30. The state of health of battery when using different strategies.

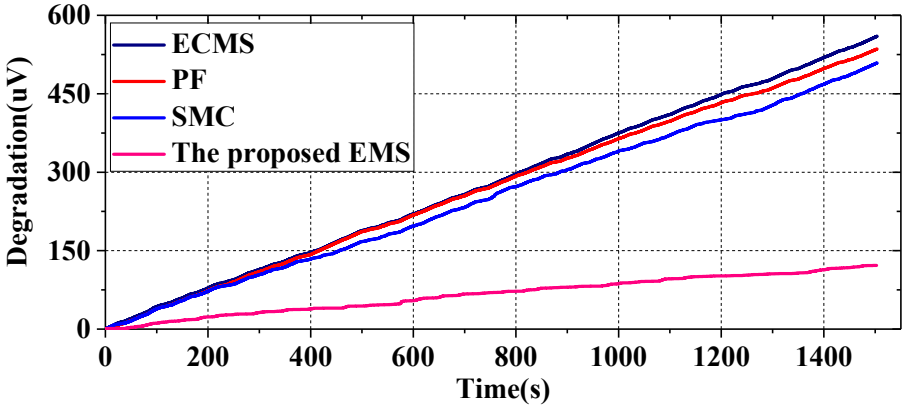

Figure 2.31. The voltage degradation of FC under the control of different strategies.

- **Comparative analysis of the system operating cost**

The main purpose of the method proposed in this chapter is to optimize the operating economy of the HEV, comprehensively consider the cost of power sources degradation, system hydrogen consumption and constrain the output power of the battery and stack. Based on the above analysis of power sources degradation cost and system hydrogen consumption, the system operating cost can be calculated as shown in Fig. 2.32 below.

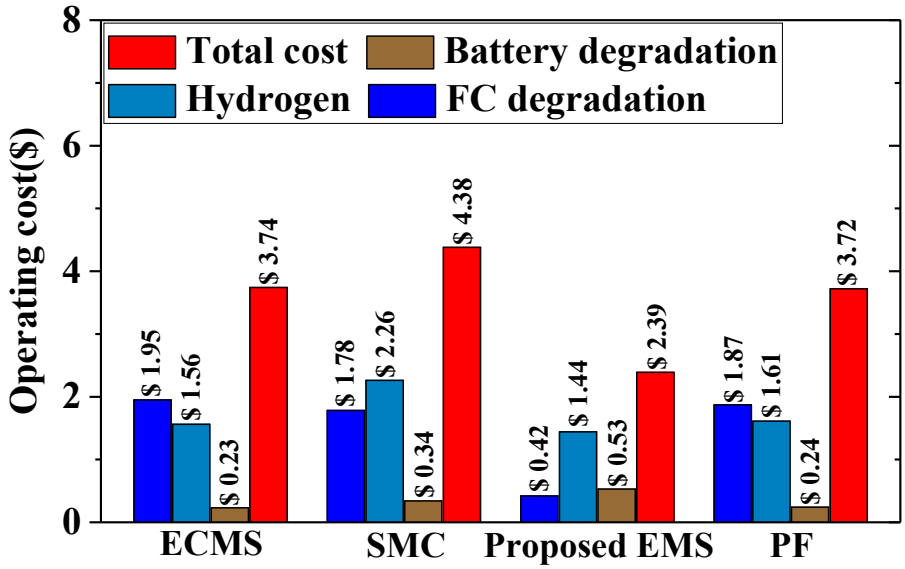

Figure 2.32. The operating cost of the HEV under the control of different strategies.

It can be seen from Fig. 2.32 that under the control of the proposed EMS, the battery degradation cost is $ 0.53, the FC degradation cost is $ 0.42, the system hydrogen consumption cost is $ 1.44 and the total system operating cost is $ 2.39. Besides, under the control of the SMC strategy, the battery degradation cost is $ 0.34, the stack degradation cost is $ 1.78, the system hydrogen consumption cost is $ 2.26 and the total operating cost is $ 4.38. What's more, under the control of the PF control strategy, the battery degradation cost is $ 0.24, the stack degradation cost is $ 1.87, the system hydrogen consumption cost is $ 1.61 and the total operating cost is $ 3.72. Furthermore, under the control of the

ECMS, the battery degradation cost is $ 0.23, the stack degradation cost is $ 1.95, the system hydrogen consumption cost is $ 1.56 and the total operating cost is $ 3.74. It can be seen that, compared with other strategies, the operating cost of the proposed method is the lowest.

TABLE 2.7. Performance comparative analysis of different strategies.

Parameter	SMC	ECMS	PF	Proposed EMS
SOC fluctuation	24.28%	3.31%	2.67%	1.91%
System hydrogen consumption	111.39 g	76.83 g	79.29 g	70.73 g
Operation efficiency	27.84%	22.76%	22.68%	37.49%
Battery operating stress	32.9083	9.0064	8.9436	10.2282
FC operating stress	32.6652	8.9185	8.9859	3.3191
Operating cost	$ 4.38	$ 3.74	$ 3.72	$ 2.39

In summary, to highlight the superiority of the presented EMS more clearly, all the results using different strategies are summarized in TABLE 2.7.

As shown in TABLE 2.7, among these strategies, the proposed EMS has advantages in terms of hydrogen consumption, operating stress, efficiency, SOC of battery, and operation cost. The experimental results demonstrate the effectiveness of the proposed EMS.

2.5. Conclusion

Through the study of existing energy management strategies in **Chapter 1**, in this chapter, an optimal system economic energy management strategy is proposed for the battery/fuel cell hybrid electric vehicle. Considering that in the hybrid power system, the operating cost of the power sources is high and the lifetime needs to be improved. Therefore, in order to further promote the use of hybrid power systems, this chapter studies the coupling relationship between lifetime degradation and output power of each power source by analyzing the impact of output power on power sources durability, and converts lifetime degradation into system operating costs. In addition, considering the equivalent hydrogen consumption cost of the battery during operation, a system operating cost function is formulated. In the cost function, the SOC fluctuation of the battery is also considered. In order to improve the operating efficiency and performance of the FC, a high-efficiency zone is also divided for the FC, and constraints are added to control the FC to operate in this zone as much as possible. Finally, in order to solve the formulated cost function, the SQP algorithm is used in this chapter. In order to verify the effect of the proposed EMS, the experimental verification is carried out on the built HIL test platform. The comparative analysis results show that the proposed EMS is superior to the results obtained by other energy management strategies in terms of power sources operating stress, operating efficiency, battery SOC fluctuation, system hydrogen consumption and system operating cost.

The **Chapter 2** discusses the application of energy management strategies in the light-duty HEV

powered by battery and FC. In addition, in the **Chapter 1**, we have studied the existing topologies of the hybrid power systems. On this basis, in order to discuss the application of hybrid power system in higher-power applications, in **Chapter 3**, we will further study the application of energy management strategies in a heavy-duty hybrid electric tram powered by supercapacitor and FC.

References

[1] N. Bizon, Load-following mode control of a standalone renewable/fuel cell hybrid power source, Energy Conversion and Management. 77 (2014) 763–772. https://doi.org/10.1016/j.enconman.2013.10.035.

[2] K. Ettihir, L. Boulon, K. Agbossou, Optimization-based energy management strategy for a fuel cell/battery hybrid power system, Applied Energy. 163 (2016) 142–153. https://doi.org/10.1016/j.apenergy.2015.10.176.

[3] T. Wang, Q. Li, X. Wang, Y. Qiu, M. Liu, X. Meng, J. Li, W. Chen, An optimized energy management strategy for fuel cell hybrid power system based on maximum efficiency range identification, Journal of Power Sources. 445 (2020) 227333. https://doi.org/10.1016/j.jpowsour.2019.227333.

[4] Q. Li, T. Wang, S. Li, W. Chen, H. Liu, E. Breaz, F. Gao, Online extremum seeking-based optimized energy management strategy for hybrid electric tram considering fuel cell degradation, Applied Energy. 285 (2021) 116505. https://doi.org/10.1016/j.apenergy.2021.116505.

[5] Q. Li, B. Su, Y. Pu, Y. Han, T. Wang, L. Yin, W. Chen, A State Machine Control Based on Equivalent Consumption Minimization for Fuel Cell/ Supercapacitor Hybrid Tramway, IEEE Trans. Transp. Electrific. 5 (2019) 552–564. https://doi.org/10.1109/TTE.2019.2915689.

[6] H. Li, A. Ravey, A. N'Diaye, A. Djerdir, Online adaptive equivalent consumption minimization strategy for fuel cell hybrid electric vehicle considering power sources degradation, Energy Conversion and Management. 192 (2019) 133–149. https://doi.org/10.1016/j.enconman.2019.03.090.

[7] T. Wang, Q. Li, X. Wang, W. Chen, E. Breaz, F. Gao, A Power Allocation Method for Multistack PEMFC System Considering Fuel Cell Performance Consistency, IEEE Trans. on Ind. Applicat. 56 (2020) 5340–5351. https://doi.org/10.1109/TIA.2020.3001254.

[8] M. Kandidayeni, J.P. Trovão, M. Soleymani, L. Boulon, Towards health-aware energy management strategies in fuel cell hybrid electric vehicles: A review, International Journal of Hydrogen Energy. 47 (2022) 10021–10043. https://doi.org/10.1016/j.ijhydene.2022.01.064.

[9] J. Jiang, Q. Jiang, J. Chen, X. Zhou, S. Zhu, T. Chen, Advanced Power Management and Control for Hybrid Electric Vehicles: A Survey, Wireless Communications and Mobile Computing. 2021 (2021) 1–12. https://doi.org/10.1155/2021/6652038.

[10] X. Meng, Q. Li, G. Zhang, T. Wang, W. Chen, T. Cao, A Dual-Mode Energy Management Strategy Considering Fuel Cell Degradation for Energy Consumption and Fuel Cell Efficiency Comprehensive Optimization of Hybrid Vehicle, IEEE Access. 7 (2019) 134475–134487. https://doi.org/10.1109/access.2019.2939047.

[11] T. Wang, Q. Li, W. Chen, Q. Li, A. Ravey, E. Breaz, F. Gao, Multi-Mode Power Allocation Strategy Based on Kalman Filter Algorithm for Hybrid Electric Vehicle, in: 2021 IEEE Transportation Electrification Conference & Expo (ITEC), IEEE, 2021. https://doi.org/10.1109/itec51675.2021.9490178.

[12] D. Zhou, A. Ravey, A. Al-Durra, F. Gao, A comparative study of extremum seeking methods applied to online energy management strategy of fuel cell hybrid electric vehicles, Energy Conversion and Management. 151 (2017) 778–790. https://doi.org/10.1016/j.enconman.2017.08.079.

[13] M.A. Roscher, D.U. Sauer, Dynamic electric behavior and open-circuit-voltage modeling of LiFePO4-based lithium ion secondary batteries, Journal of Power Sources. 196 (2011) 331–336. https://doi.org/10.1016/j.jpowsour.2010.06.098.

[14] A.A.-H. Hussein, I. Batarseh, An overview of generic battery models, in: 2011 IEEE Power and Energy Society General Meeting, IEEE, 2011: pp. 1–6.

[15] Z. Ni, R. Mével, H. Wang, M. Ouyang, Modeling of Auto-ignition of Gaseous Species formed during Lithium Battery Thermal Runaway, (n.d.).

[16] O. Tremblay, Experimental validation of a battery dynamic model for EV application, World Electric Vehicle Journal. 3 (2009) 1–10.
[17] C. Zhang, K. Li, S. Mcloone, Z. Yang, Battery modelling methods for electric vehicles-A review, in: 2014 European Control Conference (ECC), IEEE, 2014: pp. 2673–2678.
[18] C.L. Lin, D.Y. Wang, N.C. Shih, C.C. Chang, Field Demonstration of Hydrogen PEM Fuel Cell/Lithium-Ion Battery Hybrid Electric Scooters in Taiwan, Advanced Materials Research. 512–515 (2012) 1376–1379. https://doi.org/10.4028/www.scientific.net/amr.512-515.1376.
[19] T. Wang, Q. Li, L. Yin, W. Chen, E. Breaz, F. Gao, Hierarchical Power Allocation Method Based on Online Extremum Seeking Algorithm for Dual-PEMFC/Battery Hybrid Locomotive, IEEE Transactions on Vehicular Technology. 70 (2021) 5679–5692. https://doi.org/10.1109/tvt.2021.3078752.
[20] H. Li, A. Ravey, A. N'Diaye, A. Djerdir, A novel equivalent consumption minimization strategy for hybrid electric vehicle powered by fuel cell, battery and supercapacitor, Journal of Power Sources. 395 (2018) 262–270. https://doi.org/10.1016/j.jpowsour.2018.05.078.
[21] Z. Hong, Q. Li, Y. Han, W. Shang, Y. Zhu, W. Chen, An energy management strategy based on dynamic power factor for fuel cell/battery hybrid locomotive, International Journal of Hydrogen Energy. 43 (2018) 3261–3272. https://doi.org/10.1016/j.ijhydene.2017.12.117.
[22] Q. Li, T. Wang, C. Dai, W. Chen, L. Ma, Power Management Strategy Based on Adaptive Droop Control for a Fuel Cell-Battery-Supercapacitor Hybrid Tramway, IEEE Trans. Veh. Technol. 67 (2018) 5658–5670. https://doi.org/10.1109/TVT.2017.2715178.
[23] J. Larminie, A. Dicks, Fuel Cell Systems Explained, John Wiley & Sons, Ltd,., 2003. https://doi.org/10.1002/9781118878330.
[24] S.M. Njoya, O. Tremblay, L.-A. Dessaint, A generic fuel cell model for the simulation of fuel cell vehicles, in: 2009 IEEE Vehicle Power and Propulsion Conference, IEEE, 2009. https://doi.org/10.1109/vppc.2009.5289692.
[25] N.M. Souleman, O. Tremblay, L.-A. Dessaint, A generic fuel cell model for the simulation of Fuel Cell Power Systems, in: 2009 IEEE Power & Energy Society General Meeting, IEEE, 2009. https://doi.org/10.1109/pes.2009.5275853.
[26] X. Li, Z.-H. Deng, D. Wei, C.-S. Xu, G.-Y. Cao, Novel variable structure control for the temperature of PEM fuel cell stack based on the dynamic thermal affine model, Energy Conversion and Management. 52 (2011) 3265–3274. https://doi.org/10.1016/j.enconman.2011.05.013.
[27] T. Wang, Q. Li, Y. Qiu, L. Yin, L. Liu, W. Chen, Efficiency Extreme Point Tracking Strategy Based on FFRLS Online Identification for PEMFC System, IEEE Trans. Energy Convers. 34 (2019) 952–963. https://doi.org/10.1109/TEC.2018.2872861.
[28] X. Han, F. Li, T. Zhang, T. Zhang, K. Song, Economic energy management strategy design and simulation for a dual-stack fuel cell electric vehicle, International Journal of Hydrogen Energy. 42 (2017) 11584–11595. https://doi.org/10.1016/j.ijhydene.2017.01.085.
[29] P. Pei, H. Chen, Main factors affecting the lifetime of Proton Exchange Membrane fuel cells in vehicle applications: A review, Applied Energy. 125 (2014) 60–75. https://doi.org/10.1016/j.apenergy.2014.03.048.
[30] H. Chen, P. Pei, M. Song, Lifetime prediction and the economic lifetime of Proton Exchange Membrane fuel cells, Applied Energy. 142 (2015) 154–163. https://doi.org/10.1016/j.apenergy.2014.12.062.
[31] Z. Hua, Z. Zheng, E. Pahon, M.-C. Péra, F. Gao, Remaining useful life prediction of PEMFC systems under dynamic operating conditions, Energy Conversion and Management. 231 (2021) 113825. https://doi.org/10.1016/j.enconman.2021.113825.
[32] N. Marx, L. Boulon, F. Gustin, D. Hissel, K. Agbossou, A review of multi-stack and modular fuel cell systems: Interests, application areas and on-going research activities, International Journal of Hydrogen Energy. 39 (2014) 12101–12111. https://doi.org/10.1016/j.ijhydene.2014.05.187.
[33] X. Hu, J. Han, X. Tang, X. Lin, Powertrain Design and Control in Electrified Vehicles: A Critical Review, IEEE Transactions on Transportation Electrification. 7 (2021) 1990–2009. https://doi.org/10.1109/tte.2021.3056432.

[34] S.N. Motapon, L.-A. Dessaint, K. Al-Haddad, A Comparative Study of Energy Management Schemes for a Fuel-Cell Hybrid Emergency Power System of More-Electric Aircraft, IEEE Transactions on Industrial Electronics. 61 (2014) 1320–1334. https://doi.org/10.1109/tie.2013.2257152.
[35] L. Xu, J. Li, J. Hua, X. Li, M. Ouyang, Adaptive supervisory control strategy of a fuel cell/battery-powered city bus, Journal of Power Sources. 194 (2009) 360–368. https://doi.org/10.1016/j.jpowsour.2009.04.074.
[36] R. Xiong, H. Chen, C. Wang, F. Sun, Towards a smarter hybrid energy storage system based on battery and ultracapacitor - A critical review on topology and energy management, Journal of Cleaner Production. 202 (2018) 1228–1240. https://doi.org/10.1016/j.jclepro.2018.08.134.
[37] T. Wang, Q. Li, W. Chen, T. Liu, Application of energy management strategy based on state machine in fuel cell hybrid power system, in: 2017 IEEE Transportation Electrification Conference and Expo, Asia-Pacific (ITEC Asia-Pacific), IEEE, 2017. https://doi.org/10.1109/itec-ap.2017.8080854.
[38] R. Zhang, J. Tao, H. Zhou, Fuzzy Optimal Energy Management for Fuel Cell and Supercapacitor Systems Using Neural Network Based Driving Pattern Recognition, IEEE Transactions on Fuzzy Systems. 27 (2019) 45–57. https://doi.org/10.1109/tfuzz.2018.2856086.
[39] J. Han, J.-F. Charpentier, T. Tang, An Energy Management System of a Fuel Cell/Battery Hybrid Boat, Energies. 7 (2014) 2799–2820. https://doi.org/10.3390/en7052799.
[40] S. Onori, L. Serrao, G. Rizzoni, Hybrid Electric Vehicles, Springer London, 2016. https://doi.org/10.1007/978-1-4471-6781-5.
[41] J. Wang, P. Liu, J. Hicks-Garner, E. Sherman, S. Soukiazian, M. Verbrugge, H. Tataria, J. Musser, P. Finamore, Cycle-life model for graphite-LiFePO4 cells, Journal of Power Sources. 196 (2011) 3942–3948. https://doi.org/10.1016/j.jpowsour.2010.11.134.
[42] S. Zhang, X. Hu, S. Xie, Z. Song, L. Hu, C. Hou, Adaptively coordinated optimization of battery aging and energy management in plug-in hybrid electric buses, Applied Energy. 256 (2019) 113891. https://doi.org/10.1016/j.apenergy.2019.113891.
[43] Z. Song, H. Hofmann, J. Li, X. Han, X. Zhang, M. Ouyang, A comparison study of different semi-active hybrid energy storage system topologies for electric vehicles, Journal of Power Sources. 274 (2015) 400–411. https://doi.org/10.1016/j.jpowsour.2014.10.061.
[44] X. Lu, H. Wang, Optimal Sizing and Energy Management for Cost-Effective PEV Hybrid Energy Storage Systems, IEEE Transactions on Industrial Informatics. 16 (2020) 3407–3416. https://doi.org/10.1109/tii.2019.2957297.
[45] S.K. Eldersveld, Large-scale sequential quadratic programming algorithms, Office of Scientific and Technical Information (OSTI), 1992. https://doi.org/10.2172/10102731.
[46] Y. Yan, Q. Li, W. Chen, B. Su, J. Liu, L. Ma, Optimal Energy Management and Control in Multimode Equivalent Energy Consumption of Fuel Cell/Supercapacitor of Hybrid Electric Tram, IEEE Transactions on Industrial Electronics. 66 (2019) 6065–6076. https://doi.org/10.1109/tie.2018.2871792.
[47] T. Wang, Q. Li, H. Yang, L. Yin, X. Wang, Y. Qiu, W. Chen, Adaptive current distribution method for parallel-connected PEMFC generation system considering performance consistency, Energy Conversion and Management. 196 (2019) 866–877. https://doi.org/10.1016/j.enconman.2019.06.048.
[48] Q. Li, W. Chen, Z. Liu, M. Li, L. Ma, Development of energy management system based on a power sharing strategy for a fuel cell-battery-supercapacitor hybrid tramway, Journal of Power Sources. 279 (2015) 267–280. https://doi.org/10.1016/j.jpowsour.2014.12.042.
[49] M.F. Zia, E. Elbouchikhi, M. Benbouzid, Optimal operational planning of scalable DC microgrid with demand response, islanding, and battery degradation cost considerations, Applied Energy. 237 (2019) 695–707. https://doi.org/10.1016/j.apenergy.2019.01.040.
[50] V.-V. Thanh, W. Su, B. Wang, Optimal DC Microgrid Operation with Model Predictive Control-Based Voltage-Dependent Demand Response and Optimal Battery Dispatch, Energies. 15 (2022) 2140. https://doi.org/10.3390/en15062140.

Chapter 3. Online extremum seeking-based optimized energy management strategy for a heavy-duty hybrid electric tram

3.1. Introduction

As discussed in **Chapter 1** and **Chapter 2**, the energy management strategy (EMS) is one of the key technologies for hybrid power system, which can achieve the purpose of improving system efficiency and ameliorating fuel economy by optimizing the energy flow of each power source in real time. The **Chapter 2** focuses on studying EMSs for a light-duty electric vehicle power by battery and fuel cell (FC), and verifies the effectiveness of the proposed strategy on a hardware-in-the-loop test platform. Whereas, in high-power applications such as heavy-duty trams and ships, the powertrain may be composed of supercapacitor (SC) and FC [1–4]. In addition, considering that with the operation of the system, the performance of the power sources in the actual system will degrade and lead to the change of its optimal operating point, which cannot be well reflected on the simulation platform. Therefore, in order to further study the EMSs of the hybrid power system powered by other topologies on the experimental test platform, this chapter adopts the SC as the energy storage system. Since the SC has the shortcoming of low energy density, in order to ensure that the tram can operate continuously and stably, the final SOC of the SC should be consistent with the initial SOC of the SC [5].

Based on the above description and our previous work [3,6], the main purpose of this chapter is to present an online extremum seeking-based optimized EMS for a SC/FC hybrid electric tram. This strategy considers that the performance of the FC will vary with the operating conditions, so an online extremum seeking is used to estimate the maximum efficiency (ME) and maximum power (MP) operating points of the FC. Furthermore, in order to guarantee the stable and continued operation of the electric tram, the SOC fluctuation range of SC is limited in this chapter. In order to test the performance of the presented EMS in hybrid electric tram, a reduced-scale test platform powered by the SC and FC is established.

The remainder of this chapter has the following structure. The main components of the hardware experimental platform are presented in section 3.2. Section 3.3 elaborates the proposed energy management strategy. Experimental verification and results analysis is performed in section 3.4. Finally, the main conclusions and perspectives of this chapter are discussed in section 3.5.

3.2. System structure and experimental test platform

A 100% low floor light rail vehicle (LF-LRV) presented in this chapter is the world's first commercial SC/FC hybrid electric tram and is jointly developed by Chinese manufacturer of Tangshan Railway Vehicle Co. Ltd and Clean Energy Lab of Southwest Jiaotong University in 2017 [2,3]. This hybrid electric tram and its main components are depicted in Fig. 3.1. It includes two DC/DC converters, a SC,

a FC stack, some auxiliary systems, and a power distribution controller. The primary components and parameters of this tram are shown in TABLE 3.1.

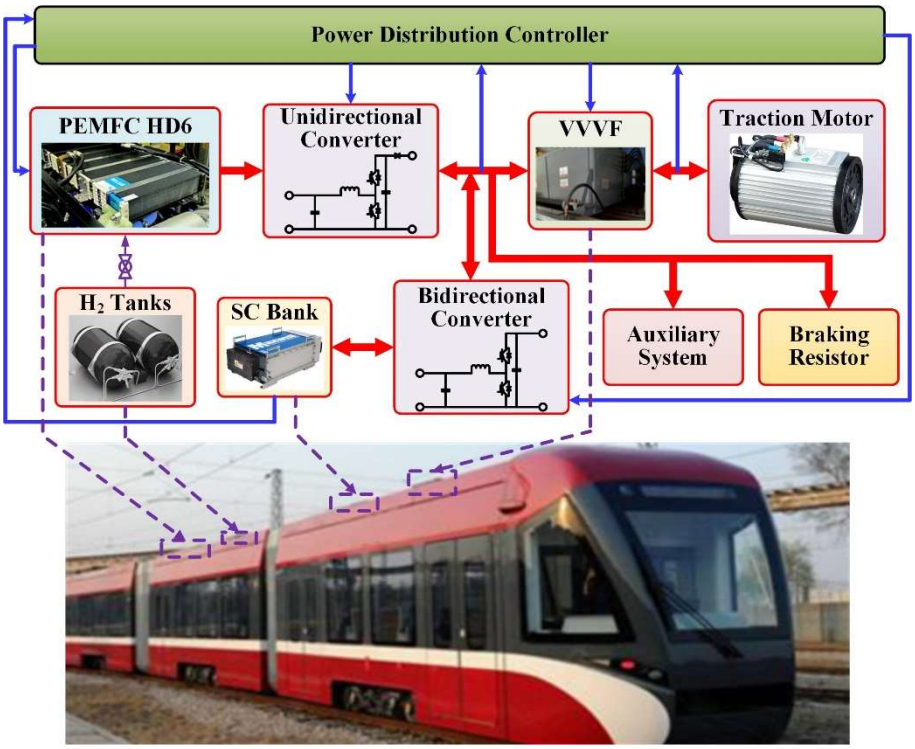

Figure 3.1. The SC/FC hybrid electric tram and its main components.

TABLE 3.1. Primary components and parameters of the hybrid electric tram.

Hybrid electric tram			
Tram weight	51.06 t	Axle weight	10.5 t
Max speed	30 kM/h	Bus voltage	750 V
Size	30.19*2.65*3.5 m^3	Capacity	300 persons
Supercapacitor			
Manufacturer	Maxwell (BMOD0615)	Current	-300-700 A
Voltage	200-528 V	Capacity	45 F
Weight	335 kG	Set Numbers	11 series & 3 parallel
FC			
Rated power	150 kW	Cell number	762
Voltage	530-710 V	Max current	320 A
Weight	305 kG	Hydrogen pressure	2.24 Bar

The SC is utilized as the power source to provide fast peak power or recover the braking power for this tram. In addition, the FC is used as the power supply to deliver the continuous and stable power demand for the tram [3,7,8]. Considering that the use of the tram directly to verify the strategy presented in this chapter is unsafe and uneconomical [9], and in order to truly reflect the changes in the operating performance of the FC to verify the effect of the proposed method, I build a reduced-scale experimental

platform in this chapter. Furthermore, the main hardware parts of the system will be described in detail in the following sections.

3.2.1. Design of the main components of the system

3.2.1.1. DC/DC converter hardware design

The main purpose of this chapter is to study the power distribution strategies for the hybrid electric tram. In order to simplify the design and manufacture of the hardware circuit, the DC/DC converter in this study adopts the non-isolated DC Buck-Boost converter (Niqor) from SynQor Company. The model is NQ60W60 (see Fig. 3.2), and its operating parameters are shown in TABLE 3.2.

TABLE 3.2. Primary parameters of the DC/DC converter module.

Parameter	Value	Parameter	Value
Operating efficiency	>90%	Input voltage range	9-60 V
Output voltage range	9-60 V	Output power range	0-2400 W
Maximum input current	40 A	Mass	158.2 g

Figure 3.2. DC/DC converter module NQ60W60.

Since the Niqor has a current sharing function, according to the system power requirements, multiple modules can be connected in parallel to increase the output power of the DC/DC converter, and the Niqor can be electrically configured, as shown in Fig. 3.3.

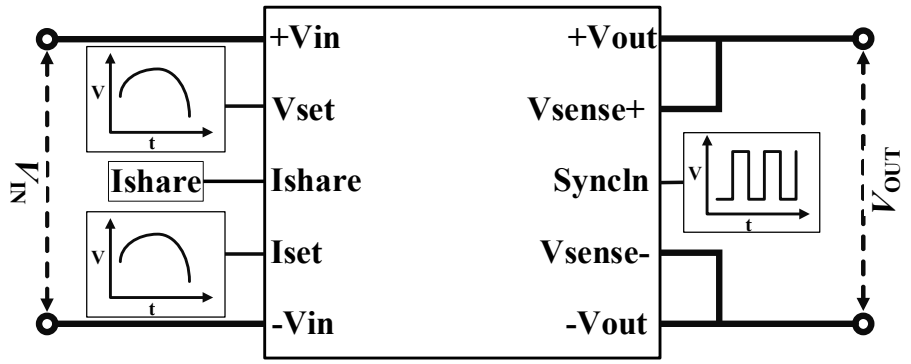

Figure 3.3. Niqor pin electrical configuration.

As shown in Fig. 3.3, the power supply output ports are connected to +Vin and -Vin of the module, and +Vout and -Vout are respectively connected to the positive and negative poles of the load. Vsense+ and Vsense- are used for module internal voltage signal acquisition. Syncln is used to provide the clock square wave of 200-300 KHz for the internal signal, which is generated by the PWM generation unit of DSP in this study. Ishare is used to control all Niqor modules to achieve an equal distribution of the power supply output current, which can be used to increase the power level of the converter. In addition, Vset is used to set the reference output voltage of Niqor, which determines the value of Vout, and the voltage input to the Iset pin determines the maximum output current of a single module. It can be known from the data sheet that they satisfy the functional relationship shown in Eq. (3.1).

$$\begin{cases} V_{\text{Iset}} = 0.0953 + 2.085 * \dfrac{I_{\text{set}}}{I_{\text{max}}} \\ V_{\text{Vset}} = 2.366 - 2.316 * \dfrac{V_{\text{set}}}{V_{\text{max}}} \end{cases} \tag{3.1}$$

where V_{Iset} represents the voltage input to the Iset pin, V_{Vset} represents the set maximum output current of the module, and I_{max} represents the maximum output current of the module. In this study, I_{max} is 40 A. In addition, V_{Vset} represents the voltage of the input Vset pin, V_{set} represents the output reference voltage of the module, and V_{max} represents the maximum output voltage of the module. In this study, the V_{max} is 60 V. The physical picture of the built DC/DC converter for cascading FC is shown in Fig. 3.4(a). In addition, the physical picture of the built DC/DC converter for connecting the SC and bus is shown in Fig. 3.4(b).

(a) DC/DC converter for FC (b) DC/DC converter for SC

Figure 3.4. The designed DC/DC converters.

3.2.1.2. Sampling conditioning circuit design

After the DC/DC converters are built, the output voltage and current of each power source and the output voltage and current signals of the converters need to be sampled and collected into the controller, so as to analyze the operating characteristics of each power source and design an energy management strategy.

The input voltage range of the A/D conversion unit of the controller (TMS320F28335) used in this paper is 0-3 V, so the controller cannot directly collect the voltage and current signals of each part, and the voltage matching needs to be achieved through the sampling conditioning circuit.

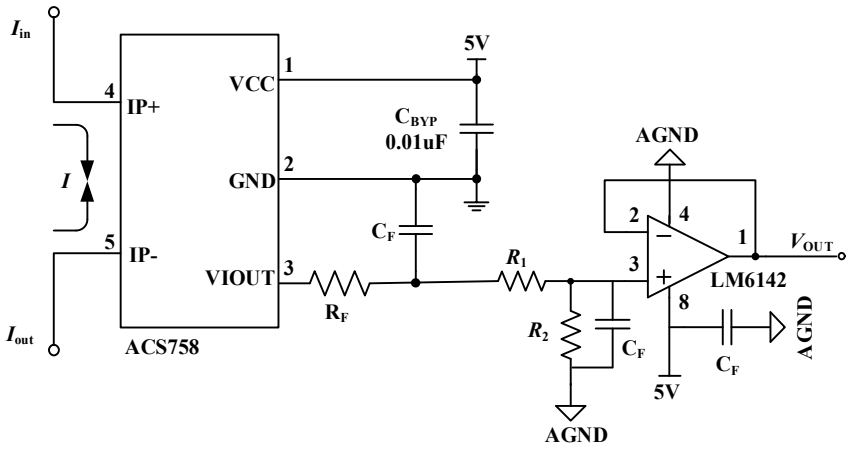

Figure 3.5. The current sampling conditioning circuit.

As can be seen from the above description, the SC and FC output current, DC/DC converter output current and the DC output current need to be collected and analyzed. The current sensor adopts ACS758 provided by Allegro Company, its maximum measurement current can reach 100 A, and the power supply voltage is 5 V. The designed current sampling and conditioning circuit is shown in Fig. 3.5.

In addition, the voltage acquisition and conditioning circuit is also an indispensable part of this study. The voltages to be acquired include the SC output voltage, the DC bus voltage and the FC output voltage. The voltage acquisition and conditioning circuit designed in this study is shown in the figure below.

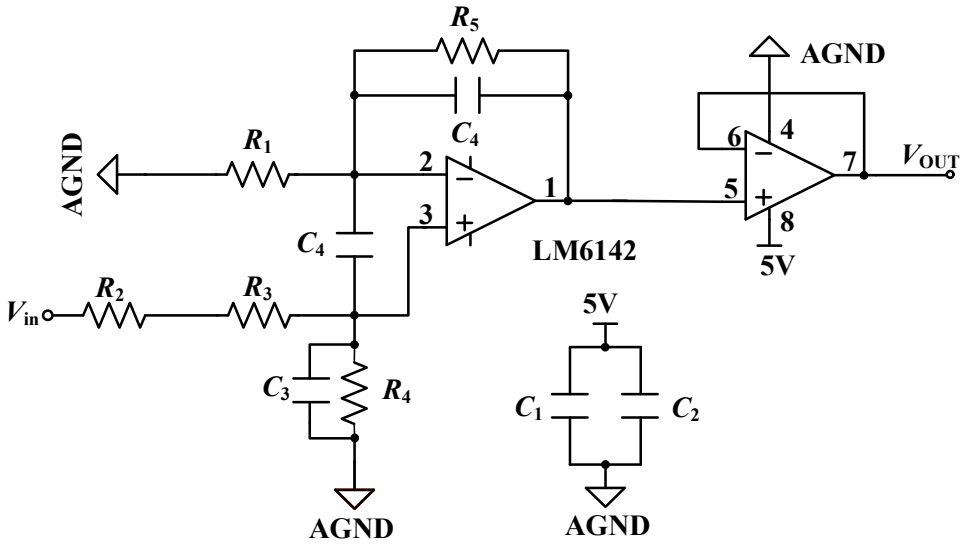

Figure 3.6. The voltage sampling conditioning circuit.

3.2.1.3. Core control circuit design

The control circuit used in this chapter is mainly composed of TMS320F28335 controller, D/A conversion circuit and display interface circuit. After analyzing the collected electrical signals in the DSP controller, this study uses the SPI communication to control the TLV5638 to realize D/A conversion, and then controls the DC/DC converter to output the reference power (refer to Eq.(3.1)) to complete the implementation of the EMSs. The built core control circuits are shown in Fig. 3.7.

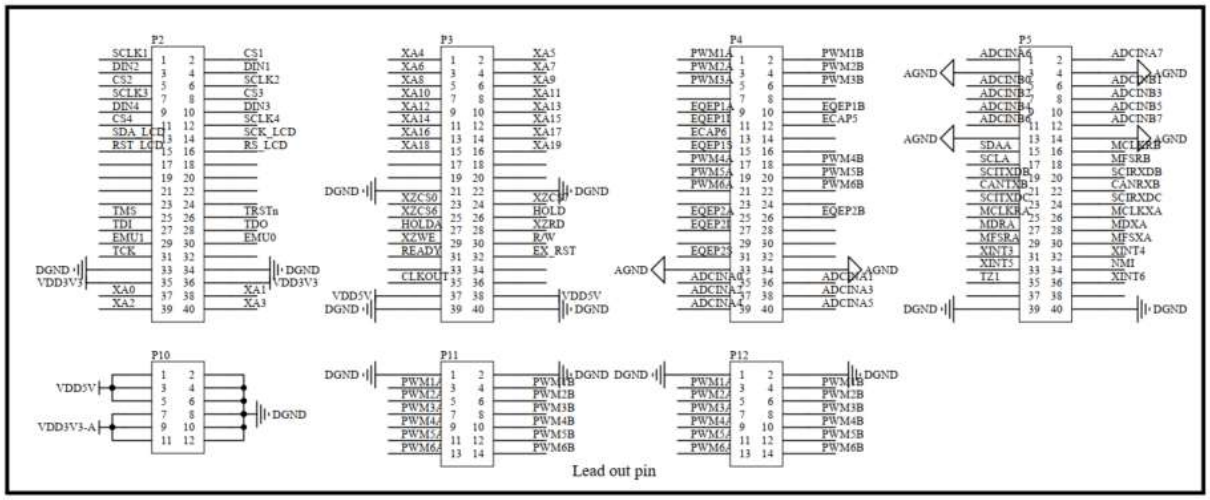

(a) Control interface circuit

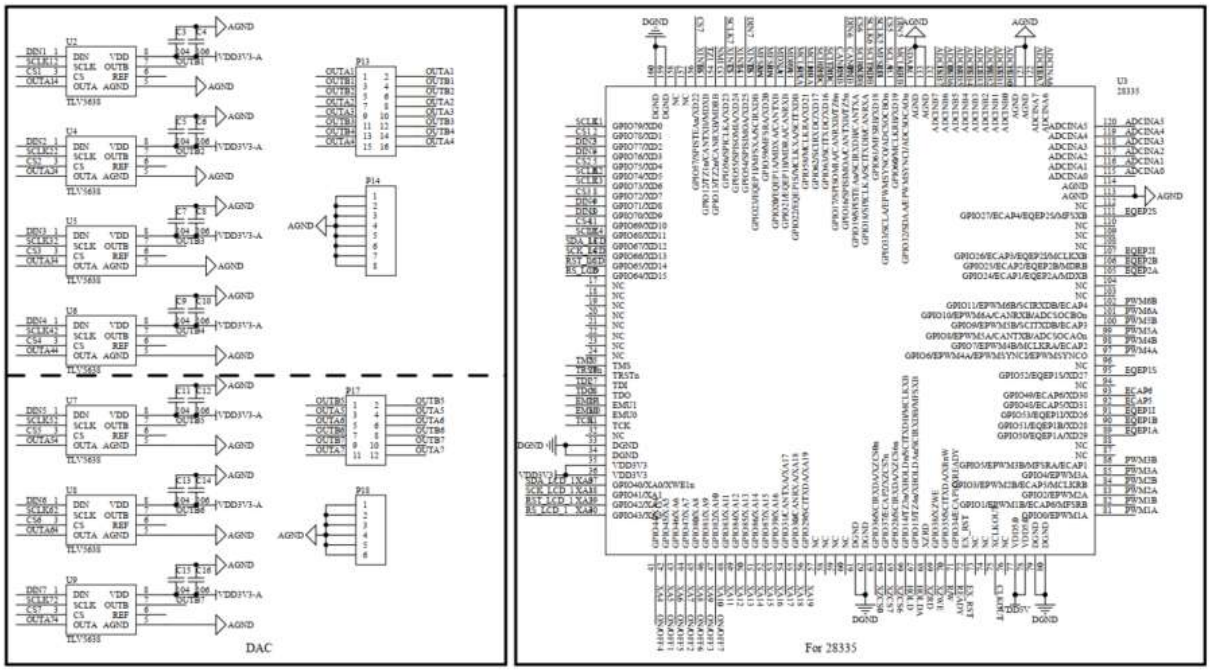

(b) DSP system circuit

Figure 3.7. The core control circuit design.

3.2.1.4. Auxiliary power supply circuit design

In this chapter, since the power sources voltages required by chips with different functions are

inconsistent, in order to ensure the normal and stable operation of each circuit, different auxiliary power supply systems need to be designed. This chapter requires two auxiliary power supplies, 3.3 V and 5 V. In order to simplify the hardware circuit, choose URB4805YMD provided by MORNSUN Company and AMS1117-3.3 provided by Advanced Monlithic Systems Inc. to meet the auxiliary power supply requirements. The designed power supply system circuit is shown in Fig. 3.8. The input voltage range of URB4805YMD module is 18-75 V, and the maximum output current can reach 2 A, which can ensure the power supply requirements of chips in all auxiliary systems. In addition, AMS1117-3.3 has good voltage regulation capability, in this system it only provides 3.3 V stable voltage for DSP controller.

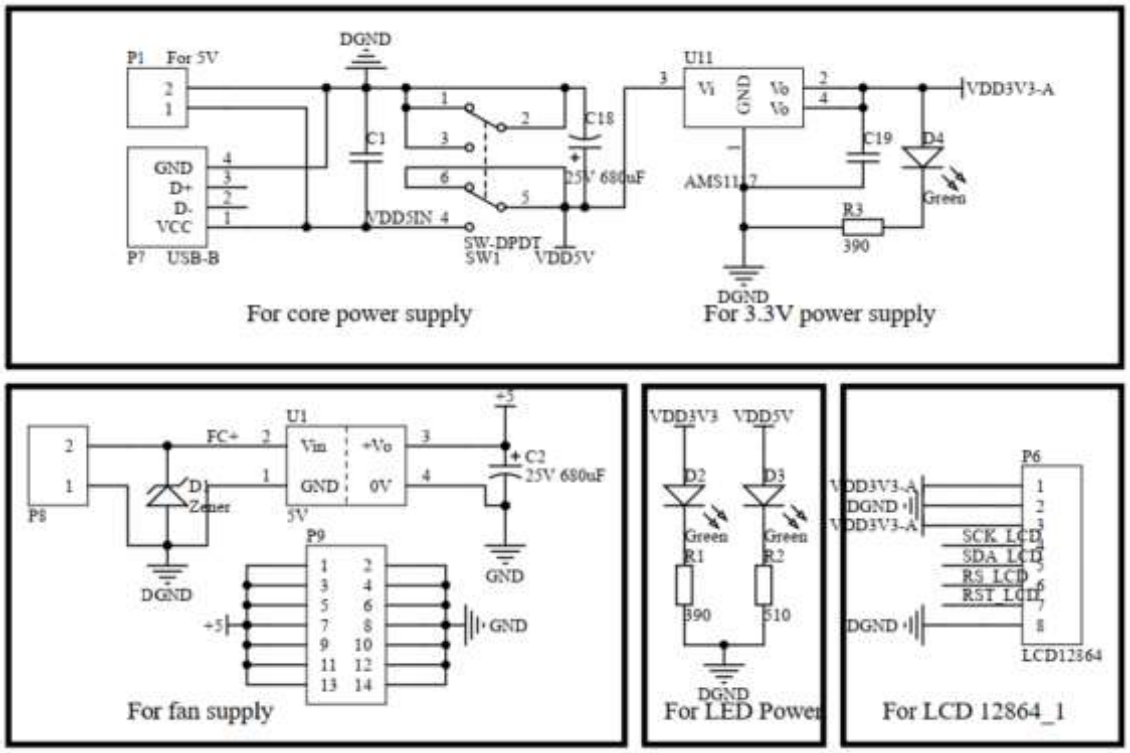

Figure 3.8. Auxiliary power supply circuit.

3.2.2. Hybrid power reduced-scale experimental bench

On the basis of completing the above hardware circuit design, according to the system topology structure (see Fig. 3.1), this chapter builds a hardware reduced-scale experimental platform as shown in Fig. 3.9. The key parameters of the power sources and the established DC/DC converters will be described in detail. In addition, the voltage and current signals of all power supplies are acquired and recorded by the NI-DAQ. Moreover, the ITECH's electrical load (IT-E502) and DC power supply (IT6522C) are used in this chapter to simulate the actual scaled-down hybrid electric tram drive cycle. In order to more clearly express the power and signal flow relationship between the components in the Fig. 3.9, the hardware structure diagram shown in Fig. 3.10 is given.

To test and verify the effectiveness of the proposed EMS, a FC stack with rated power of 1.3 kW

produced by Sunlait Company is employed in this study, and the model of this stack is S-1300. In addition, the EMSs and control algorithms of all hardware experiments in this study are implemented in DSP. This chapter uses Labview to develop a visual host computer software, and controls the electronic load and power supply through the RS232 protocol to simulate the actual scaled-down hybrid electric tram drive cycle.

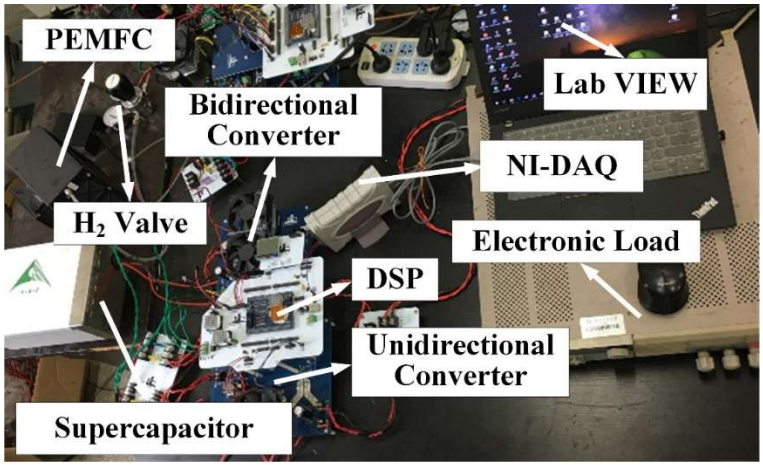

Figure 3.9. The established reduced-scale experimental bench.

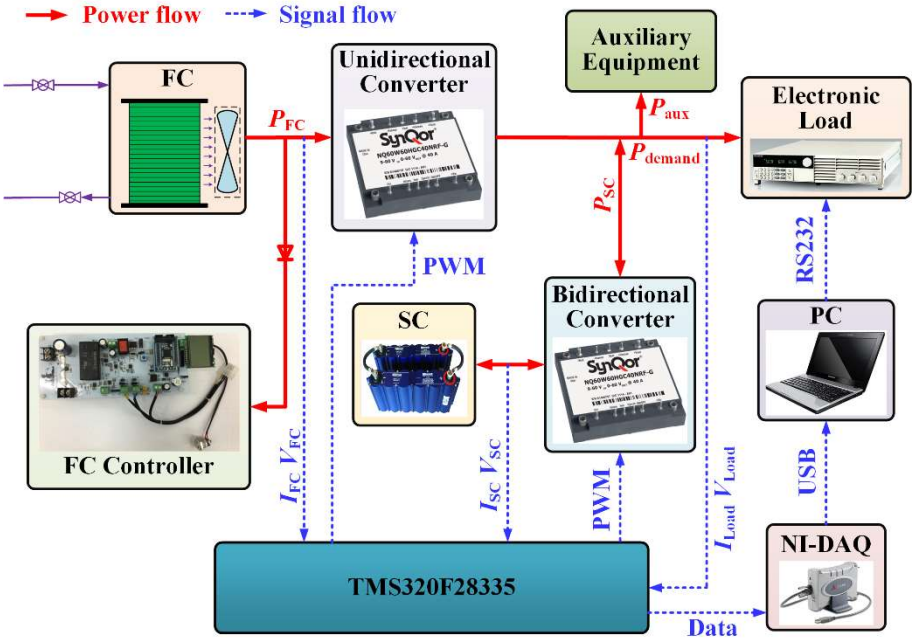

Figure 3.10. The established reduced-scale experimental bench system structure.

In the designed experimental platform, this chapter utilizes a SC and a FC for experimental testing. In addition, the primary parameters of SC and FC utilized in this chapter are listed in TABLE 3.3.

TABLE 3.3. Primary parameters of the SC and FC.

SC			
Rated capacitance	58 F	Rated voltage	32 V
Specific power	6 Wh/kg	Mass	4.3 kg
FC			
Output voltage	23-38 V	Rated current	54.2 A
Rated power	1.3 kW	Max current	58.3 A

To improve the performance of FC, the stack should work in the "safe operating zone" (bound by the stack's maximum efficiency (ME) and the maximum power (MP) points) as much as possible [10,11]. According to **Chapter 2** (see **Section 2.2.3**), the efficiency curves of S-1300 can be obtained, and the "safe operating zone" is shown in Fig. 3.11. Based on the investigation in **Chapter 1** and our previous research [3,12], it can be seen that this zone is movable. Therefore, this chapter needs to adopt the online identification algorithm to estimate the ME point and MP point.

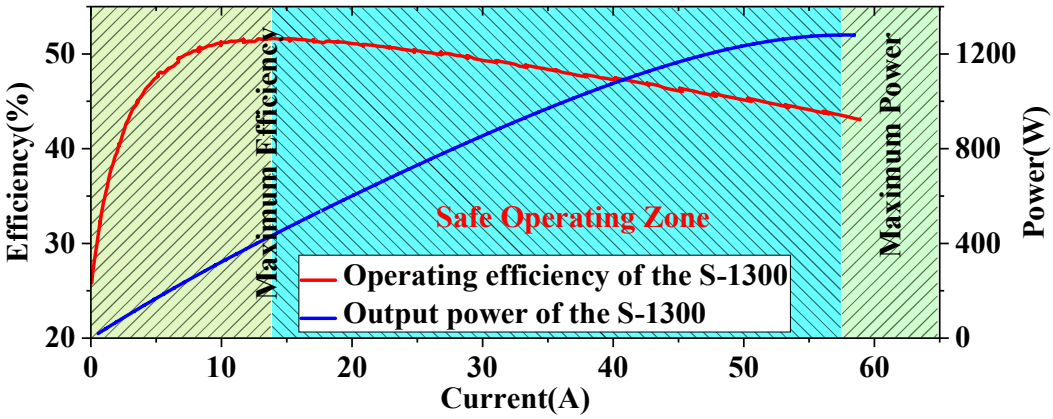

Figure 3.11. Efficiency curves and the "safe operating zone".

As previously described, a SC is used as an energy storage system to recover braking power or provide the rapidly changing power. The SOC of SC is a particularly important indicator for power distribution method, and this parameter can be calculated by the following equations [3,4]:

$$SOC(t+1) = SOC(t) + \Delta SOC(t) \tag{3.2}$$

with:

$$\Delta SOC(t) = \frac{\int_{t-1}^{t} I_{SC}\,dt}{C_{SC} V_{SC,rate}} \tag{3.3}$$

where C_{SC}, I_{SC}, and $V_{SC,rate}$ present the SC capacity, output current of SC, and rated voltage of SC, respectively. To simplify the calculation and speed up the control, the functional relationship between the output voltage and the current of the stack can be expressed by Eq. (3.4).

$$V_{FC} = f_1(I_{FC}) = \mathrm{X} \times \mathrm{A}^{\mathrm{T}} \tag{3.4}$$

with:

$$\begin{cases} \mathrm{X} = \left[I_{\mathrm{FC}}^{n} \quad \cdots \quad I_{\mathrm{FC}} \quad 1 \right] \\ \mathrm{A} = \left[a_n \quad \cdots \quad a_1 \quad a_0 \right] \end{cases} \tag{3.5}$$

where I_{FC} represents the stack's output current and V_{FC} denotes the output voltage of stack. In addition, the functional relationship between the operating efficiency and the current of the stack can be expressed by:

$$\eta_{\mathrm{FCS}} = f_2\left(I_{\mathrm{FC}}\right) = \mathrm{B} \times \mathrm{A}^{\mathrm{T}} \tag{3.6}$$

with:

$$\mathrm{B} = \left[b_n \quad \cdots \quad b_1 \quad b_0 \right] \tag{3.7}$$

where η_{FCS} is the efficiency of the FC system. In addition, the fuel consumption of the FC can be expressed by the polynomial fitting function of I_{FC}, as shown in following:

$$C_{\mathrm{FCS}} = f_3\left(I_{\mathrm{FC}}\right) = \mathrm{C} \times \mathrm{A}^{\mathrm{T}} \tag{3.8}$$

with:

$$\mathrm{C}_1 = \left[c_n \quad \cdots \quad c_1 \quad c_0 \right] \tag{3.9}$$

where C_{FCS} is the hydrogen consumption of the FC power generation system. In addition, according to the description in the **Chapter 2**, the coefficients (A and B) will change with the operation of the system. Therefore, in order to obtain the optimal operating area and operating point more accurately, it is necessary to use an online identification algorithm to update these parameters in real time in order to track these extreme points online. This online identification technique will be described in the following section.

3.3. Online extremum seeking-based optimized energy management strategy

To realize optimal power allocation between the SC and FC in the hybrid electric tram, so that the fuel consumption can be reduced and the performance of each power source can be improved, this chapter considers the factors such as SOC fluctuation constraint of SC and power sources output power constraints. In addition, considering that the operating performance of the hybrid power system will change with the external conditions, the operation polarization curves should also be identified. Therefore, the main purpose of online identification algorithm presented in this chapter is to estimate the boundary values of the "safe operating zone". Moreover, in order to highlight the superiority of the proposed strategy, the equivalent consumption minimization strategy (ECMS) and the state machine control (SMC) strategy are used for comparative analysis.

3.3.1. Design of the proposed EMS

In order to realize the purpose of minimizing fuel consumption and being able to manage power allocation between SC and FC in real-time, a power distribution strategy is developed with reference to the ECMS. The core step of the ECMS is to convert the electric energy consumption by the energy storage system into equivalent fuel consumption, and the main purpose of the ECMS is to reduce the hybrid system's total fuel consumption [13,14]. The total instantaneous fuel consumption of the system (C_{sys}) can be defined as the sum of the indirect equivalent fuel consumption of SC (C_{SC}) and the direct fuel consumption of the FC (C_{FC}). The instantaneous fuel consumption can be expressed by the following mathematical expression:

$$C_{sys}(t) = C_{FC}(t) + C_{SC}(t) = f_1\left(P_{FC}(t)\right) + f_2\left(P_{SC}(t)\right) \tag{3.1}$$

In Eq. (3.1), P_{SC}(t) and P_{FC}(t) are real-time output power of SC and FC, respectively. The $f_1(P_{FC}(t))$ can be obtained by [15]:

$$f_1\left(P_{FC}(t)\right) = \frac{P_{FC}(t)}{\Delta H_{LHV}\eta_{FCS}(t)} \tag{3.2}$$

In addition, the equivalent fuel consumption of SC can be calculated by the SOC of SC and output power of SC [4], thus, the $f_2(P_{SC}(t))$ can be calculated by:

$$f_2\left(P_{SC}(t)\right) = \begin{cases} \dfrac{P_{SC}(t)}{\Delta H_{LHV}\eta_{Bdc/dc}\eta_{FCS,avg}\eta_{dis}(t)\eta_{chg,avg}} & P_{SC}(t) \geq 0 \\ \dfrac{P_{SC}(t)\eta_{chg}(t)\eta_{dis,avg}}{\Delta H_{LHV}\eta_{Bdc/dc}\eta_{FCS,avg}} & P_{SC}(t) < 0 \end{cases} \tag{3.3}$$

In this equation, $\eta_{FCS,avg}$ represents FC average efficiency, $\eta_{dis,avg}$ and $\eta_{chg,avg}$ denote the average discharge and charge efficiency of SC, respectively, and $\eta_{Bdc/dc}$ represents the bidirectional converter efficiency. In addition, η_{dis}(t) and η_{chg}(t) represent the discharge and charge efficiency of SC, respectively. The efficiency of SC can be expressed by [2]:

$$\eta_{SC}(t) = \begin{cases} \eta_{dis}(t) = \dfrac{1}{2}\left(1 + \sqrt{1 - \dfrac{4R_{SC}P_{SC}(t)}{U_{OCV}^2}}\right) \\ \eta_{chg}(t) = 2\Big/\left(1 + \sqrt{1 - \dfrac{4R_{SC}P_{SC}(t)}{U_{OCV}^2}}\right) \end{cases} \tag{3.4}$$

where R_{SC} and U_{OCV} represent the internal resistance and output voltage of SC, respectively.

In order to keep FC working as far as possible in the "safe operating zone" while ensuring that the end-state SOC of SC is close to the beginning state, two nonlinear constraints (K_{FC} and K_{SC}) are considered

in the presented EMS. In addition, the degradation degree of FC is also considered in this work, thus to reach optimal power distribution between SC and FC, the optimization problem can be converted into a mathematical problem that solves the optimal solution of the following equation.

$$\min C_{\mathrm{sys}}(t) = \min\left(f_1^*\left(P_{\mathrm{FC}}(t)\right) + f_2^*\left(P_{\mathrm{SC}}(t)\right)\right) \tag{3.5}$$

with:

$$\begin{cases} f_1^*\left(P_{\mathrm{FC}}(t)\right) = \dfrac{1}{D_{\mathrm{FC}}} K_{\mathrm{FC}} f_1\left(P_{\mathrm{FC}}(t)\right) \\ f_2^*\left(P_{\mathrm{SC}}(t)\right) = K_{\mathrm{SC}} f_2\left(P_{\mathrm{SC}}(t)\right) \end{cases} \tag{3.6}$$

In addition, K_{FC} is the operating region constraint of FC, and this penalty coefficient is used to keep the FC operating as much as possible in its "safe operating zone". The K_{SC} is used to constrain the variation between SC initial SOC and final SOC.

The FC operating region constraint K_{FC} is described as:

$$K_{\mathrm{FC}} = \begin{cases} \left(1 + 2 \times \dfrac{\left|P_{\mathrm{FC}} - P_{\mathrm{FC,MEP}}\right|}{P_{\mathrm{FC,MPP}} - P_{\mathrm{FC,MEP}}}\right)^2 & P_{\mathrm{FC,MEP}} < P_{\mathrm{FC}} < P_{\mathrm{FC,MPP}} \\ \left(1 + 2 \times \dfrac{\left|P_{\mathrm{FC}} - P_{\mathrm{FC,MEP}}\right|}{P_{\mathrm{FC,MPP}} - P_{\mathrm{FC,MEP}}}\right)^4 & P_{\mathrm{FC}} \le P_{\mathrm{FC,MEP}} \end{cases} \tag{3.7}$$

where $P_{\mathrm{FC,MEP}}$ denotes the ME operating point power of the FC, $P_{\mathrm{FC,MPP}}$ represents the MP operating point power of the FC. According to the previous description, the ME and MP of the FC will change with the working conditions.

Moreover, the constraint of SC SOC K_{SC} is defined as follows:

$$K_{\mathrm{SC}} = \begin{cases} \left(1 - 2 \times \dfrac{SOC(t) - SOC_{\mathrm{init}}}{SOC_{\max} - SOC_{\min}}\right)^2 & SOC_{\min} \le SOC(t) \le SOC_{\max} \\ \left(1 - 2 \times \dfrac{SOC(t) - SOC_{\mathrm{init}}}{SOC_{\max} - SOC_{\min}}\right)^4 & \text{else} \end{cases} \tag{3.8}$$

where $SOC_{\max}$, $SOC_{\min}$ are the upper and lower limits of the SC SOC (0.9 and 0.2), respectively. K_{SC} can make the SC final SOC close to its initial SOC. Taking into account that the SC has the disadvantage of low energy density, therefore, the SOC variation of the beginning state and end state of SC within a driving cycle should be as small as possible to guarantee that the hybrid electric tram can operate continuously and safely [16]. In addition, it should be mentioned that the longer the stack is working under transient load conditions, the more severe is the degradation degree and the shorter is the lifespan [17–19]. Thus, the output power fluctuations should be limited when the degradation of FC is severe.

Therefore, the D_{FC} is used in this study for smoothing out the output power of the stack, to adjust FC output power based on stack's real-time degradation degree. It should be noted that since the SC has the advantages of high durability and long operating cycles, this study doesn't constrain the output power fluctuation range of the SC, and this work will take advantage of the fast response ability of the SC to quickly respond to the dynamic load fluctuation of the system.

In addition, some constraints should be added to the power sources.

$$\begin{cases} SOC_{\min} \le SOC(t) \le SOC_{\max} \\ P_{\mathrm{FC,min}} \le P_{\mathrm{FC}} \le P_{\mathrm{FC,max}} \\ D_{\mathrm{FC}}\Delta P_{\mathrm{FC,decrease}} \le \dfrac{P_{\mathrm{FC}}(t)}{dt} \le D_{\mathrm{FC}}\Delta P_{\mathrm{FC,increase}} \\ P_{\mathrm{SC,min}} \le P_{\mathrm{SC}} \le P_{\mathrm{SC,max}} \end{cases} \tag{3.9}$$

where $P_{\mathrm{FC,max}}$ and $P_{\mathrm{FC,min}}$ represent the maximal and minimum power of stack, respectively. $P_{\mathrm{FC,decrease}}$ and $P_{\mathrm{FC,increase}}$ are used to limit the dynamic power fluctuations of FC. $P_{\mathrm{SC,min}}$ and $P_{\mathrm{SC,max}}$ denote the maximal charge and discharge power of SC, respectively.

Then the FC optimal reference power $P_{\mathrm{FC,opt}}$ can be obtained.

$$P_{\mathrm{FC,opt}} = P_{\mathrm{demand}} - P_{\mathrm{SC,opt}} \tag{3.10}$$

where P_{demand} represents the load power and $P_{\mathrm{SC,opt}}$ represents the optimal power of SC. In addition, the $P_{\mathrm{SC,opt}}$ is solved by the sequential quadratic programming (SQP) algorithm [12] (the specific implementation process of the SQP algorithm is shown in **Chapter 2**).

3.3.2. Online extremum seeking approach

As can be seen from the above description, the online extremum seeking method plays a prominent role in the presented EMS. This algorithm is proposed to update the coefficients (A and B) and seek the ME and MP operating points throughout the operating cycle. Then the "safe operating zone" can be determined.

Identification method is mainly divided into online identification and offline identification [6]. Offline identification strategies can shorten the computational time and is good method to keep parameters of system constant. However, if the varying load condition results in the change of system characteristics, it is difficult to accurately reflect the operation characteristic of the research object, and the identification accuracy is unsatisfactory. In order to improve the accuracy of identification, this chapter adopts the forgetting factor recursive least square (FFRLS) algorithm to identify the efficiency and power operating curves, because the parameters of the system to be estimated are time-varying. The FFRLS algorithm is a data-driven online identification method that is often used to estimate system parameters [20]. This algorithm also can be used to identify the power source performance variations to improve the power

source output voltage [21]. In addition, the FFRLS algorithm has become one of the feasible schemes for modeling control of complex control objects due to its fast identification speed and strong linear approximation capability [22].

The specific explanation of the FFRLS algorithm is as follows:

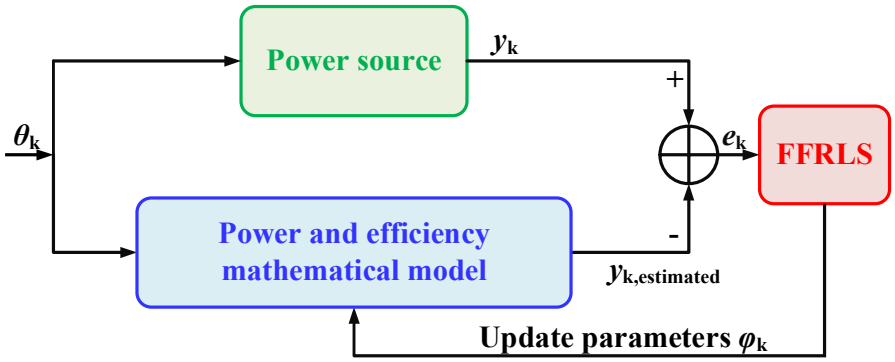

Figure 3.12. Parameters identification flowchart using the FFRLS algorithm.

As shown in Fig. 3.12, the FFRLS algorithm could be represented by a single-input single-output (SISO) model as follows [3]:

$$A(z^{-1})y(k) = B(z^{-1})u(k-d) + e(k) \tag{3.11}$$

where $y(k)$ is the discrete output variable of the model, $u(k\text{-}d)$ is the discrete input variable of the model, d is hysteresis time of the system, k is the system discrete time, and $e(k)$ is the system identification error, and

$$\begin{cases} A(z^{-1}) = 1 + a_1 z^{-1} + \cdots + a_{n_a} z^{-n_a} \\ B(z^{-1}) = b_0 + b_1 z^{-1} + \cdots + b_{n_b} z^{-n_b} \end{cases} \tag{3.12}$$

where n_a is the order number of A(z-1), n_b is the order number of B(z-1), and the Eq. (3.11) can be written as the following least-squares form

$$\begin{aligned} y(k) &= -a_1 y(k-1) - \cdots - a_{n_a} y(k-n_a) + b_0 u(k-d) + \cdots + b_{n_b} u(k-d-n_b) + e(k) \\ &= \varphi^T(k)\hat{\theta}(k) + e(k) \end{aligned} \tag{3.13}$$

where the unknown parameters of system vector θ can be defined by

$$\theta = [a_1, \cdots, a_{n_a}, b_0, \cdots, b_{n_b}]^T \in R^{(n_a+n_b+1)\times 1} \tag{3.14}$$

where $\varphi^T(k)$ is data vector which consists of measured values of output and input can be defined by

$$\varphi(k)=\begin{bmatrix} -y(k-1) \\ \vdots \\ -y(k-n_{\mathrm{a}}) \\ u(k-d) \\ \vdots \\ u(k-n_{\mathrm{b}}-d) \end{bmatrix} \in R^{(n_{\mathrm{a}}+n_{\mathrm{b}}+1)\times 1} \tag{3.15}$$

The Eq. (3.13) shows a precise description of the system, θ is parameter vector to be estimated. The unknown parameters θ are chosen in such way that the sum of squares of the error is a minimum. It can be obtained from Eq. (3.13) that, this problem can be converted into finding the parameter vector that minimizes the following performance criteria J

$$J=\frac{1}{2}\sum_{k=1}^{L}e^2(k) \tag{3.16}$$

where $e(k)$ can be calculated by the following equation

$$e(k)=y(k)-\hat{y}(k) \tag{3.17}$$

where $\hat{y}(k)=\varphi^T(k)\hat{\theta}(k)$.

Through the analysis above, the parameters of efficiency curve can be defined by

$$\eta_{\mathrm{FCS}}(k)=\left[I_{\mathrm{FC}}(k)\right]^T\theta+e(k) \tag{3.18}$$

Then define

$$\Phi_{\mathrm{k}}=\begin{bmatrix} \Phi_{\mathrm{k-1}} \\ \left[I_{\mathrm{FC}}(k)\right]^{\mathrm{T}} \end{bmatrix}, Y_k=\begin{bmatrix} Y_{\mathrm{k-1}} \\ \eta_{\mathrm{FCS}}(k) \end{bmatrix} \tag{3.19}$$

According to Eq. (3.17) and Eq. (3.19), the least squares estimation of system parameters θ at the moment k can be calculated as follows:

$$\hat{\theta}(k)=\left(\Phi_{\mathrm{k}}^{\mathrm{T}}\Phi_{\mathrm{k}}\right)^{-1}\Phi_{\mathrm{k}}^{\mathrm{T}}Y_{\mathrm{k}} \tag{3.20}$$

In order to convert formula (3.20) into recursive form, define:

$$\begin{aligned} P(k)&=\left(\left[\Phi_{\mathrm{k}}\right]^{\mathrm{T}}\Phi_{\mathrm{k}}\right)^{-1} \\ &=\left[\left[\Phi_{\mathrm{k-1}}\right]^{\mathrm{T}}\Phi_{\mathrm{k-1}}+I_{\mathrm{FC}}(k)\left[I_{\mathrm{FC}}(k)\right]^{\mathrm{T}}\right]^{-1} \\ &=\left[\left[P(k-1)\right]^{-1}+I_{\mathrm{FC}}(k)\left[I_{\mathrm{FC}}(k)\right]^{\mathrm{T}}\right]^{-1} \end{aligned} \tag{3.21}$$

Then formula (3.20) can be written as:

$$\begin{aligned}\hat{\theta}(k) &= \hat{\theta}(k\text{-}1)+P(k)I_{\mathrm{FC}}(k)\left[\eta_{\mathrm{FCS}}(k)-\left[I_{\mathrm{FC}}(k)\right]^{\mathrm{T}}\hat{\theta}(k\text{-}1)\right] \\ &= \hat{\theta}(k\text{-}1)+L(k)\left[\eta_{\mathrm{FCS}}(k)-\left[I_{\mathrm{FC}}(k)\right]^{\mathrm{T}}\hat{\theta}(k\text{-}1)\right]\end{aligned} \tag{3.22}$$

where $L(k) = P(k)I_{\mathrm{FC}}(k)$.

According to formula (3.21) and 'Matrix Inversion Lemma' [23], formula (3.23) can be obtained as follows:

$$P(k) = P(k-1) - P(k-1)I_{\mathrm{FC}}(k)\times\left[1+\left[I_{\mathrm{FC}}(k)\right]^{\mathrm{T}}P(k-1)I_{\mathrm{FC}}(k)\right]^{-1}\left[I_{\mathrm{FC}}(k)\right]^{\mathrm{T}}P(k-1) \tag{3.23}$$

The $L(k)$ can be obtained by following equation:

$$L(k) = P(k)I_{\mathrm{FC}}(k) = P(k-1)I_{\mathrm{FC}}(k)\left[1+\left[I_{\mathrm{FC}}(k)\right]^{\mathrm{T}}P(k-1)I_{\mathrm{FC}}(k)\right]^{-1} \tag{3.24}$$

Substituting (3.24) into (3.23) we get:

$$P(k) = \left[I - L(k)\left[I_{\mathrm{FC}}(k)\right]^{\mathrm{T}}\right]P(k-1) \tag{3.25}$$

When the values of system parameters change continuously and slowly, in order to weaken the influence of earlier data on the identification results, and to strengthen the sensitivity to recent estimation error, the weighting of earlier data should be reduced and the recent data should be weighted. Therefor the identification error $e(k)$ is modified by using a forgetting factor μ ($0< \mu <1$). Formula (3.16) could be corrected as the following:

$$J^{*} = \sum_{k=1}^{L}\mu^{L-k}e^{2}(k) \tag{3.26}$$

Substituting μ into formula (3.24) and formula (3.25), $P(k)$, $L(k)$, and the parameters to be estimated θ can be written as"

$$\begin{cases}\hat{\theta}(k) = \hat{\theta}(k-1)+L(k)\left[\eta_{\mathrm{FCS}}(k)-\left[I_{\mathrm{FC}}(k)\right]^{\mathrm{T}}\hat{\theta}(k-1)\right] \\ L(k) = \dfrac{P(k-1)I_{\mathrm{FC}}(k)}{\mu+\left[I_{\mathrm{FC}}(k)\right]^{\mathrm{T}}P(k-1)I_{\mathrm{FC}}(k)} \\ P(k) = \dfrac{1}{\mu}\left[\mathrm{I}-L(k)\left[I_{\mathrm{FC}}(k)\right]^{\mathrm{T}}\right]P(k-1)\end{cases} \tag{3.27}$$

Then, the presented FFRLS algorithm can be implemented by the Eq. (3.27). The parameters online identification flowchart using the FFRLS algorithm is depicted in Fig. 3.13.

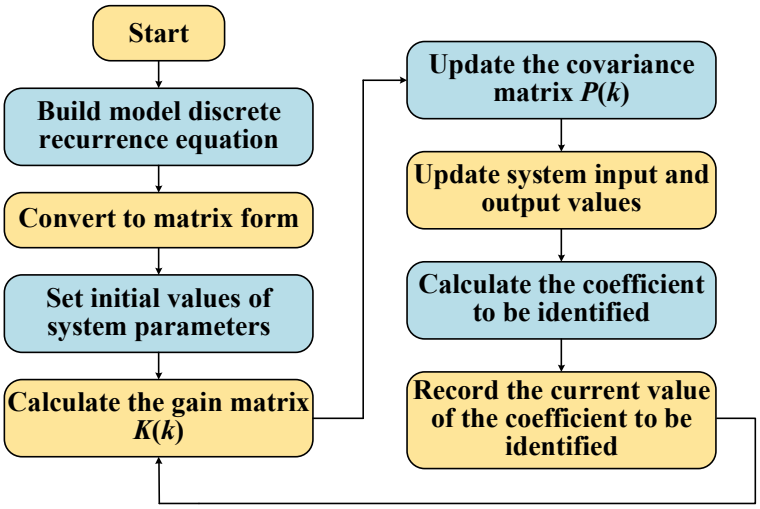

Figure 3.13. The process of parameters online identification.

The specific implementation process of the presented FFRLS algorithm is as follows:

Step 1: Convert the discrete recurrence equation of the system into the form shown in Eq. (3.13);

Step 2: Set the initial value of $\theta(k)$ to [0, 0,⋯, 0], set the initial value of the covariance matrix to [12000, 0, ⋯, 0; 0, 12000, ⋯, 0; ⋯; 0, 0, ⋯, 12000], determine the initial value of the forgetting factor;

Step 3: Calculate the matrix $K(k)$ of the FFRLS algorithm;

Step 4: Update the covariance matrix $P(k)$;

Step 5: Input the voltage and current signals into the FFRLS algorithm every 200 milliseconds, and calculate the system efficiency;

Step 6: Calculate the coefficients to be identified in the system;

Step 7: $k \rightarrow k+1$, go back to *step 3*, keep updating the system coefficients.

According to the above steps, the updated model can be used to estimate the parameters of stack. Thereafter, the optimal operating area and extreme operating point required for this chapter can be identified.

3.3.3. Specific implementation process of the proposed strategy

As shown in Fig. 3.14, the specific implementation process of the proposed EMS is as follows:

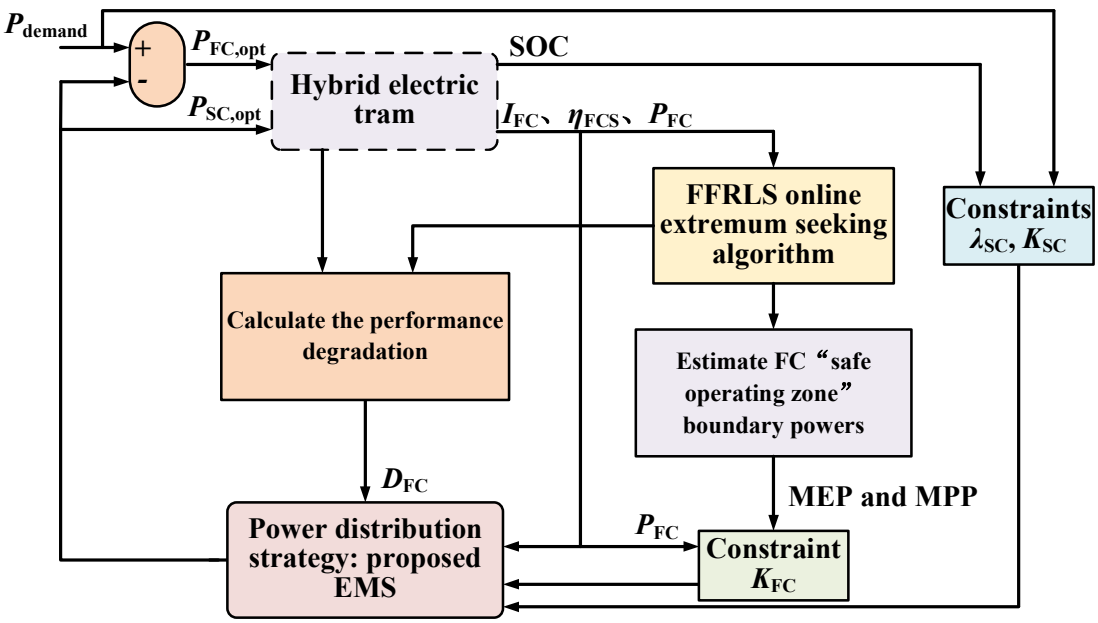

Figure 3.14. The implementation process of the proposed EMS.

STEP1: Use the online identification method based on the FFRLS algorithm shown in Eq. (3.27) to obtain the ME and MP points of the FC, thereby determining the "safe operating zone" of the stack;

STEP2: Calculate the current degradation degree of the power sources;

STEP3: According to Eq. (3.7) and Eq. (3.8), solve the penalty coefficients for power sources operation;

STEP4: Use formulas (3.1)-(3.6) and SQP algorithm to solve the real-time optimal output power of the SC, and then obtain the optimal output power of the FC according to Eq. (3.10);

STEP5: Use the DC/DC converter cascaded with the FC to control the stack output reference power.

Through above steps, the purpose of reaching optimal power distribution between SC and FC can be realized.

3.4. Experimental validation and results analysis

To better highlight the superiority of the presented EMS, the optimization-based ECMS and rule-based state machine control strategy are employed in this chapter. It should be noted that the ECMS have been analyzed in detail in **Chapter 2**, so this strategy will not be repeated in this section. In addition, this chapter redesigns the rules of the SMC based on the research [3], as shown in TABLE 3.4.

In TABLE 3.4, the SOC of SC is divided into three areas: low (SOC<0.2), normal (0.2<SOC<0.9), and high (SOC>0.9). Through the TABLE 3.4, the state machine control strategy can be realized.

TABLE 3.4. State machine control strategy decisions.

SOC state	P_{demand}	State	$P_{FC,opt}$
If SOC low	$P_{demand}>P_{FC,max}$	1	$P_{FC,opt}=P_{FC,max}$
If SOC low	$P_{demand}\leq P_{FC,max}$	2	$P_{FC,opt}=P_{FC,max}-P_{SC,min}$
If SOC normal	$P_{demand}\geq P_{FC,max}$	3	$P_{FC,opt}=P_{FC,max}$
If SOC normal	$P_{demand}\in[P_{FC,MEP}, P_{FC,max}]$	4	$P_{FC,opt}=P_{demand}$
If SOC normal	$P_{demand}<P_{FC,MEP}$	5	$P_{FC,opt}=P_{FC,MEP}$
If SOC high	-	6	$P_{FC,opt}=P_{FC,min}$

3.4.1. Experimental performance testing of FFRLS algorithm

In order to test the feasibility of the proposed online extremum seeking method, this section conducts a validation experiment using the platform shown in Fig. 3.9. The test condition is shown in Fig. 3.15. What is more, it should be noted that since it is difficult to directly verify the performance of the identification algorithm, this work first uses the FFRLS algorithm to identify the efficiency operation curves, and then sets the ME and MP points as the reference power based on the identification results to indirectly demonstrate the effectiveness of the FFRLS algorithm. This also means that in this validation experiment, the stack always works at the ME point or MP point. The function of the SC in this experiment is only to maintain the system power balance and maintain the bus voltage. Fig. 3.16 shows the results of using the proposed FFRLS algorithm to seek the ME and MP operating points.

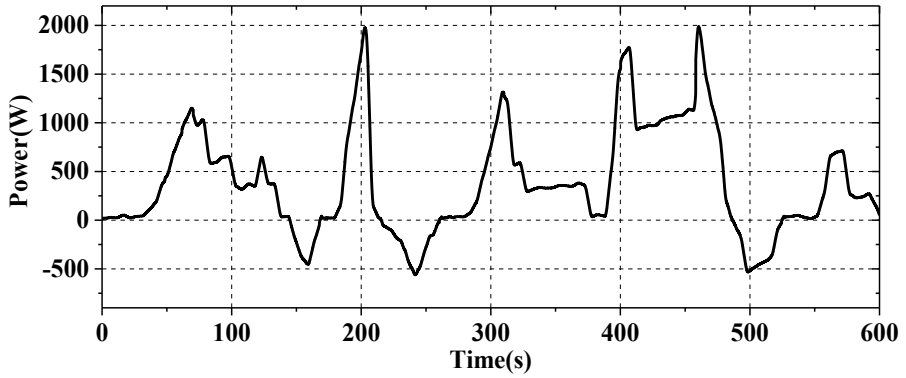

Figure 3.15. Working condition for testing the FFRLS algorithm.

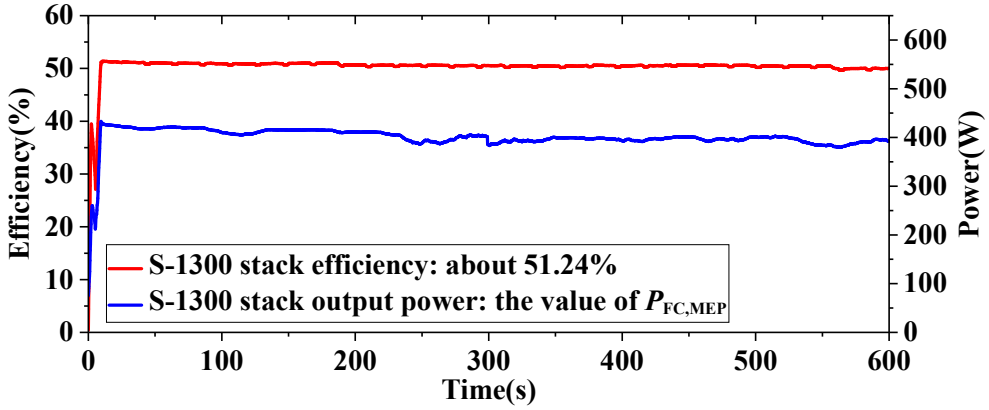

(a) S-1300 ME operating point power

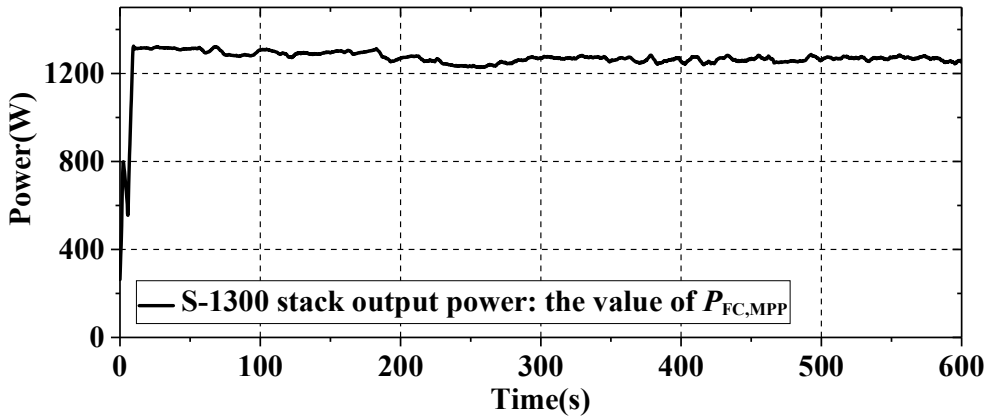

(b) S-1300 MP operating point power

Figure 3.16. The FFRLS algorithm performance verification.

The results in Fig. 3.16 show that as the external operating parameters change, the ME and MP operating points will indeed fluctuate. Besides, it can be seen from Fig. 3.11 that the maximum output efficiency of the S-1300 is about 51%, and its maximum output power is about 1300 w. Therefore, the effectiveness of the online seeking method based on the FFRLS algorithm can be verified.

3.4.2. Power allocation of power sources using different EMSs

The scaled-down power demand curve is shown in Fig. 3.17, with power ranging from -750 W to 2000 W. In addition, the SC and FC output power curves under the control of different EMSs are shown in Fig. 3.18. Specific indicators are analyzed in the next sections. It can be clearly seen that all the strategies can meet the load demand. In this hybrid system, the FC continues to deliver power to the system, so it can be seen that its output power is always positive. When the SOC of the SC is low, the FC not only needs to provide power for the load but also needs to charge the SC. Besides, the SC provides the required instantaneous power and quickly recovers system braking and excess energy. Therefore, it can be seen that the output power of the SC is alternately positive and negative.

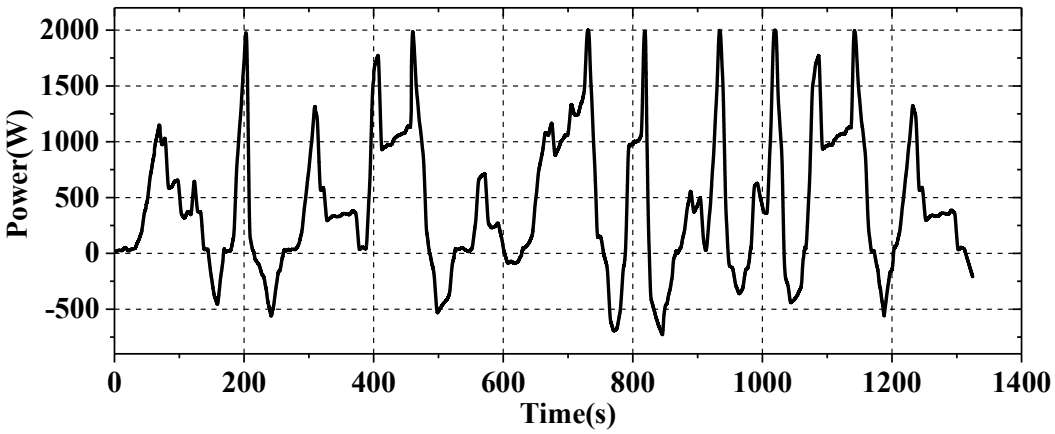

Figure 3.17. Scaled-down power demand of the hybrid electric tram.

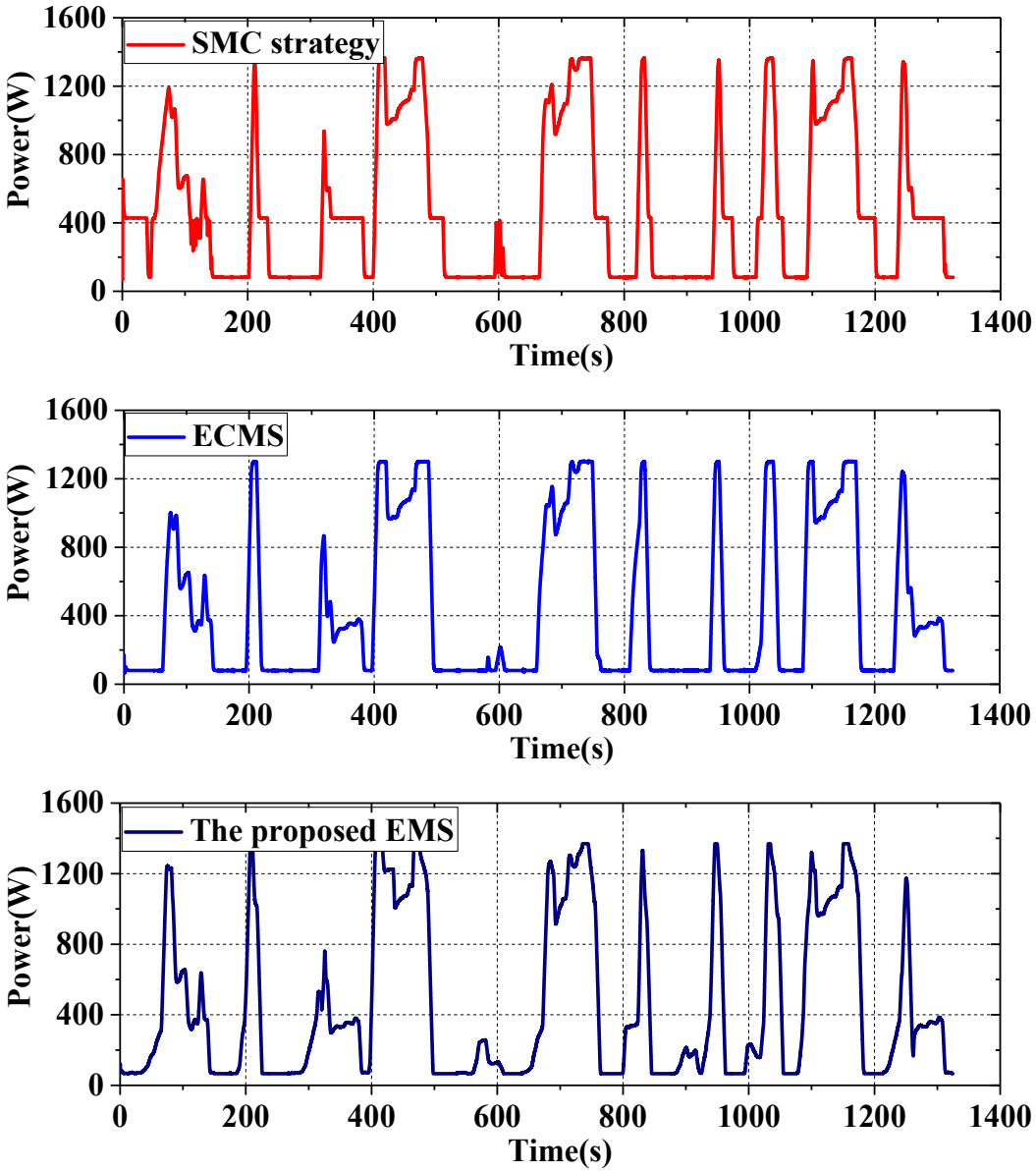

(a) FC output power curves

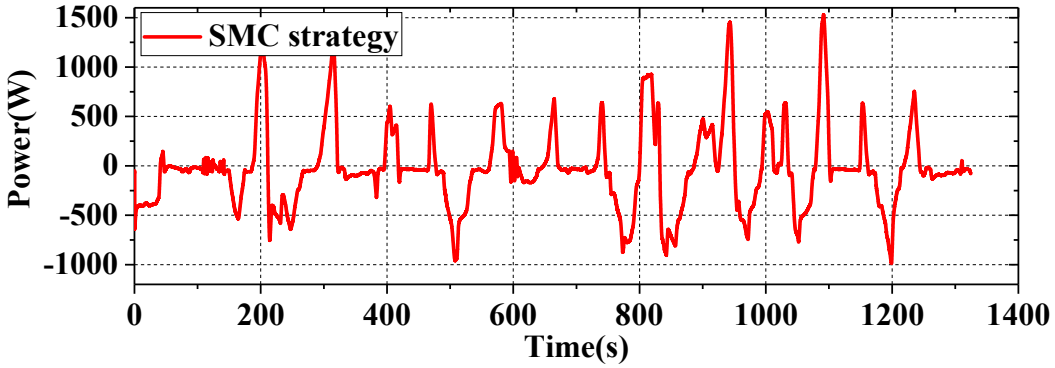

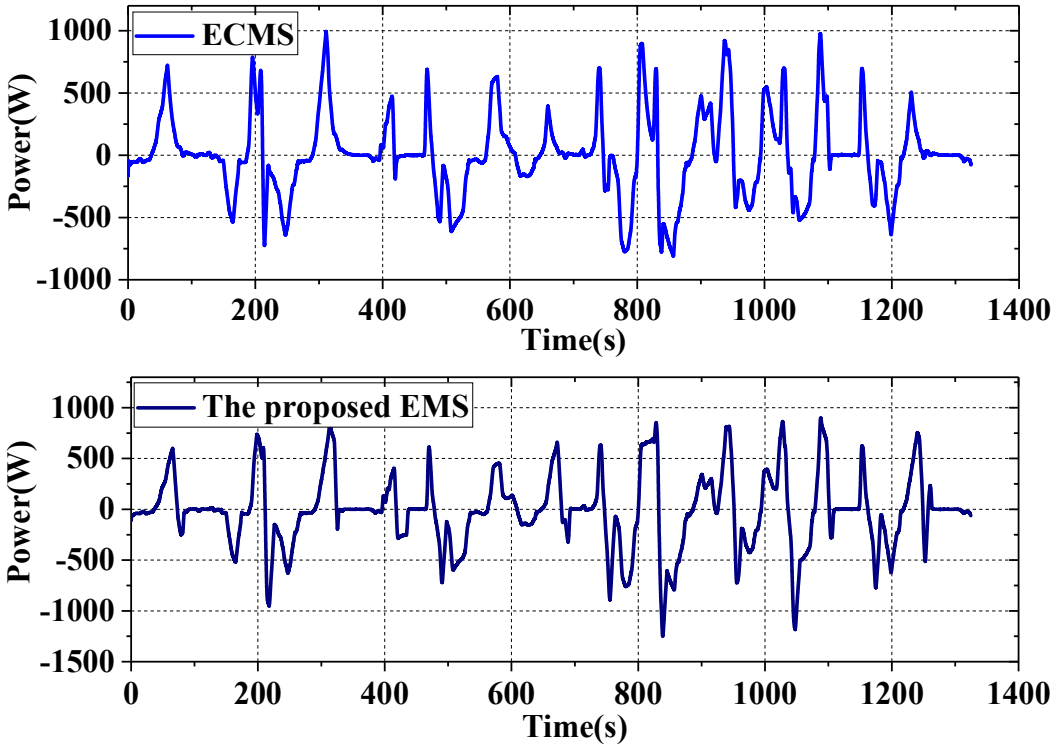

(b) SC output power curves

Figure 3.18. Power distribution curves of different power sources in different experiments.

3.4.3. Comparative analysis of different strategies

Fig. 3.18 presents the power output curves of the SC and FC when different EMSs (SMC strategy, ECMS and the presented EMS) are used. To test the performance of the presented EMS, the SOC fluctuation of SC, the efficiency of FC, system hydrogen consumption, and power sources operating stress are analyzed in this section.

3.4.3.1. SOC fluctuation range comparative analysis

As the only energy storage system in the hybrid system, the SC plays a particularly important role. The SOC curves of SC under the control of different strategies are presented in Fig. 3.19. In order to facilitate the comparison of experimental results, the initial SC SOC values in all the strategies are set to the same value (about 74%). In this section, the current and voltage of the SC can be measured directly through the sensors, and the SOC of SC is calculated through formulas (3.2) and (3.3).

In Fig. 3.19, the end-state SC SOC of the presented EMS, SMC strategy, and the ECMS are 72.65% (ΔSOC is about 2%), 88.92% (ΔSOC is about 15%), and 47.95% (ΔSOC is about 27%), respectively. Obviously, the presented strategy can ensure that the SC end-state SOC is close to its beginning state SOC. Compared with the ECMS and SMC strategy, the SOC of proposed EMS has the smallest variation between the beginning state and end state, which helps to guarantee the stable and continuous operation of the hybrid electric tram [2].

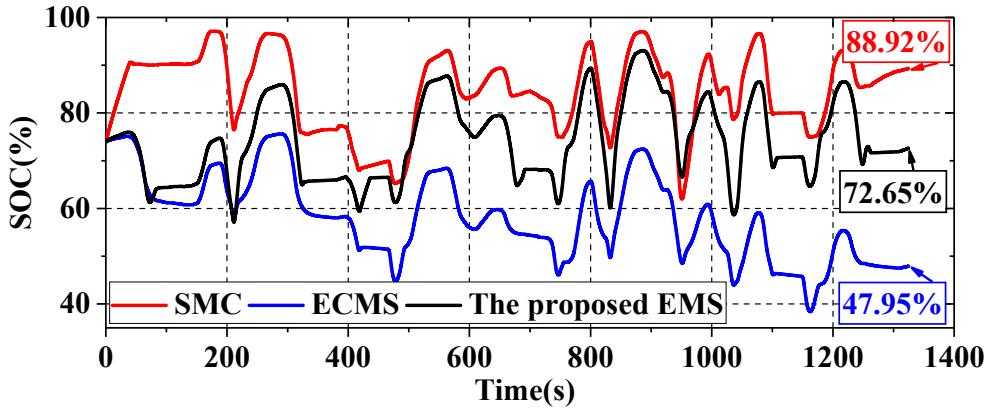

Figure 3.19. The SOC curves of SC under the control of different strategies.

3.4.3.2. Comparative analysis of the efficiency and hydrogen consumption

The efficiency of the power sources can be calculated through the research of **Chapter 2** (see **Section 2.2**). Fig. 3.20 shows the efficiency curves of FCs under the control of different strategies. When using the proposed EMS, the average efficiency of the stack is 38.09%, which is 5.62% higher than that of the ECMS and is 0.97% higher than that of the SMC strategy. It can be seen that the proposed EMS can improve the operating efficiency of the stack and improve the system economy.

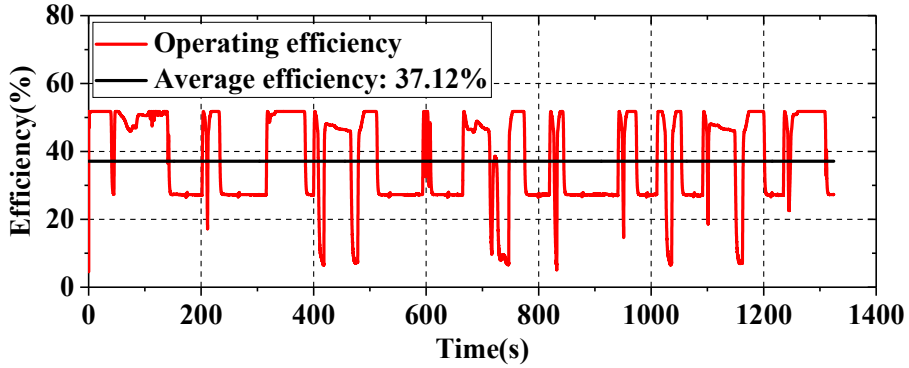

(a) SMC strategy

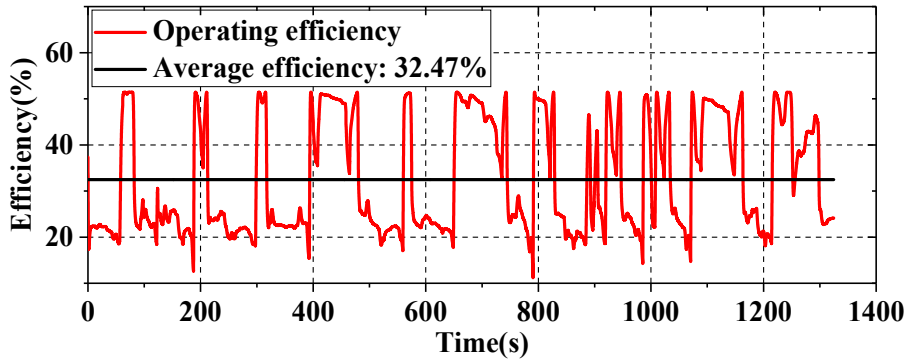

(b) ECMS

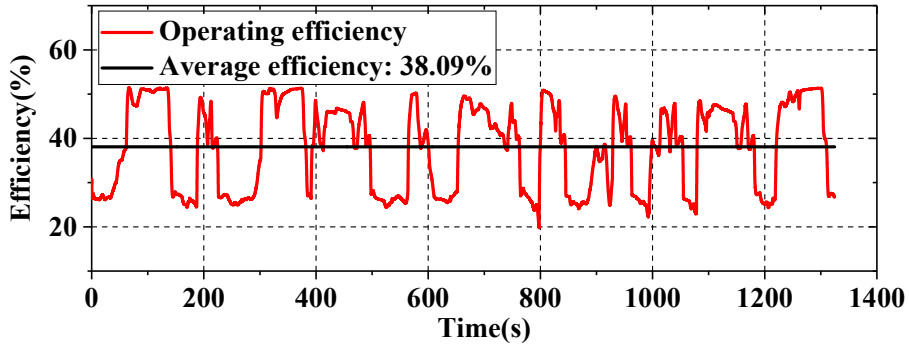

(c) The presented EMS

Figure 3.20. Operating efficiency curves using different strategies.

Moreover, the fuel consumption rate of the SC and FC could also be obtained through the research in **Chapter 2**. Then the total fuel consumption mass can be calculated by:

$$C_{\mathrm{H_2,total}} = C_{\mathrm{H_2,FC}} + C_{\mathrm{H_2,SC}} \tag{3.28}$$

with:

$$\begin{cases} C_{\mathrm{H_2,FC}} = \int_0^{\mathrm{T}} C_{\mathrm{FC}}(t)\,dt \\ C_{\mathrm{H_2,SC}} = \int_0^{\mathrm{T}} C_{\mathrm{SC}}(t)\,dt \end{cases} \tag{3.29}$$

where $C_{\mathrm{H2,SC}}$ and $C_{\mathrm{H2,FC}}$ denote the equivalent fuel consumption of the SC and hydrogen consumption of FC, respectively. By calculating the equivalent hydrogen consumption rate of the SC and the fuel consumption rate of the stack in real-time, the total amount of hydrogen consumption can be obtained, as shown in Fig. 3.21.

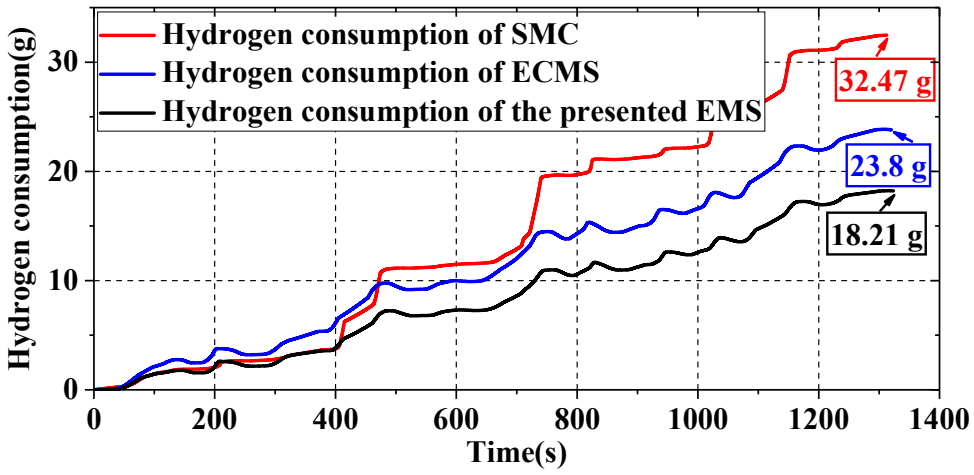

Figure 3.21. Total hydrogen consumption curves using different strategies.

The total mass of hydrogen consumed by the system using SMC strategy, ECMS, and the presented EMS is 32.47 g, 23.8 g, and 18.21 g, respectively. It can be seen that in these strategies, the total hydrogen consumption of the presented EMS is the smallest. It is proved that the proposed strategy

could effectively reduce the fuel consumption.

3.4.3.3. Comparative analysis of the power sources operating stress

According to [6,15], the key factor that affects the performance of power sources is related to power fluctuations. The operating stress analysis results of power sources using different strategies are presented in Fig. 3.22. These results are obtained using Haar wavelet transform technique, and the fluctuation distributions of SC and FC provide a clear indication of how often each power source is solicited.

As can be seen from Fig. 3.22, compared with the SMC strategy and ECMS, the operating stress of stack is the lowest under the control of the presented EMS. Thence, the presented strategy can effectively smooth the fluctuation of stack output power, thereby prolonging the lifetime of FC. Although the operating stress of SC is not the lowest, SC has the advantages of strong durability and long cycle lifespan, so it can be proved that the proposed EMS can improve the overall performance of the hybrid system.

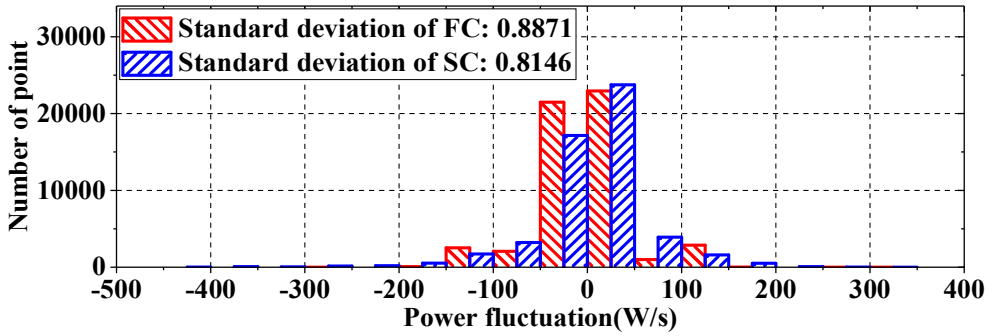

(a) SMC strategy

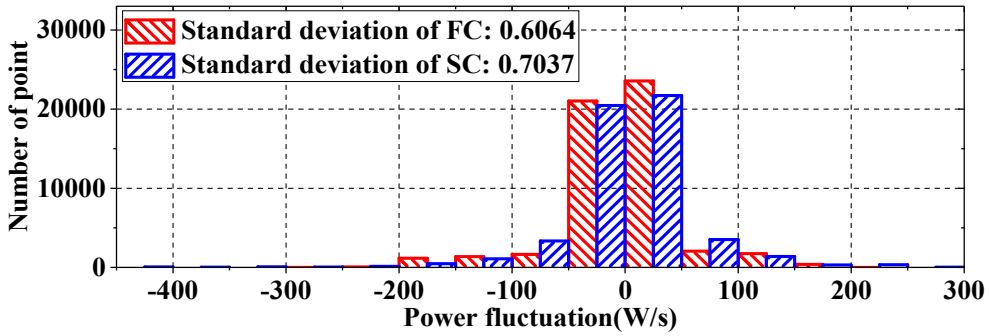

(b)ECMS

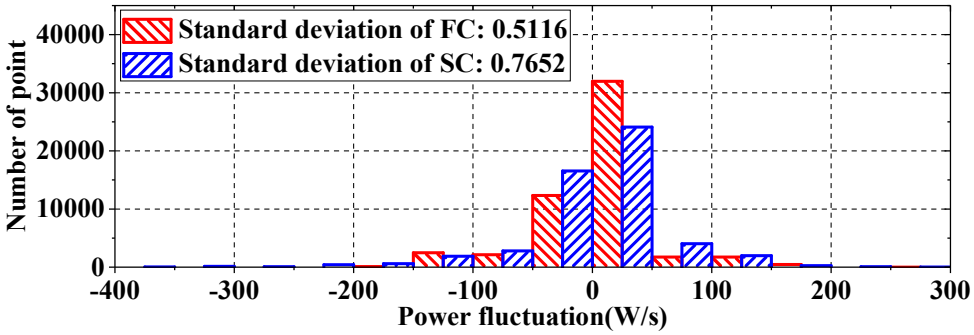

(c) The presented EMS

Figure 3.22. Power fluctuation rate distribution of SC and FC using different strategies.

Furthermore, to highlight the superiority of the presented strategy more clearly, all the results using different strategies are summarized in TABLE 3.5.

TABLE 3.5. Performance comparative analysis of different strategies.

	SMC	ECMS	The presented EMS
SOC variation of SC	74.00%-88.92%	74.00%-47.95%	74.00%-72.56%
Average operating efficiency	37.12%	32.47%	38.09%
Total fuel consumption	32.47g	23.80g	18.21g
FC operating stress	0.8871	0.6064	0.5116
SC operating stress	0.8146	0.7037	0.7652

As shown in TABLE 3.5, among these three strategies, the proposed EMS has advantages in hydrogen consumption, power sources operating stress, operating efficiency, and SOC fluctuation range of SC.

3.5. Conclusion

In this chapter, the online extremum seeking-based optimized EMS is presented for a SC/FC hybrid electric tram. Firstly, the structure and configuration of the tram are introduced. Then, to improve the operating performance of the stack, this study divides the “safe operating zone” according to its ME and MP operating points. Considering that the stack is a complex nonlinear system, an online extremum seeking method is used to estimate the ME and MP points of the FC. Therefore, the boundary values of the “safe operating zone” can be updated in real-time. The FFRLS algorithm is proposed to implement this process. Since the SC has the disadvantage of low energy density to ensure that the initial and final SOC states of the SC are consistent and to ensure the continued operating of the tram, the constraint K_{SC} is considered in the proposed EMS.

According to the structure of the studied heavy-duty hybrid electric tram (LF-LRV), a reduced-scale test platform powered by SC and FC is established, and the scaled-down working condition of the tram is adopted to test the performance of the presented EMS. The results demonstrate that the presented strategy can ameliorate power sources performance, keep the initial state SOC of SC consistent with its final state SOC, save fuel consumption, and smooth out the output power fluctuations of stack. The

presented EMS is also compared with the SMC strategy and ECMS to further certify its superiority.

The **Chapter 3** mainly studies the energy management strategy suitable for a heavy-duty hybrid electric tram powered by SC and FC, and in the next chapter, we will further investigate the study of power distribution and coordinated control methods in multi-source systems (consisting of multiple energy storage systems and multiple sets of stacks) for the higher power applications.

References

[1] Y. Yan, Q. Li, W. Huang, W. Chen, Operation Optimization and Control Method Based on Optimal Energy and Hydrogen Consumption for the Fuel Cell/Supercapacitor Hybrid Tram, IEEE Transactions on Industrial Electronics. 68 (2021) 1342–1352. https://doi.org/10.1109/tie.2020.2967720.

[2] Y. Yan, Q. Li, W. Chen, B. Su, J. Liu, L. Ma, Optimal Energy Management and Control in Multimode Equivalent Energy Consumption of Fuel Cell/Supercapacitor of Hybrid Electric Tram, IEEE Transactions on Industrial Electronics. 66 (2019) 6065–6076. https://doi.org/10.1109/tie.2018.2871792.

[3] Q. Li, T. Wang, S. Li, W. Chen, H. Liu, E. Breaz, F. Gao, Online extremum seeking-based optimized energy management strategy for hybrid electric tram considering fuel cell degradation, Applied Energy. 285 (2021) 116505. https://doi.org/10.1016/j.apenergy.2021.116505.

[4] Q. Li, B. Su, Y. Pu, Y. Han, T. Wang, L. Yin, W. Chen, A State Machine Control Based on Equivalent Consumption Minimization for Fuel Cell/ Supercapacitor Hybrid Tramway, IEEE Trans. Transp. Electrific. 5 (2019) 552–564. https://doi.org/10.1109/TTE.2019.2915689.

[5] Y. Yan, Q. Li, W. Chen, W. Huang, J. Liu, Hierarchical Management Control Based on Equivalent Fitting Circle and Equivalent Energy Consumption Method for Multiple Fuel Cells Hybrid Power System, IEEE Transactions on Industrial Electronics. 67 (2020) 2786–2797. https://doi.org/10.1109/tie.2019.2908615.

[6] T. Wang, Q. Li, Y. Qiu, L. Yin, L. Liu, W. Chen, Efficiency Extreme Point Tracking Strategy Based on FFRLS Online Identification for PEMFC System, IEEE Trans. Energy Convers. 34 (2019) 952–963. https://doi.org/10.1109/TEC.2018.2872861.

[7] N. Bizon, Efficient fuel economy strategies for the Fuel Cell Hybrid Power Systems under variable renewable/load power profile, Applied Energy. 251 (2019) 113400. https://doi.org/10.1016/j.apenergy.2019.113400.

[8] M.G. Carignano, R. Costa-Castelló, V. Roda, N.M. Nigro, S. Junco, D. Feroldi, Energy management strategy for fuel cell-supercapacitor hybrid vehicles based on prediction of energy demand, Journal of Power Sources. 360 (2017) 419–433. https://doi.org/10.1016/j.jpowsour.2017.06.016.

[9] Z. Hong, Q. Li, Y. Han, W. Shang, Y. Zhu, W. Chen, An energy management strategy based on dynamic power factor for fuel cell/battery hybrid locomotive, International Journal of Hydrogen Energy. 43 (2018) 3261–3272. https://doi.org/10.1016/j.ijhydene.2017.12.117.

[10] J. Wu, X.-Z. Yuan, J.J. Martin, H. Wang, D. Yang, J. Qiao, J. Ma, Proton exchange membrane fuel cell degradation under close to open-circuit conditions, Journal of Power Sources. 195 (2010) 1171–1176. https://doi.org/10.1016/j.jpowsour.2009.08.095.

[11] D. Feroldi, M. Serra, J. Riera, Energy Management Strategies based on efficiency map for Fuel Cell Hybrid Vehicles, Journal of Power Sources. 190 (2009) 387–401. https://doi.org/10.1016/j.jpowsour.2009.01.040.

[12] T. Wang, Q. Li, L. Yin, W. Chen, E. Breaz, F. Gao, Hierarchical Power Allocation Method Based on Online Extremum Seeking Algorithm for Dual-PEMFC/Battery Hybrid Locomotive, IEEE Transactions on Vehicular Technology. 70 (2021) 5679–5692. https://doi.org/10.1109/tvt.2021.3078752.

[13] Q. Li, T. Wang, C. Dai, W. Chen, L. Ma, Power Management Strategy Based on Adaptive Droop Control for a Fuel Cell-Battery-Supercapacitor Hybrid Tramway, IEEE Trans. Veh. Technol. 67 (2018) 5658–5670. https://doi.org/10.1109/TVT.2017.2715178.

[14] H. Li, A. Ravey, A. N'Diaye, A. Djerdir, A novel equivalent consumption minimization strategy for hybrid electric vehicle powered by fuel cell, battery and supercapacitor, Journal of Power Sources. 395 (2018) 262–

270. https://doi.org/10.1016/j.jpowsour.2018.05.078.
[15] T. Wang, Q. Li, X. Wang, Y. Qiu, M. Liu, X. Meng, J. Li, W. Chen, An optimized energy management strategy for fuel cell hybrid power system based on maximum efficiency range identification, Journal of Power Sources. 445 (2020) 227333. https://doi.org/10.1016/j.jpowsour.2019.227333.
[16] Q. Jiang, O. Béthoux, F. Ossart, E. Berthelot, C. Marchand, A comparison of real-time energy management strategies of FC/SC hybrid power source: Statistical analysis using random cycles, International Journal of Hydrogen Energy. 46 (2021) 32192–32205. https://doi.org/10.1016/j.ijhydene.2020.06.003.
[17] Z. Hua, Z. Zheng, M.-C. Péra, F. Gao, Remaining useful life prediction of PEMFC systems based on the multi-input echo state network, Applied Energy. 265 (2020) 114791. https://doi.org/10.1016/j.apenergy.2020.114791.
[18] K. Song, Y. Ding, X. Hu, H. Xu, Y. Wang, J. Cao, Degradation adaptive energy management strategy using fuel cell state-of-health for fuel economy improvement of hybrid electric vehicle, Applied Energy. 285 (2021) 116413. https://doi.org/10.1016/j.apenergy.2020.116413.
[19] M. Kandidayeni, J.P. Trovão, M. Soleymani, L. Boulon, Towards health-aware energy management strategies in fuel cell hybrid electric vehicles: A review, International Journal of Hydrogen Energy. 47 (2022) 10021–10043. https://doi.org/10.1016/j.ijhydene.2022.01.064.
[20] D. Li, Y. Yu, Q. Jin, Z. Gao, Maximum power efficiency operation and generalized predictive control of PEM (proton exchange membrane) fuel cell, Energy. 68 (2014) 210–217. https://doi.org/10.1016/j.energy.2014.02.104.
[21] Y.-P. Yang, Z.-W. Liu, F.-C. Wang, An application of indirect model reference adaptive control to a low-power proton exchange membrane fuel cell, Journal of Power Sources. 179 (2008) 618–630. https://doi.org/10.1016/j.jpowsour.2008.01.053.
[22] A. Vahidi, A. Stefanopoulou, H. Peng, Recursive least squares with forgetting for online estimation of vehicle mass and road grade: theory and experiments, Vehicle System Dynamics. 43 (2005) 31–55. https://doi.org/10.1080/00423110412331290446.
[23] S. Rhode, F. Gauterin, Online estimation of vehicle driving resistance parameters with recursive least squares and recursive total least squares, in: 2013 IEEE Intelligent Vehicles Symposium (IV), IEEE, 2013. https://doi.org/10.1109/ivs.2013.6629481.

Chapter 4. Performance consistent power distribution method for a multi-source hybrid power system

4.1. Introduction

In **Chapter 2** and **Chapter 3**, a detailed energy management study is conducted on the hybrid applications powered by a dual-source system (battery/supercapacitor and fuel cell (FC)). However, based on the existing studies, in the higher power applications (such as high-speed Electrical Multiple Unit trains), the traction power required by the vehicle is often large (for example, more than 500kW) [1]. Due to the limitation of power level and existing technology, the dual-source hybrid systems utilized in **Chapter 2** and **Chapter 3** are difficult to be applied to occasions with such high power requirements [2,3]. Therefore, some studies combine multiple energy storage systems and multiple FCs in parallel to form a multi-source hybrid power system to meet the above challenge[1,4–6]. Compared with the dual-source hybrid systems, the multi-source hybrid systems have the following advantages in the high-power applications: 1) The construction of multi-source hybrid system can increase the system power level and redundancy without increasing the development cost of high-power battery and FC; 2) Better operating performances in terms of efficiency, output power, hydrogen consumption, and operating state; 3) When a certain power source fails to operate, the faulty unit can be removed in time to avoid affecting the power supply stability of the entire system and increase the fault tolerance of the system [7–9]. However, the application of multi-source hybrid power systems also brings new challenges to the control and management of power flow. Reasonable energy management methods are beneficial to reduce the system performance degradation rate and extend its service life [10,11]. At present, the research on the power distribution among the power sources in the multi-source hybrid power system is still insufficient, and it is necessary to further explore the control of the system.

Obviously, from the research content in **Chapter 3**, when the hybrid system works in a complex environment such as rail transit, the different operating conditions (output power and operating temperature) of each power source will lead to differences in the operating performance of each power source, such as inconsistent state of charge (SOC) of batteries and inconsistent operating state of FCs. However, most studies ignore the above differences, which are not conducive to improving the overall performance of the system [1,3,4,9]. In order to fill the above-mentioned research gap, improve the system consistency (battery SOC consistency and FC operating state consistency) as much as possible and prolong the system service life, this chapter proposes a performance consistent power distribution method for a multi-source hybrid power system. In addition, in this system, referring to the research in the field of microgrid, in order to improve the fault tolerance and stability of the system, this chapter adopts a droop control technology to realize the coordinated distribution of power.

The rest of this chapter is organized as follows. The structure and droop characteristic of the multi-

source hybrid power system is analyzed in section 4.2; In section 4.3, the presented power distribution method is elaborated; Method validation and results analysis are detailed in section 4.4; Finally, the main conclusions are drawn in subsection 4.5.

4.2. Multi-source hybrid power system analysis

4.2.1. System structure analysis

Due to that parallel-connected architecture performs better than serial-connected architecture in terms of system flexibility and system performance [4,6,12–14], the structure of the multi-source hybrid power system constructed in this chapter adopts the former one. As depicted in Fig. 4.1, the powertrain of the multi-source hybrid power system developed in this chapter is mainly composed of two parts, one of which is a multi-battery system and the other is a multi-stack FC system. The multi-battery system includes N2 batteries and N2 bidirectional DC/DC converters. In addition, the multi-stack FC system consists of N1 independent stack and N1 unidirectional DC/DC converters. The hybrid power system also includes a power distribution controller, as well as some other auxiliary systems. The primary parameters of the built hybrid power system are shown in TABLE 4.1.

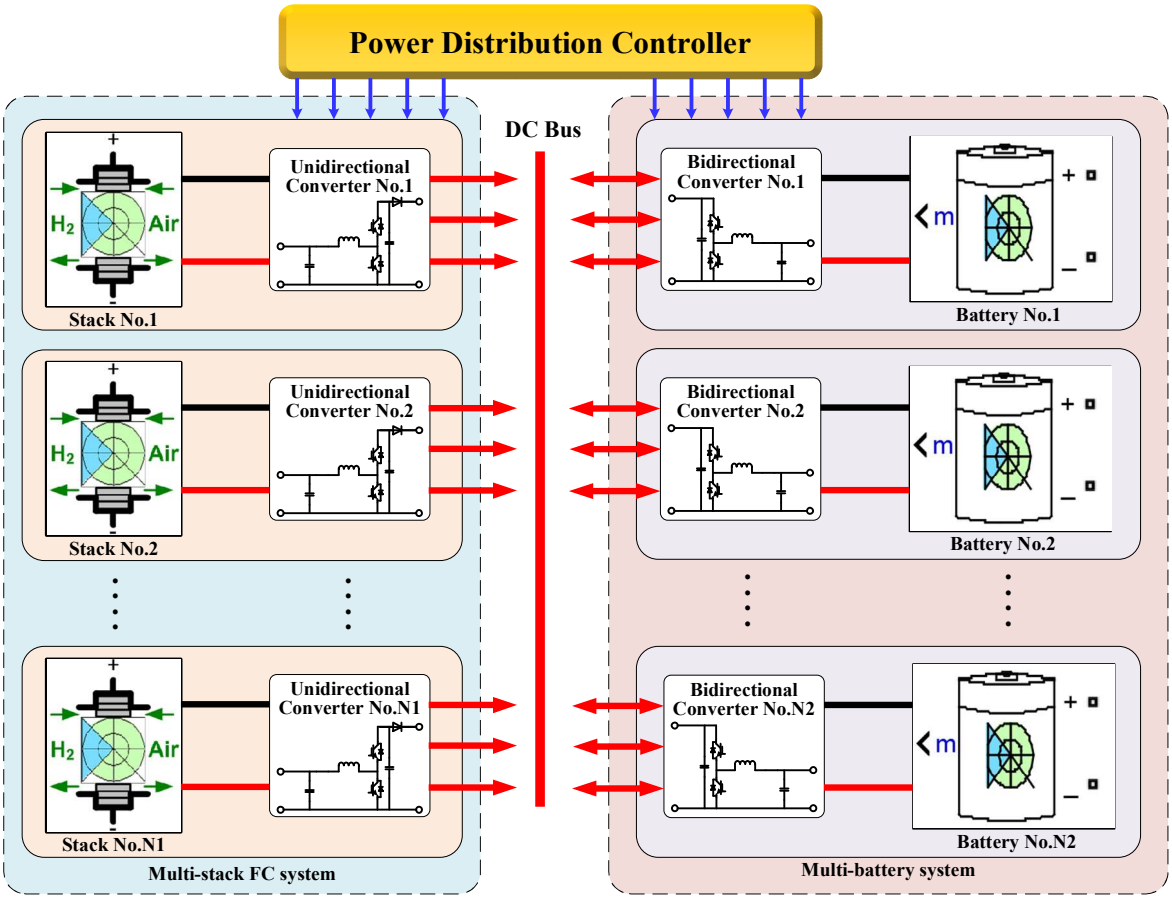

Figure 4.1. The structure of the multi-source hybrid power system.

TABLE 4.1. Primary parameters of the system.

Multi-source hybrid power system			
DC bus voltage	750 V	Power level	About 800 kW
Battery			
Type	Li-ion	Rated voltage	336 V
Capacity	15Ah	Set numbers	4 parallel
Mass	About 140 kg	-	-
FC			
Type	Water-cooled	Rated power	110 kW
Voltage	420~720 V	Set number	4 parallel
Max current	320 A	-	-

4.2.2. Components modeling

It should be mentioned that the battery and FC simulation models used in this chapter have been introduced in detail in the **Section 2.2** of **Chapter 2**, and the validity of the established models has been verified, so this chapter will not repeat the modeling of the power supplies (battery and FC) in the powertrain. In addition, as shown in Fig. 4.1, each power source delivers electric energy to the DC bus through a DC/DC converter. Taking into consideration that the traction common bus voltage is 750V, the maximum output voltage of the power sources used in this chapter (see TABLE 4.1) is lower than the bus voltage. Therefore, two boost-type DC/DC converter models are established in this chapter, one of which is a bidirectional DC/DC converter for connecting battery to the bus, and the other is a unidirectional DC/DC converter for cascading FC [3,14,15]. The topologies are shown in Fig. 4.2. Each model has two switching transistors, which can be controlled by two complementary pulse width modulation (PWM) signals with dead time. By adjusting S_1 and S_4, then the power generated by FCs and batteries can be determined.

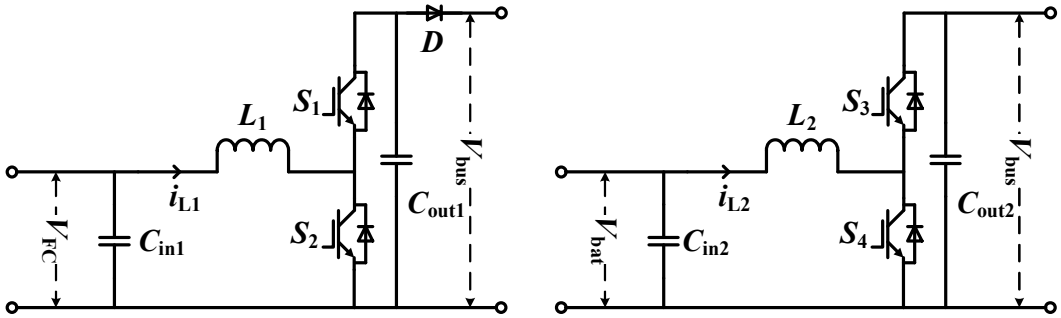

(a) The unidirectional DC/DC converter for FC (b) The bidirectional DC/DC converter for battery

Figure 4.2. The built DC/DC converter models.

4.2.3. System droop characteristic analysis

In such a multi-source hybrid system, there are a large number of power sources. In order to maintain the stable operation of the system, the droop control method is usually adopted [3,16–18]. The system

structure shown in Fig. 4.1 can be simplified to Fig. 4.3 (a), and the equivalent circuit on the load side can be depicted in Fig. 4.3 (b). Where V_{FCi} and I_{FCi} represent the voltage and current of stack No.i, respectively. V_{bati} and I_{bati} represent the voltage and current of battery No.i, respectively. In addition, V_{dci} and I_{dci} stand for the voltage and current of converter No.i respectively, V_{bus} and I_{bus} represent DC bus voltage and current respectively, and R_{li} represents the line resistance of converter No.i (i = 1, 2, ⋯ represents the i-th system branch).

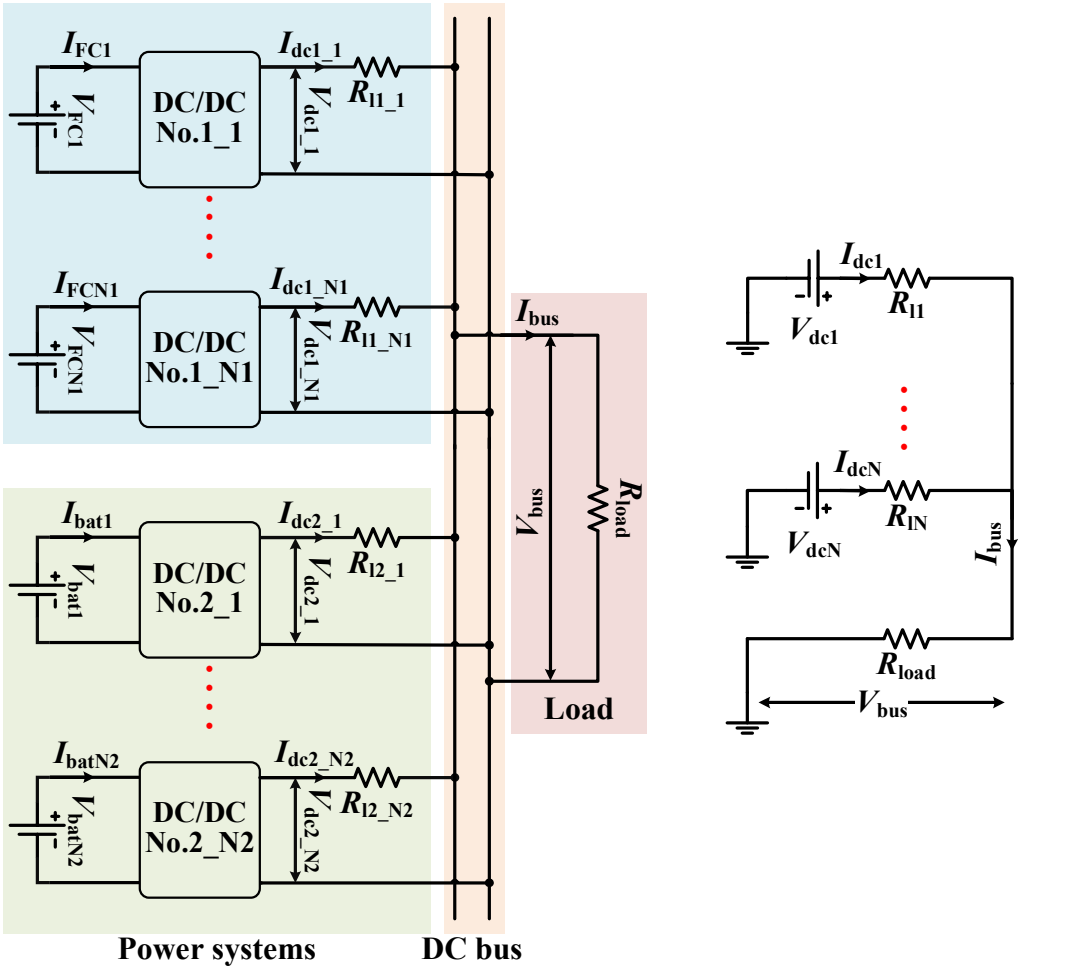

(a) Simplified diagram of the hybrid system (b) The equivalent circuit for the load side

Figure 4.3. Simplified equivalent circuit diagram of the multi-source hybrid power system.

In Fig. 4.3 (b), the I-V characteristic curve of the converter No.i can be expressed as:

$$V_{dci} = V_{dc}^{*} - I_{dci}R_{li} \tag{4.1}$$

where V_{dc}^{*} represents the reference voltage. When the output current change of the converter is ΔI, the voltage change on the line resistance is ΔV, and there are:

$$\frac{\Delta V}{\Delta I} = R_{l} \tag{4.2}$$

here, $\Delta V/\Delta I$ represents the output voltage adjustment rate of the converter. According to Eq. (4.2), the

output voltage droop characteristic curve of the converter can be drawn, as shown in the figure below [3,19].

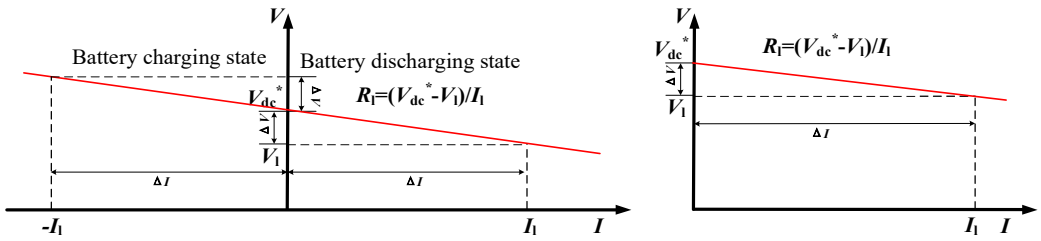

(a) Battery system output voltage droop characteristic (b) FC system output voltage droop characteristic

Figure 4.4. Output voltage droop characteristic curves.

In Fig. 4.4 (a), the positive half axis of the abscissa represents the battery discharging characteristic curve, and the negative half axis represents the battery charging characteristic curve. It can be seen from Fig. 4.4 that when the system is discharging, the droop control method will reduce the DC bus voltage, on the contrary, it will increase the DC bus voltage during charging.

In addition, according to Kirchhoff's voltage law (KVL), the relationship between the voltage, current and resistance in Fig. 4.3 (b) can be expressed by:

$$\begin{cases} V_{\mathrm{dc1}} = I_{\mathrm{dc1}} R_{\mathrm{l1}} + V_{\mathrm{bus}} \\ \vdots \\ V_{\mathrm{dcN}} = I_{\mathrm{dcN}} R_{\mathrm{lN}} + V_{\mathrm{bus}} \end{cases} \tag{4.3}$$

Moreover, according to Kirchhoff's current law (KCL), the voltage and current of the bus have the following mathematical form:

$$\begin{cases} V_{\mathrm{bus}} = I_{\mathrm{bus}} R_{\mathrm{load}} \\ I_{\mathrm{bus}} = \sum_{i=1}^{n} I_{\mathrm{dci}} \end{cases} \tag{4.4}$$

where R_{load} is the load resistance. Since the load resistance is much larger than the line resistances ($R_{\mathrm{load}} \gg R_{\mathrm{li}}$), the output current of each converter can be obtained by:

$$\begin{bmatrix} I_{\mathrm{dc1}} \\ \vdots \\ I_{\mathrm{dcN}} \end{bmatrix} = \begin{bmatrix} \dfrac{(V_{\mathrm{dc1}}/R_{l1})\prod_{i=1}^{N} R_{\mathrm{li}}}{R_{\mathrm{m}}} \\ \vdots \\ \dfrac{(V_{\mathrm{dcN}}/R_{\mathrm{lN}})\prod_{\mathrm{i=1}}^{N} R_{\mathrm{li}}}{R_{\mathrm{m}}} \end{bmatrix} + \begin{bmatrix} \sum_{\mathrm{i}\neq 1}^{N}\left(\dfrac{1}{R_{\mathrm{l1}}+R_{\mathrm{li}}}\right) & \cdots & \dfrac{-1}{R_{\mathrm{l1}}+R_{\mathrm{lN}}} \\ \vdots & \ddots & \vdots \\ \dfrac{-1}{R_{\mathrm{lN}}+R_{\mathrm{l1}}} & \cdots & \sum_{i\neq N}^{N}\left(\dfrac{1}{R_{\mathrm{lN}}+R_{\mathrm{li}}}\right) \end{bmatrix} \times \begin{bmatrix} V_{\mathrm{dc1}} \\ \vdots \\ V_{\mathrm{dcN}} \end{bmatrix} \tag{4.5}$$

with:

$$R_{\mathrm{m}} = R_{\mathrm{load}} \sum_{\mathrm{i}=1}^{N} \left(\left(\prod_{\mathrm{i}=1}^{N} R_{\mathrm{li}} \right) \Big/ R_{\mathrm{li}} \right) \tag{4.6}$$

For a multi-source hybrid power system containing N power sources, each converter output current can be calculated through the Eq. (4.5) and Eq. (4.6). In addition, it can be obtained from the equation (4.5) that the power supplied by the converters could be determined by adjusting the output voltage of converters or changing line resistances.

4.3. Power distribution method and control algorithm design

As the current research on the multi-source hybrid power system is still insufficient, related energy management methods need to be improved [4,20,21], and most of research has been summarized in **Chapter 1**. In addition, although a few studies have investigated power allocation methods for multi-stack FC systems and multi-battery systems, the main concerns are system efficiency and energy consumption, while the impact of power sources performance degradation on power allocation of the system has been barely studied [1,3,4,6,22–24]. In the multi-source hybrid power system, since the operating parameters (temperature, humidity, output power, etc.) of each power source are not completely consistent, in this state, long-term operation will lead to differences in operating performance and SOC among the power sources. If this difference in operating status is ignored and all batteries or stacks are controlled to output the same power, it will lead to over discharge of the lower SOC batteries, and cause the poorer performance stacks to degrade faster, which is not conducive to prolonging the service lifetime of the system [25,26].

In order to fill the above-mentioned research gap, keep the operating performance of each stack in the multi-stack FC system as consistent as possible, and make the SOC difference of each battery in the multi-battery system as small as possible, it is necessary to study the operating state consistent power distribution method under the premise of stabilizing the bus voltage. This chapter uses the battery SOC evaluation method proposed in the **Chapter 2** to measure the SOC (see Eq. (2.11)) of each battery in real time, and then uses the performance degradation degree evaluation method to estimate the operating state of each stack. In addition, the virtual droop control algorithm is used to adaptively adjust the output power of each power source according to the measurement results, so as to realize the adaptive control of the multi-source hybrid power system and achieve the purpose of consistent system performance [16,21].

4.3.1. Operating state consistency distribution method for the multi-source system

In the multi-battery system, battery SOC is an important indicator. The inconsistency of the SOC of each battery will lead to overcharge of the stack with large SOC and shorten the service lifetime of the entire system. Therefore, this chapter firstly conducts research on SOC consistency coordinated control in the

multi-battery system. The battery SOC can be calculated using the Eq. (2.11). When in discharging mode, a battery with a larger SOC should output more power to dissipate its power. When in charging mode, a battery with a smaller SOC should recycle more power to increase its SOC. In addition, considering the power balance relationship shown in Eq. (4.7), the reference power of batteries can be obtained, as shown in Eq. (4.8).

$$P_{\text{multi\_bat}} = P_{\text{bat1}} + P_{\text{bat2}} + \cdots + P_{\text{batN2}} \tag{4.7}$$

where $P_{\text{multi\_bat}}$ is the total required power of the multi-battery system, P_{bati} is the output power of battery No.i.

$$\begin{cases} P_{\text{bati\_ref}} = P_{\text{multi\_bat}} \times k_{\text{di}} & \text{Discharging mode} \\ P_{\text{bati\_ref}} = P_{\text{multi\_bat}} \times k_{\text{ci}} & \text{Charging mode} \end{cases} \tag{4.8}$$

with:

$$\begin{cases} \sum_{\text{i=1}}^{\text{N2}} k_{\text{di}} = 1 \\ k_{\text{di}} = \dfrac{SOC_{\text{i}}^{\text{nd}}}{SOC_{1}^{\text{nd}} + SOC_{2}^{\text{nd}} + \cdots + SOC_{\text{N2}}^{\text{nd}}} \\ \sum_{\text{i=1}}^{\text{N2}} k_{\text{ci}} = 1 \\ k_{\text{ci}} = \dfrac{2}{\text{N2}} - \dfrac{SOC_{i}^{\text{nc}}}{SOC_{1}^{\text{nc}} + SOC_{2}^{\text{nc}} + \cdots + SOC_{\text{N2}}^{\text{nc}}} \end{cases} \tag{4.9}$$

where $P_{\text{bati\_ref}}$ is the reference power of battery No.i, k_{ci} and k_{di} are the correction coefficients for battery No.i charging mode and discharging mode, respectively. In addition, SOC_{i} is the SOC of battery No.i, n_{d} and n_{c} denote the acceleration factors for discharging mode and charging mode, respectively. In summary, after the overall output power of the multi-battery system in the entire multi-source hybrid power system is determined, the reference power of each battery can be determined by Eq. (4.8) and Eq. (4.9).

In addition, according to the foregoing description, it is known that the performance among stacks in the multi-stack FC system may be inconsistent. If there is a performance difference among the stacks in the multi-stack FC system, the performance of the system will be limited by the worst performing stack [27]. Consequently, in order to minimize performance differences among the stacks and maintain the consistency of performance among the stacks, the influence of the performance difference among stacks on power splitting should be taken into account. In addition, this chapter also considers that the larger the rate of change in the output power of the stack, the faster the degradation of the stack performance and the shorter the lifespan [28–30]. Therefore, a poorly performing stack should provide less power fluctuation to improve its operating performance.

Since the output voltage and power of the stack can directly reflect the operating state of the stack [3,31], the operating state of the FC can be simply expressed as:

$$\lambda_{\mathrm{FCi}} = \frac{P_{\mathrm{FCi}}}{P_{\mathrm{ideal}}} \tag{4.10}$$

where λ_{FCi} represents the operating state of the FC No.i, and the closer its value is to 0, the worse the stack performance. P_{ideal} stands for the output power of the FC when the stack performance is good. Then the operating state of the stack can be estimated by Eq.(4.10), and its range is [0-1]. Then the ratio of the power fluctuation of each converter cascaded with the stack can be expressed by:

$$\begin{cases} K_{\mathrm{divi\_j}} = \dfrac{\lambda_{\mathrm{FCi}}}{\lambda_{\mathrm{FCj}}} = \dfrac{\Delta P_{\mathrm{dci}}}{\Delta P_{\mathrm{dcj}}} \\ \sum\limits_{\mathrm{i=1}}^{\mathrm{N1}} \Delta P_{\mathrm{dci}} = \Delta P_{\mathrm{multi\_stack}} \end{cases} \tag{4.11}$$

where $K_{\mathrm{divi\_j}}$ denotes the ratio of the output power fluctuation of converter No.i and the output power fluctuation of converter No.j, ΔP_{dci} represents the output power fluctuation of converter No.i, and $\Delta P_{\mathrm{multi\_stack}}$ stands for the multi-stack FC system demand power fluctuation. Then the output power fluctuation of each converter cascaded with the stack can be calculated by Eq. (4.12).

$$\begin{cases} \Delta P_{\mathrm{dc1}} = P_{\mathrm{dc1(t)}} - P_{\mathrm{dc1(t\text{-}1)}} = \dfrac{\Delta P_{\mathrm{multi\_stack}}}{1 + K_{\mathrm{div21}} + \cdots + K_{\mathrm{divN1\_1}}} \\ \vdots \\ \Delta P_{\mathrm{dcN1}} = P_{\mathrm{dcN1(t)}} - P_{\mathrm{dcN1(t\text{-}1)}} = \dfrac{\Delta P_{\mathrm{multi\_stack}}}{1 + K_{\mathrm{div1\_N1}} + \cdots + K_{\mathrm{div(N1\text{-}1)\_N1}}} \end{cases} \tag{4.12}$$

Then, the real-time reference power of each converter cascaded with the stack can be calculated by:

$$\begin{cases} P_{\mathrm{dc1(t)}} = P_{\mathrm{dc1(0)}} + \sum\limits_{\mathrm{i=1}}^{\mathrm{t}} \Delta P_{\mathrm{dc1(i)}} \\ \vdots \\ P_{\mathrm{dcN1(t)}} = P_{\mathrm{dcN1(0)}} + \sum\limits_{\mathrm{i=1}}^{\mathrm{t}} \Delta P_{\mathrm{dcN1(i)}} \end{cases} \tag{4.13}$$

where $P_{\mathrm{dci}}(0)$ represents the initial output power value of converter No.i. In addition, considering the power balance of the hybrid system, there is the following functional relationship between each system.

$$P_{\mathrm{multi\_stack}} + P_{\mathrm{multi\_bat}} = P_{\mathrm{demand}} \tag{4.14}$$

where P_{demand} represents the load demand power of the whole hybrid system.

4.3.2. Equal distribution method

The equal distribution method is the most common power distribution method in multi-source system, which has the advantages of strong stability and easy implementation [21,24]. Since the management research on the output power of each power source in the multi-source hybrid power system is still relatively limited, this chapter uses the above-mentioned power distribution method as a test benchmark to compare and analyze the proposed method. The equal distribution method is also called the power equal distribution control strategy, and the reference power of each power source in the system can be calculated by the following formula.

$$\begin{cases} \sum_{i=1}^{N1} K_{\mathrm{FCi}} P_{\mathrm{FCi\_ref}} + \sum_{j=1}^{N2} K_{\mathrm{batj}} P_{\mathrm{batj\_ref}} = P_{\mathrm{demand}} \\ K_{\mathrm{FC1}} = K_{\mathrm{FC2}} = \cdots = K_{\mathrm{FCN1}} \\ \sum_{i=1}^{N1} K_{\mathrm{FCi}} = 1 \\ K_{\mathrm{bat1}} = K_{\mathrm{bat2}} = \cdots = K_{\mathrm{batN2}} \\ \sum_{j=1}^{N2} K_{\mathrm{batj}} = 1 \end{cases} \tag{4.15}$$

where K_{FCi} represents the ratio of the output power of the i-th stack to the required power of the multi-stack FC system. In addition, K_{batj} represents the ratio of the output power of the j-th battery to the required power of the multi-battery system. It can be seen from Eq. (4.15) that under the control of the equal distribution method, the output power of each stack is the same, and in addition, the output power of each battery is also the same. As mentioned above, although the equal distribution method is simple, it is not conducive to maintain the consistency of system operating state.

4.3.3. Droop control algorithm based on virtual impedance

In this chapter, in order to minimize the operating state difference among the power sources in the built multi-source hybrid power system, an operating state consistency power distribution method considering multiple influencing factors (operating state of stacks and SOC of batteries) is addressed. In this method, the reference output power of each converter is determined by the operating state of each stack and the SOC of each battery, and the power splitting process could be realized by changing the values of virtual resistances. Therefore, an instantaneous virtual resistance calculation technique is proposed in this section. In addition, considering that the virtual droop control will increase the deviation between the bus voltage and the reference voltage (750 V) [9,17], a voltage regulation technology is also presented to stabilize the DC bus voltage.

4.3.3.1. Instantaneous virtual resistances calculation

According to the description in section 4.2.3, the purpose of controlling the output power of the

converters can be achieved by changing the line resistances. In order to not increase the complexity and power loss of the system, and to ensure that each converter can adjust its output power according to the operating state of each power source, a virtual droop control algorithm is added to the control strategy in this chapter [16–18]. After adding the virtual resistance R_{droop}, the simplified and equivalent circuit for the multi-source hybrid power system can be modified as shown in Fig. 4.5.

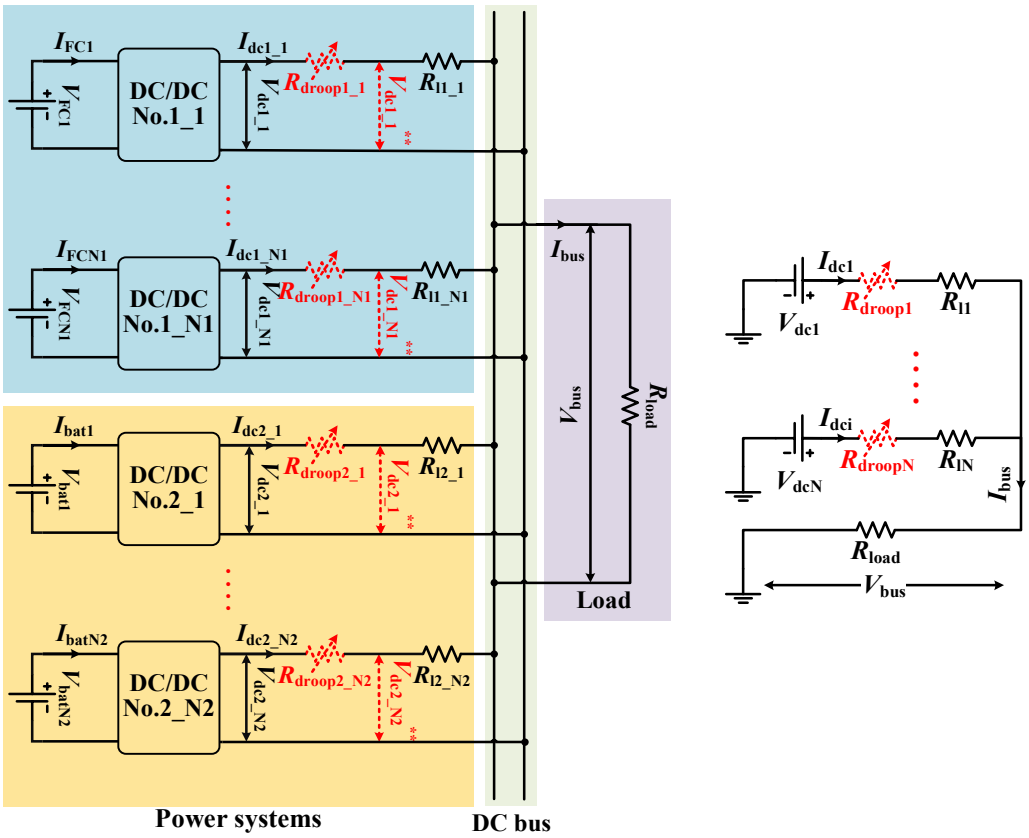

(a) Simplified diagram of the hybrid system with virtual resistances

(b) The steady-state equivalent circuit for the system with virtual resistances

Figure 4.5. Simplified equivalent circuit diagram of the multi-source hybrid system after adding virtual resistances.

According to Eq. (4.5), after adding virtual resistances to the hybrid system, the output current of each converter can be expressed as

$$\begin{bmatrix} I_{dc1} \\ \vdots \\ I_{dcN} \end{bmatrix} = \begin{bmatrix} \frac{\psi_1}{R_m^*} \\ \vdots \\ \frac{\psi_N}{R_m^*} \end{bmatrix} + \begin{bmatrix} \sum_{i\neq 1}^{N}\left(\frac{1}{R_{x1}+R_{xi}}\right) & \cdots & \frac{-1}{R_{x1}+R_{xN}} \\ \vdots & \ddots & \vdots \\ \frac{-1}{R_{xN}+R_{x1}} & \cdots & \sum_{i\neq N}^{N}\left(\frac{1}{R_{xN}+R_{xi}}\right) \end{bmatrix} \times \begin{bmatrix} V_{dc1} \\ \vdots \\ V_{dcN} \end{bmatrix} \tag{4.16}$$

with:

$$\begin{cases} \psi_{\mathrm{i}} = \left(V_{\mathrm{dci}} \Big/ \left(R_{\mathrm{li}} + R_{\mathrm{droopi}}\right)\right) \prod_{\mathrm{i}=1}^{N} \left(R_{\mathrm{li}} + R_{\mathrm{droopi}}\right) \\ R_{\mathrm{m}}^{*} = R_{\mathrm{load}} \sum_{\mathrm{i}=1}^{N} \left(\left(\prod_{\mathrm{i}=1}^{N} \left(R_{\mathrm{li}} + R_{\mathrm{droopi}}\right) \right) \Big/ \left(R_{\mathrm{li}} + R_{\mathrm{droopi}}\right) \right) \\ R_{\mathrm{xi}} = R_{\mathrm{li}} + R_{\mathrm{droopi}} \end{cases} \tag{4.17}$$

According to Eq. (4.16), the added virtual resistances can affect the output current of each converter in the hybrid system. The values of the virtual resistances added to the controller can be calculated according to the reference power obtained in the sections 4.3.1 and 4.3.2. The instantaneous virtual resistance in the controller can be calculated by substituting the obtained reference power into Eq. (4.16), as shown below.

$$\begin{bmatrix} \frac{P_{\mathrm{dc1(t)}}}{V_{\mathrm{bus(t)}}} \\ \vdots \\ \frac{P_{\mathrm{dcN(t)}}}{V_{\mathrm{bus(t)}}} \end{bmatrix} = \begin{bmatrix} \frac{\psi_{1(t)}}{R_{\mathrm{m(t)}}^{*}} \\ \vdots \\ \frac{\psi_{\mathrm{N(t)}}}{R_{\mathrm{m(t)}}^{*}} \end{bmatrix} + \begin{bmatrix} \sum_{\mathrm{i}\neq 1}^{\mathrm{N}} \left(\frac{1}{R_{\mathrm{x1(t)}} + R_{\mathrm{xi(t)}}} \right) & \cdots & \frac{-1}{R_{\mathrm{x1(t)}} + R_{\mathrm{xN(t)}}} \\ \vdots & \ddots & \vdots \\ \frac{-1}{R_{\mathrm{xN(t)}} + R_{\mathrm{x1(t)}}} & \cdots & \sum_{\mathrm{i}\neq \mathrm{N}}^{\mathrm{N}} \left(\frac{1}{R_{\mathrm{xN(t)}} + R_{\mathrm{xi(t)}}} \right) \end{bmatrix} \times \begin{bmatrix} V_{\mathrm{dc1(t)}} \\ \vdots \\ V_{\mathrm{dcN(t)}} \end{bmatrix} \tag{4.18}$$

Furthermore, due to the virtual resistances added to the multi-source hybrid power system, the reference voltage of each converter will be affected [9,32]. After the values of the virtual resistances are determined by the Eq. (4.18), the reference voltage of the converter No.i can be updated according to Eq. (4.19).

$$V_{\mathrm{dci}}^{**} = V_{\mathrm{dc}}^{*} - I_{\mathrm{dci}} R_{\mathrm{droopi}} \tag{4.19}$$

In this equation, V_{dc}^{*} denotes the traction bus reference voltage and V_{dci}^{**} represents the new reference output voltage of converter No.i.

When the line resistance is taken into consideration, Eq. (4.19) should be rewritten as:

$$V_{\mathrm{dci}}^{**} = V_{\mathrm{dc}}^{*} - I_{\mathrm{dci}} R_{\mathrm{droopi}} - I_{\mathrm{dci}} R_{\mathrm{li}} \tag{4.20}$$

Based on research [3,33], the value of the line resistance is usually between 0Ω and 1Ω. Therefore, the value of R_{li} in this study is also taken between 0-1.

4.3.3.2. Bus voltage regulation technology

From Eq. (4.20), it can be known that both the R_{droopi} and R_{li} will cause the bus voltage to drop, which is not conducive to maintaining the stable operation of the system. Consequently, in order to achieve the purpose of recovering the bus voltage variation caused by the virtual droop control without disturbing the power allocation method, a voltage control strategy is presented in this chapter. This voltage control

strategy adds a voltage correction factor (ΔV_{ref}) to the reference voltage V_{dc}^{*}. The ΔV_{ref} can be obtained by inputting the difference between the reference voltage $V_{\mathrm{dc}*}$ and the bus voltage V_{bus} into the PI controller. The solution process can be expressed by:

$$\Delta V_{\mathrm{ref}} = K_{\mathrm{P}}\left(V_{\mathrm{dc}}^{*} - V_{\mathrm{bus}}\right) + K_{\mathrm{I}}\int\left(V_{\mathrm{dc}}^{*} - V_{\mathrm{bus}}\right)dt \tag{4.21}$$

where K_{I} and K_{P} present the integral gain and proportional gain of the PI controller, respectively. In addition, the value of ΔV_{ref} is limited so that the bus voltage fluctuation never exceeds the maximum voltage deviation limit (±5% of the reference voltage). Through the voltage control strategy adjustment, the new V_{dci}^{**} value can be calculated by:

$$V_{\mathrm{dci}}^{**} = V_{\mathrm{dc}}^{*} + \Delta V_{\mathrm{ref}} - I_{\mathrm{dci}}R_{\mathrm{droopi}} - I_{\mathrm{dci}}R_{\mathrm{li}} \tag{4.22}$$

The voltage control strategy can offset the issue of bus voltage drop caused by the virtual droop control. Therefore, this strategy can ensure that the bus voltage is close to the reference voltage.

In summary, the presented power distribution method can be implemented by the framework diagram shown in Fig. 4.6.

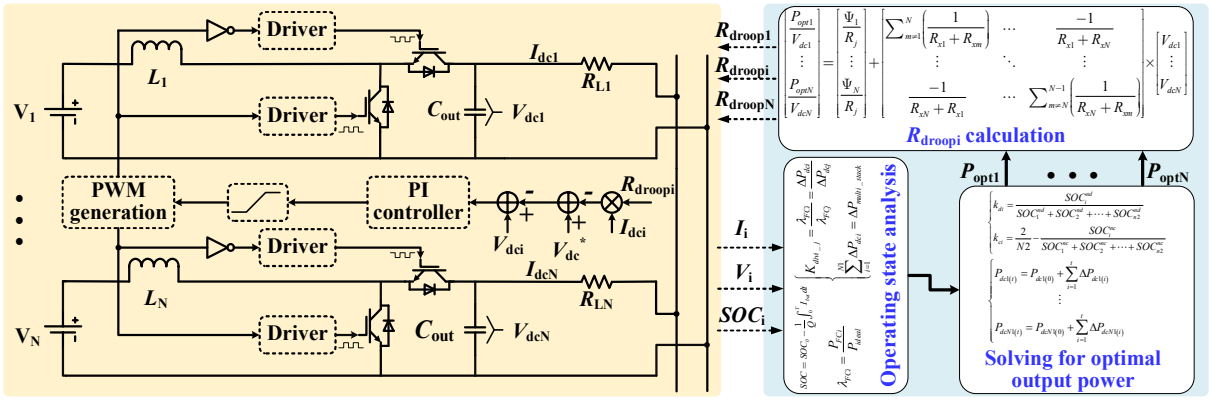

Figure 4.6. Structure diagram of the proposed power distribution method for the multi-source hybrid power system.

Firstly, the optimal output power of the multi-stack FC system and the multi-battery system can be obtained according to the energy management strategies used in the dual-source hybrid system proposed in **Chapter 2** and **Chapter 3**. Next, the proposed consistency power distribution method will be used to determine the reference power of each converter according to the real-time operating performance of the stack and the SOC of the battery. Then, based on the reference power, the added virtual resistances can be solved by using the instantaneous virtual resistance calculation technique. Finally, the voltage control strategy is presented to stabilize the bus voltage.

4.4. Comparative analysis of experimental results

In this chapter, I use the hardware-in-the-loop (HIL) simulation platform to demonstrate the effectiveness of the presented operating state consistency power distribution method. The HIL simulation platform can demonstrate the effectiveness and practicability of the presented method online. The structure of the test bench is depicted in Fig. 2.21. It should be mentioned that the HIL test bench has been introduced in detail in **Section 2.4** of **Chapter 2**, so this chapter will not repeat the introduction. In the test experiments in this chapter, 4 sets of stacks and 4 sets of batteries are used to form a multi-stack FC system and a multi-battery system, respectively. To test the effect of the proposed power distribution method when the performance of some stacks in the multi-stack FC system is degraded, this chapter uses a stack with a working time of 800 hours (stack No.3) and a stack with a working time of 1200 hours (stack No.4). In addition, in order to obtain the operating condition to test the effectiveness and performance of the presented power distribution method and droop control algorithm, this chapter adopts power following (PF) strategy presented in the **Chapter 2** to disassemble the tram driving cycle. The total required power of the multi-source hybrid power system is shown in Fig. 4.7 (a), and the respective required powers of the multi-battery system and the multi-stack FC system can be obtained by using PF strategy, as shown in Fig. 4.7 (b) and Fig. 4.7 (c).

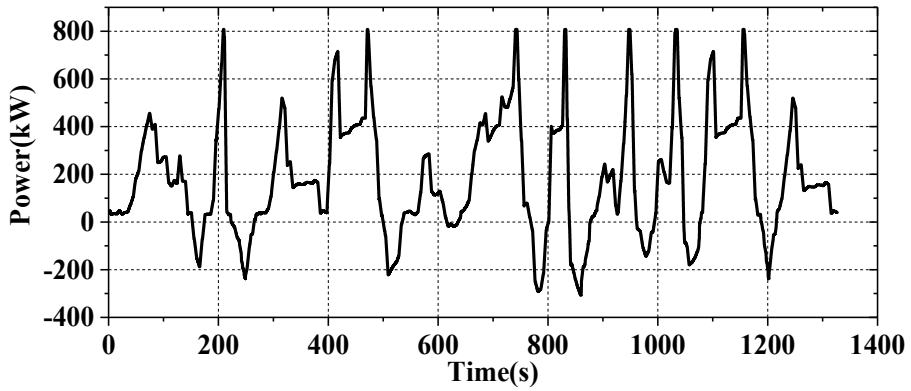

(a) Total operating condition of the multi-source hybrid power system

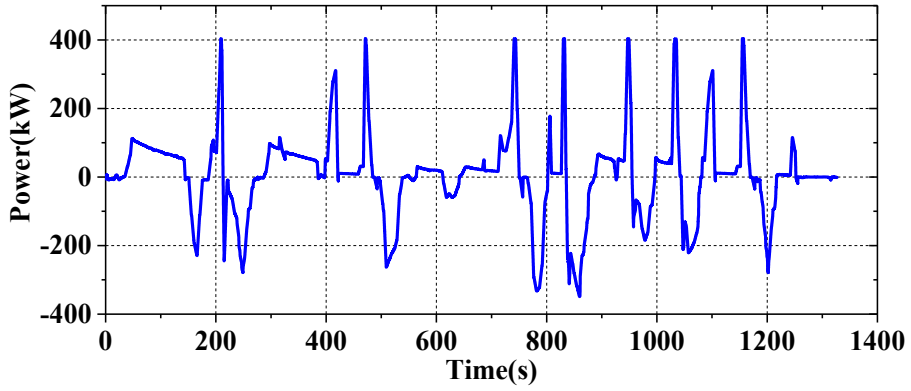

(b) Demand power for multi-battery system

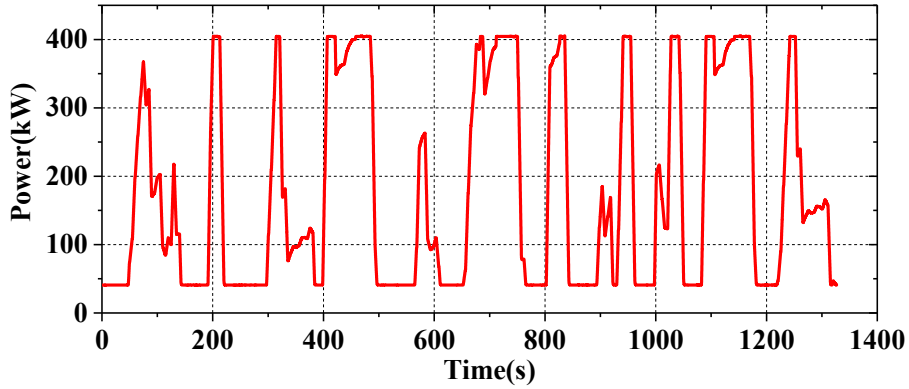

(c) Demand power for multi-stack FC system

Figure 4.7. Systems operation test conditions.

Fig. 4.7 presents the power output curves of the multi-stack FC system and multi-battery system when PF strategy is used. To test the performance of the presented power distribution method, this chapter analyzes the output power of each power source, the SOC fluctuation of battery, the stack operating stress, and also tests the fault-tolerant control capability of the hybrid system.

4.4.1. Comparative analysis of output power

On the test platform, the equal distribution method and the proposed operation consistency power distribution method are tested under the working conditions. Under the control of different power distribution methods, the output power curves of FCs and batteries are shown in Fig. 4.8.

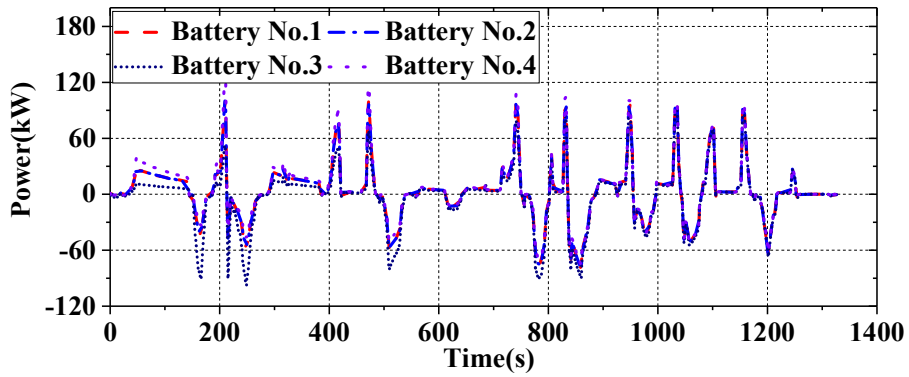

(a) The batteries output power curves under the control of the proposed distribution method

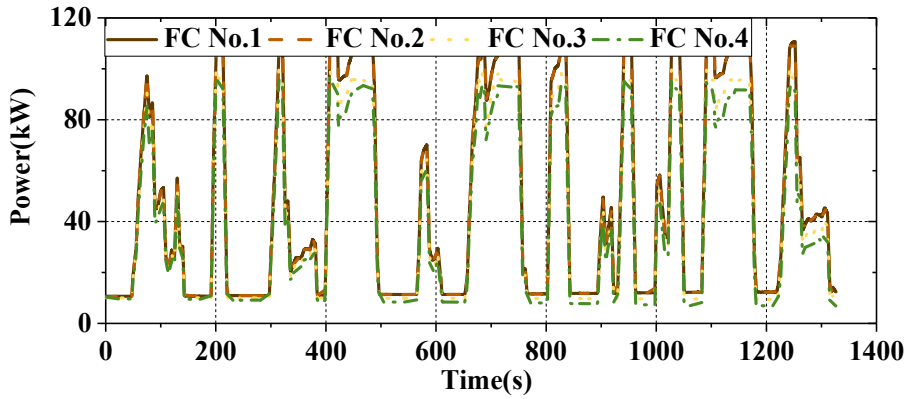

(b) The FCs output power curves under the control of the proposed distribution method

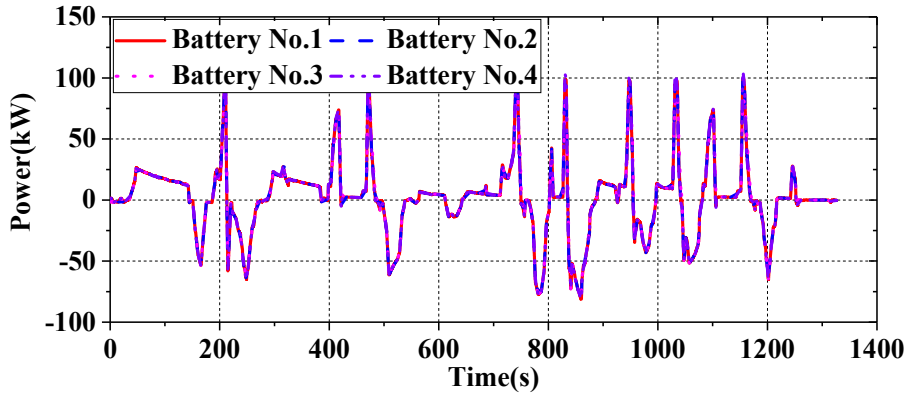

(c) The batteries output power curves under the control of the equal distribution method

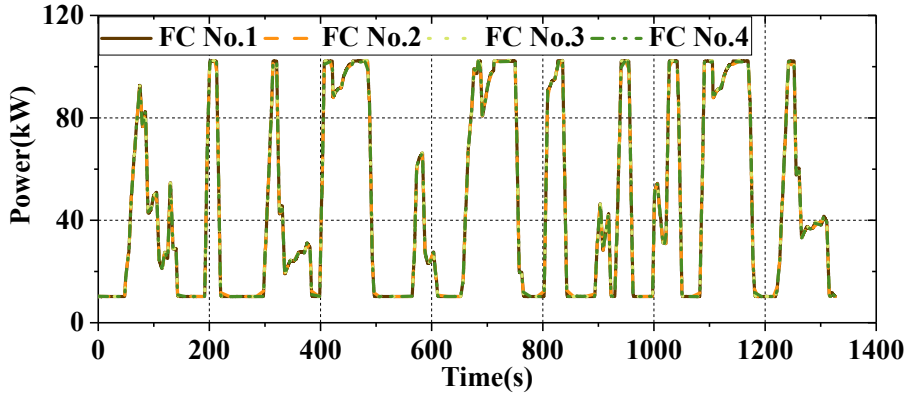

(d) The FCs output power curves under the control of the equal distribution method

Figure 4.8. Power sources output power curves using different power distribution methods.

As can be seen from Fig. 4.8, under the control of the equal distribution method, each stack outputs the same power, and each battery also outputs the same power, and the demand power of each system is equally distributed. In addition, under the control of the proposed consistency distribution method, the output power fluctuation of each stack can be adjusted in real time by its operating state, and the output power of each battery can be adjusted by its SOC. It can be seen that the constructed multi-source hybrid power system can be controlled according to the proposed power distribution method, and can operate continuously and stably.

4.4.2. Battery SOC fluctuation analysis

SOC is a particularly important indicator of the multi-battery system [34]. According to Eq. (2.11) and the output current of each battery, the real-time SOC of each battery under the control of different distribution methods can be calculated, the output current curves of the batteries and the operating SOC curves of the batteries are shown in Fig. 4.9.

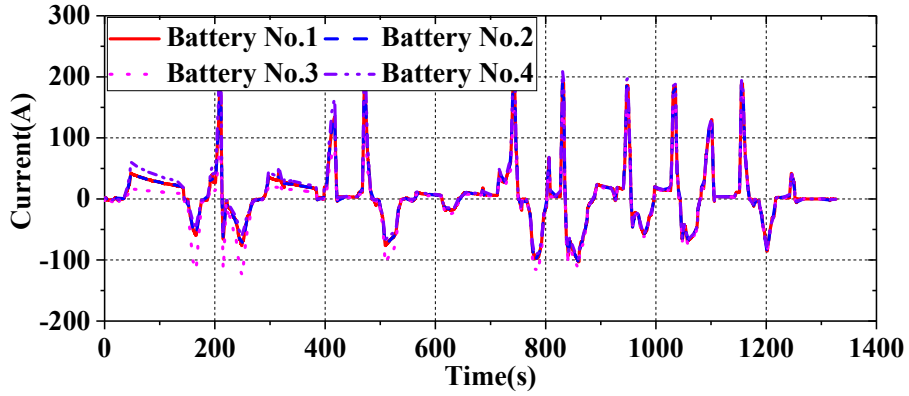

(a) The batteries output current curves under the control of the proposed distribution method

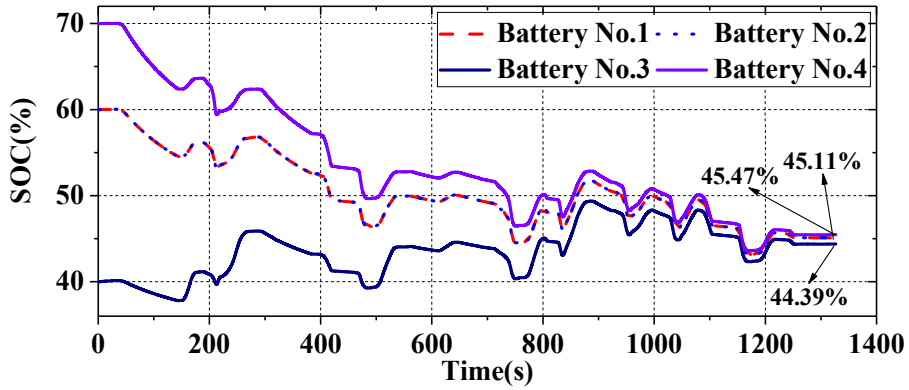

(b) The batteries SOC curves under the control of the proposed distribution method

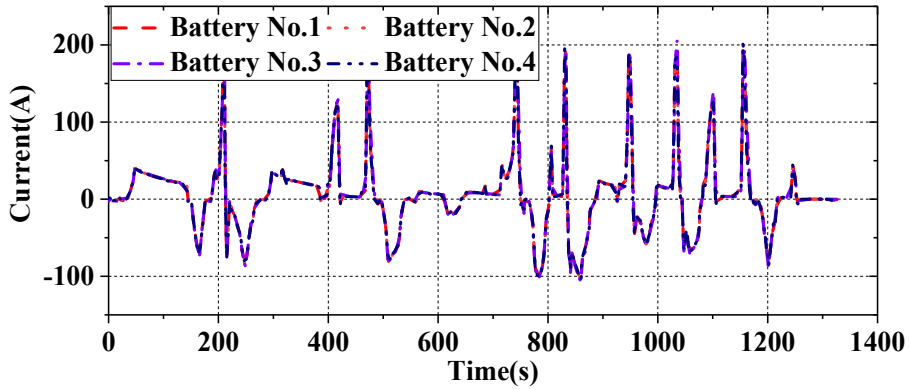

(c) The batteries output current curves under the control of the equal distribution method

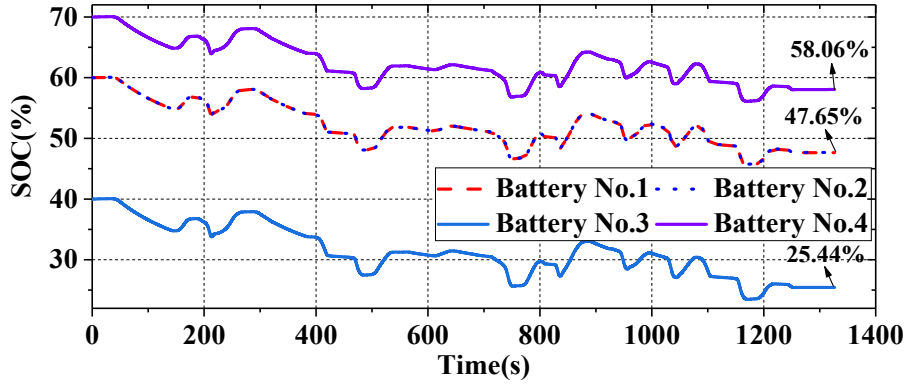

(d) The batteries SOC curves under the control of the equal distribution method

Figure 4.9. The SOC curves of batteries using the different distribution methods.

In order to highlight the advantages of the proposed consistency distributed method, the SOC initial value of battery No.1 and battery No.2 is both set to 60%, the SOC initial value of battery No.3 is set to 40%, and the SOC initial value of battery No.4 is set to 70%. In the Fig. 4.9, under the control of the proposed distribution method, the final SOC values of each battery are 45.11% (battery No.1), 45.11% (battery No.2), 44.39% (battery No.3), and 45.47% (battery No.4), respectively. In addition, under the control of the equal distribution method, the final SOC values of each battery are 47.65% (battery No.1), 47.65% (battery No.2), 25.44% (battery No.3), and 58.06% (battery No.4), respectively. It can be seen from Fig. 4.9 (a) and Fig. 4.8 (a) that under the control of the proposed distribution method, when the system is in the discharging mode, the battery with a larger SOC outputs a larger power, and when the system is in the charging mode, the battery with a smaller SOC absorbs more power. Therefore, as the system operates, the SOC difference of the batteries in the system gradually becomes smaller. It is proved that the proposed consistency distribution method is beneficial to improve the SOC consistency in the multi-battery system, thereby improving the operating performance of the system.

4.4.3. Stack operating stress analysis

According to [9,14,28], it is mentioned that the key impact on stack degradation is allocated to power dynamics. The analysis of the fluctuation of the FC output power through wavelet transform can give a clear indication of how often each stack is solicited [25]. When the change rate of the stack output power is larger, the performance of the stack decreases faster, resulting in a shorter lifespan. Therefore, the poorer the operating state of the stack, the more its output power should be smoothed. Under the control of different distribution methods, the results of the operating stress of stacks are presented in Fig. 4.10.

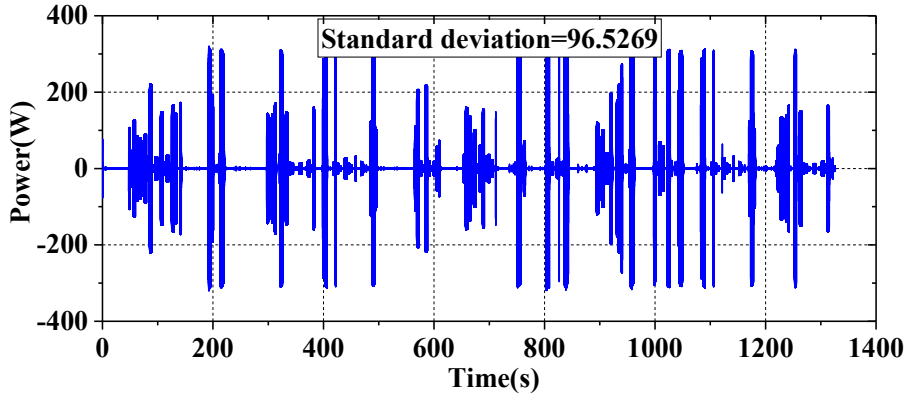

(a) The equal distribution method

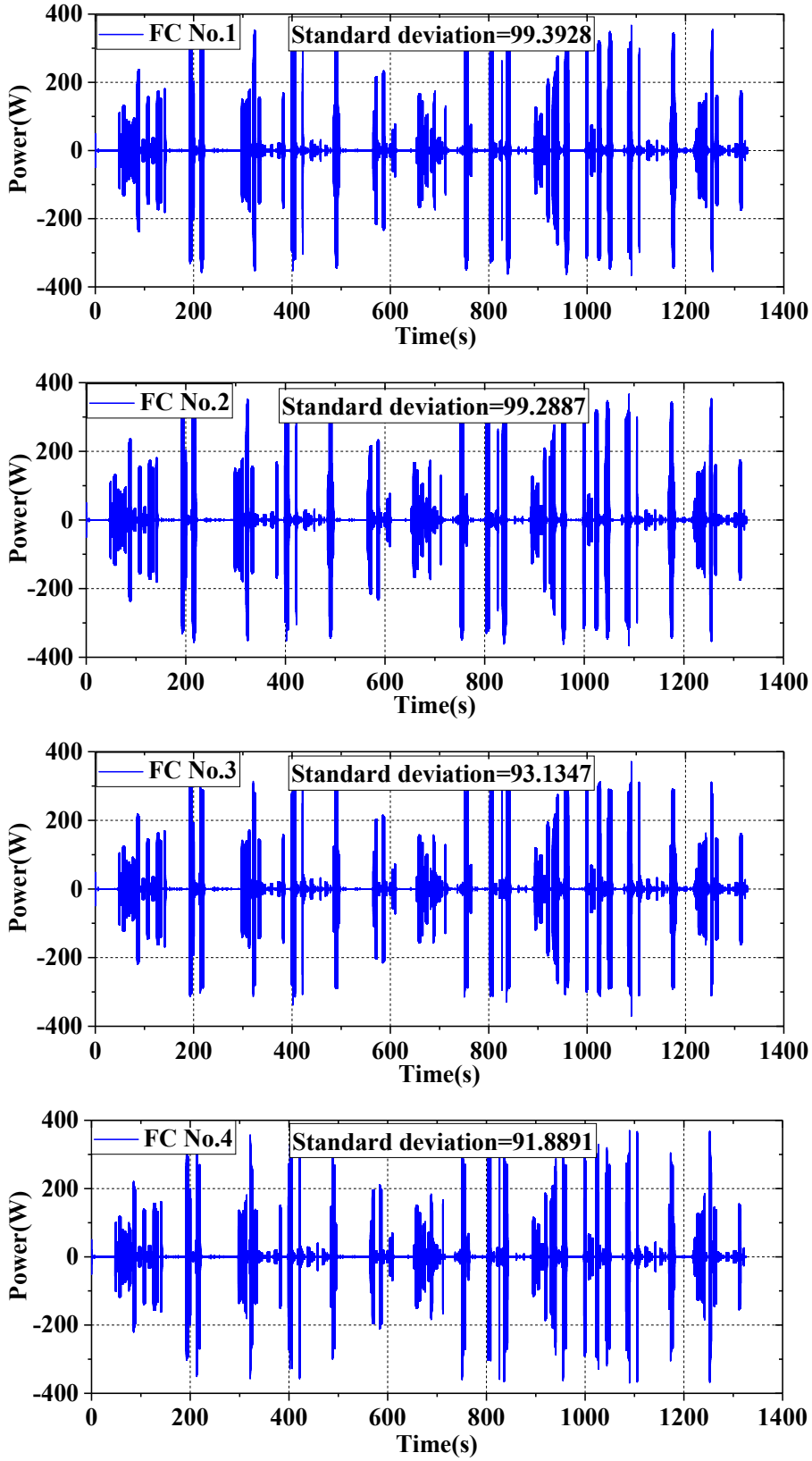

(b) The proposed consistency distribution method

Figure 4.10. The stacks operating stress using different power distribution methods.

It can be observed from the Fig. 4.10 that under the control of the equal distribution method, the output

power of each stack is the same, so the operating stress of each stack is also equal, which is 96.5269. In addition, under the control of the presented power distribution method, the more serious the performance degradation of the stack is, the smaller the output power fluctuation of the stack is. The experimental results show that the operating stress of the stacks No.1, No.2, No.3 and No.4 are 99.3928, 99.2887, 93.1347, and 91.8891, respectively. It is obvious that the proposed power distribution method helps to make the stacks' performance uniform, thereby extending the lifespan of the system.

4.4.4. Bus voltage fluctuation analysis

In addition, under the control of the droop control algorithm based on bus voltage regulation and the traditional droop control algorithm, the DC bus voltage fluctuation curves are shown in Fig. 4.11.

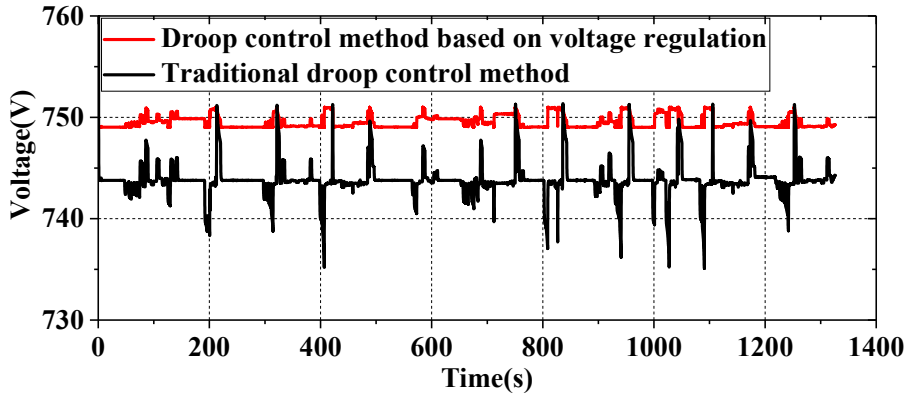

Figure 4.11. DC bus voltage fluctuation curves.

In Fig. 4.11, the black curve is the bus voltage fluctuation curve under the adjustment of the traditional virtual resistance droop control algorithm, and the voltage fluctuation range is 735 V-755 V. In addition, the red curve is the bus voltage fluctuation curve adjusted by the voltage regulation technology mentioned in section 4.3.3.2, the voltage fluctuation range is 745 V-755 V, and the voltage fluctuation is small. Therefore, compared with the traditional droop control algorithm, the proposed voltage regulation method has better performance and is more conducive to maintaining the bus voltage stability.

4.4.5. System fault-tolerant analysis

Taking into consideration that in the multi-source hybrid power system, a certain power source (battery or FC) may suddenly fail and cannot work, this chapter also tests the function of the presented method and system for fault-tolerant operation. This chapter uses the test condition shown in Fig. 4.12 to perform a plug-and-play functional test for the multi-battery system.

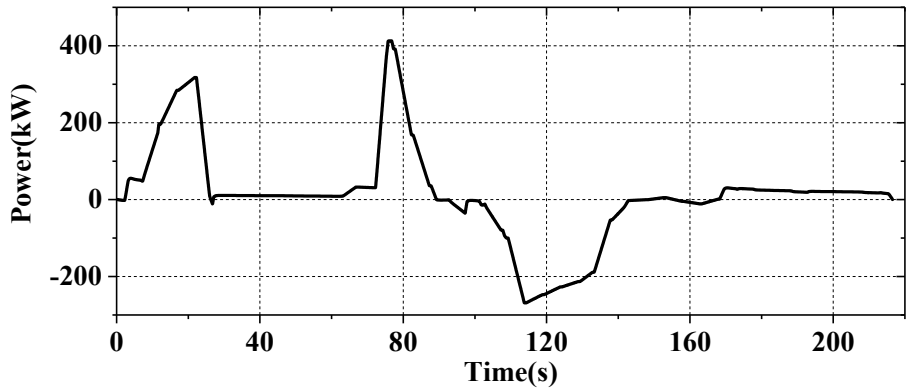

Figure 4.12. Test condition used to test fault-tolerance control of multi-battery system.

In this experiment, it is assumed that the battery No.1 failed at about 20 s, and then reconnected battery No.1 to the system at about 114 s. The experimental results are shown in Fig. 4.13.

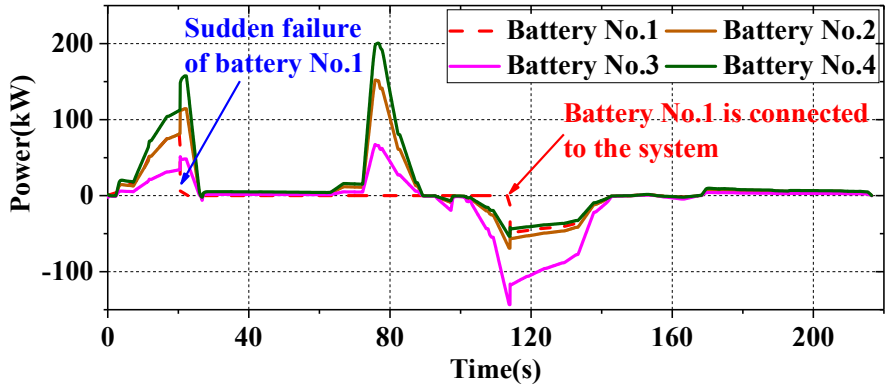

(a) Batteries output power curves

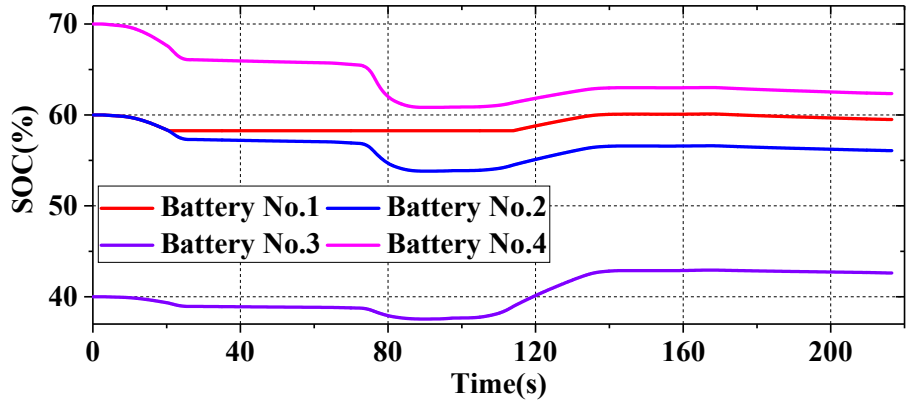

(b) Batteries SOC curves

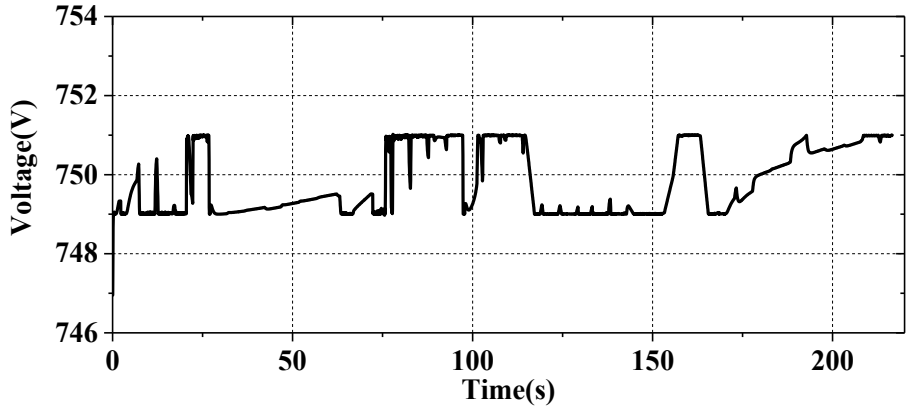

(c) Bus voltage fluctuation curve

Figure 4.13. Experimental results for testing multi-battery system fault-tolerant control capability.

It can be clearly observed in Fig. 4.13 that when the operating time is about 20 s, the battery No.1 is stopped by turning off the switch connected to the bus, which is used to simulate the sudden failure of the battery during operation. When the system operating time is about 114 s, the switch is closed, so that the battery No.1 can continue to provide power for the system. It can also be seen that before the switch is turned off (before 20 s), the four batteries distribute the demand power according to their respective SOC. After the switch is turned (between 20 s and 114 s), the output power of the battery No.1 is 0, its SOC doesn't change, and the remaining three batteries still distribute the demand power according to their respective SOC. When the switch is closed (after 114 s), the four batteries support the demand power according to their respective SOC again. Therefore, it can be seen that even if one of the batteries suddenly fails to operate, the remaining batteries can provide power to the system according to the presented consistency power distribution method, thereby verifying the plug and play function of the multi-battery system. In addition, Fig. 4.13 (c) shows the bus voltage fluctuation curve. It can be seen during the entire operation, the bus voltage fluctuation range is 748 V-752 V, which indicates that the system stability is satisfactory, and the system can ensure stable operation even in the event of a sudden failure of the battery. It should be noted that in this experiment, the multi-stack FC system only outputs the minimum power, so the operation of the stacks is not discussed.

In addition, this chapter uses the test condition shown in Fig. 4. 14 to further verify the fault-tolerant control capability of the multi-stack FC system.

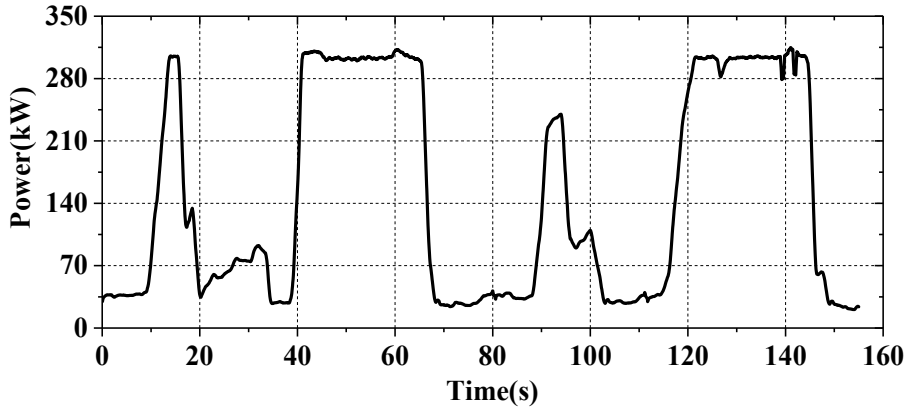

Figure 4.14. Test condition used to test fault-tolerance control of multi-stack FC system.

Assuming that the FC No.1 is out of operation due to a fault when the system operating time is about 50 s, and reconnects when the system operating time is about 100s, the operation results are shown in Fig. 4.15.

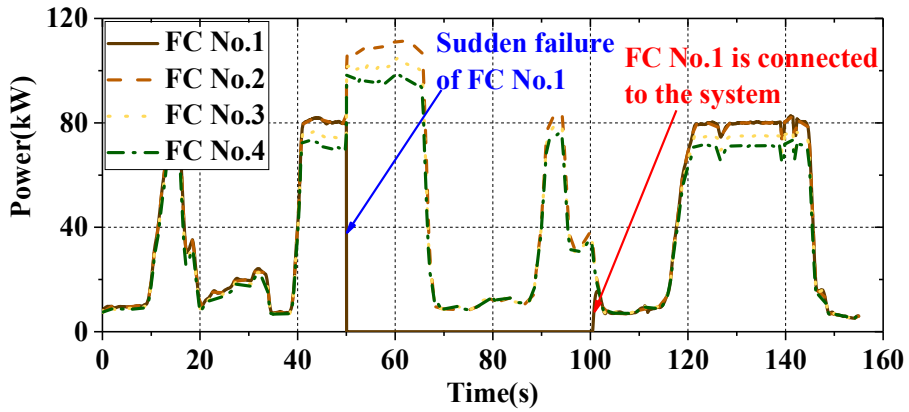

(a) FCs output power curves

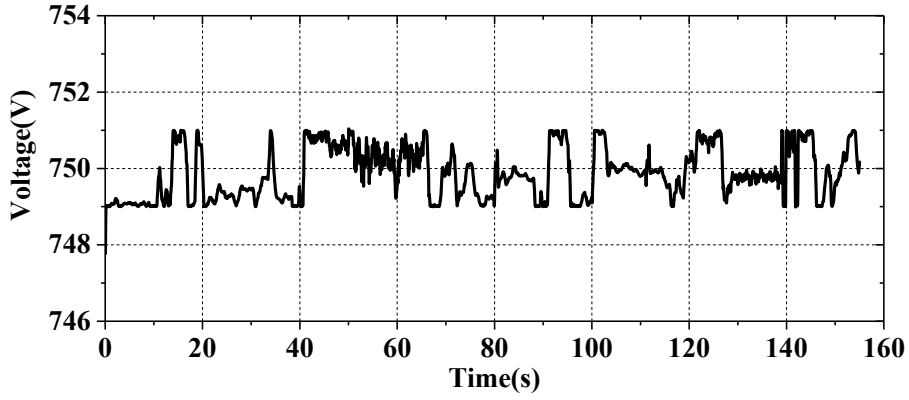

(b) Bus voltage fluctuation curve

Figure 4.15. Experimental results for testing multi-stack FC system fault-tolerant control capability.

It can be seen from Fig. 4.15 (a) that during 0 s-50 s, the system allocates the load power to four stacks according to the proposed power distribution method. When the operating time is about 50 s, the FC

No.1 is removed due to the fault, the output power of FC No.1 suddenly becomes 0, and the remaining FCs supplement the system load power according to their respective operating states. When the operating time is about 100 s, the FC No.1 is reconnected, the four FCs support the demand power according to the proposed power distribution method. In addition, from the bus voltage fluctuation curve shown in Fig. 4.15 (b), it can be seen that the bus voltage fluctuation range is small during the entire operation process, and is hardly affected by the removal and connection of the FC. In this experiment, the output power of the multi-battery system is set to 0, therefore, the operation of the batteries is not discussed.

The above experiments prove that the built system has strong robustness under the control of the proposed operating state consistency power distribution method. Even if there is a power source failure, the system can still run continuously and stably. In addition, to highlight the superiority of the proposed power distribution method more clearly, all the results using different power distribution methods are summarized in TABLE 4.2.

TABLE 4.2. Performance comparative analysis using different power distribution methods.

	Equal distribution method	The proposed method
SOC variation of battery No.1	60%-47.65%	60%-45.11%
SOC variation of battery No.2	60%-47.65%	60%-45.11%
SOC variation of battery No.3	40%-25.44%	40%-44.39%
SOC variation of battery No.4	70%-58.06%	70%-45.47%
FC No.1 operating stress	96.5296	99.3928
FC No.2 operating stress		99.2887
FC No.3 operating stress		93.1347
FC No.4 operating stress		91.8891

As shown in TABLE 4.2, the proposed power distribution method is beneficial to improve the operating consistency of the system, thereby increasing the overall service lifetime of the system.

4.5. Conclusion

This chapter mainly focuses on the research of multi-source hybrid power system suitable for high-power applications such as high-speed Electrical Multiple Unit trains, and puts forward an operating state consistency power distribution method that considers multiple factors such as the SOC of battery and operating state of FC. The presented power distribution method distributes the power among the power sources in the hybrid system according to the SOC of batteries and the operating state of stacks. Therefore, the impact of FC output power fluctuations on its operating state is analyzed in this chapter, which is also considered in the power distribution method. In addition, this chapter presents the virtual droop control algorithm and the instantaneous virtual resistances calculation technology to facilitate the expansion of system. To maintain the bus voltage stability, a voltage regulation technology is also

presented. Furthermore, this chapter also tests the practicality of the system and the effectiveness of the proposed method on the HIL platform. The results show that even if one of the power sources suddenly fails in the system, the whole hybrid system can still operate stably and allocate power according to the proposed method, which proves that the presented method has plug and play function. What is more, the experimental results show that the proposed method helps to maintain the consistent operation of the system, thereby improving the service life of the system.

References

[1] G. Zhang, Q. Li, W. Chen, X. Meng, Synthetic strategy combining speed self-adjusting operation control and adaptive power allocation for fuel cell hybrid tramway, IEEE Transactions on Industrial Electronics. 68 (2020) 1454–1465.

[2] L. Zhang, J. Liu, W. Qi, Q. Chen, R. Long, S. Quan, A parallel modular computing approach to real-time simulation of multiple fuel cells hybrid power system, International Journal of Energy Research. 43 (2019) 5266–5283. https://doi.org/10.1002/er.4515.

[3] T. Wang, Q. Li, X. Wang, W. Chen, E. Breaz, F. Gao, A Power Allocation Method for Multistack PEMFC System Considering Fuel Cell Performance Consistency, IEEE Trans. on Ind. Applicat. 56 (2020) 5340–5351. https://doi.org/10.1109/TIA.2020.3001254.

[4] N. Marx, L. Boulon, F. Gustin, D. Hissel, K. Agbossou, A review of multi-stack and modular fuel cell systems: Interests, application areas and on-going research activities, International Journal of Hydrogen Energy. 39 (2014) 12101–12111. https://doi.org/10.1016/j.ijhydene.2014.05.187.

[5] R. Suresh, G. Sankaran, S. Joopudi, S.R. Choudhury, S. Narasimhan, R. Rengaswamy, Optimal power distribution control for a network of fuel cell stacks, Journal of Process Control. 74 (2019) 88–98. https://doi.org/10.1016/j.jprocont.2017.12.006.

[6] Y. Han, Q. Li, T. Wang, W. Chen, L. Ma, Multisource coordination energy management strategy based on SOC consensus for a PEMFC–battery–supercapacitor hybrid tramway, IEEE Transactions on Vehicular Technology. 67 (2017) 296–305.

[7] N. Marx, D. Hissel, F. Gustin, L. Boulon, K. Agbossou, On Maximizing the Steady-State Efficiency of a Multi-Stack Fuel Cell System, in: 2018 IEEE Vehicle Power and Propulsion Conference (VPPC), IEEE, 2018. https://doi.org/10.1109/vppc.2018.8605036.

[8] S. Boddu, V. Agarwal, Maximum Power Extraction From Series-Connected Fuel Cell Stacks by the Current Compensation Technique, IEEE Transactions on Power Electronics. 30 (2015) 582–589. https://doi.org/10.1109/tpel.2014.2311323.

[9] T. Wang, Q. Li, H. Yang, L. Yin, X. Wang, Y. Qiu, W. Chen, Adaptive current distribution method for parallel-connected PEMFC generation system considering performance consistency, Energy Conversion and Management. 196 (2019) 866–877. https://doi.org/10.1016/j.enconman.2019.06.048.

[10] D.C.T. Cardenas, N. Marx, L. Boulon, F. Gustin, D. Hissel, Degraded Mode Operation of Multi-Stack Fuel Cell Systems, in: 2014 IEEE Vehicle Power and Propulsion Conference (VPPC), IEEE, 2014. https://doi.org/10.1109/vppc.2014.7007041.

[11] J.P. Trovão, P.G. Pereirinha, H.M. Jorge, C.H. Antunes, A multi-level energy management system for multi-source electric vehicles – An integrated rule-based meta-heuristic approach, Applied Energy. 105 (2013) 304–318. https://doi.org/10.1016/j.apenergy.2012.12.081.

[12] N. Marx, J. Cardozo, L. Boulon, F. Gustin, D. Hissel, K. Agbossou, Comparison of the Series and Parallel Architectures for Hybrid Multi-Stack Fuel Cell - Battery Systems, in: 2015 IEEE Vehicle Power and Propulsion Conference (VPPC), IEEE, 2015. https://doi.org/10.1109/vppc.2015.7352915.

[13] M. Kandidayeni, A. Macias, A.A. Amamou, L. Boulon, S. Kelouwani, H. Chaoui, Overview and benchmark analysis of fuel cell parameters estimation for energy management purposes, Journal of Power Sources. 380

(2018) 92–104. https://doi.org/10.1016/j.jpowsour.2018.01.075.
[14] Q. Li, T. Wang, C. Dai, W. Chen, L. Ma, Power Management Strategy Based on Adaptive Droop Control for a Fuel Cell-Battery-Supercapacitor Hybrid Tramway, IEEE Trans. Veh. Technol. 67 (2018) 5658–5670. https://doi.org/10.1109/TVT.2017.2715178.
[15] Q. Li, B. Su, Y. Pu, Y. Han, T. Wang, L. Yin, W. Chen, A State Machine Control Based on Equivalent Consumption Minimization for Fuel Cell/ Supercapacitor Hybrid Tramway, IEEE Trans. Transp. Electrific. 5 (2019) 552–564. https://doi.org/10.1109/TTE.2019.2915689.
[16] S. Augustine, M.K. Mishra, N. Lakshminarasamma, Adaptive Droop Control Strategy for Load Sharing and Circulating Current Minimization in Low-Voltage Standalone DC Microgrid, IEEE Transactions on Sustainable Energy. 6 (2015) 132–141. https://doi.org/10.1109/tste.2014.2360628.
[17] A distributed reactive power sharing approach in microgrid with improved droop control, CSEE Journal of Power and Energy Systems. (2020). https://doi.org/10.17775/cseejpes.2019.00530.
[18] Q. Xu, X. Hu, P. Wang, J. Xiao, P. Tu, C. Wen, M.Y. Lee, A Decentralized Dynamic Power Sharing Strategy for Hybrid Energy Storage System in Autonomous DC Microgrid, IEEE Transactions on Industrial Electronics. 64 (2017) 5930–5941. https://doi.org/10.1109/tie.2016.2608880.
[19] H. Yang, Y. Qiu, Q. Li, W. Chen, A self-convergence droop control of no communication based on double-quadrant state of charge in DC microgrid applications, Journal of Renewable and Sustainable Energy. 9 (2017) 034102.
[20] X. Han, F. Li, T. Zhang, T. Zhang, K. Song, Economic energy management strategy design and simulation for a dual-stack fuel cell electric vehicle, International Journal of Hydrogen Energy. 42 (2017) 11584–11595. https://doi.org/10.1016/j.ijhydene.2017.01.085.
[21] T. Wang, Q. Li, Y. Qiu, W. Chen, E. Breaz, A. Ravey, F. Gao, Power Optimization Distribution Method for Fuel Cell System Cluster Comprehensively Considering System Economy, IEEE Transactions on Industrial Electronics. 69 (2022) 12898–12911. https://doi.org/10.1109/TIE.2021.3135608.
[22] H. Babazadeh, B. Asghari, R. Sharma, A new control scheme in a multi-battery management system for expanding microgrids, in: ISGT 2014, IEEE, 2014: pp. 1–5.
[23] S. Zhou, L. Fan, G. Zhang, J. Gao, Y. Lu, P. Zhao, C. Wen, L. Shi, Z. Hu, A review on proton exchange membrane multi-stack fuel cell systems: architecture, performance, and power management, Applied Energy. 310 (2022) 118555.
[24] T. Wang, Q. Li, L. Yin, W. Chen, Hydrogen consumption minimization method based on the online identification for multi-stack PEMFCs system, International Journal of Hydrogen Energy. 44 (2019) 5074–5081. https://doi.org/10.1016/j.ijhydene.2018.09.181.
[25] T. Wang, Q. Li, Y. Qiu, L. Yin, L. Liu, W. Chen, Efficiency Extreme Point Tracking Strategy Based on FFRLS Online Identification for PEMFC System, IEEE Trans. Energy Convers. 34 (2019) 952–963. https://doi.org/10.1109/TEC.2018.2872861.
[26] Z. Hua, Z. Zheng, E. Pahon, M.-C. Péra, F. Gao, Remaining useful life prediction of PEMFC systems under dynamic operating conditions, Energy Conversion and Management. 231 (2021) 113825. https://doi.org/10.1016/j.enconman.2021.113825.
[27] B. Somaiah, V. Agarwal, Distributed Maximum Power Extraction From Fuel Cell Stack Arrays Using Dedicated Power Converters in Series and Parallel Configuration, IEEE Transactions on Energy Conversion. 31 (2016) 1442–1451. https://doi.org/10.1109/tec.2016.2557803.
[28] P. Pei, H. Chen, Main factors affecting the lifetime of Proton Exchange Membrane fuel cells in vehicle applications: A review, Applied Energy. 125 (2014) 60–75. https://doi.org/10.1016/j.apenergy.2014.03.048.
[29] X. Yan, M. Hou, L. Sun, H. Cheng, Y. Hong, D. Liang, Q. Shen, P. Ming, B. Yi, The study on transient characteristic of proton exchange membrane fuel cell stack during dynamic loading, Journal of Power Sources. 163 (2007) 966–970.
[30] Z. Hua, Z. Zheng, M.-C. Péra, F. Gao, Remaining useful life prediction of PEMFC systems based on the multi-input echo state network, Applied Energy. 265 (2020) 114791. https://doi.org/10.1016/j.apenergy.2020.114791.

[31] J. Chen, D. Zhou, C. Lyu, C. Lu, A novel health indicator for PEMFC state of health estimation and remaining useful life prediction, International Journal of Hydrogen Energy. 42 (2017) 20230–20238. https://doi.org/10.1016/j.ijhydene.2017.05.241.
[32] H. Yang, Q. Li, T. Wang, Y. Qiu, W. Chen, A dual mode distributed economic control for a fuel cell–photovoltaic-battery hybrid power generation system based on marginal cost, International Journal of Hydrogen Energy. 44 (2019) 25229–25239.
[33] H. Yang, S. Li, Q. Li, W. Chen, Hierarchical distributed control for decentralized battery energy storage system based on consensus algorithm with pinning node, Protection and Control of Modern Power Systems. 3 (2018). https://doi.org/10.1186/s41601-018-0081-5.
[34] T. Wang, Q. Li, L. Yin, W. Chen, E. Breaz, F. Gao, Hierarchical Power Allocation Method Based on Online Extremum Seeking Algorithm for Dual-PEMFC/Battery Hybrid Locomotive, IEEE Transactions on Vehicular Technology. 70 (2021) 5679–5692. https://doi.org/10.1109/tvt.2021.3078752.

Chapter 5. Conclusion

5.1. Summary of the research works

This thesis mainly takes the hybrid power systems used in the field of rail transit as the research object, and carries out experimental research on the energy management strategies of different hybrid power structures to ensure the economical operation of the system under the premise of stable operation. In addition, this thesis mainly conducts experimental research on extreme value tracking algorithm, energy management strategies of dual-source hybrid power systems, and energy management strategies of multi-source hybrid power system.

First of all, the research background, the current research development status of the hybrid electric vehicles, the research status of hybrid electric trams, a brief overview of the current state of research on energy management strategies, and the research status of multi-source power systems. Then, an optimal system economic energy management strategy is proposed for a battery/fuel cell hybrid electric vehicle, and compared with various energy management strategies. Thereafter, an online extremum seeking-based optimized energy management strategy is presented for a supercapacitor/fuel cell hybrid electric tram, and a detailed comparative study of energy management strategies is carried out. In the end, in order to study the multi-source hybrid power system suitable for high-power applications, an operating state consistency power distribution method that considers multiple factors is proposed. The main contributions and originality of this thesis are as follows:

The optimal system economic energy management strategy: considering that in the hybrid power system, the operating cost of the power sources is high and the lifetime needs to be improved. Therefore, in order to further promote the use of hybrid power systems, this thesis studies the coupling relationship between lifetime loss and output power of each power source by analyzing the impact of output power on power sources durability and converts lifetime loss into system operating costs. In addition, considering the equivalent hydrogen consumption cost of the battery during operation, a system optimal operating cost function is formulated.

The online extremum seeking-based optimized energy management strategy: in order to improve the operating performance of the stack, a “safe operating zone” is divided. In addition, an online identification algorithm is proposed to update the zone boundary value in real time to ensure the efficiency operation of the system. Since the supercapacitor has the disadvantage of low energy density, in order to ensure the consistency of the initial and final SOC states of the supercapacitor and ensure the continuous operation of the tram, the SOC fluctuation constraint is considered in the proposed energy management strategy.

The performance consistent power distribution method: the presented power distribution method

distributes the power among the power sources in the multi-source hybrid power system according to the SOC of batteries and the operating state of the stacks. Therefore, the impact of FC output power fluctuations on its operating state is analyzed, which is also considered in the power distribution method. In addition, the virtual droop control algorithm and the instantaneous virtual resistances calculation technology are proposed to facilitate the expansion of system. According to the real-time operating state of each power source, the adjustment factors are designed to adaptively adjust the droop coefficients to control the converters output reference power. To maintain the bus voltage stability, a voltage regulation technology is also presented.

In order to verify the effectiveness of the proposed energy management strategies and power distribution method, a hardware-in-the-loop (HIL) simulation platform for hybrid power systems is established based on RT-LAB simulation development software and OP5600 real-time digital simulator. The HIL experimental results show that all the proposed energy management strategies could be effectively embedded into the target hardware and executed correctly on the target hardware, thus verifying the effectiveness and real-time applicability of the proposed methods. In addition, in order to test the actual effect of the proposed method, a corresponding physical reduced-scale experimental platform is also built. The physical system mainly include supercapacitor, fuel cell, DC/DC converters, core control units, and sampling and conditioning peripheral hardware circuits.

5.2. Future research directions

The main focus of this thesis is on energy management strategies for different hybrid power systems. Although the corresponding research work has been carried out on the hardware-in-the-loop (HIL) simulation platform and the physical scaled-down hybrid power test bench, and certain research results have been obtained, the research content of this thesis can still be further improved. Specifically, future works concentrate on the following aspects:

1) In this thesis, only the “voltage-current” polarization curve is analyzed in the study of the method for evaluating the real-time operating performance of the stack. In order to further improve the evaluation accuracy of the performance state of the stack, the internal resistance can be also analyzed. Therefore, in the future, on-line measurement and analysis of the electrochemical impedance spectroscopy of stack can be carried out, and a new method for evaluating the state of health of stack can be proposed.

2) In recent years, with the continuous development of machine learning methods, more and more powerful algorithms with better optimization effects are emerging. Some studies have applied it to the hybrid power system to optimize the distribution of system power and predict operating conditions, and the results are satisfactory. Therefore, in the future, I intend to carry out research on optimal energy management based on machine learning methods.

3) Although this thesis has carried out a lot of research on different energy management strategies and achieved certain results, it doesn't involve the research on the methods of working condition prediction. Predicting the driving conditions of the vehicles and cooperating with appropriate energy management strategies are more conducive to improving the service life and operating performance of the power sources. Therefore, in the future research plan, the research on the working condition prediction method will be carried out.

4) The operating conditions used in this thesis are obtained from the simulation of the electronic load and power supply. In order to further prove the stability of the system and the effectiveness of the energy management strategies, the performance of the proposed strategy can be tested with actual application objects in the future.

List of Figures

List of Tables

Nomenclature

PV	Photovoltaic
WT	Wind turbines
PHEV	Plug-in hybrid electric vehicle
EV	Electric vehicle
FC	Fuel Cell
FCV	Fuel cell vehicle
ESS	Energy storage system
HEV	Hybrid electric vehicle
EMS	Energy management strategy
HIL	Hardware-in-the-loop
SOC	State of Charge
SC	Supercapacitor
GM	General Motors
SMC	State machine control
PF	Power following
FLC	Fuzzy logical control
WT	Wavelet transform
GA	Genetic algorithm
PSO	Particle swarm optimization
DP	Dynamic Programming
SDP	Stochastic Dynamic Programming
DDP	Deterministic Dynamic Programming
PMP	Pontryagin's Minimum Principle
CP	Convex programming
QP	Quadratic programming
SA	Simulated annealing
MPC	Model predictive control
ECMS	Equivalent consumption minimization strategy
RL	Reinforcement learning
DDPG	Deep Deterministic Policy Gradient
SARSA	State-action-reward-state-action
MEOP	Maximum efficiency operating point
SQP	Sequential quadratic programming
RCP	Rapid Control Prototyping
TI	Texas Instruments

ADC	Analog/digital conversion
DAC	Digital/analog conversion
ME	Maximum efficiency
MP	Maximum power
LF-LRV	100% low floor light rail vehicle
FFRLS	Forgetting factor recursive least square
SISO	Single-input single-output
PWM	Pulse width modulation
KVL	Kirchhoff's voltage law
KCL	Kirchhoff's current law